



HAL
open science

Axonal target specificity in the CRISPR/Cas9 era: a new role for Reelin in vertebrate visual sytem development

Vincenzo Di Donato

► To cite this version:

Vincenzo Di Donato. Axonal target specificity in the CRISPR/Cas9 era: a new role for Reelin in vertebrate visual sytem development. *Neurons and Cognition [q-bio.NC]*. Université Pierre et Marie Curie - Paris VI, 2016. English. NNT: 2016PA066409 . tel-01589651

HAL Id: tel-01589651

<https://theses.hal.science/tel-01589651>

Submitted on 18 Sep 2017

HAL is a multi-disciplinary open access archive for the deposit and dissemination of scientific research documents, whether they are published or not. The documents may come from teaching and research institutions in France or abroad, or from public or private research centers.

L'archive ouverte pluridisciplinaire **HAL**, est destinée au dépôt et à la diffusion de documents scientifiques de niveau recherche, publiés ou non, émanant des établissements d'enseignement et de recherche français ou étrangers, des laboratoires publics ou privés.

Université Pierre et Marie Curie

Ecole Doctorale Cerveau Cognition Comportement

Institut Curie, Unité Génétique Biologie du Développement

Equipe Développement des circuits neuronaux

Axonal target specificity in the CRISPR/Cas9 era: a new role for Reelin in vertebrate visual system development

Présenté par **Vincenzo DI DONATO**

Thèse de doctorat de Neurosciences

Dirigée par Filippo DEL BENE

Présentée et soutenue publiquement le 16/09/2016

Devant un jury composé de :

Dr. Filippo DEL BENE

Directeur de thèse

Prof. Dr. Herwig BAIER

Rapporteur

Dr. Valerie CASTELLANI

Rapporteur

Dr. Alain CHEDOTAL

Examineur

Dr. Sonia GAREL

Examineur

A mio padre

*“Cerco in tutte le canzoni
e in un passero su ramo
uno spunto per la rivoluzione”
Rino Gaetano*

Acknowledgments

When I joined Filippo's lab I barely had some beard growing on my face. If the comparison is allowed, I must say that the lab, at that time, looked exactly as the beardless face of a young guy: empty shelves, clean benches and no crazy transgenic larvae swimming around whatsoever. Then everything happened. A moderately international group of five people met at the third floor of the brand new BDD (biologie du développement) building. Indeed, we were all brand new: Filippo first year PI, Chris first year Postdoc, Karine first year lab manager, Tom first year PhD, me in a temporal limbo pre-PhD. Probably a wise player would not have bet on our team. Instead, I did decide to bet five years of my life in this game. If I look now at what the Del Bene Lab has become, I do not regret a single moment and I am just proud of having taken part an adventure that made the metaphorical young guy (the lab) and the real one (me) grow scientifically and personally. I am grateful to all the people that have contributed to this.

First and foremost I owe my deepest gratitude to my supervisor Filippo. Thank you because before meeting you I had no idea what science was about. You have shown me the good and the bad aspects of being a scientist. While on one hand you allowed me to travel all over the world to meet the greatest minds, on the other hand you pushed me to repeat the same PCR for a month. You have transmitted me your passion for discovery, for the new cutting-edge technologies and gave me the freedom to develop my research interests in any direction. I will always remember stepping in your office at anytime and bother you with any relevant biological question or stupid gossip. Thank you also for showing me that there is an explanation for everything, if you ask the right question. I will miss your way of making things just working out for everyone in the lab and your unpredictable bright suggestions on my work. Finally a non-scientifically-related thanks for all the Reelin-free moments we shared, from the organization of our Italian-style retreats, from the beers in freezing Australian bars to the apéro in unexpected gardens in Barcelona, from the rolling Superman-like crushing to the endless discussions about how the world should be. Thank you Filo for all this!

A special thanks goes to Tom. He has been my molecular biology guru; if I know how to generate triple transgenics or perform acrobatic PCRs is because of him. He has taught me everything he could (because he knew much more than that) always with a huge smile. But he has not been just a lab buddy. We have been travelling, running, partying, reflecting about life and much more together. During these years, he has been as an older brother for me. If Tom has been my molecular biology guru, then Chris has been my biology guru *tout court*. He knows about biology as much as he knows about music and, believe me, that is a lot. I want to thank him for troubleshooting with me every little or big problem I would have in my project, for patiently reading and giving suggestion on my thesis, for always giving me his honest opinion about my work and for helping me to correct it for other people to have a better opinion than his. It has been a pleasure to go to concerts, to picnics and to talk with you about deep matters around a beer. Another great thank you to Karine. You have not been just a lab manager; in a way you have been my mental and experimental order manager. You have always been there with your excellent technical skills and your perseverance to make work whatever was not. Thanks also because with you I had no need to ask, you would know already what I wanted and thank you for being the most tolerant desk mate ever.

A big thanks goes to the ever-changing Italian "ghetto" of the Del Bene Lab and of the entire BDD. Among more than 30 Italians that have been passing by a heartfelt thank you goes to Flavia. We have lived together the satisfactions and the frustrations of more than a year of insane cloning and research of mutations. Luckily you were there to share the anxiety of being scooped and the relief of publishing better than the scoopers. You have

been the core of my southern Italian experience in a lab in northern Europe made of delicious taralli, unstoppable complains about the weather, rare sunbathing on the terrace, dialect speaking and bitching in the fishroom. Thanks also for your patience and your art that contributed to the birth of this thesis. Thank you Manu for being there. I always thought that you were the pillar of the third floor of the BDD and I was surprised that it was still holding up after you left. Thanks for your wise suggestions that guided me through the tunnel of molecular biology and for trusting in me since the beginning. If I had to finish the list of Italians I want to thank, I would need to write another thesis. So, although I would like to express to all of them my gratitude just for making me feel home everyday, I will limit myself to thank Giulia and Irene for bringing a new radiant energy in the lab, Roby for trying to find solution to our constant “in pieces” condition and Federica for the continuous provision of laughs and gossips. Next, I want to thank Valerie for bringing a different point of view on my work and on many more topics during our endless discussions. Thanks for opening my mind towards new directions and for giving your Canadian touch. A very warm thanks goes to Shahad. I still remember how much fun we had when, during an exchange, she had to work on a tiny corner of my chaotic bench. At the time I was teaching her something, then, when she joined the lab for a Postdoc, I realized how much I had to learn from her. Thanks for your reflections, criticisms and suggestions in an out of the lab and thank you for always spicing them up with a great smile. A big thanks goes to Celine for helping me to value my work. Thank you for giving me guidance, teaching me how to be rigorous and to offer me you broad view on science. Also thank you, together with Shahad and Karine, for helping me to survive in the bureaucratic jungle of the French system. I also want to thank some of the former members of the lab for their support, especially Noé, Julie, the little Tom, Alessandra, Anne , Léa and as well the temporary members among which Alessio and Edoardo.

I am deeply grateful to Jean Paul. Thanks for introducing me to the flabbergasting world of genome engineering and for jumping on the bandwagon of the 2C-Cas9 even before we wisely decided to change home from the previously embarrassing CaCACreZ. Thanks you as well for making me discover the best Lebanese place in town and for sharing with me the addiction to it.

Furthermore, I am hugely indebted with the members of my TAC committee who guided my work through its different phases. Thanks Herwig for your sharp judgments and François for your advices. Thanks Silvia for your continuous support and spontaneous excitement towards my results. A sincere thanks to Yohanns for his extemporaneous maybe-too-brilliant inputs, which I would eventually understand with a couple of years of delay. Thank you for taking the time to deeply discuss about my results and making solvable apparently unsolvable mysteries. Also, thank you for organizing together the best Christmas party ever.

I would like to express my gratitude for the members of my dissertation committee. Thanks Alain, Herwig, Valerie and Sonia for accepting to be part of my jury and for taking the time to evaluate my manuscript. I am sure that fruitful discussions will arise and that your intellectual contributions will add value to my work.

I would also like to thank all the BDD people that make this an excellent, fun and vibrant place workplace.

Although I spent some time in the lab during the last years, my non-scientific Parisian experience has been unforgettable as well and I owe this to all the people that I met on my way.

I warmly thank Ale and Maria for being my Neapolitan family during my first year in town and as well Adri who nicely completed our hostel. Thanks Ricca and Mari again for our pseudo-philosophical conversations about the life and the future. Thank you Rose and Roby for reasoning with me about our paths and our choices and for never taking us seriously.

I am also grateful to the “Rue du Temple” flat mates: the Portuguese couple Simao and Sylvie for sharing the up and down of science around a cup of tea, Coralie for being so comprehensive, Damien for having taught me how to become a perfect Parisian bobo (bourgeois-bohème). Thank you Stefania, you have been the first Italian person from above Rome with whom I have shared a flat in Paris and you have convinced me that up there you can be as friendly, nice and funny as in the deep south.

Thank you Milton for being around. We have lived great moments together trying to get the best out of our lives of scientists with non-very-scientific minds. A warm thank goes to Yanina for introducing me to Erri De Luca and for thinking with me about revolution during the uncountable number of dinners she invited me for.

In addition to the people that lived at least part of these last intense years close to me, I would like to show my gratitude to all the people that, from far, have made available their support in a number of ways.

First of all, thanks to my small but always present family, my uncle, my grandpa, my aunt, and cousins for their support. Thanks Mum for believing in me much more than I do and for always understanding my states of mind despite the 2000 kilometers separating us. Thanks for taking care of me with a boost of delicious food and affection during the last phase of the thesis redaction. Thank you Fabio for supporting me from all the different countries you have moved between during these years. Although you were the one going through the most unstable steps of your career, while I was supposed to be the stable PhD student, you would always have a reassuring word for me.

Furthermore I want to thank all the friends that shared with me little parts of this journey. Thank to Imma and Francesco who won the price for the most assiduous visitors; you have stepped in my Parisian life during all the different periods and showed me that even from far we can keep on growing together. Thank you Chiara for transmitting me your “zen” attitude and helping me to look at problems from a different perspective. I am also grateful to Anna for hosting me and bringing me partying until the morning on the day of my PhD fellowship deadline and still trusting I could get funded. Thanks to Lisa and Marta for demonstrating me that we do not need constant communication if there is friendship. Then I would like to thank my “Frattamaggiore friends” Cinzia, Mario, Rosy, Antonino, Imma and Francesco again for catching up with me every time they could and for bringing me to our early years.

Last but not least, my deepest gratitude goes to Névida. I remember you back in Granada telling me that you would not come to Paris if I had chosen to go there for my PhD. Eventually this is what I choose and you did the possible and the impossible to join me. You undertook a risky PhD project to be on my side throughout these years. I can't express with words all my gratefulness to you for showing me that what binds us is more important than all the rest. Thanks for being so flexible but determined, comprehensive but tough. Thank you for sharing with me the passion of the folkloric dance and traditional music, the beauty of the world from the lost villages of the Thai jungle to the sunrise in the salt flat in Bolivia, the tears of joy during our life in Granada and the tears of sorrow for the Paris attacks, the doubts of being a scientist and the hate/love towards our job. Thanks for showing me the right way and to make me feel that this is not your way or my way but “our” way. Thank you for supporting me till the end.

Everyone knows that a PhD is not an easy path, but if I look behind me I see a straight corridor with all of you on both sides looking after me. Now that I am at the end of it, I realize that this was not a straight way by default but you made it smooth to allow me to pass by without a fear.

Thank you all for making this true.

Table of Contents

List of Figures and Tables	III
Abbreviations	IV
Preamble	VI
Chapter I: Introduction	1
1. The vertebrate visual system	1
1.1 Basic morphology and connectivity of the vertebrate retina	1
1.2 RGCs axonal navigation: a long path from the eye to the brain	3
1.2.1 Exiting the eye: intraretinal development	3
1.2.2 Midline crossing: the optic chiasm and the optic tract	5
1.2.3 The arrival: target recognition and topographic mapping	6
2. Synaptic lamination in the vertebrate visual system	8
2.1 The inner plexiform layer (IPL)	8
2.2 Development of synaptic laminae in the IPL	9
2.3 The zebrafish larval tectal neuropil	10
2.4 Development of laminar arrangement in the tectal neuropil	11
2.5 The function of layers in the organization of the visual circuitry	13
2.5.1 Wiring economy.....	13
2.5.2 Developmental speed.....	14
2.6 Molecular mechanisms of synaptic laminae formation.....	15
2.6.1 Cell-cell recognition by cell-adhesion molecules.....	15
2.6.2 Extracellular molecules	17
<i>a) Layer-specific ECM factors</i>	<i>17</i>
<i>b) Long-range guidance across multiple laminae</i>	<i>18</i>
3. Reelin: a multifunctional extracellular protein in the CNS	20
3.1 The role of Reelin in mouse cortical development	21
3.2 Modulation of cell polarity by Reelin signaling pathway	23
3.2.1 Leading process determination	23
3.2.2 Establishment of neural polarity	24
3.2.3 Cytoskeletal dynamics.....	25
3.3 Role of Reelin in axonal targeting	26
3.3.1 Function of Reelin signaling in entorhinal-hippocampal circuit formation	27
3.3.2 Function of Reelin signaling in the establishment of visual circuits.....	27

4. Conditional knock-out in the CRISPR/Cas9 era	29
4.1 The CRISPR/Cas9 system	29
4.1.1 Conditional knock-out via knock-in in zebrafish	31
4.1.2 Conditional knock-out via tissue-specific Cas9 expression	32
5. Aim of the study	34
Chapter II: Results	35
- Article 1: “A gradient of Reelin directs axonal lamination in the vertebrate visual system”	35
1. Summary Article 1	36
Submitted Article	37
- Article 2: “2C-Cas9: a versatile tool for clonal analysis of gene function” ...	65
2. Summary Article 2.....	66
Published Article	67
Chapter III: Discussion	84
1. A new function for an old protein	84
1.1 Reelin acts as a long-range molecular cue in the zebrafish tectal neuropil.....	84
1.2 Reelin signaling is involved in tectal synaptic lamination.....	86
1.3 Reelin acts as an attractive molecular cue for ingrowing RGC axons	87
1.4 Reelin spatial distribution is important for its function	88
1.5 Two gradients for laminar-specific RGC axonal targeting.....	89
2. Tissue-specific gene disruption in zebrafish	92
2.1 Genetic labeling of cas9-expressing cells via 2C-Ca9	93
2.2 Limitations and possible improvements of the 2C-Cas9 system.....	95
3. Conclusions	97
References.....	99
Publications.....	115
Attached articles	117

List of Figures and Tables

Figure 1: Schematic representation of the retina and retino-recipient nuclei in the vertebrate brain	2
Figure 2: Molecular factors involved in growth and pathfinding of RGC axons from the retina to the retinorecipient nuclei	7
Figure 3: Anatomy and development of the retinal IPL and tectal neuropil	12
Figure 4: CAMs regulating synaptic targeting in the IPL of the chick retina	17
Table 1: List of layer-specific ECM factors	18
Figure 5: Model of action of Slit1 in the zebrafish tectal neuropil	19
Figure 6: Reelin structure and function in mouse early cortical development	22
Figure 7: Reelin signaling in neuronal polarization of migrating neurons	26
Figure 8: Reelin and Dab1 are required for correct retinogeniculate targeting	28
Figure 9: Schematic illustrating sgRNA mediated recruitment of the <i>Streptococcus pyogenes</i> Cas9 endonuclease to a target site	31
Figure 10: Schematic of a CRISPRs/Cas9-based system for tissue-specific knock-out in zebrafish	33
Figure 11: Model of Reelin and Slit1 mechanisms of action in laminar patterning of zebrafish tectal neuropil	91
Figure 12: Schematic representation of the different methods and applications of tissue CRISPR/Cas9-mediated genome modifications	94

Abbreviations

ACL: amacrine cell layer

AC: amacrine cell

AF: arborisation field

AMP: adenosin monophosphate

ApoER2: apolipoprotein E receptor 2

APP: amyloid precursor protein

BAC: bacterial artificial chromosome

BC: bipolar cell

BM: basement membrane

CAMs: cell adhesion molecules

CNS: central nervous system

Cntn: contactins

CP: cortical plate

CR: Cajal-Retzius

CRISPR/Cas9: Clustered Regularly Interspaced Palindromic Repeats/CRISPR associated protein 9

CSPG: chondroitin sulfate proteoglycan

Dab1: Disabled-1

DS: direction-selective

DSB: double strand break

EBs: end-binding proteins

EC: entorhinal cortex

ECM: extracellular matrix

EGF: epidermal growth factor

GCL: ganglion cell layer

HDR: homologous directed repair

HP: hippocampus

HSPGs: heparan sulfate proteoglycans

IGL: intergeniculate leaflet

IgSF: Ig superfamily

INL: inner nuclear layer

IPL: inner plexiform layer

ipRGCs: intrinsically photosensitive RGCs

IZ: intermediate zone

LGN: lateral geniculate nucleus

LIMK1: LIM Kinase 1

LRP8: lipoprotein receptor-related protein 8
MZ: marginal zone
NgCAM: neuron-glia cell adhesion molecule
NICD: notch intracellular cleaved domain
Noi: No-isthmus
Nrp1: neuropilin-1
OFL: optic fiber layer
ONL: outer nuclear layer
OPL: outer plexiform layer
ORF: open reading frame
OT: optic tectum
Ptc1: Patched-1
PVN: periventricular neuron
ReIn= Reelin
RG: radial glia
RGC: retinal ganglion cells
SAC: stratum album centrale
SC: superior colliculus
Sdk: Sidekicks
Sema3 : Semaphorin 3
SFGS: stratum fibrosum et griseum superficiale
SFK: Src-family kinases
SGC: stratum griseum centrale
SINs: superficially located inhibitory interneurons
SO: stratum opticum
SPV: stratum periventriculare
TCA: thalamocortical axon
Tenm3: Teneurin-3
UAS: upstream activating sequence
VLDLR: very-low-density lipoprotein receptor
VZ: ventricular zone

Preamble

The extreme complexity of neural networks assembled in functional circuits in the brain represents, perhaps, the finest example of interdependence between tissue architecture and its proper function. One of the fundamental issues that the field of developmental neurobiology faces is to understand the mechanisms underlying the establishment and refinement of stereotyped patterns of connectivity between neurons. An in-depth knowledge of the processes that regulate the assembly of neural circuits is essential to shed light on how these circuits enable brain activity.

The vertebrate visual system has served as a valuable model for understanding basic principles of neural circuit formation. In particular the zebrafish retinotectal system has allowed the *in vivo* investigation of several processes, such as axonal pathfinding (Karlstrom et al 1996), establishment of retinotopic maps (Baier et al 1996, McLaughlin & O'Leary 2005), synaptic connectivity (Baier 2013) and activity dependent steps in circuit formation (Ruthazer & Aizenman 2010).

The main aim of the first part of my PhD work was to investigate the role of the extracellular matrix (ECM) protein Reelin in the establishment of the zebrafish retinotectal circuit. We tested the hypothesis that Reelin could function as a molecular cue for the axons of retinal ganglion cells (RGCs), the sole output neurons of the retina, targeting the main retinorecipient nucleus of the fish midbrain, the optic tectum. More specifically, we tried to elucidate the role of Reelin in the establishment of synaptic laminae in the tectal neuropil, a mostly cell-body free area where axons and dendrites of pre- and postsynaptic neurons form contacts.

Therefore, in the first part of the introduction, I will review current knowledge on the guidance mechanisms acting on the axons of RGCs starting from the intraretinal development until the targeting of retinorecipient nuclei in the brain. Thereafter I will focus on the anatomy and development of synaptic layers in the vertebrate visual system, as well the processes leading to this stereotyped spatial organization. Finally I will describe the role of Reelin in different processes relevant to this study.

As a second project during my PhD work, I sought to develop a strategy to enable the analysis of gene inactivation in a cell-type-specific manner. To this aim, I combined the transgenesis tools available for genetic manipulation of the zebrafish larval visual system and CRISPR/Cas9 genome editing methodology. Thus, in the last part of the introduction I will describe the CRISPR/ Cas9 system and the technologies developed so far for the generation of conditional alleles.

Chapter I: Introduction

1. The vertebrate visual system

1.1 Basic morphology and connectivity of the vertebrate retina

Five main neuronal cell types and one class of glia cells compose the vertebrate retina: photoreceptors, projection neurons (retinal ganglion cells or RGCs), three types of interneurons (horizontal, bipolar and amacrine cells), and glial cells (Müller cells). The spatial distribution of these cells within the retinal tissue gives rise to three distinct nuclear layers containing cell bodies, which are separated by two plexiform layers that contain synapses. From the apical side to the basal side of the retina, the layers are: the outer nuclear layer (ONL) hosting rod and cone photoreceptors, the outer plexiform layer (OPL), the inner nuclear layer (INL) harboring horizontal, bipolar, Müller glia and amacrine cells, the inner plexiform layer (IPL) and finally the ganglion cell layer (GCL), which is populated by displaced amacrine cells as well as RGCs (Cayouette et al 2006, Masland 2001). RGCs, the only output neurons of the retina, project their axons to more than ten areas of the zebrafish brain. In the zebrafish visual system, these areas are known as arborization fields (AF) (Burrill & Easter 1994). Some AFs are homologous to visual input receiving areas in mammals, such as the suprachiasmatic nucleus (AF1), the pretectal nucleus of the optic tract (AF9) or the optic tectum (OT)/superior colliculus (SC) (AF10). The OT receives the main proportion of retinal afferents representing the major retinorecipient nucleus in fish (Nevin et al 2010) and other non-mammalian vertebrates. In mammals, although the SC is innervated by RGC axons, the major target is represented by the dorsal lateral geniculate nucleus (LGN) in the thalamus. From the LGN and OT/SC, visual information is transmitted further into the brain (Figure 1).

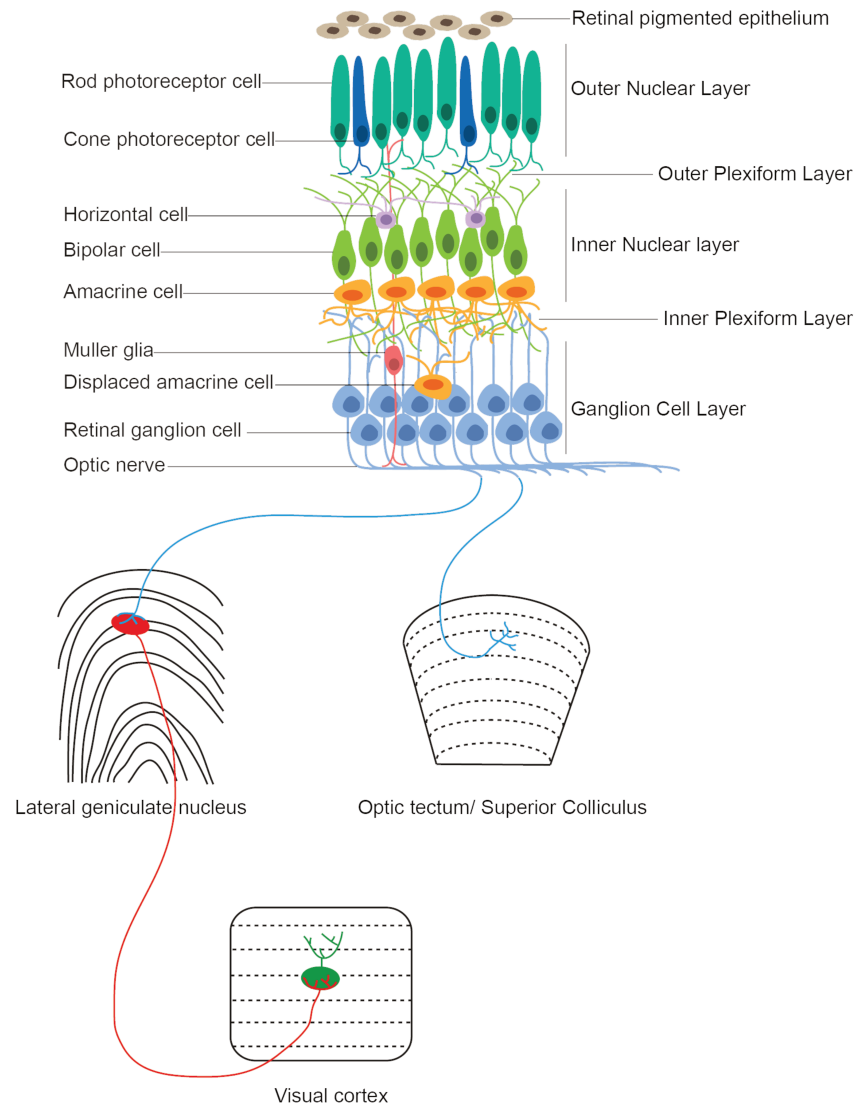


Figure 1. Schematic representation of the retina and retinorecipient nuclei in the vertebrate brain. The retina is the visual input-receiving organ of the visual system. In the retinal tissue, photoreceptors convert the light of the visual stimulus into an electric signal. The signal is then transmitted to interneurons, including bipolar cells (BCs), in a synaptic layer called the outer plexiform layer (OPL). The cell bodies of BCs and most other interneurons are placed in the inner nuclear layer (INL). The axons of BCs extend in the inner plexiform layer (IPL) where they form connections with the neurites of amacrine cells (ACs) and the dendrites of retinal ganglion cells (RGCs). RGC axons leave the eye via the optic nerve and project to the superior colliculus, SC (called optic tectum in non-mammalian vertebrates), and to the lateral geniculate nucleus (LGN) projecting thereafter to the primary visual cortex (in mammals).

1.2 RGCs axonal navigation: a long path from the eye to the brain

The development of RGC axons from the retina to their main targets in the brain can be analyzed as a multistep process. After axonogenesis, retinal axons grow inside the retina to reach the optic disk through which they can exit the eye. Thereafter, they extend towards the midline where RGC projections from both eyes meet and form the optic chiasm. Here, a proportion of RGC processes extend within the same hemisphere as their side of origin (ipsilateral axons), whereas a part of them cross over to the opposite side of the brain (contralateral axons). While across mammals the visual system displays different fractions of ipsilateral projections, these are completely absent in species that are supposed to lack binocular vision, such as *Xenopus* tadpoles, zebrafish and chick. After passing the optic chiasm, retinal afferents navigate through the optic tracts, finally projecting caudally and dorsally to their primary retinorecipient nuclei: the aforementioned SC and LGN in mammals, or the OT in non-mammalian vertebrates. The establishment of retinal axon pathway involves a plethora of finely regulated molecular signaling events. Many factors have been shown to provide guidance to RGC axonal growth cones at each step of an extremely complex developmental process (Erskine & Herrera 2014). These cues are diffusible or substrate-bound and can exert an attractive or repulsive role on RGC processes (Tessier-Lavigne & Goodman 1996). The molecular signals affecting growth cone behavior *in vivo* remains subject of intense experimental investigation.

In the following paragraphs, I will describe the basic molecular mechanisms underlying the directed growth and navigation of RGC axons from the retinal tissue towards the retinorecipient nuclei (Figure 2). Although I will discuss findings from different model organisms, particular attention will be given to the zebrafish retinorecipient system. For this reason, given that in fish all RGC axons project to the contralateral OT, the factors directing ipsilateral targeting in other systems will not be discussed here.

1.2.1 Exiting the eye: intraretinal development

As soon as axonogenesis starts, RGC axons exhibit a directed growth towards the optic disk, where they will leave the retinal tissue. Axonal extension occurs along the optic fiber layer (OFL), located at the inner surface of the retina. The OFL develops on a substrate of glial endfeet, in which cell adhesion molecules exert a growth-promoting activity. The spatial restriction of the OFL to the inner retina is ensured by Slit-Robo signaling, whose perturbation has been shown to cause intraretinal aberrant RGC projections in the outer retina (Thompson et al 2009, Thompson et al 2006b). Although OFL stability plays a crucial role in RGCs axonal outgrowth, its disruption in double *Slit1/2* or *Robo2* mouse mutants does not prevent retinal projections to reach the optic

disk, suggesting that other factors are involved in the determination of axon polarity (Thompson et al 2009, Thompson et al 2006b). Two main inhibitory gradients of CSPG (chondroitin sulfate proteoglycans) and Slit2 have been shown to guide RGC processes away from the retinal periphery, where these molecules are enriched (Brittis et al 1992). In combination with molecules exerting a repulsive action, multiple factors, in particular chemokines and cell adhesion molecules, promote centrally directed axonal growth. In zebrafish, down-regulation of the chemokine SDF-1 or its receptor CXCR4 expressed by RGCs leads to mistargeting RGC axons towards cells ectopically expressing SDF-1 within the retinal tissue (Li et al 2005). Optic-disk-directed growth is similarly impaired in chick, fish and rodents upon interference with the function of the cell adhesion molecules L1, NrCAM or BEN (Brittis et al 1995, Ott et al 1998, Weiner et al 2004). Sonic hedgehog (Shh) signaling is also required along the proximal visual pathway to instruct axonal navigation, since the induction of RGC-specific expression of Shh-insensitive Ptc1 (Patched-1) receptor in the mouse retina results in severe impairment of disk-directed growth (Sanchez-Camacho & Bovolenta 2008). In a similar manner, perturbations of Shh function in the chick retina cause disruption of centrally directed orientation of RGC axons. The proper centripetal polarity for RGC axons seems to rely on a tight spatiotemporal control of Shh expression in the ganglion cell layer (GCL). Importantly, this secreted protein is distributed in a dynamic gradient, with its expression domain moving, during early eye development, from the center to the periphery of the retina concomitantly to the RGCs differentiation wave. Once the growing axons of RGCs reach the optic disk, the exit from the eye occurs through a sharp change of direction. The signaling molecule Netrin1, localized at the optic disk glia, which acts on RGCs expressing the DCC (deleted in colorectal carcinoma) receptor, is the main molecular player in this process (Deiner et al 1997). While this protein normally functions as attractant towards RGCs as well as on commissural axons in the spinal cord (Kennedy et al 1994), its high concentration at the level of the optic disk has a repulsive effect on RGC projections driving them out of the eye field. Studies in *Xenopus* have shown that the switch of netrin-mediated attraction into repulsion depends on the decrease of cyclic AMP in the growth cones of RGCs, which in turn is induced by the ECM component laminin-1 present at the retinal surface (Hopker et al 1999) (Figure 2A).

1.2.2 Midline crossing: the optic chiasm and the optic tract

After exiting the eye at the ventral fissure, RGC axons extend towards the midline, where they meet with contralateral axons and form the optic chiasm by crossing over to the opposite side of the ventral diencephalon. Inhibitory signals ensure that RGC projections stay bundled together during midline-directed navigation and midline crossing. Slit/Robo signaling plays a major role in this process. Zebrafish *astray* mutants, carrying loss-of-function mutation in the *robo2* locus, display defasciculation of RGCs bundles at the midline as well as multiple crossings, ectopic projection patterns and ipsilateral targeting (Fricke et al 2001, Hutson & Chien 2002). Robo-expressing RGCs respond to Slit molecules. Slit factors are involved in the patterning of the so-called “glial bridges”, representing the cellular substrates for ingrowing axons across the midline tissue, and have a precise spatial distribution that is regulated by Shh signaling (Barresi et al 2005). The extracellular distribution of Slit ligands is at the same time regulated by heparan sulfate proteoglycans (HSPGs) localized at the cell surface, as genetic interaction of these factors has been shown to be crucial for midline crossing of axons in different model organisms (Inatani et al 2003, Johnson et al 2004) (Figure 2B). In zebrafish, mutant alleles (*boxer* and *dackel*) coding for two components of the exostosin glycotransferase family, respectively Ext1 and Ext2, are involved in the synthesis of HSPGs and result in strong RGCs pathfinding phenotypes in a double mutant genetic background (Lee et al 2004). Additional factors have been shown to be required for the proper formation of the optic chiasm. When the function of No-isthmus (Noi), a transcriptional regulator expressed in the CNS and belonging to the zebrafish Pax family, is disrupted retinal axons bundles from both eyes meet at the midline but fail to extend on the contralateral side thus joining the ipsilateral optic tract (Macdonald et al 1997). A comparable phenotype is observed in FgF8/Ace mutants (Shanmugalingam et al 2000). Importantly, *ace*⁻ exhibits a reduced expression of *noi* at the midline. Therefore, in both mutant fish a failure in differentiation of midline glial cells has been proposed to contribute to RGCs axon pathfinding defects and influence optic chiasm formation (Shanmugalingam et al 2000). Another signaling mechanism playing an important role in RGC axons growth through the optic chiasm is mediated by the interaction between neuropilin-1 (Nrp1) and semaphorin 3 (Sema 3D - Sema 3E) whose disruption leads to axonal stalling or retraction at the midline (Sakai & Halloran 2006). Nrp1 levels are enriched at the growth cone of retinal afferents, due to cAMP-dependent expression, and Sema3D, Sema3E expressed from midline cells would act as permissive factors to allow contralateral crossing (Dell et al 2013). The zebrafish *belladonna* (*bel*) mutation results perhaps in the most striking RGC axonal mistargeting phenotype since all retinal axons fail to cross the midline (Karlstrom et al 1996). An altered expression pattern of Slit molecules, Nrp1 and Sem3D can be detected in *bel* mutant fish, supporting the idea

that a fine spatiotemporal regulation of all these factors ensures optic chiasm formation (Seth et al 2006) (Figure 2B).

1.2.3 The arrival: target recognition and topographic mapping

After midline crossing, RGC axons navigate through the optic tracts towards their main targets in the brain, represented by the SC and LGN in mammals and the OT in other vertebrates. As is along the entire visual pathway, spatial restriction of retinal afferents to the correct trajectory is achieved by the cooperation of multiple signaling mechanisms. In the diencephalon and telencephalon, the expression of inhibitory factors such as Slits (Thompson et al 2006a), Shh (Gordon et al 2010), and CSPGs (Walz et al 2002) keep RGC axonal projections in the optic tract. In the last area of growth towards their targets, retinal axons undergo a process of topographic sorting thereby generating retinotopic maps. These maps are formed such that axons of RGCs located in neighboring positions in the retina convey visual information also to neighboring positions within the retinorecipient nucleus. In the mammalian brain gradients of Ephs and ephrins contribute to topographic targeting of retinal afferents (Triplett & Feldheim 2012) (Figure 2C). In zebrafish, a considerable effort has been directed at unraveling the molecular basis of retinotectal targeting through the isolation of mutations disrupting the normal projection patterns of RGC axons (Baier et al 1996, Karlstrom et al 1996, Trowe et al 1996).

Whereas RGC axons are topographically sorted to represent the two-dimensional aspects of the retina and thus the visual field in the visual brain areas, an additional sorting event determines the targeting of functionally different classes of RGC to distinct retinorecipient nuclei or different laminae within the retinorecipient nuclei. Although several studies have contributed to define precise projection patterns for different classes of RGCs in mouse (Hong et al 2011, Huberman et al 2009, Kim et al 2010, Kim et al 2008) and zebrafish (Nikolaou et al 2012, Robles et al 2014), the mechanisms involved in lamina-specific targeting remain to be clarified.

Being the main subject of this study, the processes leading to the establishment and refinement of synaptic laminae will be discussed in detail in the following chapter.

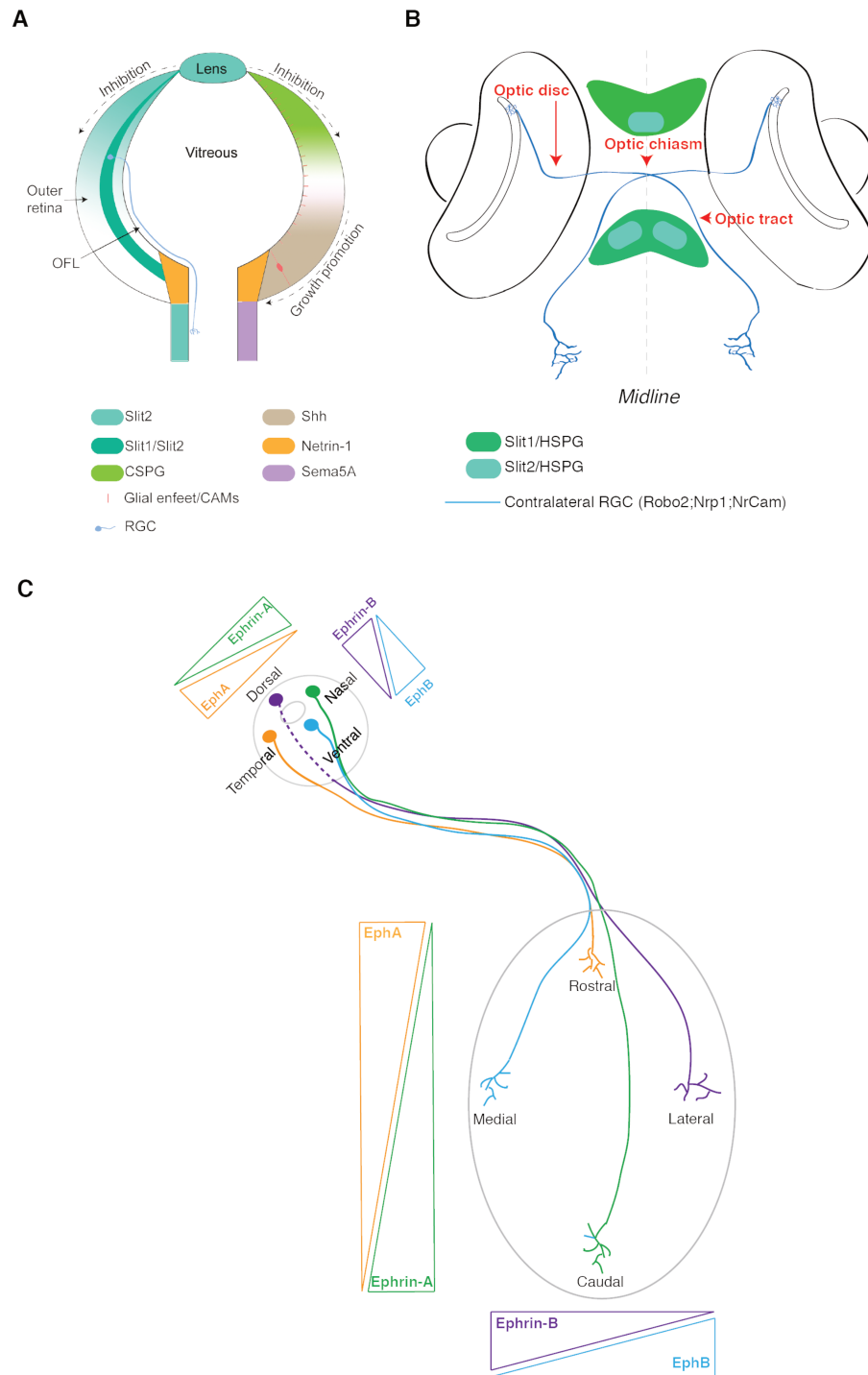


Figure 2. Molecular factors involved in growth and pathfinding of RGC axons from the retina to the retinorecipient nuclei. A) Main signaling molecules involved in intraretinal development and growth of RGC axons towards the optic disk. OFL = optic fiber layer; CSPG = chondroitin sulfate proteoglycans **B)** Expression pattern of key molecules instructing pathfinding of contralateral RGCs axons through the optic chiasm at the midline and the optic tract. HSPG = heparane sulfate proteoglycans **C)** The topographic organization between the retina and the optic tectum (OT)/superior colliculus (SC) is generated by gradients of Eph receptors (EphA and EphB) and ephrin ligands (ephrin-A and ephrin-B) on both projecting RGC axons and their targets. RGCs in the nasal retina project their axons to the caudal part of OT/SC, while RGCs in the temporal retina target the rostral OT/SC. Along the dorsoventral axis, ventral retinal afferents project to the medial OT/SC while dorsal retinal axons project to the lateral OT/SC. Adapted from (Erskine & Herrera 2014).

2. Synaptic lamination in the vertebrate visual system

In visual circuits, axonal and dendritic processes are often clustered in neuropil areas where synaptic contacts are formed between functionally related neurons, giving rise to discrete synaptic laminae (Baier 2013). Synaptic lamination is an evolutionary conserved feature. Indeed, a layered spatial organization is found in the *Drosophila* visual system and shared developmental mechanisms of lamina-specific targeting between flies and vertebrates have been shown (Huberman et al 2010, Sanes & Zipursky 2010). Furthermore, a laminated arrangement of synaptic contacts is a feature of several structures within the visual pathway such as the retina, the OT/SC, LGN and cortex (Sanes & Zipursky 2010). The mostly cell-body-free neuropil laminae represent structural units for the detection of particular features of the visual scene, such as color and motion. The visual information coming from different laminae is conveyed to downstream circuits where is further processed.

In the following paragraphs, I will describe the anatomy and development of synaptic layers in the retina and the optic tectum, as well as models that have been proposed to explain their emergence during evolution and basic molecular mechanisms driving the process of laminar-specific targeting of neuronal process in neuropil areas.

2.1 The inner plexiform layer (IPL)

In the vertebrate retina, the IPL harbors synaptic contacts between three distinct cell populations (ACs, BCs and RGCs), each of them accounting for multiple genetically specified cell types (Siegert et al 2009). The processes of around one hundred different cellular subtypes are clustered in at least ten spatially defined sublaminae (Marc & Cameron 2001, Roska & Werblin 2001) (Figure 3).

In 1953 an observed differential response of RGCs to illumination, depending on the discharge pattern displayed upon stimulation of the cell receptive fields with dark or bright light spots, led to the definition of ON- and OFF-center cells (Kuffler 1953). This characterization paved the ground for following studies that showed a stereotypical dendritic clustering of the two subsets of cells, thus proposing a partitioning of the IPL in distal (the inner half) OFF and proximal (the outer half) ON layers (Famiglietti & Kolb 1976, Nelson et al 1978). Such division is still broadly accepted, even if some exceptions have been reported (Hoshi et al 2009, Odermatt et al 2012). Nevertheless, the division in ON and OFF zones is not sufficient to justify the response of visual circuits to the immense variety of visual features. The subdivision in multiple parallel synaptic sublaminae seems more accurate, with each lamina harboring a microcircuit that

preferentially responds to a specific visual feature such as color or motion (Azeredo da Silveira & Roska 2011, Wassle 2004). To date, a precise and comprehensive pattern of co-stratification between the three cells types (ACs, BCs and RGCs) forming specialized laminar microcircuits in the IPL neuropil has not been described.

2.2 Development of synaptic laminae in the IPL

During early eye development newborn ACs migrate basally towards the future IPL. While the cells initially display a non-directed exuberant neurite outgrowth, subsequently a plexus is formed between the majority of ACs, whose soma is located in the INL, and a reduced number of displaced ACs whose cell body is the GCL. This plexus, composed of neuritic arborization of one AC population directed towards the other, represents a rudimental IPL that, in few hours, acquires a laminated structure. Lamina-specific targeting of neurites extending from the INL-localized ACs is highly precise from the beginning, as the projections do not undergo extensive remodeling (Godinho et al 2005). This suggests the requirement of laminar cues to direct the first steps of IPL formation. Although there is evidence of a transient role of RGCs in IPL lamination pre-patterning (Kay et al 2004) and it has been proposed that displaced ACs can provide initial guidance of INL-localized AC neurites to the proper layer (Godinho et al 2005), it seems that cell-surface cues are also important in this process (Deans et al 2011, Yamagata & Sanes 2012). In zebrafish, AC processes provide a laminar scaffold for ingrowing RGC dendrites which will target five different strata developing in an inside-out fashion with the exception of the fifth and last stratum (Mumm et al 2006). Interestingly, this lamination strategy is not always adopted by single RGCs, which display highly plastic dendritic arborization. The axons of BCs reach the IPL when synaptic contacts between ACs and RGCs processes have already formed (Schroeter et al 2006). In zebrafish and mice, BC processes initially develop along the entire depth of IPL extending branches in multiple sublaminae, and subsequently undergo selective restriction to specific layers (Morgan et al 2006) (Figure 3B).

2.3 The zebrafish larval tectal neuropil

The major retinorecipient area of the fish brain is the OT. The OT functions as the main visual processing center which, in response to visual cues, initiates appropriate motor programs, such as prey capture (Gahtan et al 2005) or looming evoked escape response (Dunn et al 2016, Temizer et al 2015). The zebrafish larval tectum is separated in two regions, a deeper layer, the stratum periventriculare (SPV), containing the cell bodies of radial glia (RG) and periventricular neurons (PVNs) and a superficial neuropil area. The neuropil area harbors synapses between the axons of RGCs, which convey the visual input from the retina to the dendrites of PVNs. PVNs, in turn, transmit the visual information to downstream circuits in premotor areas. The dendrites of superficially located inhibitory interneurons (SINs) also extend in the tectal neuropil (Del Bene et al 2010, Preuss et al 2014).

The tectal neuropil displays a precise pattern of synaptic lamination. Although the analysis of laminar segregation of PVN projections has been carried out in some studies (Nevin et al 2010, Robles et al 2011), a more considerable effort has been directed at analyzing lamina-specific targeting of retinal afferents. RGC axons innervate four main retinorecipient layers in the neuropil of the OT: the most superficial stratum opticum (SO), the stratum fibrosum et griseum superficiale (SFGS), the stratum griseum centrale (SGC), and a deeper layer located at the boundary between the stratum album centrale (SAC) and the stratum periventriculare (SPV) (Figure 3 C). Among these layers, the SO and SFGS layers are targeted by the majority of RGC axons, with a single RGC axon almost always innervating exclusively one tectal layer (Xiao & Baier 2007). An elegant study performed by Robles and colleagues (Robles et al 2013) has taken advantage of the Brainbow multicolor fluorescent labeling method (Livet et al 2007) to analyze the lamina-specific segregation of retinal axon terminals. The examination of the trajectories of differentially labeled RGC axons revealed the presence of ten distinct sublaminae clustered on top of each other, with the SO being composed of two layers and the SFGS of six layers. Another degree of complexity is added to the system by two factors: 1. individual sublaminae can be innervated by multiple RGC classes; 2. RGCs displaying similar dendritic morphology at the level of the IPL exhibit different axonal projection patterns in the tectal neuropil. More than 50 structural RGC types with unique combinations of axonal and dendritic morphologies have been described in a recent study on single-cell lamination patterns in the retinotectal system (Robles et al 2014).

The previous observations suggest that one individual synaptic lamina in the tectal neuropil is characterized by a complex connectivity pattern arising from the combination of different classes of retinal inputs and retinorecipient tectal neurons.

Despite the morphological heterogeneity of pre- and postsynaptic neurons, RGCs and PVNs respectively, that characterize a single lamina, it is becoming clearer from different studies that the synaptic composition of each lamina correlates with precise functional properties. For instance, the analysis of visually evoked calcium signals, used as indirect measure of neuronal activity, in zebrafish larvae has revealed preferential activation of individual retinorecipient sublayers to size (Barker & Baier 2015, Del Bene et al 2010, Preuss et al 2014), orientation and direction of visual stimuli (Gabriel et al 2012, Gebhardt et al 2013, Nikolaou et al 2012).

2.4 Development of laminar arrangement in the tectal neuropil

In zebrafish, the laminar positioning of single RGC axons in the tectal neuropil is precise from early innervation and is not achieved by gradual refinement (Robles et al 2013). Importantly, retinal axons maintain the same laminar position throughout larval development. In fact, although dynamic changes in axonal arbor morphology can be observed during development, they are restricted to the retinotopic position, thus within the plane of a single lamina, and do not lead to changes of axonal targeting between laminae. Moreover, laminar choice of ingrowing RGC processes is not determined by neural activity, since a precise projection pattern can be detected in absence of synaptic transmission (Nevin et al 2008). Together, these observations suggest a model according to which, during early development of the tectal neuropil, RGC axons and PVN dendrites project to precise laminae in an activity-independent manner. Here, a first phase of extensive branching is followed by activity-dependent refinement of the arborization fields (Ben Fredj et al 2010). This last reduction of arbor complexity and refinement of synaptic contacts might lead to a gradual increase over time in responsiveness of the circuit to the visual scene (Smear et al 2007).

In mouse, a different developmental strategy has been shown to regulate lamina-specific targeting of RGC axons to the SC. In this case, axons of certain RGC subtypes are initially more diffusely targeted, across multiple laminae, and subsequently restricted, by pruning, to a single lamina (Cheng et al 2010, Kim et al 2010). Nevertheless, other RGC subtypes directly target the appropriate lamina *ab initio*, as in the fish retinotectal system (Kim et al 2010).

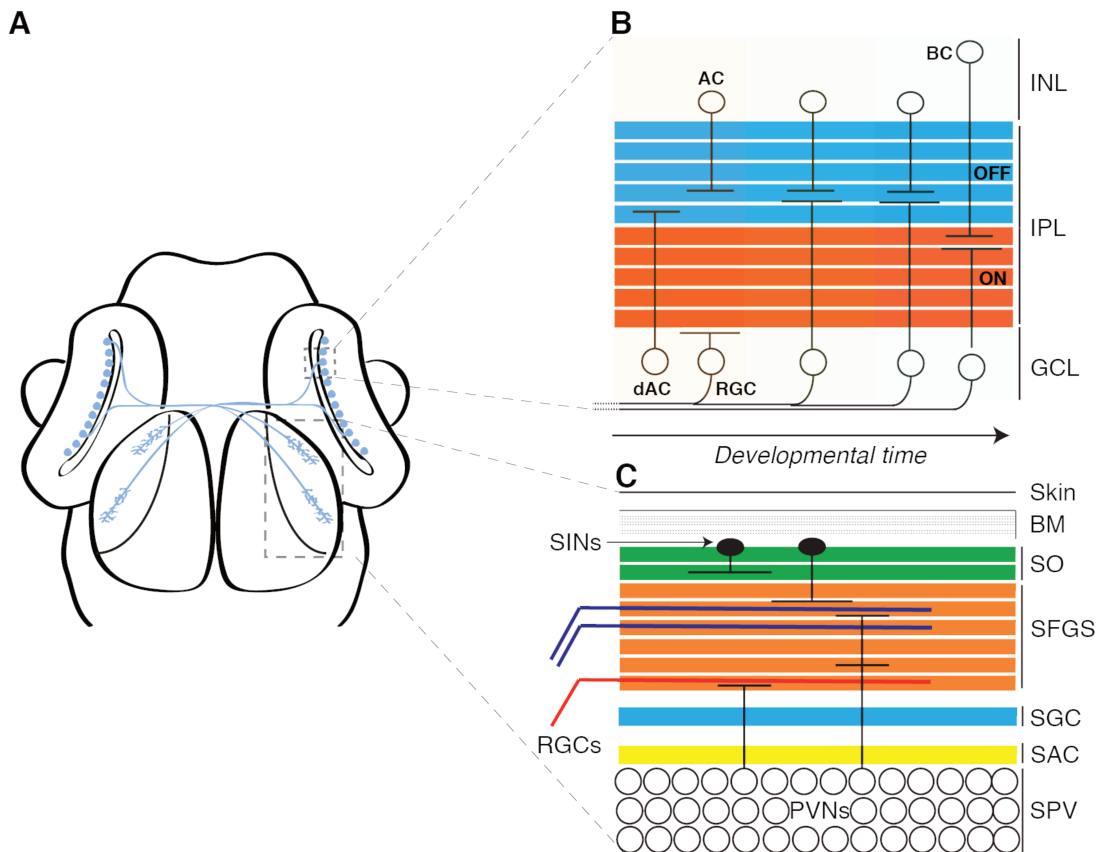


Figure 3. Anatomy and development of the retinal IPL and tectal neuropil.

A) Schematic representation of the zebrafish retinotectal system highlighting the IPL and the tectal neuropil (dashed boxes). **B)** Developmental steps leading to lamination in the zebrafish inner plexiform layer (IPL). Amacrine cells (ACs) and displaced amacrine cells (dACs) are the first cell populations extending their processes in the future OFF and ON strata of the nascent IPL. Subsequently different subtypes of retinal ganglion cells (RGCs) project their dendrites into the IPL forming synaptic contacts with projections of ACs and dACs in approximately ten layers. Later on, BC axons target the stratified IPL. Developmental windows are shown in different colors. **C)** Neuropil of the zebrafish optic tectum. RGC axons navigate from the retina to the optic tectum where they target one of the ten layers of the tectal neuropil. Periventricular neurons (PVNs), whose cell bodies are situated in the deep neuropil, also project their dendrites to the neuropil. A population of interneurons, the SINs, resides in the superficial layers of the neuropil. BM = basement membrane; SO = stratum opticum; SFGS = stratum fibrosum et griseum superficiale; SGC = stratum griseum centrale; SAC = stratum album centrale, SPV = stratum periventriculare. Adapted from (Baier 2013).

2.5 The function of layers in the organization of the visual circuitry

Synaptic laminae represent a fundamental anatomical unit of neural circuits. The laminar spatial arrangement of neural processes in fly, chick, mouse and fish visual systems (Huberman et al 2010) suggests that a selection pressure may have driven the emergence of such stereotyped pattern of organization.

In the next paragraphs, I will discuss two non-mutually exclusive models that offer a possible interpretation of the presence of synaptic laminae in nature.

2.5.1 Wiring economy

The establishment of connections between distant neurons is a costly developmental process. Thus, placement of connected neurons in adjacent areas reduces wiring costs and represents an evolutionary advantage. More than a century ago Santiago Ramon y Cajal observed that “all of the various conformations of the neuron and its various components are simply morphological adaptations governed by laws of conservation for time, space, and material” (Cajal 1899). According to this principle, the wiring economy theory, nervous systems are arranged in those configurations that tend to minimize the wiring length, the cellular material used and the conductance time of nerve impulses.

Several features of the nervous system, such as the shape and size of dendritic and axonal arbors (Chklovskii 2004, Cuntz et al 2010) and topology of neural networks (Bullmore & Sporns 2012), seem to be the result of the wiring economy principle. In the vertebrate visual system, the composition of receptive fields is based on connections between neurons representing adjacent points in the visual field. The length of these connections is minimized by the generation of retinotopic maps, a spatial arrangement where neurons representing partially overlapping parts of the visual field are situated in neighboring areas (Kaas 1997). In the retina, the wiring economy model can explain the spatial segregation of axons and dendrites in the IPL. Such “segregated” arrangement would favor the exclusion of cell bodies from the tightly packed IPL in order to reduce neuropil volume (Rivera-Alba et al 2014). Possibly, wiring minimization may have also driven the evolution of synaptic laminae in the IPL and the neuropil of the OT. Consistently, a neurite targeting a specific lamina can undergo extensively branching on a single plane and contact with several pre- or postsynaptic partners. This would offer a more economical solution in terms of wire lengths if compared to a non-laminar arrangement.

2.5.2 Developmental speed

A recent study on the zebrafish larval retinotectal system suggests that the emergence of synaptic lamination in evolution may have arisen to ensure a rapid assembly of functional neural networks (Nikolaou & Meyer 2015). This study analyzes the impact that the loss of RGCs axonal lamination has on the functional development of direction-selective (DS) circuits whose pre- and postsynaptic inputs are normally confined to superficial retinorecipient laminae of the optic tectum neuropil (Nikolaou et al 2012). To this aim the authors take advantage of the *astray* (*astti272z*) mutant zebrafish (Hutson & Chien 2002), exhibiting aberrant lamina-specific targeting of retinal afferents. This mutant strain lacks functional Robo2, the only Slit1 receptor expressed by RGCs. The disruption of laminated architecture of Robo2-depleted RGC axons may depend on the inability of those to respond to a superficial-to-deep gradient of Slit1 within the tectal neuropil (Xiao et al., 2011). Nikolaou and Meyer (2015) show that the laminar arrangement of not only DS-RGCs axons but also DS-tectal cell dendrites is strongly affected in *astti272z* mutants, suggesting that Slit/Robo signaling provides positional information for both pre- and postsynaptic partners in the developing neuropil. Surprisingly, despite the loss of a laminated architecture, *in vivo* recording of the activity of DS-RGCs and DS-tectal neurons in mutant tecta reveals tuning properties comparable to those detected in wild-type larvae, albeit the establishment of a functional circuit is developmentally delayed. In a series of elegant transplantation experiments where one synaptic partner is mutant for *robo2* while the other expresses the wild-type receptor the authors show that wild-type RGC axons can provide positional information for Robo2 mutant tectal cells dendrites and *vice versa*. In this context, the structural plasticity of Robo2-defective axonal or dendritic projections allows them to target the proper synaptic partner, thereby compensating for the loss of guidance otherwise provided by Robo2. Such structural plasticity at the neuropil level would ensure functional recovery in the *astray* tectum. Nevertheless, the fact that the formation of a functional DS-circuit in the *astray* tectal neuropil is delayed to later stages of development indicates that lamination cues are required for a fast and thus probably more energy efficient assembly of the circuit. According to this hypothesis, the multiple sublaminae in which the tectal neuropil is divided would be pre-patterned before the innervation of RGCs retinal inputs into the tectum. In the case of Slit/Robo signaling, a gradient of Slit1 across the tectal neuropil would bring in spatial proximity RGCs axons and tectal cell dendrites, expressing comparable levels of Robo2. This mechanism would greatly reduce the time required to develop a functional visual system. Importantly, the ability of extracting motor information for a visual scene is crucial to animals to perform behaviors such as prey capture and escape response. Therefore it is fair to assume that the purpose of a rapid circuit assembly may have

exerted evolutionary pressure towards a laminated architecture of the neural circuits operating in the visual system.

2.6 Molecular mechanisms of synaptic laminae formation

The molecular mechanisms underlying the laminar arrangement of synapses in the vertebrate visual system are only beginning to be understood. Pioneer work from Langley (1895) and Sperry (1963) paved the way for the study of synaptic specificity. Their observations suggested the presence of “specific chemical affinities” between synaptic partners. According to this hypothesis, the recognition of the correct target cell would rely on “individual identification tags” displayed by different types of neurons and neuronal processes.

Results from a considerable number of studies support the concept of a combinatorial molecular code for different neuronal types regulating the specificity of synaptic contacts (de Wit & Ghosh 2016). This strategy would allow the cell-type specific expression of cell-surface molecules whose combination would determine a sort of unique molecular tag. Consequently, these cell-recognition molecules would regulate the appropriate laminar targeting of the processes of synaptically connected neurons (Missaire & Hindges 2015). In addition to a cell-type specific molecular code other studies have suggested that several molecules deposited in the extracellular matrix would be responsible for a pre-patterning of the laminar scaffold in neuropil areas (Robles & Baier 2012). Thereby a combination of cell-cell recognition molecules and extracellular cues provide guidance for ingrowing axons and dendrites and directing them to their correct laminar position.

Although other molecules have been shown to play a role in laminar segregation of axons and dendrites, such as transmembrane semaphorins (Matsuoka et al 2011), I will limit myself to the description of the two aforementioned classes of molecular factors.

2.6.1 Cell-cell recognition by cell-adhesion molecules

Studies on the chick retina have unraveled a crucial role for cell adhesion molecules (CAMs) in the establishment of laminar specificity in the IPL. The first identified factors were four closely related transmembrane Ig superfamily (IgSF) adhesion molecules, Dscam, DscamL, Sidekick-1 and 2, expressed by mutually exclusive groups of ACs and RGCs (Yamagata & Sanes 2008, Yamagata et al 2002). Presynaptic and postsynaptic neurons expressing one of these four molecules extend their processes in a specific sublamina of the IPL where they make synaptic contacts. Homophilic interactions between Dscams and Sdks have been proposed to mediate synaptic

partner matching at the level of each lamina. In a more recent study, five additional Ig-related CAMs, the Contactin 1-5 (Cntn1-5), have been shown to contribute to the correct synaptic laminar targeting (Yamagata & Sanes 2012) (Figure 4). These proteins, unlike Dscams and Sdks, might drive laminar specificity, at least in part, through heterophilic interactions with their ligands. This hypothesis is supported by the identification of several transmembrane proteins interacting with Contactins, as the neuron-glia cell adhesion molecule NgCAM, protein tyrosine phosphatases, and the amyloid precursor protein (APP) (Kuhn et al 1991, Kunz et al 1998, Osterfield et al 2008, Pavlou et al 2002, Shimoda & Watanabe 2009, Suter et al 1995, Zuko et al 2011). Some of these display expression in the IPL (Drenhaus et al 2003). Interestingly, loss-of-function studies of Dscam or DscamL1 in the developing mouse retina reveals no alterations in the laminar organization of the IPL, suggesting that the function of Dscams in synaptic adhesion is not conserved in mammals (Fuerst et al 2009).

Other classes of CAMs have been recently shown to regulate not only morphological but also functional connectivity in the mouse and zebrafish visual systems. In the mouse retina, a role for the type II cadherins *Cdh8* and *Cdh9* has been found in laminar targeting of a direction-selective circuit (Duan et al 2014). Two types of retinal bipolar cells (BCs), each expressing a different type II cadherin, extend their processes into different synaptic laminae in IPL. While axons of *Cdh8*-expressing type 2 BCs (BC2s) innervate the outer IPL, those of *Cdh9*-expressing BC5s target the inner IPL. Disruption of either gene in the expressing cell population results in partial perturbation of this arborization pattern, indicating that that *Cdh8* and *Cdh9* act to bias BC axon laminar choice between inner and outer IPL. This observation is further supported by the fact ectopic expression of *Cdh8* in BCs normally expressing *Cdh9* redirects their axons towards the outer IPL and *vice versa*. Interestingly, the introduction of *Cdh8* or *Cdh9* into BCs in *cdh8*^{-/-} or *cdh9*^{-/-} backgrounds still leads to a correct lamina-specific targeting. Since in *cdh8* or *cdh9* mutant mice BCs expressing ectopic cadherins extend their axons in a cadherin-depleted IPL, the last observation suggests that *Cdh8* and *Cdh9* act through heterophilic interaction to instruct laminar choice of BC processes. In zebrafish, a study of Teneurin-3 (*Tenm3*) showed that this cell-adhesive transmembrane protein is required for synaptic targeting of RGCs at both dendritic and axonal level (Antinucci et al 2013). Laminar specificity of RGCs dendrites in the IPL and RGC axons in the tectal neuropil is severely perturbed by knockdown of *Tenm3*. Remarkably, the analysis of RGCs visual response properties reveals strong impairment of a specific functional subtype of RGCs (orientation-selective RGCs) suggesting that Teneurin-3 contributes to the functional wiring of the retinotectal system. These findings have been further supported in a recent report showing that

Tenm3 is in fact responsible for the IPL laminar dendritic targeting of a subtype of ACs co-stratifying with dendrites of orientation-selective RGCs (Antinucci et al 2016).

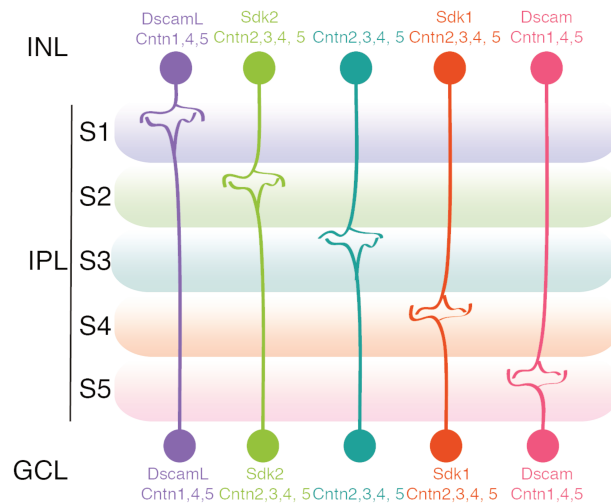


Figure 4. CAMs regulating synaptic targeting in the IPL of the chick retina. Different combinations of cell-surface recognition molecules are expressed by amacrine, bipolar and retinal ganglion cells extending their projections in the IPL. Here, synaptic contacts are formed between neurites of pre- and postsynaptic cells expressing the same isoform combination of Dscams, Sidekicks (Sdk), and Contactins (Cntn). These molecules ensure a precise laminar targeting. INL = inner nuclear layer; GCL = ganglion cell layer. Adapted from (Missaire & Hindges 2015).

2.6.2 Extracellular molecules

a. Layer-specific ECM factors

In fish, mouse and chick, the expression patterns of different ECM proteins, such as Tenascin-R, Tenascin-C, Versican, Ne1 and Reelin, are restricted to specific anatomical layers in retinorecipient nuclei (Table1). Moreover, *in vitro* and *in vivo* experiments show that some of these molecules inhibit RGC axons outgrowth or act as a repulsive cue for retinal afferents (Becker et al 2004, Jiang et al 2009, Perez & Halfter 1994).

Therefore, the spatial distribution of these factors and the interaction with ingrowing RGC axons might suggest that they act at the level of discrete laminae to instruct laminar specificity of retinotectal or retinocollicular projections.

Table 1. List of layer-specific ECM factors

ECM protein	Spatial distribution in retinorecipient layers	References
Versican	In the chick tectum, Versican, belonging to the Chondroitin sulphate proteoglycans (CSPGs) family, displays a gradient of expression from deep-to-superficial in different laminae of the SFGS.	(Yamagata & Sanes 2005)
Reelin	In the mouse superior colliculus (SC), the large secreted protein Reelin is present in most superficial anatomical layers. Reelin-expressing cells can be also observed in the SO of the developing OT in the common brown trout and zebrafish.	(Baba et al 2007, Candal et al 2005, Del Bene et al 2010)
Ne1	In the developing chick tectum, the glycoprotein Ne1 is expressed in four layers (predominantly in one layer at the border between retinorecipient and non-retinorecipient laminae) that are not innervated by RGC axons. Albeit secreted, this protein does not diffuse across several laminae.	(Jiang et al 2009)
Tenascin-R	In the tectum of adult zebrafish this glycoprotein is present in the outermost layer, the stratum marginale (above the SO) and in the deeper layers SAC and SGC. This distribution borders the main retinorecipient laminae of the SO and SFGS that do not display Tenascin-R expression	(Becker et al 2004)
Tenascin-C	In the chick tectum, it is highly concentrated in three laminae of the SFGS (C,E and G). The pattern is complementary to that of ingrowing RGC axons (SFGS B,D and F)	(Yamagata et al 1995)

b. Long-range guidance across multiple laminae

One of the first evidences of a role of ECM in synaptic lamination through the modulation of a guidance cue-receptor signaling in the tectal neuropil has been provided by Xiao et al (2011). In this study, the authors show that Slit1/Robo2 signaling conveys lamina-specific positional information to RGC axons innervating the neuropil of the optic tectum. A loss-of-function of the receptor Robo2, expressed by RGCs, resulted in aberrant layering of retinal afferents. Similar defects were caused by knockdown of the secreted guidance factor Slit1. Interestingly, the same phenotype had been previously observed in the *dragnet* mutant fish deficient for (Col4 α 5), an

ECM component of the basement membrane located at the tectal surface (Xiao & Baier 2007). These observations argued for a link between Slit/Robo signaling and ECM molecules of the basement membrane. Indeed, a direct interaction between Slit1 and Col4 α 5 could be shown. Furthermore, the enrichment of a GFP-tagged version of Slit1 at the tectal surface detected in wild-type tecta was abolished in *dragnet* mutant fish. This result led to the hypothesis that the endogenous Slit1 is distributed in superficial-to-deep gradient within the tectal neuropil and that is bound to the basement membrane through Collagen IV. Such spatial distribution has been proposed to regulate axonal lamination of RGC processes across several synaptic laminae (Figure 5). Tectum-derived Slit would mainly function as a repulsive cue since loss of Slit/Robo signaling biases the targeting of RGC axons towards the tectal surface. Interestingly, a subset of axons meandered towards deeper layers despite the absence of Slit1 indicating that the responsiveness of distinct subsets of RGCs to this guidance factor is differentially regulated (Figure 5). Furthermore, this result also suggests the presence of additional ECM-bound factors to achieve a fine modulation of laminar segregation of axons.

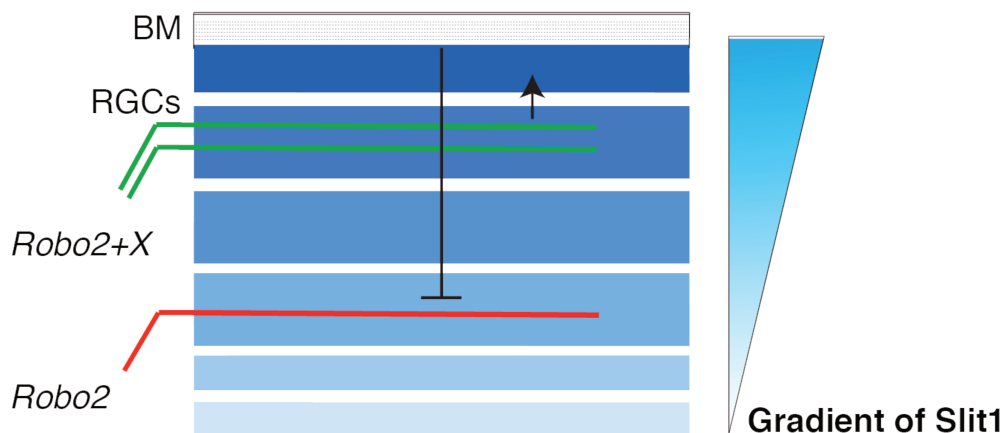


Figure 5. Model of action of Slit1 in the zebrafish tectal neuropil. Slit1 is presumably distributed in a superficial-to-deep gradient in the neuropil of the zebrafish optic tectum. Here, it regulates laminar targeting of Robo2-expressing RGC axons. It acts as long-range repellent for subpopulations of RGCs and attractant for other RGCs types, possibly via an additional co-receptor. BM = basement membrane. RGC = retinal ganglion cell.

3. Reelin: a multifunctional extracellular protein in the CNS

In 1951 a mouse strain carrying a spontaneous autosomal recessive mutation was described for the first time (Falconer 1951). This mutant mouse strain was named *reeler* due to its distinctive reeling gait. During the following decades, several studies contributed to the characterization of abnormal neuroanatomical phenotypes displayed by the *reeler* mouse, among which are inverted cortical lamination, ectopic positioning of neurons and abnormal orientation of cell bodies causing to some extent defects in dendritic and axonal polarity (Goffinet 1979). In this mouse mutant the normal inside-out development of cortex lamination (discussed in detail in the next paragraph), which leads to late-born neurons being continuously localized in more superficial positions than the early-born neurons, is disrupted. Instead, cortical neurons are roughly laminated in an inverted outside-in birth order. In cortical structures of the *reeler* mouse, even though the spatiotemporal patterns of neurogenesis are not affected, migrating neurons do not recognize their appropriate final location therefore fail to form proper cellular layers in various brain areas such as the cerebellum, the hippocampus and the cerebral cortex (Caviness 1976, Mikoshiba et al 1980, Stanfield & Cowan 1979). Multiple experimental evidences accumulated over almost 50 years after the original description of the *reeler* mouse until the discovery of the *reelin* gene indicated an involvement of the protein coded by the disrupted locus in the process of neuronal migration. Indeed, the majority of the studies that followed the identification and cloning of the *reelin* gene in 1995 have focused on the role that the Reelin protein plays in neuronal migration during CNS development (Tissir & Goffinet 2003). The mouse Reelin protein, 3461 amino acids long (D'Arcangelo et al 1995), is a large secreted extracellular matrix (ECM) glycoprotein. It has a modular structure composed of eight repeats, each formed by two sub-repeats (A and B) separated by a central epidermal growth factor (EGF) motif. The N-terminal region comprises a signal peptide required for secretion, a following region with similarity to the extracellular F-spondin (Klar et al 1992) and a unique region displaying an epitope recognized by the commonly used CR-50 monoclonal antibody (Ogawa et al 1995). The short and highly basic C-terminal region of the protein is required for efficient activation of the canonical Reelin signaling (Nakano et al 2007) (Figure6A). A recent comparative study showed that the aminoacidic sequence of the Reelin protein domains is very well conserved across species (Manoharan et al 2015). Sequence analysis across 105 genomes revealed that each repeat presents an average 88% identity to its corresponding repeat in different species. These high similarity values could indicate specific functional roles for each individual domain in the Reelin protein. It is known that, after secretion, the Reelin protein undergoes proteolytic cleavage generating three fragments among which the

central one (composed of the repeats 3 to 6) seems to be sufficient to exert, although at a lesser extent, the function of the full-length protein (Jossin et al 2004).

Nevertheless, to date, a possible function for the different Reelin repeats has not been fully investigated.

3.1 The role of Reelin in mouse cortical development

The function of Reelin has been mainly analyzed in embryonic brain development, since the protein is predominantly expressed in a spatiotemporally restricted fashion during early forebrain patterning (Alcantara et al 1998, Schiffmann et al 1997). Here, Reelin is secreted by the Cajal-Retzius cells, which are located in the superficial marginal zone (MZ) of the cerebral cortex and hippocampus (Ogawa et al 1995). This is a transient cell population that dies 1-2 weeks after birth, corresponding to the time point during development when the establishment of laminated structures in the forebrain is completed. Although Cajal-Retzius cells were described over a century ago, only after the analysis of Reelin expression pattern, their role in neural migration during neocortical development was unraveled. The first phase of the process consists of the formation of the preplate which is composed of the Cajal-Retzius cells and another population of postmitotic neurons, the subplate neurons, above the ventricular zone (VZ) (Marin-Padilla 1998, Super et al 1998). Shortly thereafter, the first cohort of differentiated neurons from the VZ migrate above the subplate and settles beneath the Cajal-Retzius cells. Following waves of newborn neurons will migrate from the VZ towards the preplate, switching from an initial multipolar migration to a directed migration, through the intermediate zone (IZ), along radial glial fibers. When these cortical neurons, displaying a characteristic bipolar morphology, reach the MZ, they undergo a process called “terminal translocation”. In this phase the cell soma detach from the radial fibers and move toward the most superficial layer of the cortical plate, while the leading process remains attached to the MZ, stopping neuronal migration just beneath the MZ (Nadarajah et al 2001, Sekine et al 2011). Since newborn neurons migrate above the older neurons of the subplate and the cortical plate before the placement in the cellular layer located just beneath Cajal-Retzius cells, the resulting laminated structure displays a characteristic “inside-out” pattern. In absence of Reelin, the first group of migrating neurons does not invade the preplate. Therefore, the preplate fails to divide into the marginal zone and the subplate (Ogawa et al 1995, Sheppard & Pearlman 1997). Under these conditions, the following cohorts of migrating newborn neurons are unable to bypass previously generated neurons leading to an abnormal “outside-in” lamination pattern (Figure 6B).

However, a recent in-depth analysis of the *reeler* cortex suggests that the “inverted cortical layering” represents an oversimplification (Wagener et al 2016). In this report, the detailed anatomical characterization enabled by the combination of novel layer-specific molecular markers (Molyneux et al 2007) and suitable transgenic mice (Gerfen et al 2013, Madisen et al 2010) did not reveal an evident cortical inversion despite a severe cellular misplacement.

However, over the years, most of the studies on Reelin have focused on the molecular mechanisms underlying the characteristic cortical inversion and the defective neuronal migration in the *reeler* mouse model. Just recently, an interest towards the role of Reelin in different processes, such as polarization of neural processes or axonal targeting, has arisen. Some of the findings in these fields will be relevant for the interpretation of the results from our first study. Therefore I will introduce them in the next paragraphs.

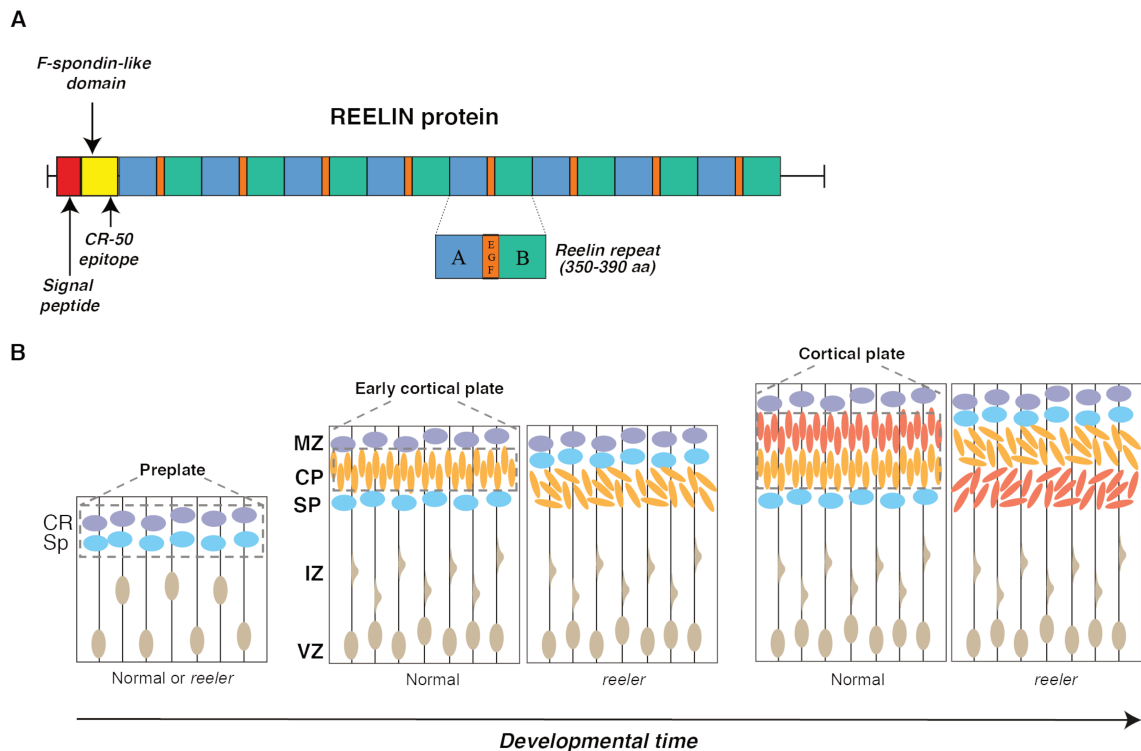


Figure 6. Reelin structure and function in mouse early cortical development.

A) Schematics of the Reelin protein. Reelin is a large secreted ECM protein, consisting of 3461 amino acids (aa). The N-terminus contains a cleavable signal peptide, which is followed by a region of similarity to F-spondin, a protein secreted by floor plate cells regulating cell migration and neurite growth. The downstream sequence contains a stretch of aa recognized by the monoclonal antibody CR-50. This region is followed by a series of eight internal repeats of 350–390 aa, each of them containing two subdomains, A and B, separated by an epidermal growth factor (EGF)-like motif. **B)** Schematics of early cortical development in wild-type and *reeler* mice. At embryonic day (E) 13.5, during the preplate stage (left panel) two cell populations

reside above the ventricular zone (VZ), the Cajal-Retzius (CR) cells, which express Reelin, and subplate (Sp) neurons. At this stage, the *reeler* cortex is indistinguishable from the wild-type counterpart. At E14.5 (central panel), the first cohort of cells migrates along radial glial fibers and passes above the Sp, splitting the preplate into two zones. Preplate splitting does not occur in the *reeler* cortex plate. At E15.5 (right panel), a second cohort of cells migrates through the normal cortical plate and settles superficially, generating a characteristic inside-out lamination pattern. In *reeler* mice, the second cohort of cells settles in deeper layers, forming an outside-in pattern. Adapted from (Rice & Curran 2001, Tissir & Goffinet 2003). MZ: marginal zone; CP: cortical plate; SP: subplate; IZ: intermediate zone; VZ: ventricular zone.

3.2 Modulation of cell polarity by Reelin signaling pathway

Canonical Reelin signal transduction is initiated by the binding of the secreted ECM protein to the transmembrane lipoprotein receptors low-density lipoprotein receptor-related protein 8 (LRP8), also known as apolipoprotein E receptor 2 (ApoER2), or very-low-density lipoprotein receptor (VLDLR) (D'Arcangelo et al 1999, Hiesberger et al 1999). Upon Reelin binding, the receptors cluster and internalize (Strasser et al 2004), thereby inducing the activation of Src-family kinases (SFK) (Arnaud et al 2003), which in turn are responsible for the phosphorylation of the adaptor protein Dab1, the mammalian homolog of *Drosophila Disabled-1* (Howell et al 1997).

A Reelin-induced intracellular cascade, mediated by the phosphorylated Dab1, activates a large number of downstream effectors, many of them regulating, directly or indirectly, the establishment and/or maintenance of neuronal polarity (Figure 7) (Forster 2014).

3.2.1 Leading process determination

In the developing cortex newly generated neurons migrate through the intermediate zone (IZ) towards the forming cortical plate (CP). During the initial migratory phase neurons display a multipolar morphology with many unspecified processes. Later on in development, when migrating neurons reach the emerging CP, they adapt a characteristic bipolar morphology with a *trailing process*, which corresponds to the axon and is oriented toward the ventricular zone (VZ), and a *leading process* oriented toward the MZ. During neuronal differentiation, the selection of the neural process that will develop into an axon requires the localization of the Golgi apparatus at the axon initial segment (Zmuda & Rivas 1998). Following axon specification, the Golgi apparatus translocates from this position to the future leading process at the opposite site of the cell soma (Horton et al 2005). Reelin has been shown to promote a fast translocation of Golgi vesicles to the apical dendrite in neocortical and hippocampal neurons *in vivo* and *in vitro*, with this process being arrested in a *reelin* or *dab1* deficient cortex (Matsuki et al 2010, Meseke et al 2013a, Meseke et al 2013b, Nichols

& Olson 2010, O'Dell et al 2012). Additionally, the exposition of differentiating neurons *in vitro* to an external source of Reelin results in an earlier translocation of the Golgi in the neuronal process closer to the Reelin source (Meseke et al 2013b). Taken together, these observations point towards a possible contribution of Reelin to the selection and determination of the leading process in migrating cortical neurons. According to this putative mechanism of action, in migrating neurons the neurite that is the most proximal to the Reelin-enriched MZ will be in contact with a high Reelin concentration. This neurite will be reached by Golgi vesicles and will be specified into the apical dendrite displaying a surface-directed orientation. Therefore, the spatial distribution of Reelin in the tissue seems to be relevant for a correct mode of migration.

3.2.2 Establishment of neural polarity

The results from various studies indicate that the serine/ threonine-kinase LKB1 an important molecular factor influencing neural polarity (Asada et al 2007). This kinase promotes axon specification in radially migrating neurons (Barnes et al 2007, Shelly et al 2007), as its down-regulation leads to a defective specification of leading and trailing processes resulting in an arrest of migration (Asada et al 2007). These defects are reminiscent of those affecting migrating neurons in the *reeler* mutant (Pinto Lord & Caviness 1979). Additionally, overexpression of the LKB1 complex has been shown to induce the formation of multiple axons from an undifferentiated neurite (Shelly et al 2007), a phenotype that is suppressed by Reelin treatment (Matsuki et al 2010). An indirect regulation of LKB1 function by Reelin could be achieved by crosstalk with the Notch signaling pathway (Artavanis-Tsakonas et al 1999). Notch is a transmembrane receptor that, upon binding of the ligand to the extracellular domain, undergoes proteolytic cleavage and releases the notch intracellular cleaved domain (NICD) (Schweisguth 2004). Very low levels of NICD in the developing cortex of the *reeler* mouse indicate an involvement of Reelin signaling in the activation of Notch 1 (Sibbe et al 2009). Such a role is further supported by the fact that aberrant process orientation in a *reelin* mutant background is rescued by overexpression of NCDI (Hashimoto-Torii et al 2008). Moreover, impaired polarization of neuronal processes is also observed in NCDI-depleted neurons (Hashimoto-Torii et al 2008). Considering that NCDI is capable of activating LKB1 by inducing its phosphorylation (Androutsellis-Theotokis et al 2006), Reelin may control LKB1 via NCDI ensuring proper neuronal polarity development.

3.2.3 Cytoskeletal dynamics

Reelin signaling has been shown to induce the stabilization of the cytoskeleton at the level of the leading process by indirectly regulating the turnover of proteins involved in cytoskeletal dynamics. One of these proteins is the actin depolymerizing factor n-cofilin, whose function is inhibited by phosphorylation at serine residue 3 mediated by LIM Kinase 1 (LIMK1) (Arber et al 1998). During somal translocation, the last phase of radial migration, Reelin activates LIMK1, thus inducing an increase in n-cofilin phosphorylation and subsequent blocking of its actin disassembling function. This signaling mechanism would lead to the stabilization of the leading process resulting in the anchoring to the MZ (Chai et al 2009). Another Reelin-mediated mechanism guaranteeing the stabilization of the leading process is the regulation of the activity of the GTPase Rap, which is responsible for N-cadherin localization at the cell membrane (Franco et al 2011). In addition to these mechanisms, Reelin is also known to interfere with microtubule dynamics. In this case, Reelin signaling enhances the activity of end-binding proteins (EBs), which bind to microtubule plus-ends, thus increasing microtubule assembly (Meseke et al 2013a). Another pathway that allows the Reelin-mediated modulation of microtubule dynamics relies on the binding of the VLDLR receptor to the downstream effector Lis1 (PAFAH1B1) (Assadi et al 2003), which in turn interacts with microtubule-associated proteins Dynein, NudE and Nudel (Assadi et al 2003, McKenney et al 2010).

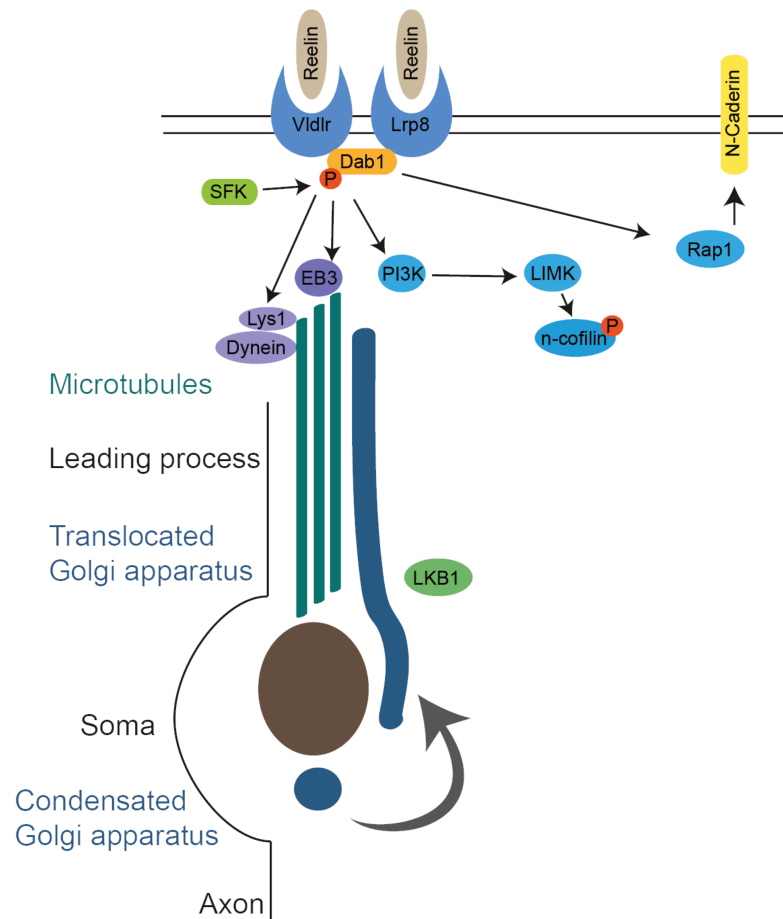


Figure 7. Reelin signaling in neuronal polarization of migrating neurons.

The activity of multiple factors is modulated by Reelin signaling during various processes underlying neuronal migration: neural process orientation (factors are represented in green), microtubule dynamics (factors are represented in violet), leading process stabilization (factors are represented in blue). Adapted from (Forster 2014).

3.3 Role of Reelin in axonal targeting

Only a few studies have highlighted the involvement of Reelin signaling in the development and guidance of axons. Such studies have analyzed the role of the ECM protein in the regulation of axonal targeting in mainly two neural circuits, the entorhinal-hippocampal circuit and the visual system.

3.3.1 Function of Reelin signaling in entorhinal-hippocampal circuit formation

Shortly after the discovery of Reelin, the observation that CR cells were present not only in the MZ of the neocortex but also in the MZ of the hippocampus (HC), suggested that these Reelin-expressing cells could contribute to the establishment enthorinal-hippocampal connections. Indeed, the *reeler* mouse displayed multiple abnormalities at the level of entorhinal cortex (EC) projections innervating distinct target regions of the HP (Borrell et al 1999, Del Rio et al 1997). These defects were mainly the presence of misrouted fibers and the formation of ectopic termination patches. Further analysis performed in *dab1*-deficient mice (*scrambler*) revealed a similar phenotype characterized by entorhinal afferents targeting inappropriate layers in the HC, thus indicating that in this system Reelin could act as guidance factor trough the adaptor Dab1 (Borrell et al 2007). Moreover, experiments based on the use of organotypic co-cultures of combinations of wild-type and mutant EC and HC showed that Dab1 is required in both ingrowing axons and in the target tissue to ensure a normal projection pattern. Interestingly, exposure of entorhinal axons to Reelin increased growth cone collapse and reduced axonal growth. Together the results from these studies suggest that Reelin signaling modulates both targeting and refining of axonal connections at the target site.

3.3.2 Function of Reelin signaling in the establishment of visual circuits

The first evidence of an involvement of Reelin in the regulation of anatomy and function of visual circuits was provided by Rice et al (2001). In this study, the authors showed that Reelin and Dab1 loss-of-function alters the projection patterns rod bipolar cells and type All amacrine cells in the retinal IPL. Subsequent studies focusing on the trajectories of retinal afferents to the SC in the visual system of the *reeler* mouse and Reelin-deficient rat revealed targeting defects in this retino-recipient nucleus (Baba et al 2007, Sakakibara et al 2003). However, an abnormal SC cytoarchitecture in the mutant mouse suggested that the aberrant retinocollicular targeting might be a secondary effect of disorganized neural lamination in the SC, ruling out a direct influence of the Reelin signaling on RGCs axonal trajectories. A different scenario has been observed during the establishment of RGCs projection patterns in the thalamic region of the LGN (Su et al 2011). This retinorecipient nucleus consists of three anatomically and functionally separated subnuclei – the ventral LGN (vLGN), the intergeniculate leaflet (IGL) and the dorsal LGN (dLGN). The vLGN and IGL are reached by projections of non-image-forming intrinsically photosensitive RGCs

(ipRGCs), whereas the dLGN receives input from image-forming RGCs (Figure 8A). Interestingly, a peak of Reelin expression can be detected at the level of vLGN and IGL and not in the dLGN during the developmental stage coinciding with the arrival of RGC afferents. Analysis of the RGCs axonal targeting to LGN subnuclei, in *reeler* and *scambler* mice, reveals misrouted projections of ipRGCs, which fail to target the appropriate partners and innervate other non-retino-recipient thalamic regions (Figure 8B). These observations indicate a role for Reelin signaling in class-specific retinogeniculate targeting. Importantly, the authors show that the synaptic partners of ingrowing RGC axons are not misplaced in the LGN of mutant mice. Therefore, in this case, the mistargeting phenotype is unlikely to arise from lamination defects due to neural mispositioning prior to RGCs innervation, as observed in the SC (Baba et al 2007). On the contrary, similarly to what was observed in the entorhino-hippocampal pathway (Borrell et al 2007), in the retinogeniculate system Reelin functions as molecular cue for the axons of *dab1*-expressing cells.

Interestingly, retinogeniculate projections in compound *vldlr/lrp8* mutants display targeting defects which are substantially different from those observed in the *reeler* and *scambler* mice. This observation suggests that these two receptors might also be involved in retinogeniculate targeting via a Reelin-independent mechanism (Su et al 2013).

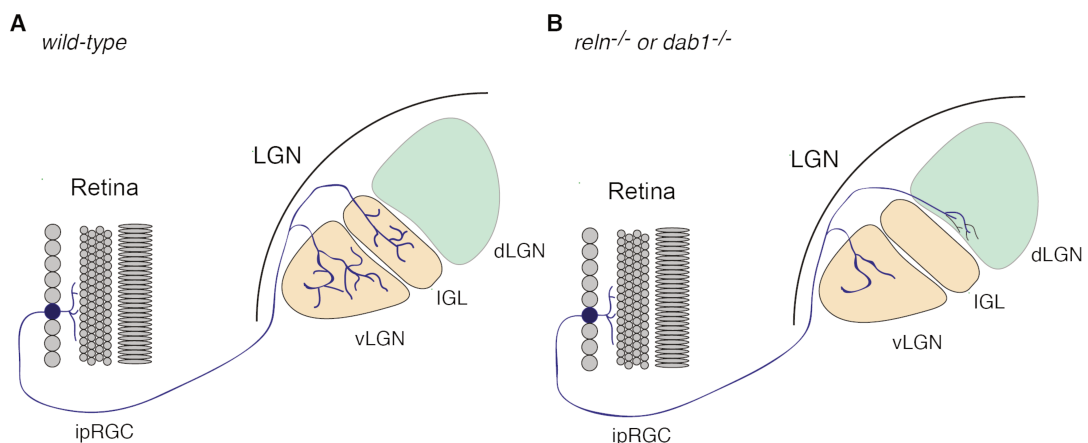


Figure 8. Reelin and Dab1 are required for correct retinogeniculate targeting.

A) Retinogeniculate projections in wild-type mouse. The axons of non-image-forming intrinsically photosensitive RGCs (ipRGCs) target two retinorecipient nuclei of the lateral geniculate nucleus (LGN), the ventral LGN (vLGN) and the intergeniculate leaflet (IGL). **B)** *reeler* (*reln^{-/-}*) and *scambler* (*dab1a^{-/-}*) mutants display a strongly reduced pattern of innervation of the vLGN and IGL. Additionally, ipRGCs are heavily mistargeted to the dLGN and other non-retinorecipient thalamic nuclei.

4. Conditional knock-out in the CRISPR/Cas9 era

Over the last decades the analysis of gene function has relied on mutagenesis approaches leading to the generation of loss-of-function alleles. The TALEN and most importantly the CRISPR/Cas9 systems represent a major step forward towards achieving precise and targeted gene disruption (Doudna & Charpentier 2014, Joung & Sander 2013). Being readily applicable for the creation of knock-out loci in a great variety of animal models used in neuroscience studies, this technology has led to significant advances in the field of developmental and functional neurobiology (Heidenreich & Zhang 2016).

However, constitutive gene disruption is often associated with side effects, as compensation mechanisms and embryonic lethality, representing an important limitation for the analysis of phenotypes specific to the nervous system, since neural circuits are fully established at late stages of development. In recent years, different approaches have pioneered the use of the CRISPR/Cas9 methodology to achieve conditional gene inactivation in worms (Shen et al 2014), fruit fly (Port et al 2014), mouse (Platt et al 2014) and zebrafish (Ablain et al 2015).

In the next paragraphs, I will introduce the basic principles of the CRISPR/Cas9 system and the strategies that have been developed in the last years to achieve conditional gene inactivation by taking advantage of this system.

4.1 The CRISPR/Cas9 system

The CRISPR/Cas (clustered regularly interspaced palindromic repeats/CRISPR-associated) system was discovered in prokaryotes as an adaptive defensive mechanism against the invasion of nucleic acids from exogenous bacteriophages or plasmids (Barrangou et al 2007, Bhaya et al 2011, Garneau et al 2010, Hale et al 2009, Marraffini & Sontheimer 2008). The system is composed of three factors: a small CRISPR RNAs (crRNAs), a *trans*-activating crRNA (tracrRNA) and a nuclease associated with the CRISPR locus (CRISPR associated = Cas). The CRISPR locus contains short palindromic repeats that flank unique spacer sequences. These spacers are generated by the incorporation of foreign nucleic acids into the CRISPR locus after a first infection of the host by an invading pathogen. Such spacers determine target recognition of invading nucleic acids during future infections. They are used as template for the transcription of short RNAs (crRNAs) from the CRISPR locus which will recognize foreign nucleic acid based on Watson-Crick base pairing. Thereafter, a second component, the tracrRNA, is recruited. This crRNA/tracrRNA/DNA complex promotes binding of the Cas nuclease that catalyzes the cleavage of the intruding DNA

(Sashital et al 2012, Wiedenheft et al 2012). Different CRISPR/Cas systems are adopted by prokaryotes. Among these, the type II CRISPR/Cas9 system has been adapted for genome engineering (Makarova et al 2011). The three components of the bacterial system have been reduced to two by fusion of the crRNA and the tracrRNA into a single guide RNA (sgRNA). This sgRNA is composed of a 5' sequence (20 nucleotides) complementary to a chosen target locus and a 3'-placed secondary structure (reminiscent of the tracrRNA) required for the interaction with the Cas9 nuclease. Additionally, the sequence coding for the Cas9 nuclease has been modified to allow efficient activity in eukaryotic cells via codon optimization and addition of nuclear localization signals (Cong et al 2013, Jinek et al 2012). Furthermore the Cas9 enzyme requires a protospacer adjacent motif (PAM), directly adjacent to the sgRNA site, to discriminate between the CRISPR locus and the nucleic acids of the invading pathogen. The Cas9 protein derived from *Streptococcus pyogenes* is the most widely used and requires NGG as PAM sequence for efficient activity (Figure 9).

The artificial system is based on the combined activity a single guide RNA (sgRNA) recognizing the target genomic sequence and the Cas9 endonuclease catalyzing double-strand breaks (DSBs) at the targeted locus. Following DNA cleavage, mutations are induced upon imperfect repair by the nonhomologous end-joining (NHEJ) pathway at the targeted sequence. Therefore a simple replacement within the sgRNA of the 20bp responsible for target site binding allows targeted mutagenesis at any genomic locus of interest.

This versatility of the CRISPR/Cas9 system, combined with a relatively simple molecular design, has contributed to its wide application for reverse genetic approaches and, more in general, for genome editing in a variety of model organisms.

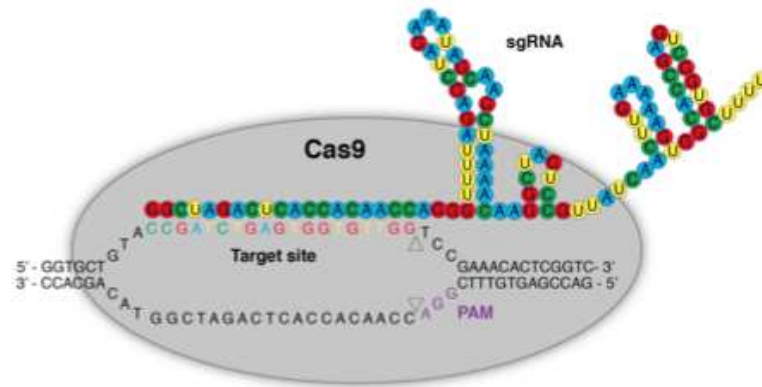


Figure 9. Schematic illustrating sgRNA-mediated recruitment of the *Streptococcus pyogenes* Cas9 endonuclease to a target site. The N-terminal 20bp of the sgRNA hybridize to the DNA target by Watson-Crick base pairing while the rest forms a *trans*-crRNA mimicking the secondary structure to bind the Cas9 enzyme. In purple the NGG protospacer adjacent motif (PAM) just downstream of the hybridizing base pairs. Cas9 introduces a DSB just upstream of this spacer motif. Adapted from (Auer & Del Bene 2014).

4.1.1 Conditional knock-out via knock-in in zebrafish

In recent years, TALEN or CRISPR/Cas9-based approaches have been developed in zebrafish to insert DNA fragments of variable size at defined genomic sites (Auer & Del Bene, 2014). These technologies have broadened the repertoire of genome engineering applications, previously limited to site-specific mutagenesis. Importantly, the ability to insert exogenous sequences at DSB target sites offers the possibility to generate conditional loss-of-function alleles. A first experimental strategy exploring this possibility was introduced by Bedell et al (2012). In this study, the authors co-delivered a high-efficiency TALEN with a single-stranded DNA (ssDNA) carrying left and right homology arms flanking the cutting site. Upon TALEN-mediated induction of the DSB, the ssDNA would serve as a template to “knock-in” at the target locus any sequence is placed between the both homology flanks via homologous directed repair (HDR) mechanism. Using this technique, Bedell et al (2012) were able to introduce loxP sites in the zebrafish genome. The “knock-in” of these sequences, if targeted to the flanking genomic regions of a gene of interest, allows the generation of animals carrying a so-called floxed allele. Cre recombinase catalyzes site-specific recombination of the loxP sites and can be used to excise the floxed target allele (Sauer & Henderson 1988). By crossing transgenic animals carriers of a floxed sequence with transgenic animals in which a tissue-specific promoter drives Cre expression, it is possible to induce the excision of the target locus in the desired cell population (Kuhn et al 1995, Theodosiou & Xu 1998). Since the first demonstration of site-directed integration of exogenous sequences in the fish genome, several CRISPR/Cas9-based methods, potentially

capable of inducing targeted integration events of loxP sites at any genomic locus, have been developed in the zebrafish scientific community (Auer & Del Bene 2014).

The latest advance on the knock-in approaches successfully applied for the generation of floxed alleles has been developed by (Hoshijima et al 2016). In this case, genome-editing events are made traceable by tagging donor sequences with reporter genes, thereby allowing the easy recovery of edited alleles.

Nonetheless, the long generation time of zebrafish transgenic lines carrying stable conditional alleles and challenging homologous recombination-based genomic manipulations represent important constraints for further developments.

4.1.2 Conditional knock-out via tissue-specific Cas9 expression

Recently, an alternative way to achieve tissue-specific inactivation of target genes has been developed by combining the Tol2 transgenesis (Kawakami 2004) and CRISPR/Cas9 technologies (Ablain et al 2015). In this study, the authors propose a modular vector-based system providing cell-type-specific expression of the Cas9 endonuclease and ubiquitous transcription of the sgRNA by a U6 promoter (Mosimann et al 2011). This approach allows induction of conditional gene disruption in chosen cell populations, offering the possibility to analyze the cell-autonomous phenotypes resulting from gene loss-of-function. Furthermore, the integration of the vector in the fish genome via Tol2 transposition permits the generation of stable transgenic animals, displaying specific phenotypes with higher penetrance than in transient experiments (Figure 10). The versatility of the vector system relies on the possibility to readily change the promoter driving Cas9 expression and the sgRNA sequence to target a specific open reading frame (ORF) to achieve spatially restricted gene loss-of-function. A similar approach has been proposed to obtain a tight temporal regulation of Cas9 expression (Yin et al 2015). This methodology is based on the generation of two transgenic lines: one carries a transgene allowing heat-shock induction of Cas9 expression after Cre mRNA injection (*hp70:loxP-mCherry-STOP-loxP-cas9*); the other harbors U6 cassettes for the transcription of sgRNAs (*U6:sgRNA*). Therefore, double carriers would show tissue-specific phenotypes subsequent to heat-shock and Cre activation.

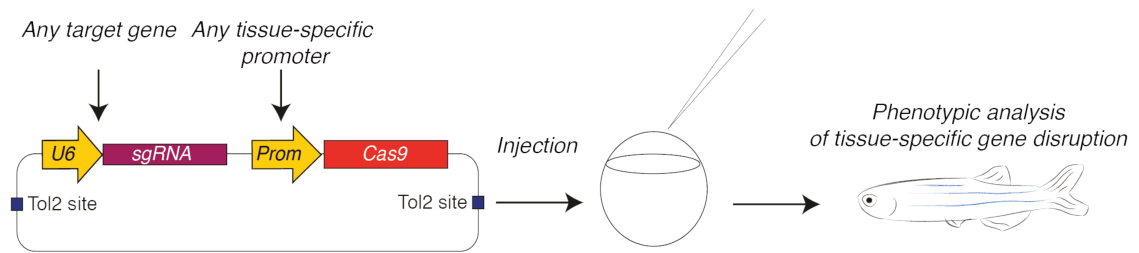


Figure 10. Schematic of a CRISPRs/Cas9-based system for tissue-specific knock-out in zebrafish. The modular vector system allows the cloning of a tissue-specific promoter of choice to induce cell-specific expression of the Cas9 endonuclease. The insertion of the target sequence of the desired locus under the transcriptional control of a ubiquitous promoter (U6) leads to the constitutive expression of the specific sgRNA. Tol2 sites enable stable integration of the vector in the zebrafish genome. Injection at one-cell stage embryos permits the analysis of the phenotypic effects of tissue-specific gene knock-out.

The strategies presented above enable the analysis of the phenotypic effects of gene disruption in a cell population of interest. Importantly, in these previous reports conditional knock-out led to visually distinguishable phenotypes, such as loss of pigmentation (Yin et al 2015) or heart edema (Hoshijima et al 2016). Up to date, there is no method available for the zebrafish community allowing the visualization of cells carrying loss-of-function alleles. This represents an important feature for the direct correlation between genotype and phenotype, needed for an in-depth analysis of gene function.

5. Aim of the study

Aim of the study 1

During the development of the CNS, the secreted Reelin controls the migration and laminar arrangement of neurons in various structures including the neocortex, hippocampus, cerebellum and spinal cord. In the mammalian visual system few studies have addressed its role in axonal targeting. In this study we have taken a combined genetic, molecular biology and *in vivo* imaging approach in the developing zebrafish larvae to investigate the function of Reelin, secreted by a population of superficial interneurons (SINs) residing on the surface of the tectal neuropil, in retinotectal circuit establishment. In particular we tested whether Reelin signaling has a role in the guidance of RGC axons to appropriate retinorecipient synaptic sublaminae. By doing so, we aimed to gain insights into how ECM factors contribute to organize synaptic lamination in the optic tectum and thereby hoped to unravel general mechanisms of neural circuit development.

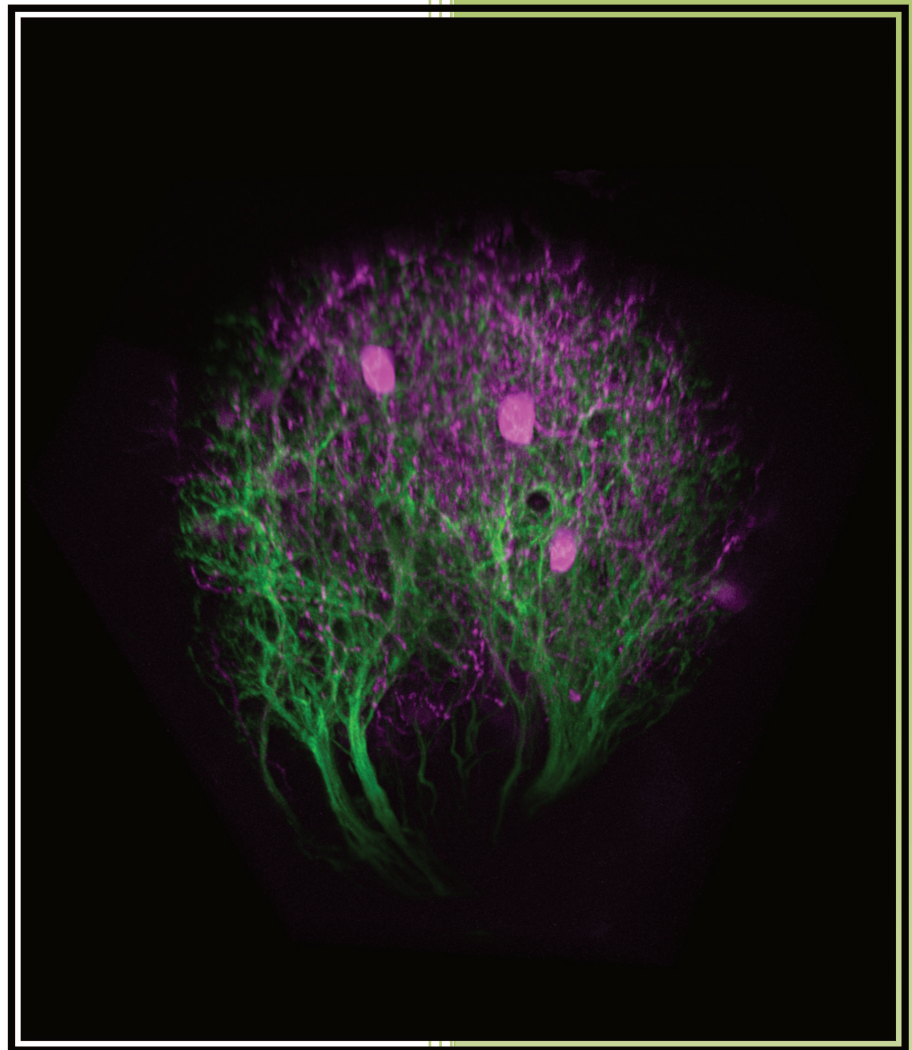
Aim of the study 2

The CRISPR/Cas9 technology has revolutionized reverse genetic approaches in a variety of model organisms including zebrafish. Nevertheless, interference with gene function in a spatiotemporally controlled manner remains challenging. In this study we sought to develop a strategy to enable the analysis of gene inactivation in a cell-type-specific manner. In particular, we explored the possibility to induce simultaneously tissue-specific somatic mutations and genetic labeling of cell clones or single cells, in order to follow mutant cells *in vivo* via reporter gene expression. To this aim, we combined the transgenesis tools available for genetic manipulation of the zebrafish larval visual system and CRISPR/Cas9 genome editing methodology.

Chapter II: Results

Article 1:

“A gradient of Reelin directs axonal lamination in the vertebrate visual system”



1. Summary Article 1

Neuronal connections in the retina as well as in the retino-recipient nuclei are arranged in synaptic laminae. During the last decade, extracellular molecular cues have been shown to play a role in directing lamina-specific targeting of axons and dendrites of synaptically connected neurons (Robles & Baier 2012). The aim of this paper was to investigate the *in vivo* function of the ECM protein Reelin and the downstream effectors of its signaling pathway in the process of axonal targeting and synaptic lamination. We addressed these questions in the context of the zebrafish developing retinotectal system where the axons of RGCs project to precise layers of the optic tectum neuropil.

The main results of the paper are:

- A population of superficial inhibitory interneurons (SINs) located at the surface of the tectal neuropil highly expresses Reelin.
- Reelin is spatially distributed in a superficial-to-deep gradient within the tectal neuropil.
- The gradient distribution requires heparane sulphate proteoglycans (HSPGs), one of the ECM components associated with the basement membrane at the tectal surface.
- RGCs express the receptor VLDLR and the intracellular adaptor protein Dab1a, both factors of Reelin canonical signaling pathway.
- Loss-of-function alleles of *reln*, *vldlr* or *dab1a* genes cause severe disruption of RGC axonal laminar targeting within the tectal neuropil.
- Wild-type RGC axons show aberrant layering in *reln* mutant tecta.
- Induced over-expression of VLDLR receptor in RGC axons biases the laminar choice towards superficial tectal sublaminae.

Altogether our data suggest that:

- The secreted protein Reelin establish a concentration gradient that contributes to the patterning of synaptic laminae in the zebrafish developing tectal neuropil before the arrival of RGC axons.
- Tectum-derived Reelin acts as long-range, presumably attractive, molecular cue to direct laminar-targeting of ingrowing RGC axons that express VLDLR and Dab1a.

In conclusion, our findings elucidate a novel role for the Reelin pathway in the vertebrate visual system development. More importantly, we identified a new extracellular guidance system organizing synaptic lamination in the brain.

A gradient of Reelin directs axonal lamination in the vertebrate visual system

Vincenzo Di Donato ¹, Thomas O. Auer ^{1*}, Flavia De Santis ¹, Karine Duroure ¹, Marine Charpentier ², Filippo Del Bene ¹

1. Institut Curie, PSL Research University, INSERM, U 934, CNRS UMR3215, F-75005, Paris, France. 5. Muséum National d'Histoire naturelle, Paris F-75231, France

2. Muséum National d'Histoire naturelle, INSERM U1154, CNRS UMR 7196, Paris F-75231, France

* Present address: Center for Integrative Genomics, Faculty of Biology and Medicine, University of Lausanne, Lausanne, Switzerland

ABSTRACT

Neural circuit function requires the establishment of precise connections between neurons. Axons and dendrites of functionally related neuronal populations form synapses, which can be spatially organized in discrete layers¹. This is a prominent feature of the vertebrate visual system, where the clustering in synaptic laminae of projections from retinal afferents to retinorecipient areas promotes a rapid establishment of the network². One way to achieve a fast and precise axonal targeting is via the pre-patterning of neuropil layers by extracellular matrix (ECM) proteins and secreted factors, as has been shown for Slit1 and its interaction with collagen IV^{3,4}. With this exception, the signaling network of molecular cues involved in the process of synaptic lamination remains largely unknown. Here, we show that the ECM protein Reelin⁵ imparts lamina-specific positional information to retinal axons through a concentration gradient in the zebrafish optic tectum neuropil. We demonstrate that Reelin secreted by a specific class of tectal superficial inhibitory neurons (SINs)⁶ exerts an attractive role on Retinal Ganglion Cell (RGC) axons via the receptor VLDLR and the Dab1a intracellular transducer. The spatial distribution of Reelin in the tectal neuropil requires heparan sulfate proteoglycans (HSPGs) anchoring of the protein within the ECM. Finally, we disrupt axonal lamination by genetically inducing an ectopic source of Reelin, showing that RGC projections depend on a gradient distribution of Reelin to target a single discrete synaptic layer. Together, our results

demonstrate that the Reelin/VLDLR signaling pathway is required for the formation of a correct axonal lamination pattern during the development of the vertebrate visual system, presumably acting in parallel to Slit1/Robo2.

This study thus provides, to our knowledge, the first *in vivo* proof for synaptic lamination through an endogenous concentration gradient of an ECM-bound molecule and provides a framework for the investigation of mechanisms of neural circuit establishment and maintenance.

INTRODUCTION

The assembly of synapses between functionally connected neurons in discrete neuropil areas is an important evolutionary conserved feature of the central nervous system¹. In these regions, the clustering of dendritic and axonal processes leads to the formation of synaptic layers³. These anatomically organized areas are a prominent feature of the vertebrate visual system⁷. The mechanisms ruling the formation of synaptic laminae as well as the impact that such spatial organization has on the processing of the visual input and the transmission to downstream circuits are poorly understood. Wiring economy has been proposed to justify laminar arrangement of cell bodies in invertebrate neural circuits^{8,9}, and similar principles may act to reduce wiring length in the retina and retinorecipient nuclei³. In the larval zebrafish midbrain, the neuropil of the optic tectum is innervated by the vast majority of the axons of retinal ganglion cells (RGCs)¹⁰. Each RGC displays a precise projection pattern by targeting only one of the multiple sublaminae of the four main layers (from the superficial to the deepest: stratum opticum (SO), stratum fibrosum et griseum superficiale (SFGS), stratum griseum centrale (SGC), stratum album centrale (SAC)) in which the tectal neuropil is divided¹¹. Previous studies suggest that laminar-specific arrangement of retinotectal axons underlies functional specialization of RGCs devoted to the transmission of a related feature of the visual field¹². Nevertheless, when lamination is lost, RGC axons do not fail to connect with the proper synaptic partners, the dendrites of the periventricular neurons (PVNs), but the process is developmentally delayed². This indicates that a layered anatomical organization ensures a rapid assembly of the visual neural microcircuit. Therefore, given that a timely establishment of the retinotectal system depends on the spatially organized targeting of RGC projections at early stages of innervation of the optic tectum, a pre-patterning of the synaptic laminae is most likely required. Extracellular short-range cues have been shown to act on retinal afferents¹³⁻¹⁵ restricting their targeting areas. However, to date, the Slit/Robo pathway is the only extracellular matrix (ECM)-based long-range signaling mechanism that has been shown to provide positional

information for ingrowing RGC axons in the tectal neuropil^{4,16}. The secreted protein Slit1, a known repulsive guidance factor, is presumably distributed in a concentration gradient along the optic tectum being enriched at the tectal surface⁴. Although Slit1 is proposed to have a repellent effect on the projections of RGCs expressing the receptor Robo2, a significant proportion of RGC populations is attracted to the most superficial part of the tectal neuropil. This leads to the hypothesis that an additional pathway might be involved in lamina-specific axonal targeting by forming an opposite gradient repelling axons from deeper layers of the neuropil. Alternatively, an additional long-range cue may work as a complementary gradient to Slit1, attracting RGC axons towards the tectal surface.

RESULTS

Reelin is distributed in a superficial-to-deep gradient within the tectal neuropil

We found that a previously characterized population of inhibitory interneurons, the SInNs⁶, located at the surface of the tectal neuropil (Fig. 1a, b and c) show high expression of the ECM protein Reelin during early zebrafish embryonic development (Fig. 1d, e). In vertebrates, secreted Reelin controls the migration and the laminar arrangement of neuronal cell bodies in several brain structures including neocortex, hippocampus, cerebellum and spinal cord^{5,17-19}. Immunohistochemical analysis on sectioned fish tecta revealed local enrichment of Reelin at the basement membrane near the tectal neuropil surface, progressively decreasing towards the periventricular zone (Fig. 1d-f). Such a spatial distribution indicates that a gradient of Reelin is present along the neuropil.

Tectum-derived Reelin is required for lamina-specific targeting of RGC axons

The concentration gradient of Reelin is detectable starting from 3 days post fertilization (dpf) (Extended data Fig. 1a,b), a developmental stage when the optic tectum is anatomically defined and RGC axons from the contralateral eye start projecting into the tectal neuropil. As laminar innervation of RGCs and tectal expression of Reelin temporally coincide, we explored the hypothesis of an instructive role of tectal Reelin on axonal laminar choice. We generated a loss-of-function allele at the *reelin* locus via transcription activator like nucleases (TALENs)²⁰, resulting in a null mutation as confirmed by the absence of the protein in *reln*^{-/-} fish (Extended data Fig.1 c-e). Genetic labeling of RGC axons by transient expression of *Isl2b:GFP-Caax*,

showed a fully penetrant layering defect phenotype in *reln*^{-/-} 5dpf larvae. Misrouted axons meandering between multiple tectal laminae were observed in every mutant fish (n=13/13) (Fig. 2b) and not in the wild-type siblings (n=0/9) (Fig. 2a). This result is consistent with the aberrant axonal stratification induced by global knock-down of the *reelin* transcript with an antisense splice blocking morpholino (Extended data Fig. 2). To confirm that impairment of Reelin signaling affects specifically the tectal lamination process and not the overall patterning of RGC axons we performed axon tracing by retinal injection of DiO and Dil dyes. Normal retinotopic maps were detected in *reln*^{-/-} fish (Extended data Fig. 3). We next determined whether in the tectum Reelin functions in a cell- or non-cell-autonomous manner to control RGC lamination. For this purpose, we generated chimeric embryos by transplanting green labeled RGCs from *Tg(Brn3C:memGFP)*²¹, wild-type donor fish into *reln*^{-/-} mutant hosts. Transplant-derived RGC axons from wild-type animals exhibited defects in sublaminar segregation when innervating the tectal neuropil of *reln*^{-/-} hosts (n=8/8), while axons from *reln*^{-/-} donor fish transplanted into wild-type hosts displayed normal layering (n=0/11) (Extended data Fig.4). These observations demonstrate that the concentration gradient of Reelin acts as a molecular cue in axon wiring in the tectum in a non-cell-autonomous manner, ruling out the possibility that Reelin expressed at the level of RGCs²² contributes to the laminar targeting.

Reelin directs axonal laminar specificity via VLDLR and Dab1a

In order to define downstream signaling events for Reelin-mediated retinotectal projection patterning, we analyzed the expression of canonical Reelin receptors, very low-density lipoprotein receptor (VLDLR) and low-density lipoprotein receptor-related protein 8 (LRP8), also known as ApoER2²³. Whole mount *in situ* hybridization on zebrafish larvae revealed, at 72 hours post fertilization (hpf), specific signal for VLDLR (Fig. 2c) but not LRP8 (Extended data Fig. 5a) in the RGC population arguing for responsiveness of RGCs to the Reelin pathway via VLDLR. To assess the requirement of VLDLR for precise axonal laminar positioning, we generated a loss-of-function allele of the *vdldr* gene (Extended data Fig. 5c) by CRISPR/Cas9 targeted mutagenesis²⁴. Mosaic labeling of RGCs in *vdldr*^{-/-} fish revealed abnormal axon targeting (Fig. 2d, n=12/12), while no layering defects were observed in wild-type siblings (n=0/11). To further dissect Reelin signaling pathway in RGCs, we focused on the intracellular transducer downstream of VLDLR, Dab1²⁵. RNA expression analysis showed that of the two Dab1 paralog genes present in the zebrafish genome^{26,27} only Dab1a (Fig. 2e) is expressed in the RGC layer of the developing

retina, whereas Dab1b expression is restricted to the amacrine cell (AC) population (Extended data Fig. 5b). Importantly, loss-of-function of *dab1a* induced by CRISPR/Cas9 technology (Extended data Fig. 5d) recapitulates the aberrant layering phenotype observed in *reelin* and *vldlr* mutants, characterized by RGCs axons exhibiting laminar mistargeting in mutant fish (n=9/9) compared to siblings (n=0/10) (Fig. 2f). Altogether these results demonstrate that Reelin and its downstream effectors are critical molecular players in the lamination process of the tectal neuropil.

Reelin functions as a long-range attractive molecular cue for RGC axons

We next examined whether Reelin acts as an attractive or repulsive guidance cue on ingrowing axons. We sought to influence the laminar choice of single RGC axons by increasing the intracellular levels of the Reelin receptor VLDLR. To this aim, we transiently over-expressed a GFP-fused version of VLDLR (*UAS:vldlr-GFP*) or a control membrane bound GFP (*UAS:lyn-GFP*) in a subset of RGCs. Using a stable RFP transgene (*Tg(Isl2b:Gal4;UAS:RFP)*) to label the whole RGC axonal terminals for precise spatial reference, we evaluated the lamina-specific projection pattern of the GFP labeled cells (Fig. 3a, b). While in both conditions, in all embryos analyzed, green fluorescent RGC axons were detected in the SO and SFGS, approximately 65% of *Tg(Isl2b:Gal4;UAS:RFP)* embryos displayed GFP-positive axons in the SGC and 65% in the SAC (the deeper layers) upon expression of the *UAS:lyn-GFP* transgene (n=20 fish analyzed). By contrast, overexpressing *vldlr-GFP* in RGCs led to a significant decrease in the targeting of these deeper layers with about 40% of fish displaying GFP-positive axons at the level of the SGC and only 10% for the SAC (Fig. 3c) (n=20 fish analyzed). The shift of axons highly expressing the *vldlr-GFP* transgene towards more superficial sublaminae at the expense of the deeper ones underlies a preferential targeting of the Reelin-enriched neuropil zone. These data are consistent with an attractive guidance role of Reelin on *vldlr*-expressing RGCs.

Reelin spatial distribution is important for lamina-specific axonal targeting and requires heparane sulphate proteoglycans (HSPGs)

To test whether Reelin distribution in a gradient is necessary for the laminar targeting of RGC axons, we provided an additional source of the Reelin protein from the periventricular zone, anatomically opposite to the SIN location. Expression of a *UAS:relnT2AGFP* transgene in PVNs and Radial Glia cells (Extended data Fig 6) caused a perturbation of retinotectal lamination likely due to interference with the

endogenous Reelin distribution (Fig. 3d, e). We therefore conclude that spatial organization of the ECM protein is crucial for pre-patterning of tectal sublaminae.

We next examined the mechanism of Reelin gradient formation by analyzing the spatial distribution of the Reelin protein in *drg*^{s510} and *dak*^{t0273b} mutant fish^{21,28}. These mutants are known to exhibit striking RGCs layering defects^{4,29} as a result of the deficiency in respectively Collagen IV and HSPGs (heparan sulphate proteoglycans) assembly that disrupts basement membrane integrity. First we checked that Reelin expressing SINS were not changed in number and location in these mutants. Anti-Reelin immunostaining on tectal sections of *drg*^{s510} mutant embryos revealed local enrichment of Reelin at the basement membrane and a gradual decrease towards the PV zone similar to that observed in the wild-type counterparts (Fig. 4 a, b – d, e). In contrast, in *dak*^{t0273b} tecta, no clear surface localization of Reelin could be detected and the gradient distribution of the protein was abolished (Fig. 4 c, f and g). These results argue for a requirement of HSPGs for the superficial accumulation of Reelin. As the guidance factor Slit1 is bound to the basal membrane through Collagen 4a5⁴, the Reelin and Slit pathways may act simultaneously in retinotectal system development but require different ECM components for their gradient formation.

DISCUSSION

Taken together, our data provide experimental evidences for a role of the ECM protein Reelin in the establishment of synaptic laminae in neuropil areas of the vertebrate visual system. An involvement of Reelin signaling in retinogeniculate targeting has been previously reported^{30,31}, however, the process of axonal lamination in the brain of *reeler* mice⁵ has not been investigated. This study shows that an endogenous concentration gradient of Reelin, secreted by the superficial interneurons SINS and stabilized at the basement membrane by HSPGs, allows the pre-patterning of the tectal neuropil in sub-layers. Such layers are precisely targeted by ingrowing RGC axons that may differentially express VLDLR and that therefore respond to different concentrations of Reelin.

Importantly, we demonstrate, for the first time, that Reelin acts as an attractive cue towards RGC axons. These findings support the idea that two extracellular gradients with similar distribution but opposite functions, repellent in the case of Slit1 and attractant in the case of Reelin, are in place to ensure a proper and fast axonal spatial segregation in laminae in the visual system. Giving the widespread expression of these two molecules in various regions of the vertebrate nervous system, it is likely that this represents a conserved patterning mechanism in other regions of the central

system that show lamination and discrete synaptic distribution. From an evolutionary perspective, the pre-patterning of synaptic laminae might be the result of a selective pressure because it ensures a timely circuit assembly by bringing the neurites of pre- and postsynaptic neurons in spatial proximity². An appropriate speed of synaptic contact formation is crucial to perform certain behaviours at appropriate stages of development, such as feeding or escape behaviour for the zebrafish larva. In this contest, our study proposes ECM lamination cues as key factors of a strategy that the developing brain adopts to shape neuropil architecture for the timely establishment of a functional circuit. Although our results refer to the zebrafish retinotectal system, they provide a framework for the analysis of ECM contribution to neural networks assembly in other species or areas of the brain.

Finally, Reelin misexpression has been involved in the molecular pathogenesis of numerous neurodevelopmental disorders such as schizophrenia, bipolar disorder and autism³²⁻³⁴ where impaired neuronal connectivity and synaptic plasticity are observed. This study describes therefore a novel molecular mechanism of Reelin function that could be at the basis of several major human neurological disorders and offers new insights into their pathogenesis.

FIGURE LEGENDS

Figure 1 SINS generate a superficial-to-deep gradient of Reelin within the neuropil of the larval optic tectum. **a-c**, Anatomical localization of SINS and RGC axons in the neuropil of a zebrafish larva. **a**, Schematic representation of a 5 days post-fertilization (dpf) fish larva (lateral view). **b**, Schematic representation of the tectal neuropil region showing the relative positions of different cell populations. SINS: Superficially Inhibitory Neurons (in purple). RGC axons: Retinal Ganglion Cell axons (in green). PVNs: Periventricular Neurons (in white). In yellow: Reelin gradient. **c**, Confocal z-projection lateral view of 5 dpf double transgenic *Tg(s1156tEt;UAS:RFP)*³⁵ x *Tg(Brn3C:mGFP)*²¹ embryo displaying SINS in magenta and RGC axons in green. **d, e**, Transversal sections of a 5 dpf larval tectum showing Reelin spatial distribution. Reelin protein accumulates at the basement membrane (the tectal surface), while the concentration decreases towards the periventricular zone. **d**, Anti-reln (in green) and DAPI (in blue); **e**, anti-reln. **f**, Densitometric plot of anti-reelin signal intensity on 5 different 5dpf tecta.. Data are represented as mean \pm SE. Scale bars = 30 μ m.

Figure 2 Reelin signaling is required for lamina-specific targeting of RGCs axons. **a, b**, Z-projection of confocal images showing mosaic GFP labeling of RGC

axons in wild-type (**a**) and *reln*^{-/-} (**b**) 5dpf live larval fish. Left panels: respective schematics of the targeted tectal laminae. Disruption of the *reln* locus impairs axonal lamination in the tectal neuropil. **c-f**, Expression pattern and loss-of-function analysis of *vdllr* and *dab1a*. **c**, Cross-section of a 3 dpf zebrafish retina shows mRNA expression of *vdllr* in RGC and amacrine cell (AC) populations. **d**, Aberrant layering (arrowheads) of GFP-labeled RGC axon in *vdllr*^{-/-} fish at 5 dpf. **e**, Cross-section of a 3 dpf zebrafish retina shows mRNA expression of *dab1a* in RGCs and ACs. **f**, Aberrant layering (arrowheads) of GFP-labeled RGC axon in *dab1a*^{-/-} mutant larva at 5 dpf. Scale bars = 20 μ m.

Figure 3 Reelin acts as attractive guidance cue on retinal afferents. **a, b**, Lateral view of confocal images projections showing RGC axons at 5 dpf. The entire population of RGCs expresses RFP (magenta) labeling all tectal laminae; GFP (green) is expressed in a mosaic subset of RGCs indicating the transient expression of the control *UAS:lyn-GFP* (**a**) or *UAS:vdllr-GFP* (**b**) transgenes. The box highlights the neuropil area where the most ventral layers SGC and SAC can be easily identified. Higher magnification of the boxed areas shows axonal targeting within these laminae by GFP-positive control cells (**a**) and absence of targeting upon over-expression of *vdllr-GFP* (**b**). **c**, Quantification of the percentage of fish displaying one or more GFP-labeled RGCs in the main layers of the tectal neuropil (*UAS:lyn-GFP* expressing fish analyzed n=20; *UAS:vdllr-GFP* expressing fish analyzed n=20). The superficial laminae SO and SFGS are merged as their close proximity renders their unequivocal discrimination difficult. **d, e**, Interference with the reelin gradient in the tectal neuropil causes aberrant layering of RGC axons. Schematics and projection of confocal images of a control 5dpf *Tg(rlp5bGal4:UAS:GFP)* embryo (**d**) and an embryo overexpressing the *relnT2AGFP* transgene, *Tg(rlp5bGal4:UAS:relnT2AGFP)* (**e**). The Gal4 transcriptional activator drives expression of the GFP or *relnT2AGFP* in a subset of neurons in the periventricular zone (in green). PVNs: periventricular neurons. RG: radial glia cells. **d**, A single RGC axon (magenta) targets a defined lamina of the neuropil. **e**, RFP-positive RGC projections (magenta) meander between multiple laminae, crossing them at multiple locations (white arrowheads). Scale bars = 20 μ m.

Figure 4 Heparan sulphate proteoglycan, but not Collagen IV, is required for binding of reelin to the basement membrane. **a-c**, Spatial distribution of the Reelin protein in wild-type (**a**), *drg*^{s510} (**b**) and *dak*^{10273b} (**c**) fish revealed on cryosectioned tectum of 5dpf larvae by immunohistochemistry with anti-reln (in green) and DAPI (in blue). Scale bar = 30 μ m. **d, f**, Densitometric plots of anti-Reelin signal intensity from the yellow highlighted areas in **a** and **b** or **a** and **c** respectively. Data are represented

as mean \pm SEM calculated on 5 samples. **e, g**, Graphic quantification of relative fluorescence intensities 0 μ m and 30 μ m away from the neuropil surface, derived from **d** and **f** respectively. Error bars represent SEM. (***) *P*-value < 0.001 following Wilcoxon Mann-Whitney test.

Extended data Figure 1 Reelin immunoreactivity in the developing tectal neuropil is abolished in the reelin mutant. a, Cross-section of the tectum showing reelin spatial distribution detected by immunohistochemistry in a 3 dpf wildtype fish larva. Anti-reln (in green) and DAPI (in blue) stainings are shown. **b**, Densitometric plots of anti-Reelin signal intensity from the yellow highlighted area in **a**. **c, d**, Sections of the tectum showing Reelin spatial distribution detected by immunohistochemistry in a 5 dpf wild-type fish larva (**b**, see also Fig 1d) or a *reln*^{-/-} mutant (**c**). **e**, Schematic representation of TALEN-mediated gene disruption at the *reelin* locus. Scale bars = 30 μ m.

Extended data Figure 2 Reelin downregulation by morpholino oligonucleotides causes axonal lamination defects in RGCs. a, b, Z-projections of confocal images showing mosaic GFP labeling of RGC axons in the *BGUG* transgenic line injected with control (**a**) or *reelin* splice blocking morpholino oligonucleotides (**b**). The arrowhead indicates a representative lamination mistake. **c**, Quantification of the percentage of tecta showing normal or altered RGC axon lamination in control (n=0/23) or splice blocking morpholino (n=16/32) injected larvae. **d**, RT-PCR on cDNA extracted from 48dpf larvae injected with Control Morpholino or Splice blocking Morpholino. The presence of an upper band in the Splice blocking Morpholino-injected samples is the consequence of intron retention. The two first lanes show molecular markers.

Extended data Figure 3 Reelin mutant larvae show normal retinotopic organization. a, b, Schematic representation of retinotopic targeting of RGC axons coming from different retina locations (left panels). Injections of the lipophilic dyes Dil and DiO in different quadrants of the contralateral retina (depicted in the left upper panels) show that retinotopic mapping to the optic tectum is not altered in *reelin* mutants (right panels) compared to wild-type embryos (central panels).

Extended data Figure 4 Reelin expression is required in the tectal neuropil and not in RGCs for correct lamina-specific targeting. a-c, Representative pictures of in vivo imaged RGC axons after blastula stage transplants from wild-type donors into a wild-type tectum (**a**), from a wild-type donor into a *reelin* mutant tectum (**b**) or

from *reelin* mutants into a wild-type tectum (c). Donor derived cells are labeled by GFP expression driven by the RGC specific *Tg(Brn3C:mGFP)²¹* transgenic line. Images are projections of confocal image stacks, rotated to best show laminae. Lamination defect could be detected only in wildtype RGC axons where transplanted into a *reelin*-depleted tectum (b). Scale bars = 30mm.

Extended data Figure 5 Components of the Reelin pathway in the visual system

a,b, Expression patterns of *Irp8* and *dab1b* in the developing retina. **a**, Cross-section of a 3 dpf zebrafish retina shows mRNA expression of *Irp8* (**a**) and *dab1b* (**b**) in the AC population but not in RGCs. **c,d**, Schematic representation of CRISPR/Cas9-mediated gene disruptions at the *vldlr* (**c**) and *dab1a* (**d**) genomic loci.

Extended data Figure 6 Ectopic expression of *reelin* in the retinotectal system

a,b, The *Tg(rpl5b:Gal4)* transgenic line drives expression of *UAS:GFP* control or *UAS:relnT2AGFP* in periventricular neurons (PVNs) and radial glia (RG) cells. Sections of the tectum showing reelin spatial distribution and GFP fluorescence detected by immunohistochemistry in 5 dpf fish larvae. **a**, *UAS:GFP* expressing cells in the periventricular zone do not express Reelin. **b**, Reelin protein is present in PVNs and RG cells expressing the *UAS:relnT2AGFP* transgene as shown by co-labeling of Reelin and GFP (right panel). Anti-reln (in magenta), anti-GFP (in green) and DAPI (in blue). Scale bars = 30 μ m.

MATERIALS AND METHODS

DiDo injections

For tracing of axonal projections into the tectal neuropil, 5dpf embryos were fixed in 4% PFA/PBS for 2 hours following injection of the two lipophilic dyes DiO and Dil into opposite quadrants of the contralateral eye as previously described³⁶.

Vibratome sections

Whole-mount embryos were washed twice in 1X PBS/0.1% Tween-20 (PBS-Tw) solution. The samples were embedded in gelatin/albumin with 4% of Glutaraldehyde and sectioned (20 μ m) on a VT1000 S vibrating blade microtome (Leica). Sections were mounted in Fluoromount Aqueous Mounting Medium (Sigma).

Cryosections

Zebrafish larvae at the developmental stage of 3 or 5 dpf were fixed in 4% paraformaldehyde in 1X phosphatebuffered saline (PBS; pH 7.4) for 2h at room temperature and, thereafter, cryoprotected overnight in a 30% sucrose/0.02% sodium azide/PBS solution. Embryos were transferred to plastic molds and embedded in O.C.T. Compound (Sakura Finetech) after removal of the sucrose. Blocks were then frozen at -80°C on dry ice. The 14- μ m sections were mounted on Fisherbrand Superfrost Plus slides (Fisher Scientific).

Immunohistochemistry (IHC)

Tectal cryosections were washed three times in 1X PBS/0.1% Tween-20 (PBS-Tw) solution. For Anti-Reelin IHC antigen retrieval was performed: sections were pretreated with Sodium Citrate buffer (10g sodium citrate, 30mL TX-100 into 1L PBS) for 5 minutes, heated at 75 °C for 15 minutes and subsequently treated with a 1% SDS in PBS solution. Consequently, they were incubated 1 hour at room temperature in 10% Normal Goat Serum (Invitrogen) in PBS-Tw blocking solution followed by overnight incubation, at 4 °C, with 1/200 dilution of mouse Reelin monoclonal antibody Millipore (# MAB5366). The Alexa Fluor 488 secondary antibody goat anti-mouse IgG (Life Technologies) and DAPI (Sigma) were diluted at a final concentration of 1/200 and 1/500 dilution respectively in blocking solution and were added for 2 hours at room temperature. Sections were washed five times in wash buffer (1X PBS/0.1% Tween-20) prior to addition of Vectashield drops for the coverslip placement. Slides were left at room temperature for 1 hour before microscopy analysis. For Anti-GFP IHC no antigen retrieval was performed and 1/500 dilution of chicken primary anti-GFP antibody (Genetex) and Alexa Fluor 488 secondary antibody goat anti-chicken IgG (1/500, Molecular probes) were used.

Microscopy

Imaging of retinal sections following whole mount *in situ* hybridization was performed with a Leica MZ FLIII stereomicroscope (Leica) equipped with a Leica DFC310FX digital camera. A Zeiss LSM 780 confocal microscope (Zeiss) was used for confocal microscopy, employing a 40x water immersion objective. Z-volumes were acquired with a 1- to 2- μ m resolution and images processed using ImageJ, Adobe Photoshop and Adobe Illustrator software. 3D reconstructions of single RGCs axons Z- volumes were done using Imaris. For *in vivo* imaging embryos were anesthetized using 0.02% tricaine (MS-222, Sigma) diluted in egg water and embedded in 1% low melting-point agarose in glass-bottom cell tissue culture dish (Fluorodish, World Precision Instruments, USA).

Image analysis

For the analysis of the gradient images were processed with ImageJ. The fluorescence intensity in the ROI (yellow rectangles areas) was analyzed using the Plot Profile function and normalized to the maximum fluorescence value of the ROI. Analysis was performed on neuropil tissue adjacent to the SINs, excluding cell bodies.

Morpholino knockdown assay

A standard control morpholino oligonucleotide (MO) and a splice-blocking MO (Gene Tools) were injected (4ng) at 1-4 cell stage *Tg(Pou4f3:Gal4;UAS:mGFP)^{s318t}*, otherwise named (*BGUG*)²⁹, transgenic embryos. The sequences were as follows: Standard control MO: 5' - CCT CTT ACC TCA GTT ACA ATT TAT A - 3'; *reln* splice site MO: 5' - CAC AGC TAA AGA GAA CAC ACA TACA - 3'.

TALENs generation

TALENs were assembled by a method derived from as previously described²⁰. For each TALEN subunit, the fragment containing the 16 RVD segment was obtained from single unit plasmids. The assembled TALE repeats were subcloned in a pCS2 vector containing appropriate Δ 152 Nter TALE, +63 Cter TALE and FokI cDNA sequences with the appropriate half-TALE repeat (derived from the original pCS2 vector²⁰).

sgRNAs and Cas9 mRNA generation

sgRNA guide sequences were cloned into the Bsal digested DR274 (Addgene ref 42250) plasmid vector. The sgRNAs were synthesized by *in vitro* transcription (using the Megascript T7 transcription kit, Ambion ref AM1334). After transcription, sgRNAs

were purified using RNAeasy Mini Kit (Quiagen). The quality of purified sgRNAs was checked by electrophoresis on a 2 % agarose gel. Cas9 mRNA was generated as previously described²⁴.

DNA extraction and sequencing for analysis of TALENs and CRISPR/Ca9-mediated mutagenesis

For genomic DNA extraction, pools of 25 5-dpf embryos were digested for 1 h at 55°C in 0.5mL lysis buffer (10 mM Tris, pH 8.0, 10 mM NaCl, 10 mM EDTA, and 2% SDS) with proteinase K (0.17 mg/mL, Roche Diagnostics). To check for frequency of indel mutations, target genomic loci were PCR amplified using Phusion High-Fidelity DNA polymerase (Thermo Scientific). PCR amplicons were subsequently cloned into the pCR-bluntII-TOPO vector (Invitrogen). Plasmid DNA was isolated from single colonies and sent for sequencing. Mutant alleles were identified by comparison with the wild-type sequence.

Genotyping of mutant lines

Genotyping of *reln* mutants was performed as follows : after genomic DNA extraction PCR amplification reactions were conducted in final volumes of 20 µl containing 1x PCR reaction buffer, 1,5mM MgCl₂, 70 ng of gDNA, 0.5 µM of Forward and Reverse primers (fwd : 5'- GTC GTA GAG CGT CCG CGG GTG GCT GAG-3' and rev : 5'- CTC CAC TGC AGG TGT TGC GGA GCG CTG-3'), dNTP (0,2 mM each) and Taq DNA Polymerase (5U/µl) (LifeTechnologies). The gDNA amplification was performed with 30 cycles at the annealing temperature of 68 °C. The PCR amplification product were subsequently digested with BsaHI (NEB) at 37°C for 4-6hours. Digestion reaction was checked on 2 % agarose gel. The wildtype allele results in two fragments of 120bp and 160bp length, respectively. The mutant alleles are not digested and show a band at 280 bp. For genotyping of *vldlr* mutants PCR amplification was performed at the annealing temperature of 60 °C. The Forward and Reverse primers used were : fwd : 5'- ATA GGA ACT CGG ACT ATG ATT GTT TCT - 3' and rev : 5'- CTC GCA TTT GTA TCC TCC TTT AAG ATT -3'. The PCR amplicon was digested with BstNI (NEB) at 60°C for 4-6hours. Digestion reaction was checked on 3 % agarose gel. The wildtype allele results in two fragments of 80 length. The mutant alleles are not digested and show a band at 160 bp. For genotyping of *dab1a* mutants PCR amplification was performed at the annealing temperature of 60 °C. The Forward and Reverse primers used were : fwd : 5'- ATA GGA ACT CGG ACT ATG ATT GTT TCT -3' and rev : 5'- CTC GCA TTT GTA TCC TCC TTT AAG ATT -3'. The PCR amplicon was digested with BclI (NEB) at 37°C for 4-6hours. Digestion reaction was checked on 3 % agarose gel. The wildtype allele results in two fragments of

around 125bp and 140bp band. The mutant alleles show an indigested band at 265 bp. Genotyping of *drg*^{s510} and *dak*^{t0273b} was carried out as previously described^{28,29}.

In situ hybridization

In vitro transcription of Digoxigenin-labeled probes was performed using the RNA Labeling Kit (Roche Diagnostics Corporation) according to manufacturer's instructions. Decorionated embryos at the appropriate developmental stage(s) were fixed in 4% paraformaldehyde in 16 phosphate buffered saline (pH 7.4) for 2 h at room temperature and whole-mount in situ hybridisation was performed as previously described³⁷.

Transplantations

Mutant/wild-type chimeric embryos were generated by blastomere transplantations at the 1000-cell stage as previously described³⁸. Donor RGCs were derived from transgenic *Tg(Brn3C:memGFP)*²¹ *reelin* mutant or wild-type embryos and visualized by the expression of a fluorescent membrane-targeted GFP.

Molecular cloning

The *pIsl2b:Gal4:eGFP-Caax* and *pIsl2b:Gal4:RFP-Caax* constructs were generated by a Gateway reaction (MultiSite Gateway Three-Fragment Vector Construction Kit, ThermoFisher Scientific, Waltham, MA) using the *p5E-Isl2b*³⁹, *pME-eGFP-Caax* or *pME-RFP-Caax*, *p3E-pA* and the *pDest-Tol2;cmlc2:eGFP*⁴⁰ vectors. To generate the *rp15b:Gal4* vector we cloned a 5700 bp promoter fragment of the ribosomal gene *rp15b* in a 5' entry vector and recombined it with a Gal4 middle entry, a polyA 3' entry vector and a Tol2 destination vector⁴⁰. The *pUAS:relnT2AGFP* construct was generated by PCR amplification, Phusion High-Fidelity DNA Polymerase (Thermo Scientific), of two fragments of 5266 bp and 5426 bp respectively from the vector PMM-rIM⁴¹ containing the full-length cDNA of the mouse *reelin*. The T2A sequence was amplified from the *pUAS:Cas9T2AGFP;U6:sgRNA1;U6:sgRNA2*⁴² plasmid and the *lyn-GFP* sequence was amplified from the *cl دنب:lyn-GFP*⁴³ plasmid. The four fragments were inserted into the *pT1UciMP*⁴⁴ plasmid containing 14xUAS with the Gibson Assembly Cloning Kit (New England Biolabs). The *pUAS:lyn-GFP* was generated by amplification of the *lyn-GFP* sequence from the *cl دنب:lyn-GFP*⁴³ plasmid and subsequent cloning into the *pT1UciMP*⁴⁴ plasmid with the Gibson Assembly Cloning Kit. For the generation of the *pUAS:vdrl-GFP* plasmid full cDNA of *vdrl* was PCR amplified from total cDNA of 2dpf zebrafish embryos and the GFP sequence amplified from a *pME-eGFP* plasmid. The two fragments, separated by a short linker

sequence (GGTGGATCTGGT), were cloned into the pT1UciMP⁴⁴ plasmid with the Gibson Assembly Cloning Kit.

cDNA cloning for in situ hybridisation probes

The cDNA fragments of *vldlr*, *lrp8* (*apoer2*), *dab1a* and *dab1b* were amplified by PCR from total cDNA of 3dpf zebrafish embryos using the following primers: *vldlr* : *fw* - GTGAGCAGTCTCAGTTCCAGTGTGG, *rev* - ACTCACAGCAGGGTACGTGTGGCC;
lrp8: *fw* - GCATGTAAGAACGGCCAGTGTGTCC, *rev* - GGGTAGACGTGTCCGATCTGCTCG;
dab1a: *fw* - TCTGTCAGGACTCAATGATGAACT, *rev* - GTCATGTGCATTGAACACAGTGCGA ; *dab1b*: *fw* - GTCAACAGAGGCTGAACCTCAAGC, *rev* - CATGCTGGCGAGGGGGATCAGAC.
 Previously described sequences²² were used for *reelin* cDNA amplification.

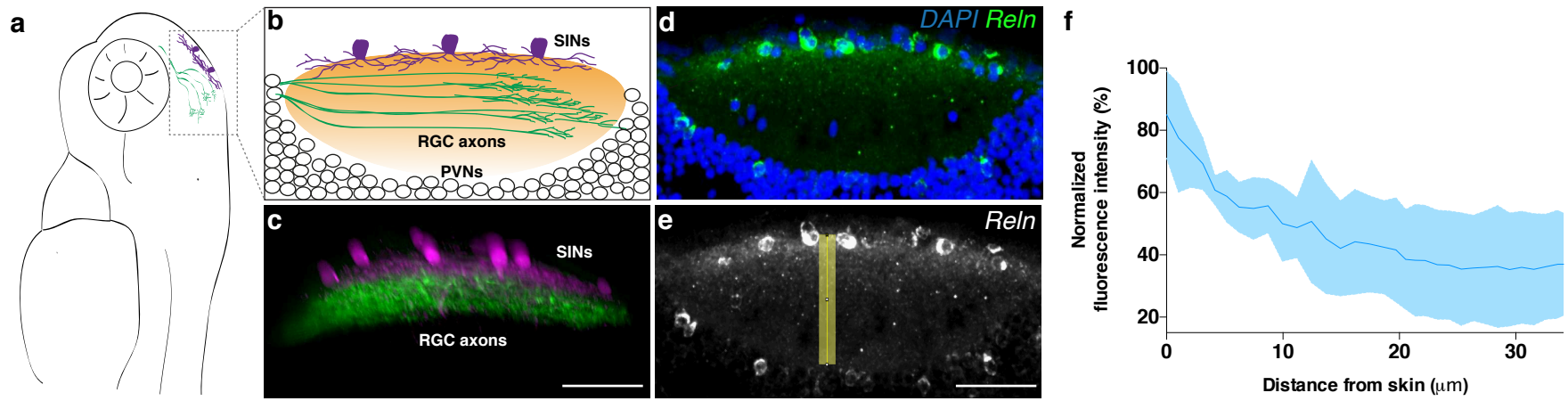
REFERENCES

- 1 Sanes, J. R. & Yamagata, M. Many paths to synaptic specificity. *Annual review of cell and developmental biology* **25**, 161-195, doi:10.1146/annurev.cellbio.24.110707.175402 (2009).
- 2 Nikolaou, N. & Meyer, M. P. Lamination Speeds the Functional Development of Visual Circuits. *Neuron* **88**, 999-1013, doi:10.1016/j.neuron.2015.10.020 (2015).
- 3 Baier, H. Synaptic laminae in the visual system: molecular mechanisms forming layers of perception. *Annual review of cell and developmental biology* **29**, 385-416, doi:10.1146/annurev-cellbio-101011-155748 (2013).
- 4 Xiao, T. *et al.* Assembly of lamina-specific neuronal connections by slit bound to type IV collagen. *Cell* **146**, 164-176, doi:10.1016/j.cell.2011.06.016 (2011).
- 5 D'Arcangelo, G. *et al.* A protein related to extracellular matrix proteins deleted in the mouse mutant reeler. *Nature* **374**, 719-723, doi:10.1038/374719a0 (1995).
- 6 Del Bene, F. *et al.* Filtering of visual information in the tectum by an identified neural circuit. *Science* **330**, 669-673, doi:10.1126/science.1192949 (2010).
- 7 Sanes, J. R. & Zipursky, S. L. Design principles of insect and vertebrate visual systems. *Neuron* **66**, 15-36, doi:10.1016/j.neuron.2010.01.018 (2010).
- 8 Rivera-Alba, M. *et al.* Wiring economy and volume exclusion determine neuronal placement in the Drosophila brain. *Current biology : CB* **21**, 2000-2005, doi:10.1016/j.cub.2011.10.022 (2011).
- 9 Perez-Escudero, A. & de Polavieja, G. G. Optimally wired subnetwork determines neuroanatomy of *Caenorhabditis elegans*. *Proceedings of the National Academy of Sciences of the United States of America* **104**, 17180-17185, doi:10.1073/pnas.0703183104 (2007).
- 10 Robles, E., Laurell, E. & Baier, H. The retinal projectome reveals brain-area-specific visual representations generated by ganglion cell diversity. *Current biology : CB* **24**, 2085-2096, doi:10.1016/j.cub.2014.07.080 (2014).
- 11 Robles, E., Filosa, A. & Baier, H. Precise lamination of retinal axons generates multiple parallel input pathways in the tectum. *The Journal of neuroscience : the official journal of the Society for Neuroscience* **33**, 5027-5039, doi:10.1523/JNEUROSCI.4990-12.2013 (2013).
- 12 Nikolaou, N. *et al.* Parametric functional maps of visual inputs to the tectum. *Neuron* **76**, 317-324, doi:10.1016/j.neuron.2012.08.040 (2012).
- 13 Inoue, A. & Sanes, J. R. Lamina-specific connectivity in the brain: regulation by N-cadherin, neurotrophins, and glycoconjugates. *Science* **276**, 1428-1431 (1997).
- 14 Becker, C. G., Schweitzer, J., Feldner, J., Becker, T. & Schachner, M. Tenascin-R as a repellent guidance molecule for developing optic axons in zebrafish. *The Journal of neuroscience : the official journal of the Society for Neuroscience* **23**, 6232-6237 (2003).

- 15 Jiang, Y. *et al.* In vitro guidance of retinal axons by a tectal lamina-specific glycoprotein Nel. *Molecular and cellular neurosciences* **41**, 113-119, doi:10.1016/j.mcn.2009.02.006 (2009).
- 16 Robles, E. & Baier, H. Assembly of synaptic laminae by axon guidance molecules. *Current opinion in neurobiology* **22**, 799-804, doi:10.1016/j.conb.2012.04.014 (2012).
- 17 Vaswani, A. R. & Blaess, S. Reelin Signaling in the Migration of Ventral Brain Stem and Spinal Cord Neurons. *Frontiers in cellular neuroscience* **10**, 62, doi:10.3389/fncel.2016.00062 (2016).
- 18 Borrell, V. *et al.* Reelin and mDab1 regulate the development of hippocampal connections. *Molecular and cellular neurosciences* **36**, 158-173, doi:10.1016/j.mcn.2007.06.006 (2007).
- 19 Sekine, K., Kubo, K. & Nakajima, K. How does Reelin control neuronal migration and layer formation in the developing mammalian neocortex? *Neuroscience research* **86**, 50-58, doi:10.1016/j.neures.2014.06.004 (2014).
- 20 Huang, P. *et al.* Heritable gene targeting in zebrafish using customized TALENs. *Nature biotechnology* **29**, 699-700, doi:10.1038/nbt.1939 (2011).
- 21 Xiao, T., Roeser, T., Staub, W. & Baier, H. A GFP-based genetic screen reveals mutations that disrupt the architecture of the zebrafish retinotectal projection. *Development* **132**, 2955-2967, doi:10.1242/dev.01861 (2005).
- 22 Costagli, A., Kapsimali, M., Wilson, S. W. & Mione, M. Conserved and divergent patterns of Reelin expression in the zebrafish central nervous system. *The Journal of comparative neurology* **450**, 73-93, doi:10.1002/cne.10292 (2002).
- 23 Hiesberger, T. *et al.* Direct binding of Reelin to VLDL receptor and ApoE receptor 2 induces tyrosine phosphorylation of disabled-1 and modulates tau phosphorylation. *Neuron* **24**, 481-489 (1999).
- 24 Hwang, W. Y. *et al.* Heritable and precise zebrafish genome editing using a CRISPR-Cas system. *PLoS one* **8**, e68708, doi:10.1371/journal.pone.0068708 (2013).
- 25 Howell, B. W., Gertler, F. B. & Cooper, J. A. Mouse disabled (mDab1): a Src binding protein implicated in neuronal development. *The EMBO journal* **16**, 121-132, doi:10.1093/emboj/16.1.121 (1997).
- 26 Imai, H. *et al.* Dynamic changes in the gene expression of zebrafish Reelin receptors during embryogenesis and hatching period. *Dev Growth Differ* **54**, 253-263, doi:10.1111/j.1440-169X.2012.01327.x (2012).
- 27 Herrero-Turrion, M. J., Velasco, A., Arevalo, R., Aijon, J. & Lara, J. M. Characterisation and differential expression during development of a duplicate Disabled-1 (Dab1) gene from zebrafish. *Comparative biochemistry and physiology. Part B, Biochemistry & molecular biology* **155**, 217-229, doi:10.1016/j.cbpb.2009.11.003 (2010).
- 28 Lee, J. S. *et al.* Axon sorting in the optic tract requires HSPG synthesis by ext2 (dackel) and extl3 (boxer). *Neuron* **44**, 947-960, doi:10.1016/j.neuron.2004.11.029 (2004).
- 29 Xiao, T. & Baier, H. Lamina-specific axonal projections in the zebrafish tectum require the type IV collagen Dragnet. *Nature neuroscience* **10**, 1529-1537, doi:10.1038/nn2002 (2007).

- 30 Su, J. *et al.* Reelin is required for class-specific retinogeniculate targeting. *The Journal of neuroscience : the official journal of the Society for Neuroscience* **31**, 575-586, doi:10.1523/JNEUROSCI.4227-10.2011 (2011).
- 31 Su, J., Klemm, M. A., Josephson, A. M. & Fox, M. A. Contributions of VLDLR and LRP8 in the establishment of retinogeniculate projections. *Neural development* **8**, 11, doi:10.1186/1749-8104-8-11 (2013).
- 32 Folsom, T. D. & Fatemi, S. H. The involvement of Reelin in neurodevelopmental disorders. *Neuropharmacology* **68**, 122-135, doi:10.1016/j.neuropharm.2012.08.015 (2013).
- 33 Lammert, D. B. & Howell, B. W. RELN Mutations in Autism Spectrum Disorder. *Front Cell Neurosci* **10**, 84, doi:10.3389/fncel.2016.00084 (2016).
- 34 Guidotti, A., Grayson, D. R. & Caruncho, H. J. Epigenetic RELN Dysfunction in Schizophrenia and Related Neuropsychiatric Disorders. *Front Cell Neurosci* **10**, 89, doi:10.3389/fncel.2016.00089 (2016).
- 35 Scott, E. K. & Baier, H. The cellular architecture of the larval zebrafish tectum, as revealed by gal4 enhancer trap lines. *Frontiers in neural circuits* **3**, 13, doi:10.3389/neuro.04.013.2009 (2009).
- 36 Baier, H. *et al.* Genetic dissection of the retinotectal projection. *Development* **123**, 415-425 (1996).
- 37 Thisse, C. & Thisse, B. High-resolution in situ hybridization to whole-mount zebrafish embryos. *Nature protocols* **3**, 59-69, doi:10.1038/nprot.2007.514 (2008).
- 38 Gosse, N. J., Nevin, L. M. & Baier, H. Retinotopic order in the absence of axon competition. *Nature* **452**, 892-895, doi:10.1038/nature06816 (2008).
- 39 Ben Fredj, N. *et al.* Synaptic activity and activity-dependent competition regulates axon arbor maturation, growth arrest, and territory in the retinotectal projection. *The Journal of neuroscience : the official journal of the Society for Neuroscience* **30**, 10939-10951, doi:10.1523/JNEUROSCI.1556-10.2010 (2010).
- 40 Kwan, K. M. *et al.* The Tol2kit: a multisite gateway-based construction kit for Tol2 transposon transgenesis constructs. *Developmental dynamics : an official publication of the American Association of Anatomists* **236**, 3088-3099, doi:10.1002/dvdy.21343 (2007).
- 41 Pujadas, L. *et al.* Reelin regulates postnatal neurogenesis and enhances spine hypertrophy and long-term potentiation. *The Journal of neuroscience : the official journal of the Society for Neuroscience* **30**, 4636-4649, doi:10.1523/JNEUROSCI.5284-09.2010 (2010).
- 42 Di Donato, V. *et al.* 2C-Cas9: a versatile tool for clonal analysis of gene function. *Genome research* **26**, 681-692, doi:10.1101/gr.196170.115 (2016).
- 43 Dona, E. *et al.* Directional tissue migration through a self-generated chemokine gradient. *Nature* **503**, 285-289, doi:10.1038/nature12635 (2013).
- 44 Horstick, E. J. *et al.* Increased functional protein expression using nucleotide sequence features enriched in highly expressed genes in zebrafish. *Nucleic acids research* **43**, e48, doi:10.1093/nar/gkv035 (2015).

Figure 1



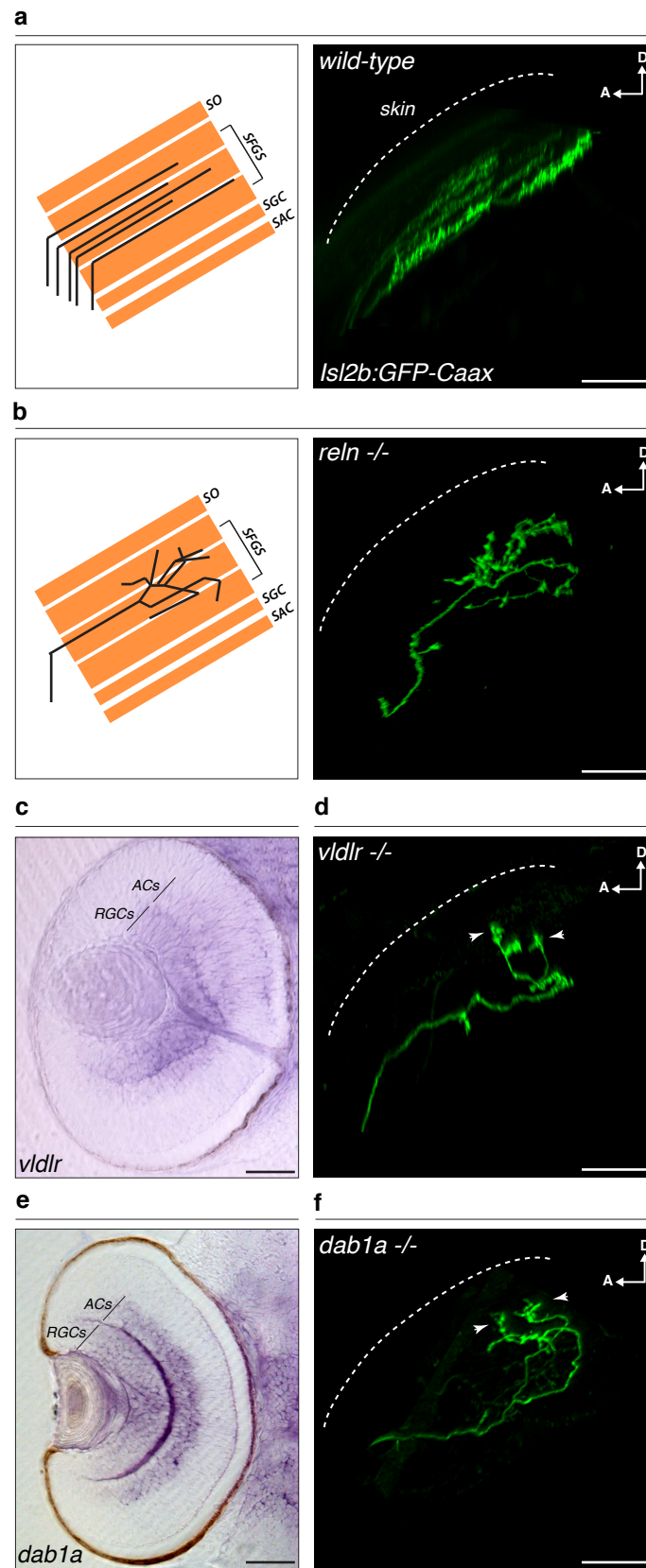
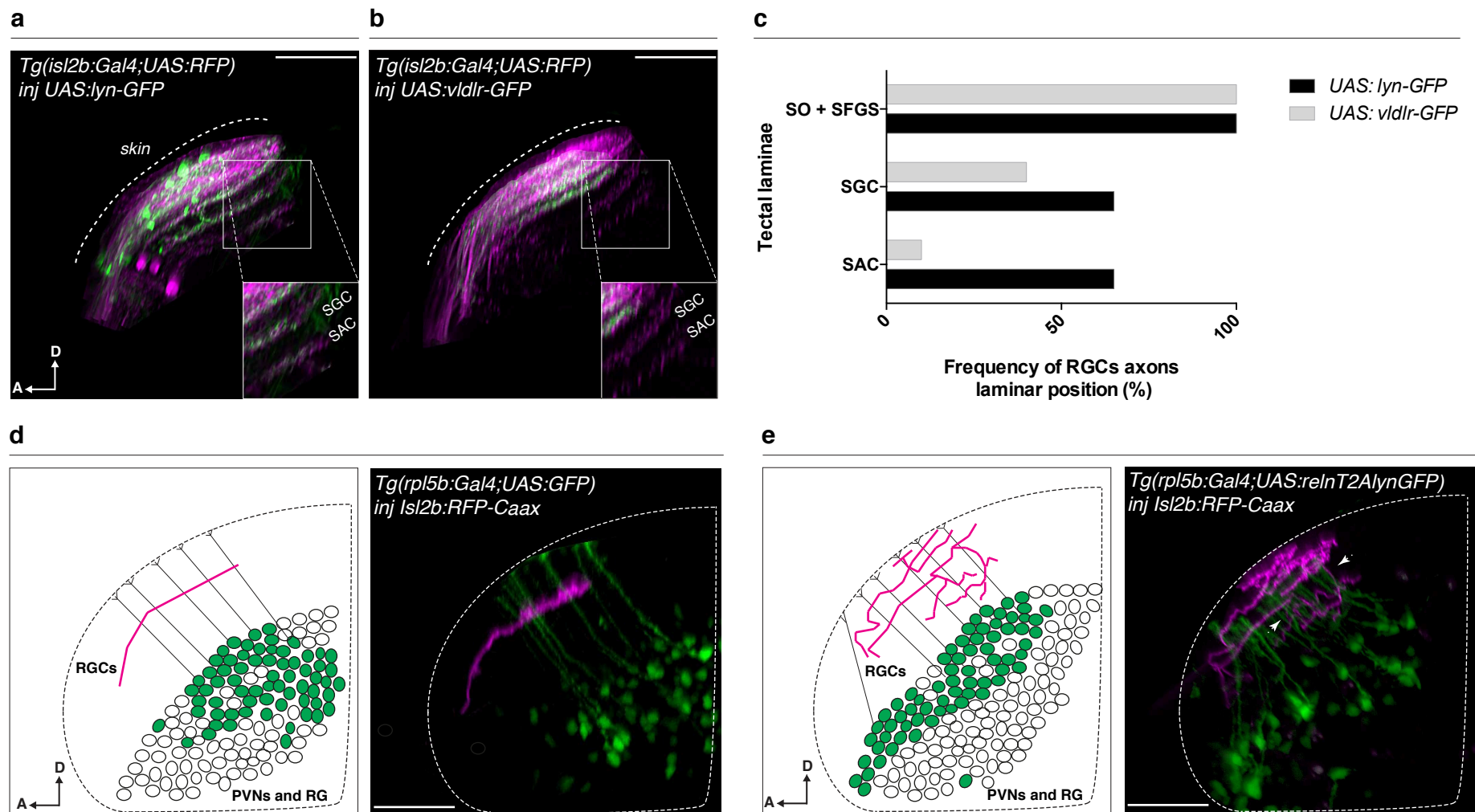


Figure 2

Figure 3



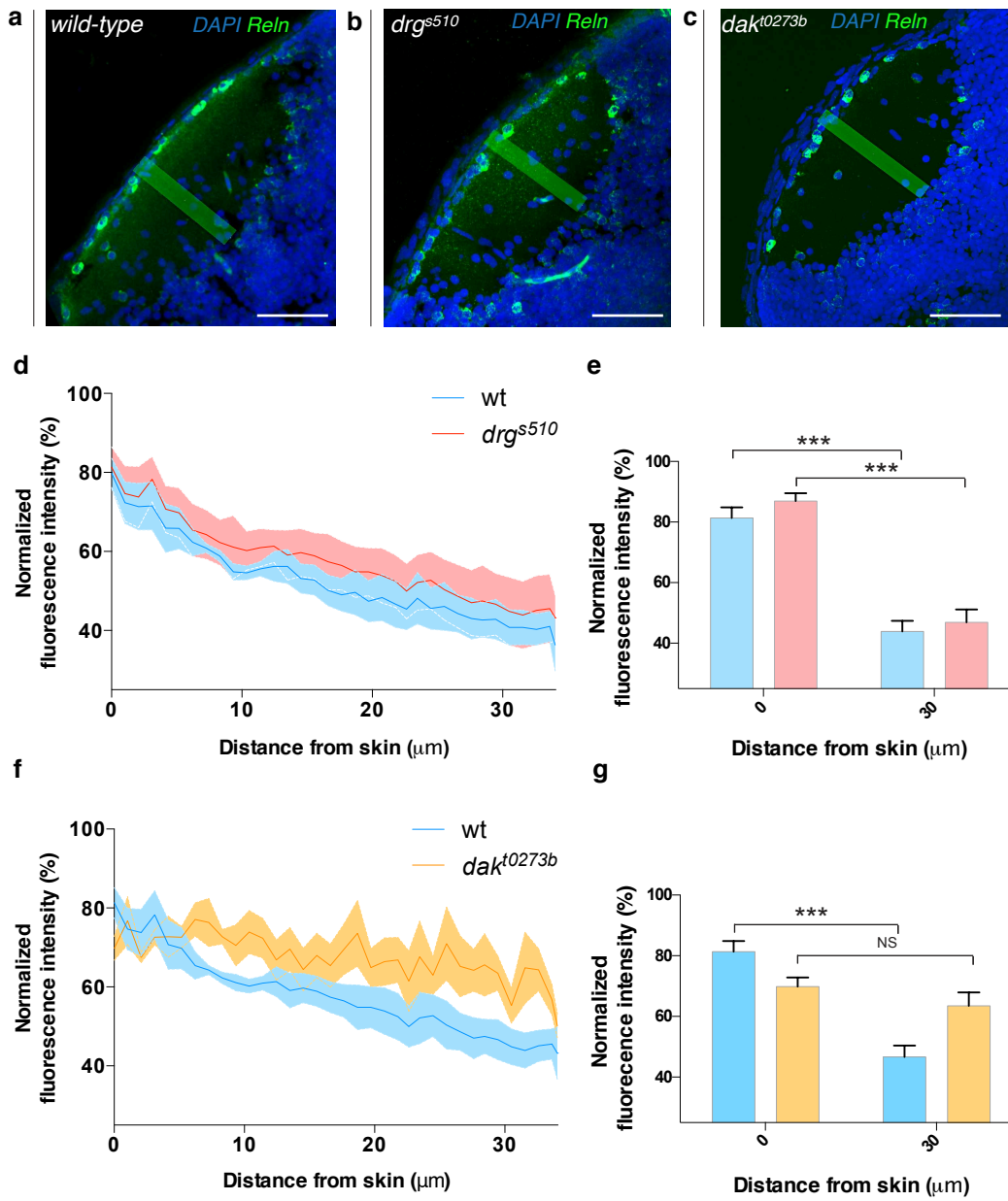
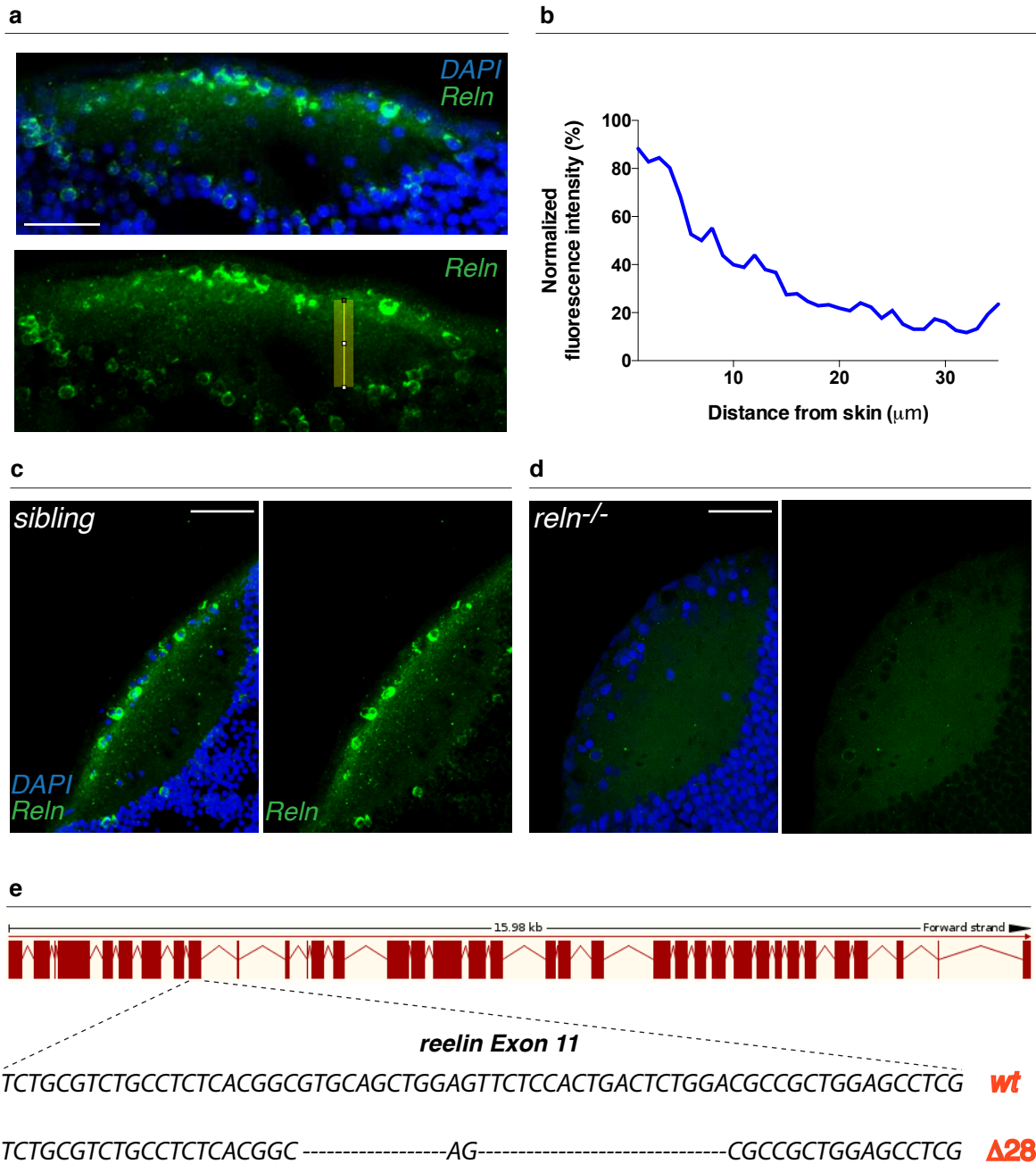
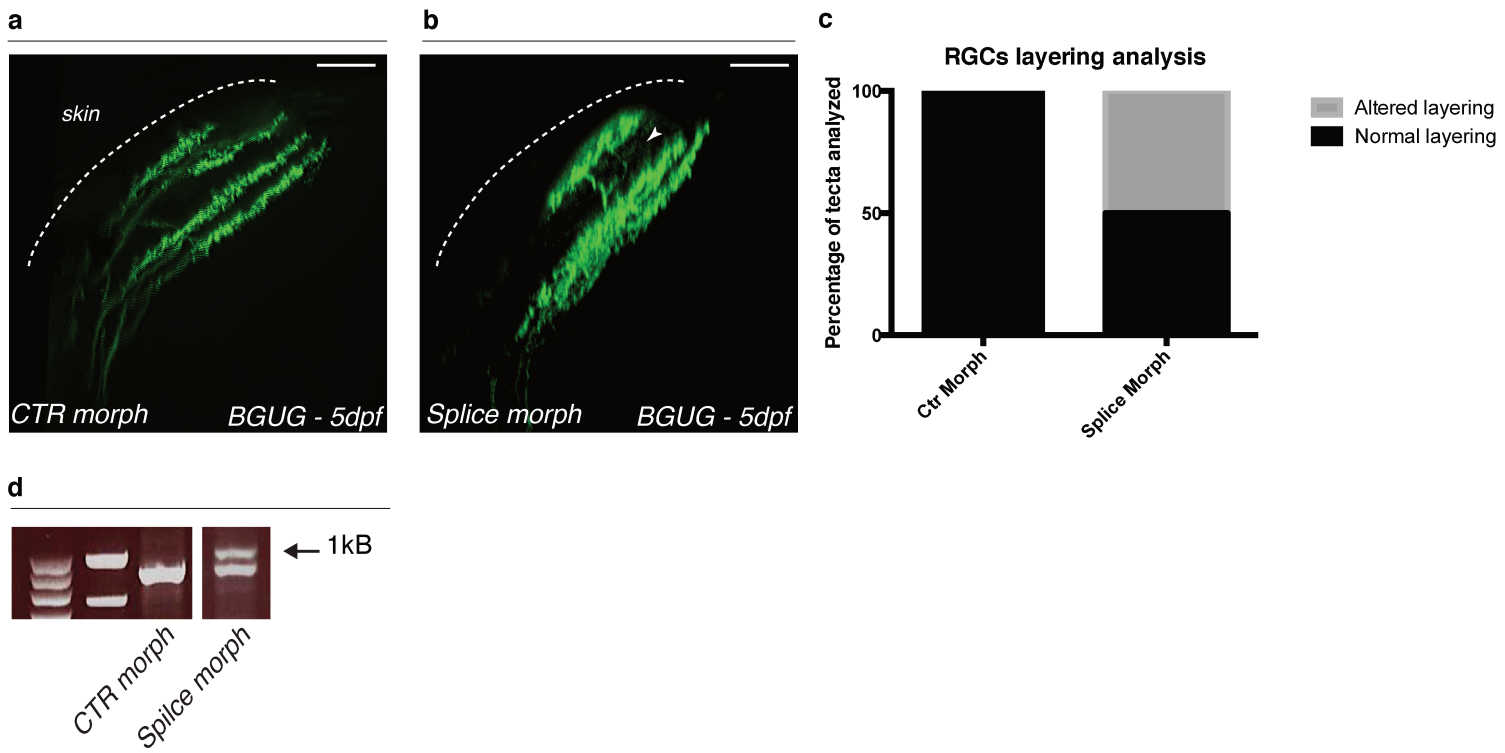


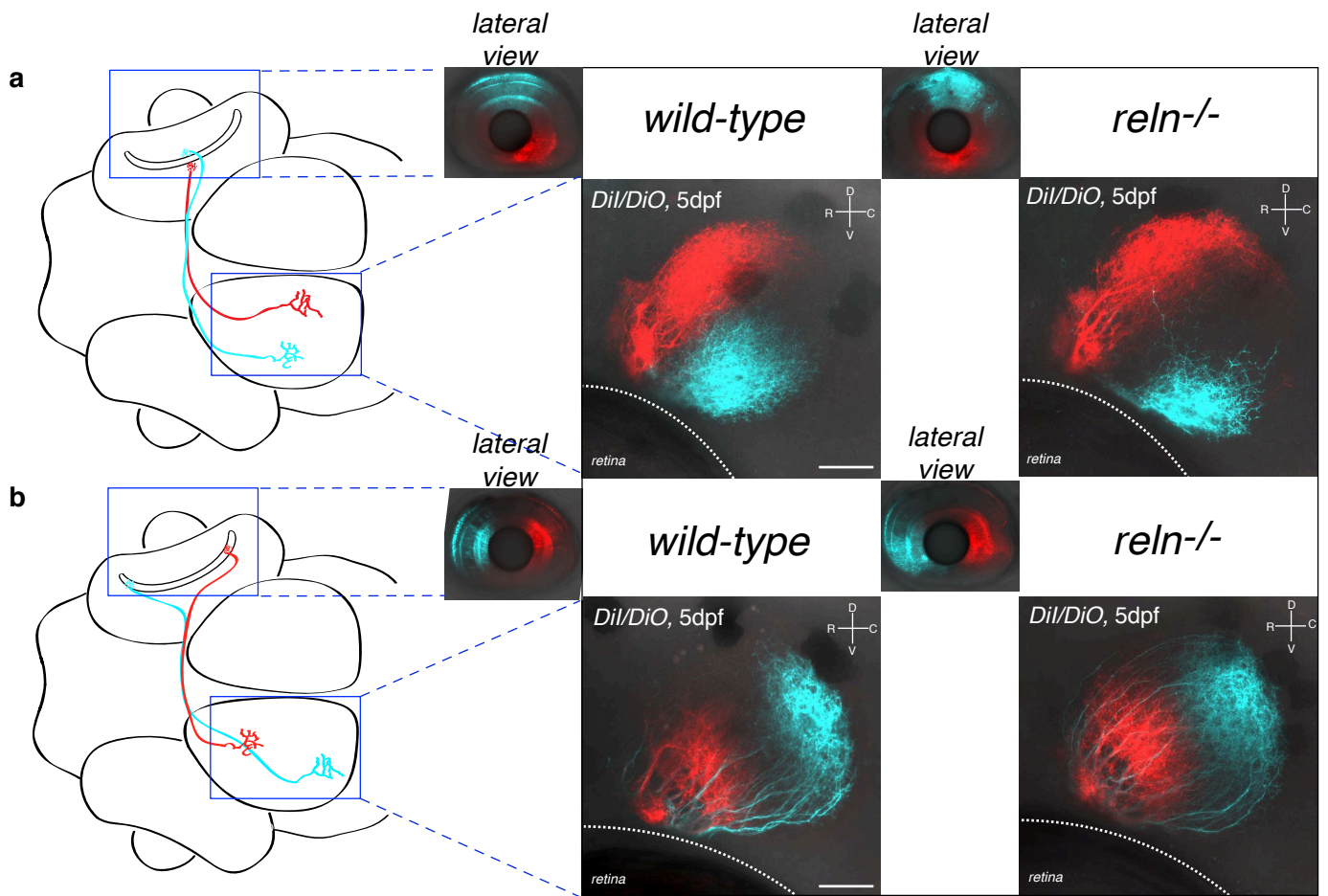
Figure 4



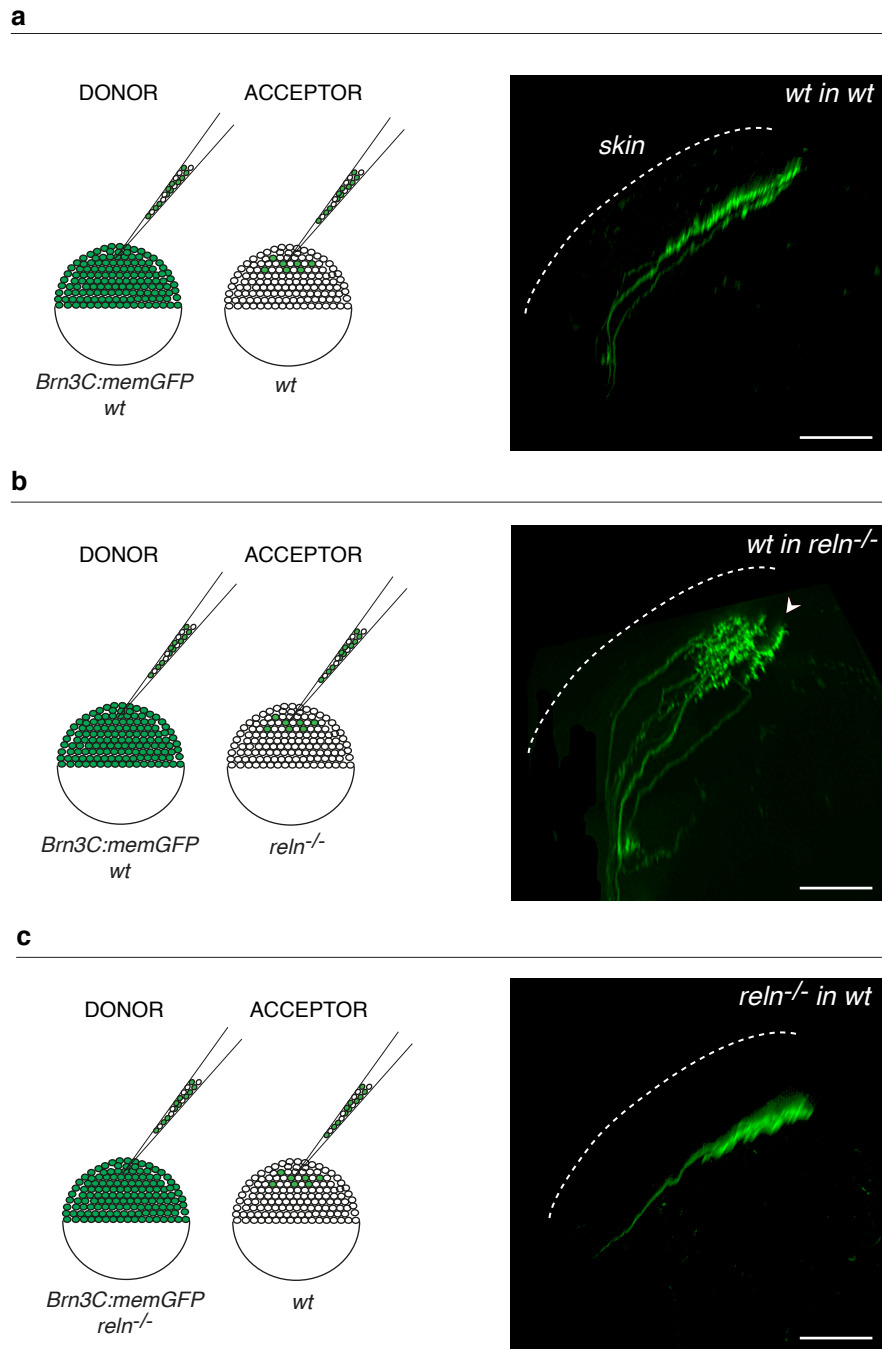
Extended data Figure 1



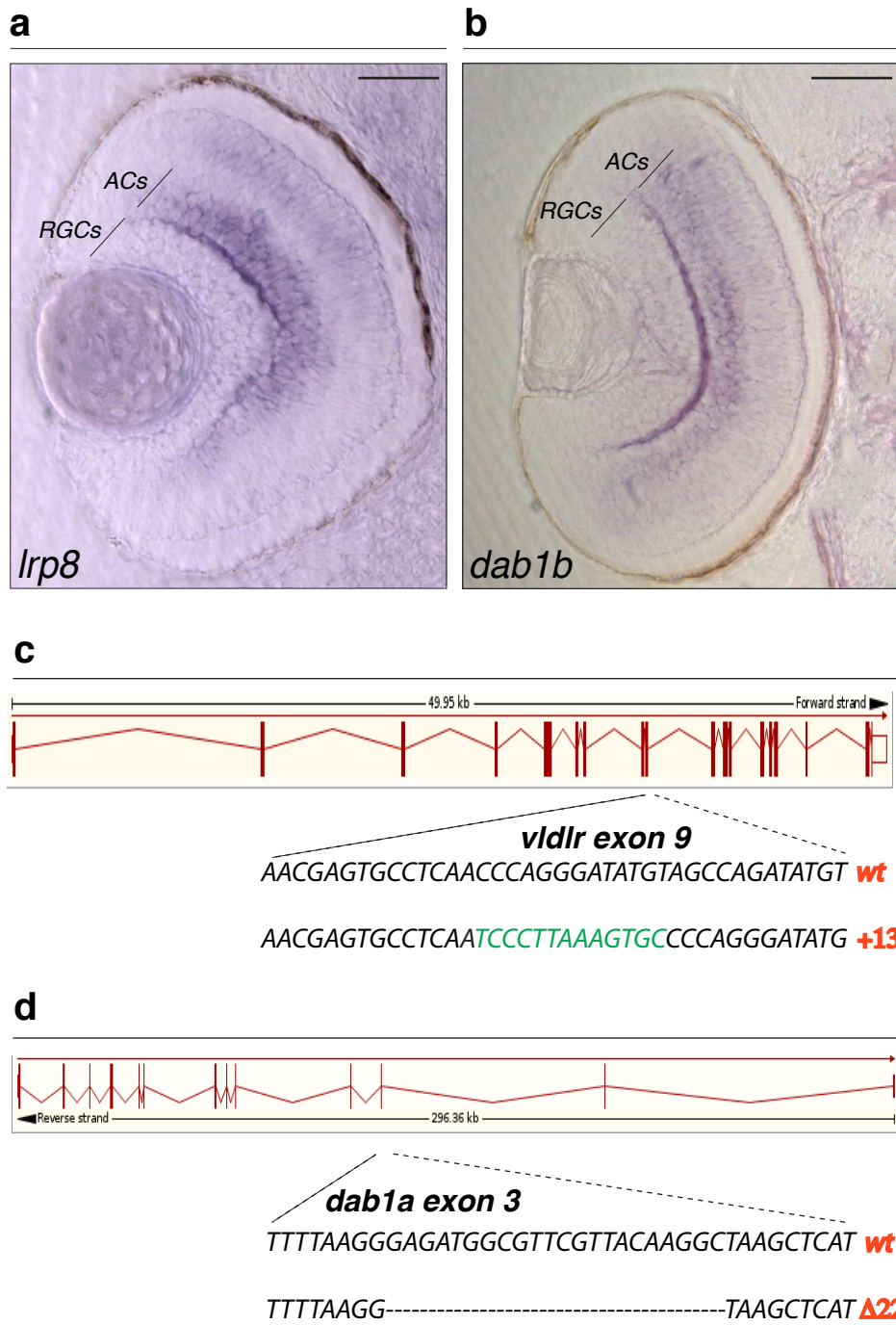
Extended data Figure 2



Extended data Figure 3



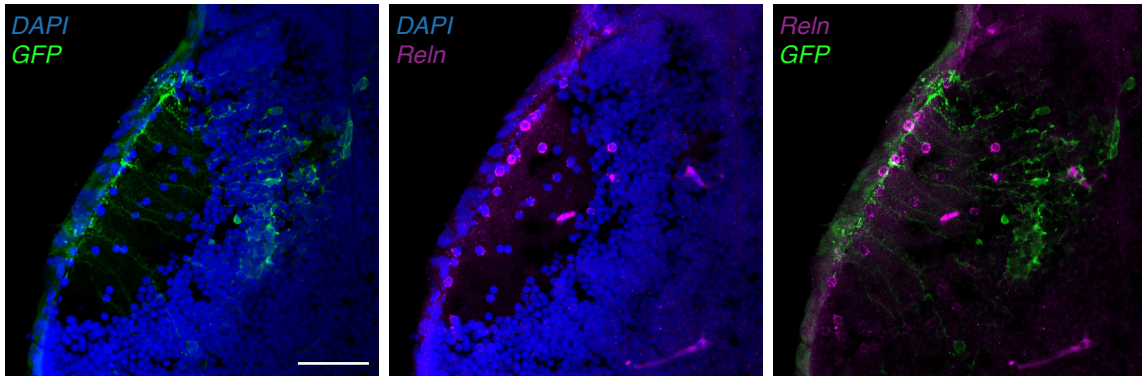
Extended data Figure 4



Extended data Figure 5

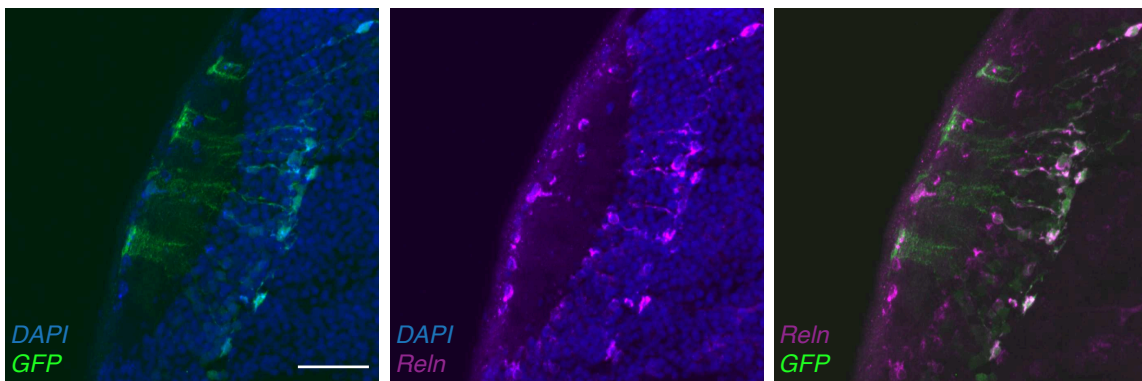
a

Tg(rpl5b:Gal4) x Tg(UAS:GFP)



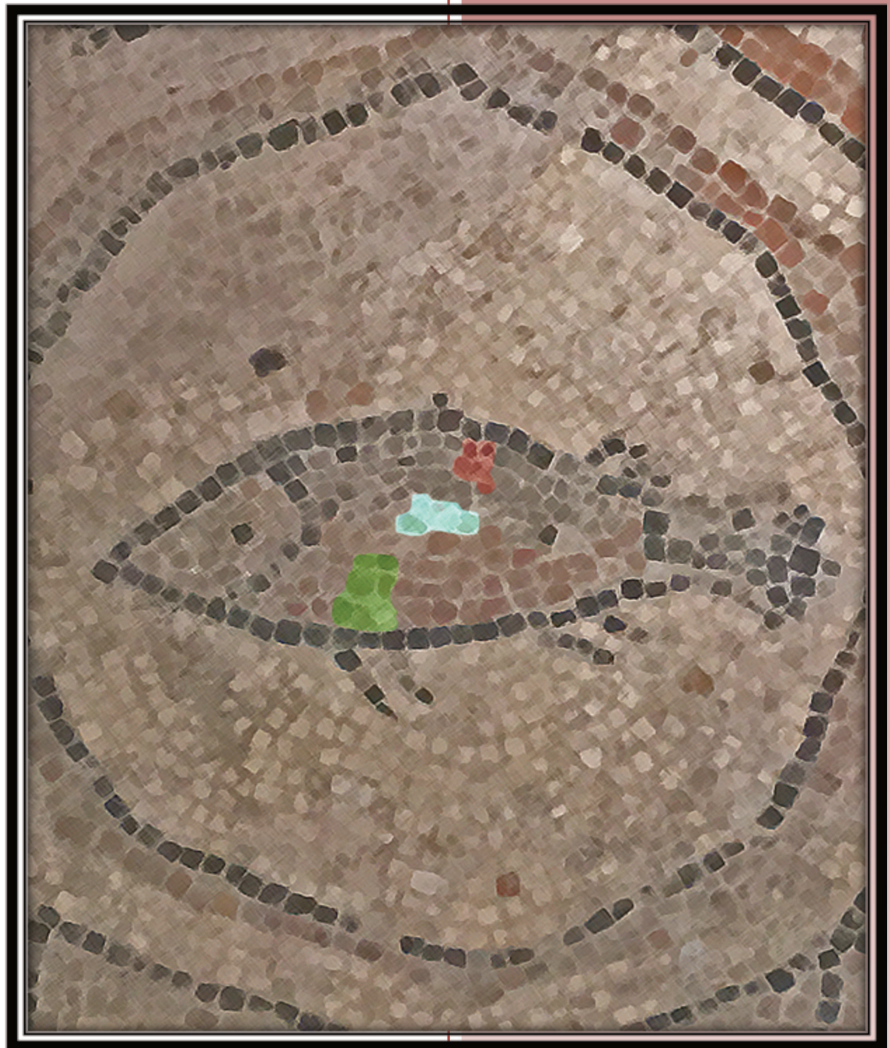
b

Tg(rpl5b:Gal4) x Tg(UAS:relnT2AGFP)



Extended data Figure 6

*Article 2:
“2C-Cas9: a versatile tool for clonal analysis
of gene function”*



2. Summary Article 2

In the last few years the development of CRISPR/Cas9-mediated genome editing techniques has allowed the efficient generation of loss-of-function alleles in several model organisms including zebrafish (ref). However, these methods are mainly devoted to target-specific genomic loci leading to the creation of constitutive knock-out models. On the contrary, the analysis of gene function via tissue- or cell-specific mutagenesis remains challenging in zebrafish. To circumvent this limitation, we combined the transgenesis tools available for genetic manipulation of the zebrafish larval visual system and CRISPR/Cas9 technique to develop a strategy to achieve tissue-specific gene disruption.

Results:

- We generated a vector system for spatiotemporal control of Cas9 activity via Gal/UAS simultaneous genetic labeling of *cas9*-expressing cells with GFP.
- By Gal4-driven expression of our vector system in retinal progenitor cells (RPCs) we successfully disrupted the *tyrosinase* gene, encoding for a key regulator of melanin synthesis. We were therefore able to induce loss of pigmentation in the differentiated retinal pigmented epithelium.
- To allow long-term tracking of *cas9*-expressing cells, we combined our knock-out strategy with the activity of the Cre recombinase (2C-Cas9 system).
- By using the 2C-Cas9 system, we targeted in RPCs the *atho7* locus, encoding for a transcriptional factor involved in retinal ganglion cell (RGC) specification. Thereby we could modify retinal progenitor cell fate determination and generate labeled loss-of-function clones lacking the population of retinal ganglion cells.
- By further combining the 2C-Cas9 vector system with the Brainbow technology, we achieved differential labeling of potentially mutant and wild-type cells in the same animal. As proof of principle, we targeted the genomic locus coding for the motor protein Kif5aa in differentiated RGCs. Our system allowed direct comparison of mutant RGCs, displaying reduced axonal branching due to *kif5aa* loss-of-function, and the wild-type counterpart.

In conclusion, we present for the first time the possibility to express Cas9 under the control of the Gal4/UAS system in a tissue-specific way in a vertebrate model. The genetic lineage tracing of potentially mutant cells allows the phenotypic analysis of cell populations of interest until adulthood, broadening the use of the 2C-Cas9 in fields ranging from stem cells and regeneration to cancer biology and aging.

2C-Cas9: a versatile tool for clonal analysis of gene function

Vincenzo Di Donato,^{1,4} Flavia De Santis,^{1,4} Thomas O. Auer,^{1,5} Noé Testa,¹ Héctor Sánchez-Iranzo,² Nadia Mercader,² Jean-Paul Concordet,³ and Filippo Del Bene¹

¹Institut Curie, PSL Research University, INSERM U 934, CNRS UMR3215, F-75005, Paris, France; ²Department of Cardiovascular Development and Repair, Atherothrombosis and Imaging, Centro Nacional de Investigaciones Cardiovasculares (CNIC), 28028 Madrid, Spain; ³Muséum National d'Histoire Naturelle, INSERM U1154, CNRS UMR 7196, Paris F-75231, France

CRISPR/Cas9-mediated targeted mutagenesis allows efficient generation of loss-of-function alleles in zebrafish. To date, this technology has been primarily used to generate genetic knockout animals. Nevertheless, the study of the function of certain loci might require tight spatiotemporal control of gene inactivation. Here, we show that tissue-specific gene disruption can be achieved by driving *Cas9* expression with the Gal4/UAS system. Furthermore, by combining the Gal4/UAS and Cre/loxP systems, we establish a versatile tool to genetically label mutant cell clones, enabling their phenotypic analysis. Our technique has the potential to be applied to diverse model organisms, enabling tissue-specific loss-of-function and phenotypic characterization of live and fixed tissues.

[Supplemental material is available for this article.]

The CRISPR (Clustered Regularly Interspaced Short Palindromic Repeats)/CRISPR-associated (Cas) system has recently emerged as a powerful tool to generate constitutive loss-of-function alleles, enabling detailed analyses of gene function (Cho et al. 2013; Cong et al. 2013; Hwang et al. 2013b; Mali et al. 2013). Gene disruption is achieved by the activity of two components: a single guide RNA (*sgRNA*) that contains 20 nt complementary to a DNA target, and a *Cas9* endonuclease that catalyzes DNA cleavage at the target site after complex formation with the *sgRNA*. Following DNA cleavage, mutations are efficiently induced upon imperfect repair by the nonhomologous end-joining (NHEJ) pathway at the targeted sequence. *sgRNAs* that bind within the coding region of a gene thereby allow disruption of the open reading frame (ORF), leading to loss of gene activity. Pioneer studies in worms (Shen et al. 2014), fruit fly (Port et al. 2014), mouse (Platt et al. 2014), and, more recently, zebrafish (Ablain et al. 2015) have taken advantage of this methodology to induce conditional gene knockouts by driving tissue-specific expression of *Cas9*. However, in zebrafish, this approach relies on cell-type-specific promoter sequences to control *Cas9* expression, usually requiring the screening of several lines to achieve sufficient and nonectopic transgene expression. One alternative and powerful method for cell-specific expression of transgenes in model organisms is the Gal4/UAS binary system (Asakawa and Kawakami 2008), in which transcription is driven by the binding of the Gal4 transcription factor to tandem upstream activation sequences (UAS) placed at the 5' end of a gene of interest. An important resource of Gal4 transgenic lines has been established by gene- and enhancer-trap screens (Davison et al. 2007; Asakawa et al. 2008; Scott and

Baier 2009; Kawakami et al. 2010; Balciuniene et al. 2013) based on random integration of the Gal4 ORF via Tol2 transposition (Kawakami 2004) into the fish genome. In particular, Gal4 driver lines have been identified for many tissues as well as for novel and previously uncharacterized cell types, especially in the nervous system (Scott et al. 2007; Asakawa et al. 2008). More recently, we have developed a simple and efficient method for converting GFP- into Gal4-transgenic lines, significantly expanding the potential resource of Gal4 driver lines (Auer et al. 2014a,b). Finally, Gal4-driven expression of transgenes from UAS promoters is robust and can often be revealed in cells where *Gal4* expression itself is difficult to detect. In this report, we show that flexible and efficient gene disruption is achieved as a result of tissue-specific expression of *Cas9* via the Gal4/UAS system. In addition, we overcome the challenge of visualizing loss-of-function mutations in specific cells by coexpressing the *Cas9* endonuclease with GFP or Cre recombinase, allowing the labeling of potentially mutant cells and thereby facilitating their phenotypic analysis. This step is essential to correlate phenotype with genotype for analysis of gene function, a task that was not addressed with previously published methods.

Results

Design of a vector system for spatiotemporal control of *Cas9* activity via Gal/UAS

The generation of conditional knockout models requires the specific targeting of a gene of interest in a given tissue and, ideally, the labeling of targeted cells. In order to develop a flexible tool

⁴These authors contributed equally to this work.

⁵Present address: Center for Integrative Genomics, Faculty of Biology and Medicine, University of Lausanne, 1015 Lausanne, Switzerland
Corresponding authors: filippo.del-bene@curie.fr, jean-paul.concordet@mnhn.fr

Article published online before print. Article, supplemental material, and publication date are at <http://www.genome.org/cgi/doi/10.1101/gr.196170.115>.

© 2016 Di Donato et al. This article is distributed exclusively by Cold Spring Harbor Laboratory Press for the first six months after the full-issue publication date (see <http://genome.cshlp.org/site/misc/terms.xhtml>). After six months, it is available under a Creative Commons License (Attribution-NonCommercial 4.0 International), as described at <http://creativecommons.org/licenses/by-nc/4.0/>.

for efficient spatiotemporal control of gene disruption, we generated a Tol2-based vector ensuring Gal4/UAS-mediated cell-type-specific expression of the Cas9 enzyme and ubiquitous expression of sgRNAs. Due to its strong transactivating properties, the Gal4/UAS system directs effective expression of the Cas9 endonuclease, even in the case of weak tissue-specific *Gal4* transcription by an endogenous promoter. Furthermore, this system renders our vector design compatible with many readily available Gal4 transgenic lines generated in previous Gal4 gene- and enhancer-trap screens (including those where the regulatory elements driving *Gal4* expression are not known) (Davison et al. 2007; Asakawa et al. 2008; Scott and Baier 2009; Kawakami et al. 2010; Balciuniene et al. 2013). In our vector design, the use of a viral T2A self-cleaving peptide (Provost et al. 2007) to synthesize a GFP reporter from the same transgene (*UAS:Cas9T2AGFP*) allows Cas9-positive cells to be unambiguously marked by GFP fluorescence. This feature is critical for the analysis of cellular phenotypes resulting from Cas9-induced gene inactivation. Our vector also contains two sgRNA expression cassettes, each driven by the ubiquitous *U6-1* promoter (Halbig et al. 2008; Yin et al. 2015) (*UAS:Cas9T2AGFP;U6:sgRNA1;U6:sgRNA2*) (Fig. 1A). By using two sgRNAs, we sought to increase the probability of generating loss-of-function alleles, since genomic deletions might be induced, in addition to frame-shifts caused by insertions and deletions (indels). To verify that cell-type-specific expression of *Cas9* can be driven by Gal4 transcriptional activation, we generated a stable transgenic line with this vector, *Tg(UAS:Cas9T2AGFP;U6:sgRNA1;U6:sgRNA2)*, and crossed it to different Gal4 driver lines (Fig. 1B). The motor neuron-specific *Tg(mnx1:Gal4)* transgenic line, the enhancer-trap line *Tg(s1020t)* expressed in the thalamus and spinal cord, and the optic tectum-specific gene-trap line *Tg(SA2AzGFF49A)* were used as drivers. We compared the expression of the *UAS:Cas9T2AGFP* with an independent reporter of the Gal4 activity by crossing the same driver lines with a *Tg(UAS:RFP;cry:GFP)*. In the embryos analyzed, GFP was specifically detected in the expected Gal4 transactivation domain, indicating nonectopic *Cas9* expression. Modest differences in GFP and RFP expression were observed, the RFP-positive cells being on average more numerous than the GFP-positive ones. This might be due to transgene specific differences likely linked to positional effect of the integration as commonly seen for other zebrafish transgenic lines. Overall, these expression patterns demonstrate that our approach can be used to both express Cas9 nuclease in a tissue-specific manner and to simultaneously label *Cas9*-expressing cells with GFP.

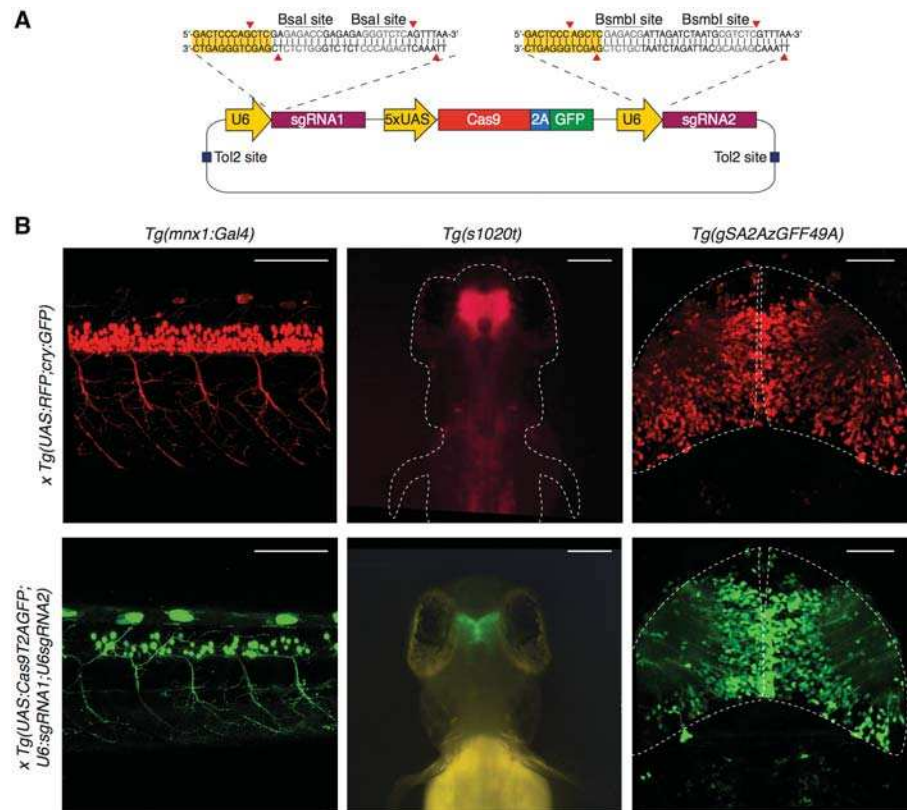


Figure 1. Spatiotemporal control of Cas9 activity via the Gal4/UAS expression system. (A) Schematic illustration of the expression vector design. Spatial and temporal control of Cas9 synthesis is achieved by the Gal4/UAS system and monitored by GFP expression. Two constitutively active *U6* promoters drive the transcription of single guide RNAs (*sgRNAs*) specifically targeting a gene of interest. To facilitate cloning of *sgRNA* target sequences, Bsmbl and Bsal restriction sites (red arrows) were introduced. Tol2 allows efficient transgenesis after injection into one-cell stage zebrafish embryos. (B) (Left panel) Confocal imaging of the spinal cord of 2 dpf *Tg(mnx1:Gal4)* embryos. The upper image shows the Gal4-induced RFP expression of a double transgenic embryo deriving from a cross between *Tg(mnx1:Gal4)* and *Tg(UAS:RFP; cry:GFP)* fish. The same pattern is observed in the GFP channel in a double transgenic *Tg(mnx1:Gal4) × Tg(UAS:Cas9T2AGFP;U6:sgRNA1;U6:sgRNA2)* embryo (lower image). Scale bar = 100 μ m. (Middle panel) Imaging of whole-mount 3 dpf *Tg(s1020t)* enhancer-trap line. The GFP expression pattern (lower panel) recapitulates RFP (upper panel). Scale bar = 100 μ m. (Right panel) Confocal imaging of 5 dpf optic tectum in the double transgenic embryos deriving from a cross of *Tg(gSA2AzGFF49A)* gene-trap line and *Tg(UAS:RFP; cry:GFP)* (upper image) and *Tg(UAS:Cas9T2AGFP;U6:sgRNA1;U6:sgRNA2)* (lower image). Scale bar = 50 μ m. No target sequence was inserted in the vector for the generation of the *Tg(UAS:Cas9T2AGFP;U6:sgRNA1;U6:sgRNA2)* line.

Targeting the *tyrosinase* gene in the optic primordium leads to loss of pigmentation in the retinal pigmented epithelium (RPE)

To test the efficiency of our approach for tissue-specific gene disruption, we targeted the *tyrosinase* (*tyr*) gene, which codes for a key enzyme in melanin production (Camp and Lardelli 2001), by including two *sgRNAs* targeting the *tyr* in our vector locus (*pUAS:Cas9T2AGFP;U6:tyrsgRNA1;U6:tyrsgRNA2*). We previously assessed the mutagenesis rate of each *sgRNA* by injection of in vitro-transcribed *sgRNA* with synthetic *Cas9* mRNA into one-cell stage wild-type embryos (Supplemental Table S1). Loss-of-function of the *tyr* locus results in pigmentation defects, offering a clear visual read-out of biallelic gene inactivation (Jao et al. 2013). We used fluorescence-activated cell sorting (FACS) to verify that site-specific cleavage only occurs in GFP-expressing cells and to quantify the mutation rate induced by our vector. The quasi-ubiquitous *Tg(rpl5b:Gal4)* line (Amsterdam et al. 2004) was chosen to enlarge

the number of GFP-positive cells in the assay (Supplemental Fig. S1A). We thereby transiently expressed the pUAS: *Cas9T2AGFP*; *U6:tyrsgRNA1*; *U6:tyrsgRNA2* by injection into one-cell stage *Tg(rpl5b:Gal4)* embryos. After separating the pool of GFP-positive cells from the GFP-negative control cells derived from 200 injected embryos, total DNA was extracted from the two cell populations. Upon PCR amplification and sequencing of single amplicons from the DNA of GFP-positive cells, we detected indel out-of-frame mutations at the *tyr* target region in 30% (4/12) of the analyzed sequences (Supplemental Fig. S1B). In this cell population, we also observed a 488-bp deletion at the *tyr* gene resulting from simultaneous targeting of the locus by both sgRNAs. In contrast, no *tyr* mutations were found in the GFP-negative cells (0/15). These data confirm that locus-specific knockout events are restricted to the cells expressing the fluorescent reporter. Subsequently, we tested whether spatiotemporally regulated *tyr* loss-of-function can be induced by our vector system. For this purpose, we used a transgenic line expressing *Gal4* under the promoter of the zebrafish *retinal homeobox gene 2 (rx2)* (Heermann et al. 2015), *Tg(rx2:Gal4;myl7:GFP)*. We identified transgenic embryos using the *myl7 (myosin, light chain 7, regulatory)* promoter, driving heart-specific *GFP* expression, which was incorporated in the same transgene. *Rx2* is active in the optic primordium in the progenitors of the neural retina and the retinal-pigmented epithelium (RPE) (Chuang and Raymond 2001). Thus, transient, cell-specific expression of *Cas9* from the pUAS: *Cas9T2AGFP*; *U6:tyrsgRNA1*; *U6:tyrsgRNA2* in *Tg(rx2:Gal4;myl7:GFP)* embryos should promote targeted disruption of the *tyr* locus uniquely in *Gal4*-positive cells, leading to pigmentation defects exclusively in the RPE after biallelic gene inactivation. In agreement with the known expression pattern of the *rx2* promoter (Supplemental Fig. S2A), we detected sparse green fluorescent cells in the embryonic retina of *Gal4*-positive larvae, at 24 hours post-fertilization (hpf) (Fig. 2A). Of the embryos analyzed at 5 days post-fertilization (dpf), 15% displayed loss of pigmentation specifically in the RPE (16/107 embryos in three independent experiments) compared to 0% (0/116 in three independent experiments) in embryos injected with a plasmid containing control sgRNA sequences (Fig. 2B,C). We observed a variable degree of pigmentation loss, and all the embryos displaying the phenotype were scored as positives. Importantly, no pigmentation defects were detected outside of the eye-specific *Gal4* expression domain. Together, these results indicate that knockout of the *tyr* gene driven by the *rx2* promoter leads to tissue-specific pigmentation defects. Having this proof of principle for our approach, we decided to create a stable integration of the UAS-based transgene to achieve a more robust and more reliable expression and to evaluate the penetrance of the pigmentation phenotype. We generated a *Tg(UAS:Cas9T2AGFP;U6:tyrsgRNA1;U6:tyrsgRNA2)* transgenic line

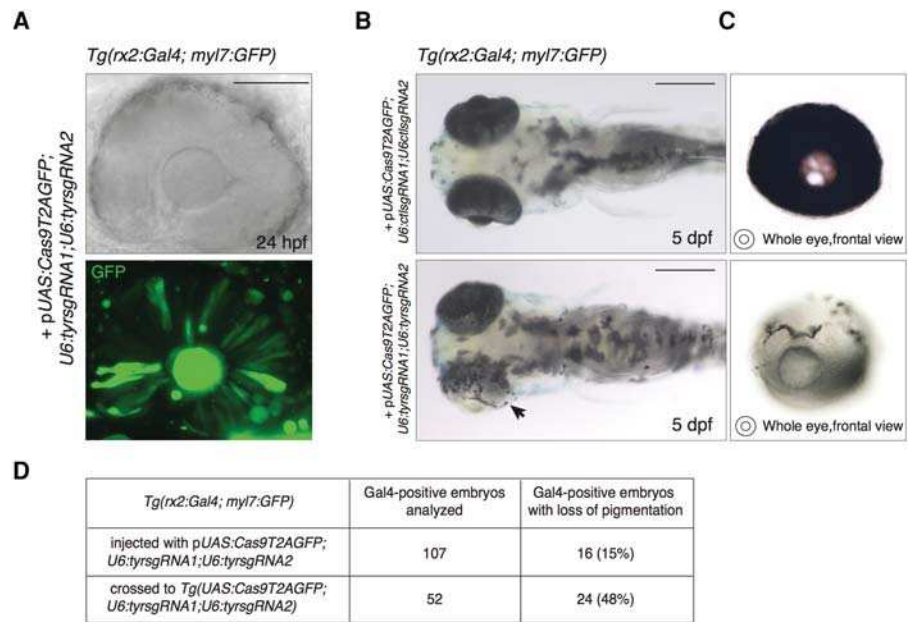


Figure 2. Tissue-specific disruption of the *tyrosinase* locus induced by the expression of the UAS-based vector in the retinal progenitor cells. (A) Transmitted light and confocal imaging of eye of a 24 hpf *Tg(rx2:Gal4;myl7:GFP)* embryo injected with pUAS: *Cas9T2AGFP*; *U6:tyrsgRNA1*; *U6:tyrsgRNA2* together with *Tol2* mRNA. GFP fluorescence indicates *Gal4*-driven expression of the *Cas9* enzyme in the retinal progenitor cells (RPCs) giving rise to the retinal pigmented epithelium (RPE) and to the neural retina. Scale bar = 100 μ m. (B) (Lower panel) Specific loss of pigmentation in the RPE of a 5 dpf zebrafish embryo induced by injection of pUAS: *Cas9T2AGFP*; *U6:tyrsgRNA1*; *U6:tyrsgRNA2* in *Tg(rx2:Gal4; myl7:GFP)* at one-cell stage. Arrowhead indicates the eye with lost pigmentation. (Upper panel) Control embryo injected with the same vector containing a control sgRNA sequence (*ctfsgRNA*). Scale bar = 300 μ m. (C) Frontal view of eyes with absent pigmentation (lower panel) and wild-type (upper panel) explanted from the larvae shown in B. (D) Table showing the percentage of *Gal4*-positive larvae displaying loss of pigmentation in the RPE. (First row) Injection of the pUAS: *Cas9T2AGFP*; *U6:tyrsgRNA1*; *U6:tyrsgRNA2* into one-cell-stage *Tg(rx2:Gal4; myl7:GFP)* embryos. (Second row) Cross of *Tg(rx2:Gal4; myl7:GFP)* fish with *Tg(UAS:Cas9T2AGFP;U6:tyrsgRNA1;U6:tyrsgRNA2)*.

and crossed it with *Tg(rx2:Gal4;myl7:GFP)* fish. *Gal4*-positive embryos were prescreened by *myl7:GFP* expression and subsequently analyzed to assess *tyr* inactivation. The rate of larvae displaying RPE pigmentation defects increased to 48% (24/52) (Fig. 2D); therefore, *tyr* loss-of-function most likely occurred in all double transgenic progeny of the cross, as only half of the *Gal4*-positive larvae were expected to carry the UAS transgene. This observation shows that stable expression of the *Cas9*/sgRNA complex dramatically improves the efficiency of gene inactivation, most likely due to higher levels and more widespread expression in retinal progenitor cells (RPCs). Based on these data, we conclude that our vector system is capable of inducing loss-of-function alleles at given genomic loci in a defined spatiotemporal manner. However, at the developmental stage of the phenotypic analysis (5 dpf), GFP fluorescence could no longer be detected since the *rx2* promoter is not active in the differentiated RPE. This result reflects the fact that *GFP* expression is strictly dependent on the temporal activity of the promoter driving *Gal4* expression, thus restricting direct detection of potential mutant cells to a limited time window.

Cre-mediated recombination allows permanent labeling of *Cas9*-expressing cells

By using the pUAS: *Cas9T2AGFP*; *U6:sgRNA1*; *U6:sgRNA2* vector, potentially mutated cells are labeled by simultaneous expression

of the Cas9 endonuclease and a *GFP* reporter. Nevertheless, the possibility of phenotypic analysis of the cells expressing the transgene strongly depends on the activity window of the chosen promoter, as it determines when the GFP reporter can be detected. Therefore, the long-term visualization of cells displaying loss-of-function phenotypes that are not self-revealing (unlike the loss of pigmentation induced by mutations on the *tyr* locus) requires permanent labeling of *Cas9*-expressing cells and their progeny. To obtain such a labeling, we replaced the *GFP* ORF with the one of *Cre* recombinase (Fig. 3A), an enzyme catalyzing site-specific recombination events (Branda and Dymecki 2004; Pan et al. 2005). In order to detect Cre-mediated labeling of *Cas9*-expressing cells, we used transgenic lines carrying a cassette where a ubiquitous promoter drives constitutive expression of a fluorescent reporter only upon excision of a floxed STOP sequence by Cre recombinase. The tissue-specific Gal4-driven transcription of a *UAS:Cas9T2ACre* transgene ensures concomitant expression of the Cas9 and Cre enzymes inducing, respectively, double-strand breaks (DSBs) at the target locus and activation of the floxed reporter transgene within the same cell (Fig. 3B). Most importantly, Cre-dependent expression of the fluorescent reporter will persist in all cells derived from a specific *Cas9*-expressing precursor. This approach, that

we name 2C-Cas9 (Cre-mediated recombination for Clonal analysis of Cas9 mutant cells) allows targeted mutagenesis of a cell population and the genetic labeling of the derived mutant cell clones.

Visualizing 2C-Cas9-mediated gene inactivation

In order to explore the possibility of directly visualizing protein loss, we sought to induce eye-specific loss-of-function at the *parvalbumin 6* (*pvalb6*) locus, coding for a calcium-binding protein expressed in a subpopulation of amacrine cells (ACs) in the inner nuclear layer (INL) and retinal ganglion cell layer (GCL) of the differentiated retina (Fig. 4A). The *pvalb6* gene is the only paralog expressed in mature retinal neurons as reported by the ZFIN in situ database (Sprague et al. 2008). This gene represents an ideal target for unbiased detection of locus disruption, since its expression can be easily revealed by immunohistochemistry with a commercially available antibody (Nevin et al. 2008). To achieve *pvalb6* inactivation, we first generated a *pUAS:Cas9T2ACre;U6:pvalb6sgRNA1;U6:pvalb6sgRNA2* vector. The mutagenesis rate of the *sgRNA* used was tested in transient injection in wild-type embryos prior to cloning in the 2C-Cas9 vector (Supplemental Table S1). As a single efficient *sgRNA* could be identified for this gene, the same target sequence was inserted downstream from each of the two *U6* promoters. We chose the *rx2:Gal4* driver to express this UAS construct targeting *pvalb6* in multipotent retinal progenitor cells as the *rx2* promoter is active during early eye field development (Chuang and Raymond 2001; Heermann et al. 2015). It has been previously reported that one single RPC can give rise to clones including all of the different retinal cell types spanning all retinal layers (Livesey and Cepko 2001). Thus, a loss-of-function mutation, when induced at the level of a RPC, is expected to propagate to a clone of cells derived from the progenitor. To obtain clonal labeling of mutant retinal cells, we injected the *pUAS:Cas9T2ACre;U6:pvalb6sgRNA1;U6:pvalb6sgRNA2* into one-cell stage embryos of a cross of *Tg(rx2:Gal4;myl7:GFP)* and *Tg(-3.5Subb:loxP-lacZ-loxP-eGFP)cn2* fish. The latter reporter line allows visualization of Cre-mediated recombination by switching from *lacZ* to *GFP* expression. This cross enables the detection in the retina of radial columns of GFP-positive cells arising from RPCs having expressed the *Cas9* during the activation time of the *rx2* promoter. Discrete clones of GFP-positive *Cas9*-expressing cells were analyzed in retinas of 5 dpf larvae after double immunohistochemistry for GFP and Pvalb. For each clone, we counted the total number of cells labeled by the GFP reporter, excluding photoreceptors, and the number of cells simultaneously stained for GFP and Pvalb. This second

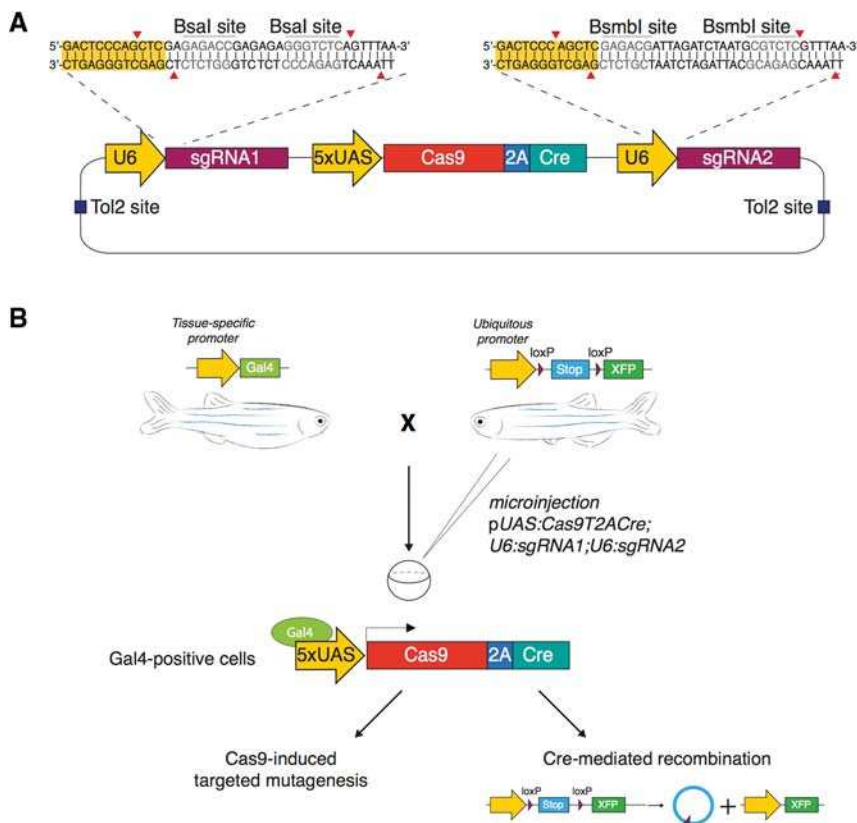


Figure 3. Permanent labeling of *Cas9*-expressing cells by Cre-mediated recombination. (A) Schematic illustration of the *pUAS:Cas9T2ACre;U6sgRNA1;U6sgRNA2* expression vector design. The vector contains two *U6-sgRNA* expression cassettes targeting the same gene. Bsal and BsmBI restriction sites are used for the *sgRNA* target sequence cloning. UAS elements drive the expression of *Cas9* and *Cre* recombinase linked via the T2A peptide. (B) Microinjection of the *pUAS:Cas9T2ACre;U6sgRNA1;U6sgRNA2* construct in the double transgenic embryos *Tg(Tissue specific promoter:Gal4) × Tg(Ubiquitous promoter:loxP-STOP-loxP-XFP)* triggers simultaneous synthesis of *Cas9* and *Cre* in a chosen spatiotemporal pattern, defined by the promoter driving *Gal4* expression. Cell-specific *Cas9* endonuclease activity induces targeted disruption of the gene of interest and Cre-mediated recombination induces permanent expression of a fluorescent reporter gene (*XFP*) by deletion of the floxed stop sequence.

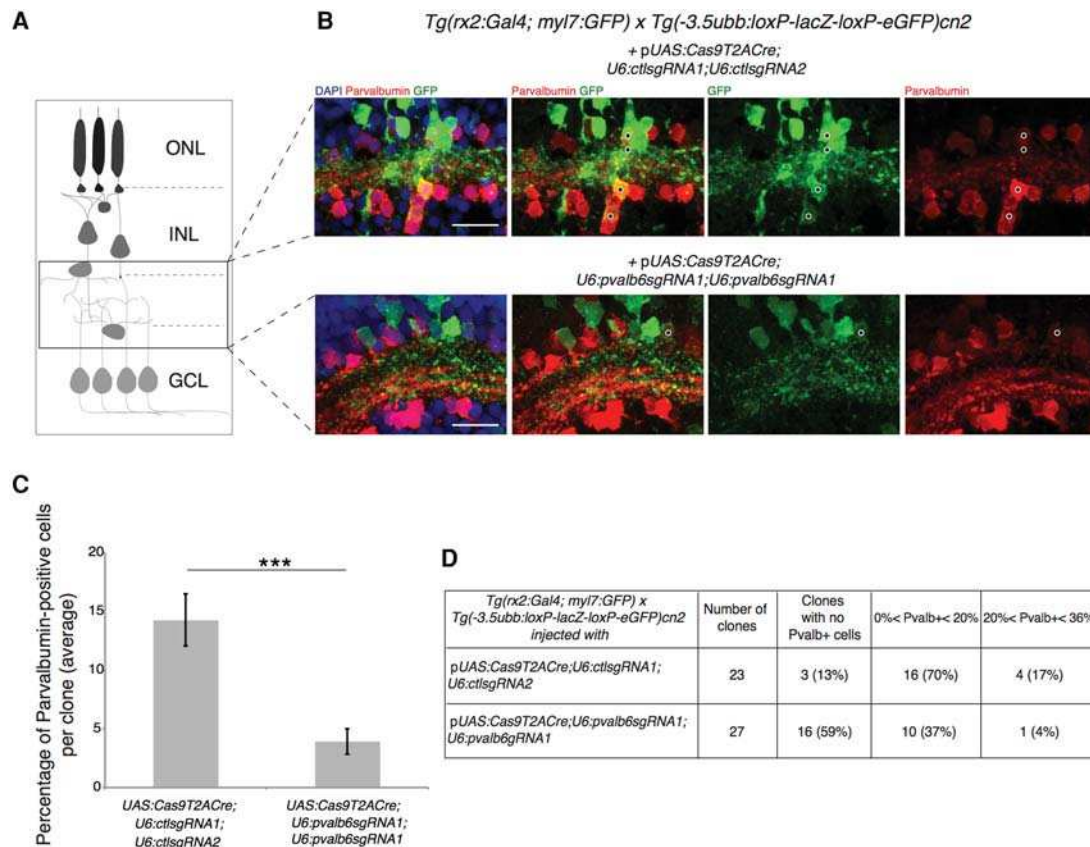


Figure 4. Targeting of the *pvalb6* locus leads to loss of Pvalb expression in ACs. (A) Schematic of a clone of cells deriving from a single RPC. The black frame defines the position of the amacrine cell population. (ONL) Outer nuclear layer, (INL) inner nuclear layer, (GCL) ganglion cell layer. (B) GFP-positive Cas9-expressing cells in the retinal section of a 5 dpf double transgenic *Tg(rx2:Gal4; myl7:GFP) × Tg(-3.5ubb:loxP-lacZ-loxP-eGFP)cn2* embryos transiently expressing the 2C-Cas9 vector containing control sgRNAs (upper panel) or *pvalb6*-specific sgRNAs (lower panel). The same sgRNA target sequence was inserted downstream from each U6 promoter (*U6:pvalb6sgRNA1*). The number of Pvalb- and GFP-double-positive cells (black dots) is reduced if *pvalb6* is targeted compared to control. Scale bar = 50 μ m. (C) Quantification of the percentage of Pvalb-positive cells per GFP-positive clone. Data are represented as mean \pm SEM. (***) *P*-value < 0.001 following Wilcoxon Mann–Whitney test. (D) Table showing the percentage of Pvalb-positive cells per GFP-positive clone in the retinal sections of double transgenic *Tg(rx2:Gal4; myl7:GFP) × Tg(-3.5ubb:loxP-lacZ-loxP-eGFP)cn2* larvae microinjected with the 2C-Cas9 plasmid containing control sgRNAs (first row) or *pvalb6*-targeting sgRNAs (second row).

population represents the subset of amacrine cells deriving from Cas9-expressing RPCs that escaped *pvalb6* biallelic inactivation. We observed that the total number of cells was not affected in the examined clones (15 ± 1 in controls vs. 16 ± 1 in *pvalb6* sgRNA clones; $P = 0.9$, Wilcoxon Mann–Whitney test), while the number of cells showing colocalization of Pvalb and GFP signals was considerably reduced by the targeting of *pvalb6* (1.9 ± 0.3 in controls vs. 0.8 ± 0.2 in *pvalb6* sgRNA clones; $P < 0.005$, Wilcoxon Mann–Whitney test) (Fig. 4B). Overall, in control retinas the number of GFP-positive cells expressing Pvalb represented 12% of each clone on average ($n = 23$ clones; 345 cells analyzed). On the contrary, in clones where the *pvalb6* gene was targeted, only 4% of GFP-positive cells were also positive for Pvalb ($n = 27$ clones; 435 cells analyzed), representing cells that escaped biallelic *pvalb6* inactivation (Fig. 4C,D). Altogether, *pvalb6* targeting led to a reduction of two thirds of the *pvalb6*-expressing ACs. These results confirm that 2C-Cas9 can mediate gene loss-of-function and that antibody staining can efficiently reveal protein loss at a cellular resolution, offering a clear read-out of the proportion of cells carrying biallelic mutations within the analyzed population.

atoh7 gene inactivation in retinal progenitors inhibits determination of retinal ganglion cells (RGCs) in clonally derived cell populations

We next wanted to test the utility of the 2C-Cas9 system in the analysis of a loss-of-function phenotype in cell clones. We chose to target the *atoh7* gene because a characterized loss-of-function allele (*lakritz*) shows a clearly identifiable retinal phenotype (Kay et al. 2001). The *lak* mutation results in the loss of retinal ganglion cell (RGC) specification during eye development. Because *rx2* expression precedes *atoh7* activation, mutations induced by *rx2*-driven Cas9 may give rise to *atoh7* mutant cells in RPCs before endogenous *atoh7* is expressed. We therefore transiently expressed a pUAS:Cas9T2ACre;U6:atoh7sgRNA1;U6:atoh7sgRNA2 vector in double transgenic embryos deriving from a cross of *Tg(rx2:Gal4;myl7:GFP)* and *Tg(-3.5ubb:loxP-lacZ-loxP-eGFP)cn2* fish to induce targeted mutations at the *atoh7* locus in RPCs. The mutagenesis efficiency of the sgRNAs used was assessed prior to insertion in the transgenesis vector (Supplemental Table S1) in transient injection experiments. Clones of GFP-positive cells were analyzed in sections of

differentiated retinas of 5 dpf larvae (Fig. 5A–C). For this analysis, we chose to quantify only spatially well-separated clones that could be unambiguously identified, ranging from 10 to 55 cells per clone. We observed that the total number of cells per clone was not affected (25 ± 3 in controls vs. 24 ± 2 in *atoh7* sgRNA clones; $P = 0.91$, Wilcoxon Mann–Whitney test), while the number of RGCs was significantly reduced in *atoh7* targeted clones (6.1 ± 1.2 in controls vs. 2.4 ± 0.5 in *atoh7* sgRNA clones; $P < 0.01$, Wilcoxon Mann–Whitney test). On average, in control retinas the RGC population represented 23% of the cells in each clone (57/247 cells analyzed). In contrast, in potentially *atoh7*-depleted clones only 9% of GFP-positive cells corresponded to differentiated RGCs (48/532 cells analyzed) (Fig. 5D). In the retinas of embryos injected with the control plasmid, all clones of cells (10/10) contained RGCs, representing, in the majority of clones (7/10), >20% of the GFP-positive cell population (Fig. 5E). In the

retinal sections of embryos where the *atoh7* locus was targeted, one third of the examined clones (7/22) displayed complete absence of RGCs, while only in a few cases (2/22 clones) the percentage of specified RGCs per clone was higher than 20% (Fig. 5E). These observations indicate that *atoh7* loss-of-function is effectively induced by our vector system in *rx2*-expressing retinal progenitors.

Analysis of genetic chimeras by combining tissue-specific loss-of-function with Brainbow single-cell labeling

To gain insights into complex loss-of-function phenotypes, it is necessary to understand if the biological effect of gene inactivation is cell-autonomous or non-cell-autonomous. Our method can be applied to generate genetic mosaics in which the phenotype of single mutant cells can be analyzed in a wild-type

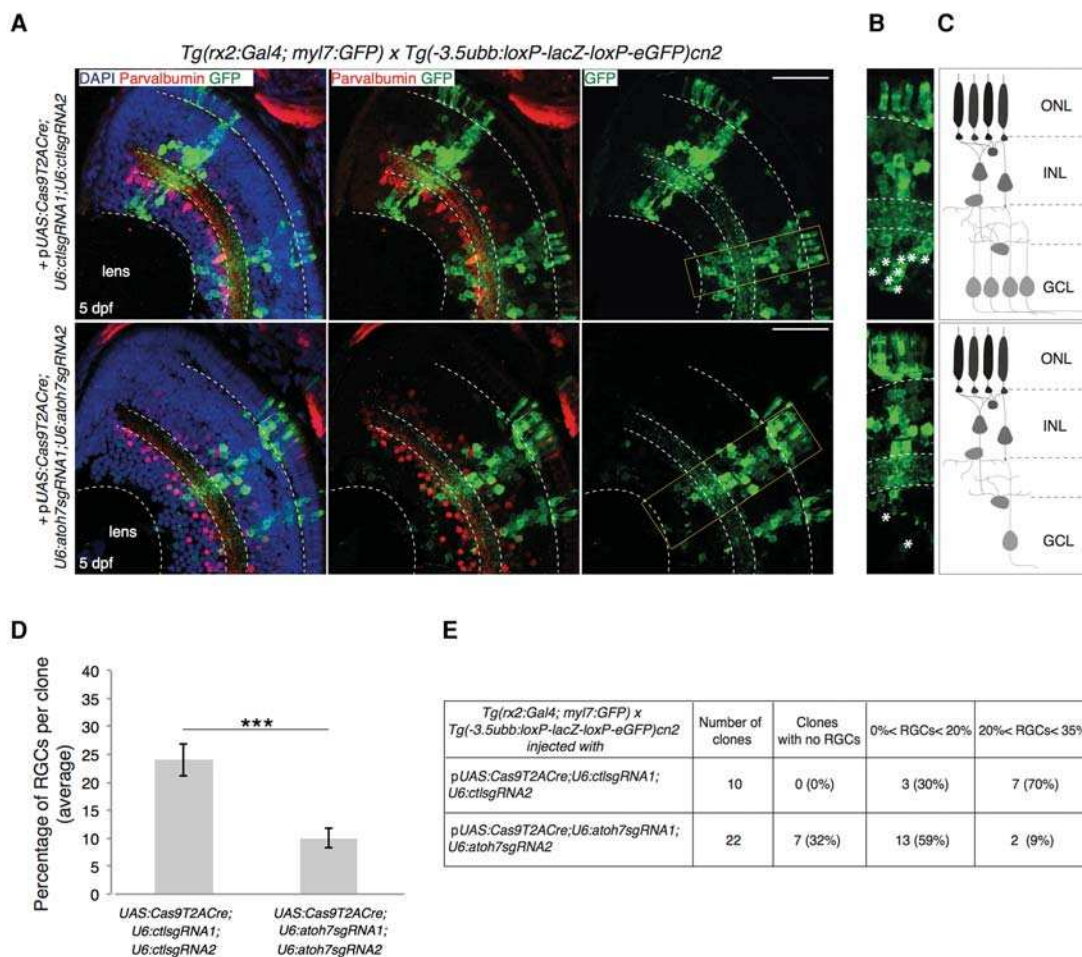


Figure 5. Clonal deletion of *atoh7* leads to reduction in RGCs differentiation. Targeting of the *atoh7* gene. *Atoh7* is a transcription factor essential for the differentiation of retinal ganglion cells (RGCs). The pUAS:Cas9T2ACre;U6sgRNA1;U6sgRNA2 construct, with control or *atoh7*-specific sgRNAs, was injected in double transgenic embryos *Tg(rx2:Gal4; myl7:GFP) × Tg(-3.5ubb:loxP-lacZ-loxP-eGFP)cn2*. The latter transgene drives *Gal4* expression in retinal progenitor cells. (A) (Upper panel) Differentiated RGCs are detected in wild-type clones injected with the DNA construct containing control sgRNAs. (Lower panel) GFP-labeled mutant clones show reduction of RGCs in the retinal section of a 5 dpf larva, as expected from *atoh7* loss-of-function. Quantification of RGCs was done according to soma location in the ganglion cell layer (GCL), and displaced amacrine cells were distinguished by Parvalbumin counterstaining. Scale bar = 100 μ m. (B) Higher magnification of the wild-type (upper panel) and *atoh7* (lower panel) mutant retinal cell layers. RGCs are indicated by asterisks. (C) A schematic of labeled clones in the zebrafish retinal layers. (ONL) Outer nuclear layer, (INL) inner nuclear layer, (GCL) ganglion cell layer. (D) Quantification of the percentage of RGCs per clone derived from *Cas9*-expressing cells. Data are represented as mean \pm SEM. (***) P -value < 0.001 following Wilcoxon Mann–Whitney test. (E) Table showing the percentage of RGCs per GFP-positive clone in the retinal sections of double transgenic *Tg(rx2:Gal4; myl7:GFP) × Tg(-3.5ubb:loxP-lacZ-loxP-eGFP)cn2* embryos microinjected with the 2C-Cas9 vector containing control sgRNAs (first row) or *atoh7*-specific sgRNAs (second row).

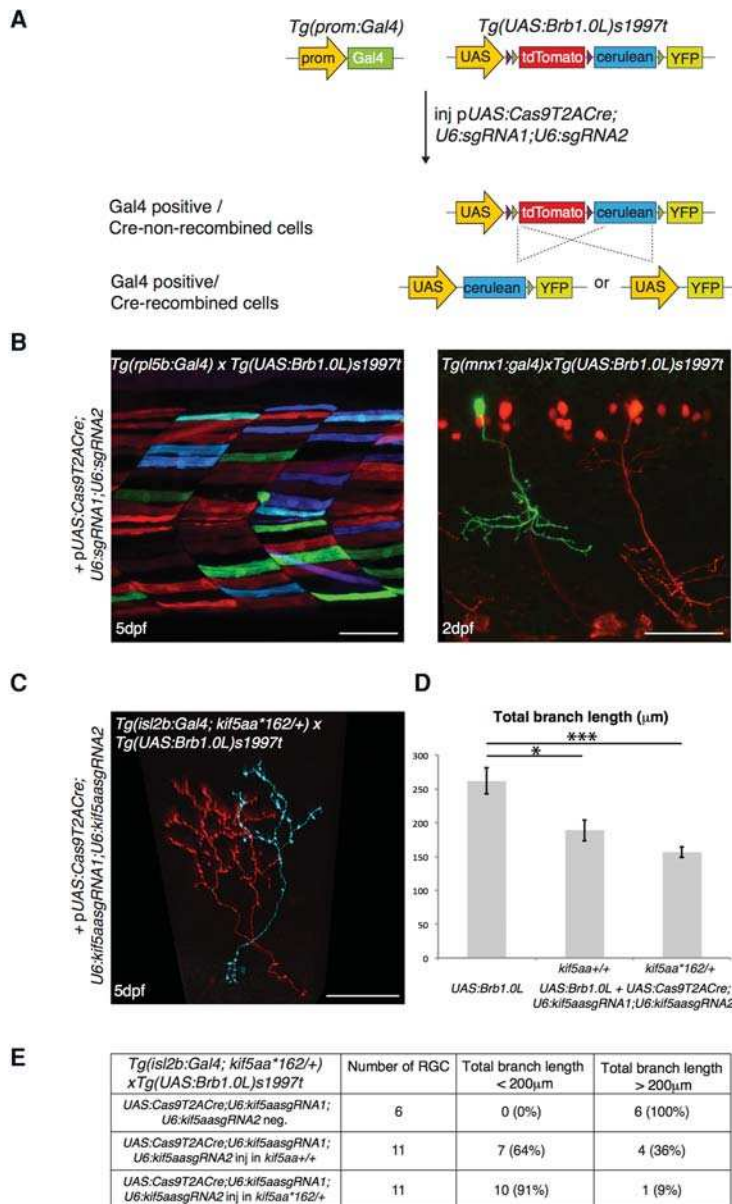


Figure 6. Labeling of mutant single cells by combining the 2C-Cas9 and the Brainbow methodologies. (A) Microinjection of the *pUAS:Cas9T2ACre; U6sgRNA1; U6sgRNA2* construct in the double transgenic embryos *Tg(promoter:Gal4) × Tg(UAS:Brb1.0L)s1997t* leads to synthesis of both Cas9 and Cre. In *Gal4*-expressing cells, Cas9 promotes targeted cleavage of the chosen genomic locus. At the same time, Cre activity induces stochastic recombination of the *UAS:Brb1.0L* cassette, thus promoting a switch from the default tdTomato to YFP or Cerulean fluorescence in the same cells. (B) Recombination of the *UAS:Brb1.0L* cassette in a tissue-specific pattern induced by injection of the *pUAS:Cas9T2ACre; U6sgRNA1; U6sgRNA2* plasmid. No target sequence was inserted in the vector prior to injection. (Left panel) Multicolor labeling of muscle cells in the *Tg(rpl5b:Gal4)* transgenic line. (Right panel) Single YFP motor neuron labeled by expression of *UAS:Cas9T2ACre; U6sgRNA1; U6sgRNA2* transgene in the double transgenic embryos *Tg(mnx1:Gal4) × Tg(UAS:Brb1.0L)s1997t*. tdTomato marks motor neurons that do not express the *UAS* transgenic cassette. Scale bar = 50 μm. (C) Double transgenic *Tg(isl2b:Gal4; kif5aa*162/+)* × *Tg(UAS:Brb1.0L)s1997t* larva, injected with *pUAS:Cas9T2ACre; U6:Kif5aasgRNA1; U6:Kif5aasgRNA2*. *isl2b:Gal4* drives the expression of *UAS:Brb1.0L* transgene in RGC axons in the optic tectum. Note that the axon marked by *cerulean* expression, and therefore by Cre recombinase activity, shows reduced arbor size as expected from the phenotype of *kif5aa^{-/-}* RGCs transplanted in wild-type host (Auer et al. 2015). Scale bar = 30 μm. (D) Quantification of total branch length in tdTomato-positive wild-type and potentially mutant Cerulean- or YFP-positive RGC axons (analyzed in *kif5aa^{+/+}*; [*] *P*-value < 0.05 following Wilcoxon Mann-Whitney test, and *kif5aa*162/+*; [***] *P*-value < 0.001 following Wilcoxon Mann-Whitney test). Data are represented as mean ± SEM. (E) Table describing the percentage of RGCs displaying a wild-type-like (axonal length > 200 μm) and a mutant-like (axonal length < 200 μm) phenotype in the tectum of double transgenic *Tg(isl2b:Gal4; kif5aa*162/+)* × *Tg(UAS:Brb1.0L)s1997t* larva, injected with *pUAS:Cas9T2ACre; U6:Kif5aasgRNA1; U6:Kif5aasgRNA2*. (First row) tdTomato-positive cells (*UAS:Cas9T2ACre; U6:Kif5aasgRNA1; U6:Kif5aasgRNA2*-negative). (Second row) Cerulean- or YFP-positive neurons (*UAS:Cas9T2ACre; U6:Kif5aasgRNA1; U6:Kif5aasgRNA2*-positive) in *kif5aa^{+/+}* fish. (Third row) Cerulean- or YFP-positive neurons (*UAS:Cas9T2ACre; U6:Kif5aasgRNA1; U6:Kif5aasgRNA2*-positive) in *kif5aa*162/+* fish.

background, thus allowing the evaluation of cell-autonomous gene function. To this end, we combined our conditional knockout strategy with the Brainbow technology (Livet 2007; Pan et al. 2013), in which Cre recombinase stochastically activates the expression of different fluorescent proteins, allowing the differential labeling of single mutant cells in a wild-type tissue. In the *UAS:Brainbow* transgene (*Tg[UAS:Brb1.0L]^{s1997t}*) (Robles et al. 2013), Cre recombinase sites separate the cDNAs of the fluorescent proteins tdTomato, Cerulean, and YFP. When crossing a transgenic line carrying this cassette to cell-type-specific *Gal4* lines, the *Gal4* transactivator leads to the expression of *tdTomato*, in the absence of Cre-mediated recombination. In contrast, if Cre recombinase expression is induced, transcription of either *cerulean* or *YFP* is triggered (Fig. 6A). We first verified that transient expression of the *pUAS:Cas9T2ACre; U6:sgRNA1; U6:sgRNA2* construct induces stochastic recombination of the *UAS:Brainbow* allele by injecting the plasmid into one-cell stage

Tg(rpl5b:Gal4) or *Tg(mnx1:Gal4) × Tg(UAS:Brb1.0L)^{s1997t}* double transgenic embryos. Mosaic expression of fluorescent proteins was detected, as expected, in *Gal4*-positive cells (Fig. 6B) in agreement with the known *Gal4* expression patterns of the two promoters (Fig. 1B; Supplemental Fig. S2B). We next used the 2C-Cas9 vector system to generate genetic chimeras where tdTomato-fluorescent cells are wild-type, while Cerulean- or YFP-labeled cells represent potentially mutant cells. In order to achieve this differential labeling, we injected the 2C-Cas9 vector in double transgenic embryos (carrying tissue-specific *Gal4* driver and *UAS:Brainbow*). In our construct, *Cas9* and *Cre* expression occur from the same transcript; therefore, *Gal4*-expressing cells that received the *Cas9T2ACre* plasmid will recombine the *UAS:Brb1.0L* allele, inducing expression of *cerulean* or *YFP* and will potentially be knockout for the target gene. On the contrary, *Gal4*-expressing cells that did not receive the *Cas9T2ACre* plasmid will be marked by tdTomato fluorescence and wild-type (Fig. 6A).

To confirm that cell-autonomous gene function can be examined by this method, we targeted the *kif5aa* gene, coding for the motor protein Kinesin family member 5A, a (Campbell and Marlow 2013; Auer et al. 2015). We selected this gene because we have recently shown that *kif5aa* inactivation results in the reduction of axon arbor complexity via a cell-autonomous mechanism: *kif5aa*^{-/-} cells transplanted into wild-type host, after differentiation into RGCs, showed a severe reduction in axon arbor total length (Auer et al. 2015). We decided to apply the 2C-Cas9 system to inactivate the *kif5aa* gene in single RGCs while differentially labeling wild-type and potentially mutant cells in the same embryos. We used *Tg(isl2b:Gal4)* larvae to express the *Gal4* transactivator in RGCs and drive 2C-Cas9-mediated gene disruption in this neuronal population. To further increase the efficiency of the knockout strategy, we used *Tg(isl2b:Gal4)* embryos heterozygous for an existing loss-of-function mutation in the *kif5aa* locus (*kif5aa*^{*162/+}). We hypothesized that, if only one wild-type allele needs to be targeted by the Cas9/sgRNA complex, a loss-of-function phenotype would be generated with a higher probability. We therefore cloned two sgRNAs targeting the *kif5aa* locus (Auer et al. 2014b) (Supplemental Table S1) in the 2C-Cas9 vector and injected the resulting pUAS:*Cas9T2ACre;U6:kif5aasgRNA1;U6:kif5aasgRNA2* in double transgenic embryos *Tg(isl2b:Gal4;kif5aa*^{*162/+}) × *Tg(UAS:Br1.0L)s1997t*. In the injected embryos, YFP- or Cerulean-fluorescent RGCs (potentially *kif5aa* mutant) showed a decrease of total branch length compared to *tdTomato*-expressing RGCs (wild-type). As expected, an overall reduction of axonal length was detected in YFP or Cerulean RGCs compared to *tdTomato* RGCs, and it was more severe in *kif5aa*^{*162/+} than in *kif5aa*^{+/+} embryos (*tdTomato*-expressing RGCs = 261.8 ± 19.3 μm, *n* = 6; *cerulean*- or *YFP*-expressing RGCs in *kif5aa*^{+/+} = 188.8 ± 15.7 μm, *n* = 11, *P* < 0.05, Wilcoxon Mann–Whitney test; *cerulean*- or *YFP*-expressing RGCs in *kif5aa*^{*162/+} = 156.6 ± 7.7 μm, *n* = 11, *P* < 0.001, Wilcoxon Mann–Whitney test) (Fig. 6D). In addition, we noted the presence of two distinct RGC phenotypes in the Cre-labeled neurons: a wild-type-like (axonal length >200 μm) and a mutant-like (axonal length <200 μm). Remarkably, the number of cells showing a mutant-like phenotype was more abundant in the *kif5aa*^{*162/+} fish (91% of analyzed axons, *n* = 11) than in the *kif5aa*^{+/+} embryos (64% of analyzed axons, *n* = 11) (Fig. 6E). This observation confirms that the activation of the 2C-Cas9 system in a heterozygous genetic background leads to an increase of the proportion of mutant cells.

Our results demonstrate the utility of this method to generate genetic mosaic embryos and allow the labeling of multiple axons with different genotypes in distinct color combinations.

Discussion

The constant improvement of CRISPR/Cas9-mediated technologies over the past years is revolutionizing reverse genetic approaches in model organisms. Using the Gal4/UAS system for the first time in a vertebrate model to drive *Cas9* expression, our method expands the possibility of spatiotemporally regulated gene knockout, allowing researchers to tap into the resource of existing Gal4 driver lines. The generation of a stable *Tg(UAS:Cas9T2AGFP;U6:sgRNA1;U6:sgRNA2)* transgenic line, represents an advantage in the study of in vivo gene function in diverse cell types and tissues, as tissue-specific gene inactivation can be obtained simply by crossing to already established Gal4 driver lines. Although this transgenic expression system has been shown to experience somatic mosaicism from epigenetic silencing (Akitake et al.

2011), this has not diminished its great popularity and use in zebrafish and other organisms. Indeed, in some applications mosaic gene expression can even be a positive feature, allowing the analysis of the effect of gene inactivation in a sparse manner in single cells or cell clones. However, even when tissue-specific gene inactivation is achieved, the visualization of mutant cells is essential to the phenotypic analysis, an integral element that was not possible with previously published approaches.

In our work, we tested two methods to identify cells carrying loss-of-function alleles. In both cases, the use of a T2A self-cleaving peptide allows for the stoichiometric expression of the *Cas9* and a reporter gene that are translated as a single polypeptide from the same mRNA (Provost et al. 2007; Kim et al. 2011). First, we used a GFP reporter whose expression is linked to that of the *Cas9* to allow for efficient visualization of *Cas9*-expressing cells. *Cas9T2AGFP* transcription being dependent on transactivation by Gal4, the analysis of gene loss-of-function can be performed during the time frame of *Gal4* expression, which is detected by GFP fluorescence. In some cases, the phenotypic evaluation of mutant cells may be required after *Gal4* expression has terminated. For instance, when targeting the *tyr* gene with a Gal4 driver active in retinal progenitors, we could observe cells lacking pigmentation in larvae, but they did not express GFP, and therefore, absence of pigmentation could not be strictly correlated to inactivation of the *tyrosinase* gene in the unpigmented cells. The second method that we tested, 2C-Cas9, addresses the time frame issue by enabling both conditional generation of mutant cells and their permanent lineage tracing. In this assay, we used Cre activity to permanently label the population of *Cas9*-expressing cells, making it possible to analyze the phenotype resulting from targeted gene disruption after *Cas9* expression has ceased. Importantly, if Cre-mediated recombination of a floxed allele results in the expression of a fluorescent protein driven by a constitutive promoter, the label would be transmitted from the *Cas9*-expressing founder cell to its progeny and remain detectable, thus generating a clone of labeled mutant cells. By using this method in retinal progenitor cells, we successfully disrupted the *pvalb6* and *atoh7* genomic loci, thus modifying molecular identity and cell-fate determination of their progeny, respectively.

To expand further the possibility to analyze tissue-specific gene inactivation, we took advantage of the flexibility of the pUAS:*Cas9T2ACre;U6:sgRNA1;U6:sgRNA2* construct to achieve labeling of single mutant cells in an otherwise wild-type animal. So far, generation of genetic chimeras in biological systems has mainly been possible in the mouse and the fruit fly, greatly contributing to the preeminence of these animal models in genetic studies (Perrimon 1998; Wijgerde et al. 2002). In these models, the use of recombination-based approaches such as Cre/LoxP has been accepted as a gold standard technique for conditional mutagenesis. Until now, a similar approach has not been available in zebrafish. The phenotypic analysis of single mutant cells in a wild-type genetic background has relied on technically challenging transplantation experiments limited to embryonic development, which could not be temporally controlled. For this reason, genetic chimera experiments allow the investigation of only early phenotypes and cannot be used to examine the role of genes and pathways that are used repeatedly during development. Our multicolor labeling approach, that we achieved by combining the 2C-Cas9 system with the Brainbow technology (Livet 2007; Pan et al. 2013), permits the analysis of tissue-specific phenotypes of gene inactivation at a single cell resolution and enables the direct comparison of potentially mutant cells with their wild-type

counterpart in the same animal. Cre/LoxP-based approaches in zebrafish, if properly developed, could also circumvent these limitations but would require much longer generation time and challenging homologous recombination-based genomic manipulations. Furthermore the efficiency of Cre-mediated recombination is well known to depend strongly on the Cre driver line used and the target locus, and potential mosaic inactivation needs to be taken into account also in this case (Branda and Dymecki 2004).

Although the 2C-Cas9 system is meant to allow the phenotypic evaluation of mutant cells, different parameters may influence the interpretation of phenotypes arising from the targeting of a specific locus with this method. To unambiguously follow the fate of mutant cells (or clones of cells), it would be necessary to activate a reporter gene exclusively in these populations. However, in the zebrafish model system, the tools to obtain this kind of tracking are still missing. As an alternative, we propose to mark potentially mutant cells by coexpressing the Cas9 enzyme together with GFP or Cre reporters. By using this approach, not all the analyzed cells will be mutant and each mutant cell will have independently induced mutations (a percentage of these might be silent in-frame mutations). If an antibody recognizing the protein encoded by the targeted gene is available, a single staining could identify all the cells carrying protein null-mutations. Indeed, we could reveal *pvalb6* loss-of-function in the zebrafish neural retina by staining the population of Cas9-expressing cells with an antibody directed against this protein. In other cases, a molecular evaluation of the proportion of truly mutant cells within the analyzed population would be ideally needed to facilitate the statistical analysis of the behavior of the Cas9-expressing cells. A possibility to estimate the rate of mutation in the targeted tissue would be the separation of the marked Cas9-expressing cells by fluorescence-activated cell sorting (FACS). To be efficient, this procedure requires a highly pure and concentrated single-cell suspension, and it might be prone to contamination with debris or nonfluorescent cells. In addition, many transgenic lines contain fluorescent transgenesis markers (such as *myl7:GFP* or *cry:GFP*), which are wild-type fluorescent cells limiting the accuracy of the FACS for the evaluation of the mutagenesis efficiency.

In addition, the strength of the Gal4 driver used is essential in determining the efficiency of the 2C-Cas9 system, and its variability may result in differences in gene disruption. For instance, when using the *Tg(rpl5:Gal4)* line to target the *tyr* locus, we detected a mutagenesis rate that appeared lower than when using the *rx2:Gal4* driver, where we observed phenotypes suggesting a highly efficient gene disruption. This result suggests that, in driver lines displaying low expression of the Gal4 transactivator, gene inactivation may be insufficient to observe phenotypic effects of loss-of-function. Therefore strong Gal4 carrier lines need to be used in order to achieve high mutagenesis rates. The intra-cellular levels of Cas9 expression provided by the 5xUAS of our vector system were sufficient to induce gene inactivation in cell clones or single cells in our experiments. Nevertheless, further improvements in the Cas9 expression cassette could increase Cas9 protein levels. Recently, noncoding elements of the zebrafish genome have been used to increase expression of transgenes and have been incorporated in UAS vectors (Horstick et al. 2015). The addition of such features to our vector design may have a strong impact on the expression of the Cas9, thus leading to a more penetrant tissue-specific loss-of-function. In addition to strong and stable Cas9 expression, the generation of a high rate of biallelic mutations re-

quires highly active sgRNAs that will be facilitated by recently reported efficiency predictions (Moreno-Mateos et al. 2015). Furthermore, the design of sgRNAs recognizing genomic loci coding for essential domains of a protein would increase the possibility of inducing a null phenotype, even in the case of in-frame mutations (Shi et al. 2015). Importantly, we also show that one simple and powerful way to increase the efficiency of gene disruption is to inject the *pUAS:Cas9T2ACre;U6:sgRNA1;U6:sgRNA2* in a heterozygous mutant background, where one allele is already constitutively mutated.

In this report, we present for the first time in zebrafish a strategy to track the fate of individual genetically modified cells within a wild-type whole animal environment, thus allowing detection of cell-autonomous defects resulting from mutations. The genetic lineage tracing of potentially mutant cells allows the phenotypic analysis of cell populations of interest until adulthood, broadening the use of the 2C-Cas9 in fields ranging from stem cells and regeneration to cancer biology and aging. Finally, because none of the tools that we generated are restricted to zebrafish, similar experiments are readily possible in virtually any organism where transgenesis and DNA injection are feasible.

Methods

Fish lines and husbandry

For this study, the transgenic and mutant lines used are listed in Supplemental Table S2. Zebrafish strains were maintained according to standard protocols (Westerfield 2000).

Molecular cloning

The *Cas9T2AGFP* fragment was generated by inserting a PCR-amplified fragment containing the *T2AGFP* sequence from the *pCas9_GFP* plasmid (Addgene, #44719) into the *pCS2-nCas9n* plasmid (Addgene, #47929). Primers used (5' to 3') were *Bgl*III-Cas9-T2A fwd: GGTGAGATCTCCTAAGAAGAAGAGAAAGGTGA GGTCCGGCCGGCCGGAG, and *GFP* *Xba*I rev: AGCTTCTAGATTA CTTGTACAGTTC. *Bgl*III and *Xba*I enzymes were used to digest both plasmid and PCR product prior to ligation.

The *U6:sgRNA1* sequence was synthesized as G-block from IDT. *Bsm*BI restriction sites were introduced to clone the 20-bp target sequence at the predicted transcription start site (+1). The Gibson assembly kit (NEB) was used to clone the *U6:sgRNA1* and the *Cas9T2AGFP* fragments into a *pminiToI2* vector (Balciunas et al. 2006) containing a 5xUAS cassette and digested with *Eco*RI and *Cla*I. Primers used were (5' to 3'): *U6* fwd: GCAATAAACCTTGTACAAAGTGGGGGATC, and *U6* rev: GAGC TCGAATTAATTCATAATTGAAAAAAGCACCGAC to amplify the *U6:sgRNA* fragment, and *Cas9-T2A-GFP* fwd: CTGAATAGGGAA TTGGGGCCACCATGGCTTCTCCA, and *Cas9-T2A-GFP* rev: TTG TACAAGGTTTATTGCAGCTTATAATGGTTACAAATAAAG to amplify the *Cas9T2AGFP* fragment.

The second *U6:sgRNA2* cassette was designed with *Sal*I overhangs for insertion into the *p(UAS:Cas9T2AGFP;U6:sgRNA1)* plasmid linearized with the same enzyme. *Bsa*I sites were used to clone the 20-nt sgRNA target sequence at the +1 position.

The *Cas9T2ACre* fragment was synthesized by fusion of individual PCR products using Phusion High-Fidelity DNA Polymerase (Thermo Scientific). The Cre sequence was amplified from the *pCR8GW-Cre-FRT-kan-FRT 2* plasmid (Suster et al. 2011). Primers used (5' to 3') were *T2A-Cre* fwd: GAGGAAGTCTTCTAACAT GCGGTGACGTGGAGGAGAATCCCGGCCCAATGGCCAATTTAC TGACCGTACAC, and *Cre-Xba*I rev: CGATTCTAGACTAATCGCC

ATCTTCCAGC. The *Cas9T2A* fragment was amplified from the pUAS:*Cas9T2AGFP;U6:sgRNA1;U6sgRNA2*. Primers used (5' to 3') were Cas9 KpnI fwd: GGTCGGTACCGCACTGATCAAGAAATAC, and T2A rev: GTCACCGCATGTTAGAAGACTTCC. Both fragments were fused, amplified, and inserted into the pUAS:*Cas9T2AGFP;U6:sgRNA1;U6sgRNA2* digested with KpnI and XbaI. The sequence of all constructs was verified by sequencing.

Generation of stable transgenic lines

The *Tg(UAS:Cas9T2AGFP;U6:sgRNA1;U6:sgRNA2)* and *Tg(UAS:Cas9T2AGFP; U6:tyrsgRNA1;U6:tyrsgRNA2)* were generated by injecting the previously described plasmids into one-cell stage wild-type embryos. The *rx2:Gal4* vector was generated by three-way-Gateway cloning recombining a 5' entry vector carrying the *rx2* promoter fragment (Heermann et al. 2015) with a Gal4 middle entry, a polyA 3' entry vector, and a *myl7:eGFP-Tol2* destination vector (Kwan et al. 2007). To generate the *rpl5b:Gal4* vector, we cloned a 5700-bp promoter fragment of the ribosomal gene *rpl5b* in a 5' entry vector and recombined it with a Gal4 middle entry, a polyA 3' entry vector, and a Tol2 destination vector (Kwan et al. 2007). To generate the *Tg(-3.Subb:loxP-lacZ-loxP-eGFP)cn2* transgenic line (also known as cn2Tg or Hulk), we used a three-way-Gateway cloning system. p5E -3.*Subb:loxP-lacZ-loxP* was generated by inserting the result of digesting the iZEG plasmid (Novak et al. 2000) with XbaI and XhoI and making blunt ends into the p5E *ubi* (Mosimann et al. 2011) after being linearized with BamHI and blunting the ends. pDest *cry:GFP* was generated by inserting the result of digesting the p1 *cry:GFP* (Love et al. 2011) with SacII and making blunt ends into the pDestTol2pA2 (Kwan et al. 2007) that was linearized with BglII. The -3.*Subb:loxP-lacZ-loxP-eGFP; cry:GFP* construct was generated combining these four plasmids into a single one using Gateway LR Clonase II, Life Technologies: p5E -3.*Subb:loxP-lacZ-loxP*, pME GFP (Kwan et al. 2007), p3E pA (Kwan et al. 2007), and pDest *cry:GFP*. Stable transgenic lines were generated injecting plasmid DNA with Tol2 mRNA transposase and founders identified by genetic crossing and transgene transmission. The *cry:GFP* cassette contained in this transgene allows the selection of transgenic embryos due to the GFP expression in the developing lens under the control of the *gamma-crystallin* promoter.

Injections

To test the mutagenesis efficiency of *sgRNAs*, a mixture of *sgRNA* and *Cas9* mRNA was injected into one-cell stage zebrafish embryos. The final concentration was 75 ng/μL for *sgRNA* and 150 ng/μL for *Cas9* mRNA. For Tol2-mediated transgenesis, p(UAS:*Cas9T2AGFP;U6:sgRNA1;U6sgRNA2*) or p(UAS:*Cas9T2ACre;U6:sgRNA1;U6sgRNA2*) were co-injected at a concentration of 30 ng/μL with the Tol2 transposase mRNA (50 ng/μL) into the selected Tg(*Promoter:Gal4*) lines. Genomic DNA was extracted from either single embryos or pools of embryos and then used for PCR and DNA sequencing experiments.

Whole-embryos DNA extraction

For genomic DNA extraction, pools of 25 embryos at 5 dpf were digested for 1 h at 55°C in 0.5 mL lysis buffer (10 mM Tris, pH 8.0, 10 mM NaCl, 10 mM EDTA, and 2% SDS) with proteinase K (0.17 mg/mL, Roche Diagnostics). To check for frequency of indel mutations, target genomic loci were PCR-amplified using Phusion High-Fidelity DNA polymerase (Thermo Scientific). PCR amplicons were subsequently cloned into the pCR-bluntII-TOPO vector (Invitrogen). Plasmid DNA was isolated from single colonies and

sent for sequencing. Mutant alleles were identified by comparison with the wild-type sequence.

Cryosections

Embryos at the stage of 5 dpf were fixed in 4% paraformaldehyde in PBS (pH 7.4) for 2 h at room temperature and subsequently cryoprotected overnight in a 30% sucrose/0.02% sodium azide/PBS solution. Embryos were transferred to plastic molds and embedded in OCT after removal of the sucrose. The blocks were placed on dry ice before sectioning. The sections were cut with a thickness of 14 μm and mounted on Fisherbrand Superfrost plus slides (No. 12-550-15).

Immunohistochemistry

Cryosections of 5 dpf retinas were washed twice in 1× PBS/0.1% Tween-20 (PBS-T) solution. Subsequently, they were incubated 1 h at room temperature in 10% normal goat serum (Invitrogen) in PBS-T blocking solution followed by overnight incubation with 1/500 dilution of chicken primary anti-GFP (Genetex) or mouse anti-Parvalbumin antibody (Millipore). The Alexa Fluor 488 secondary antibody goat anti-chicken IgG or the Alexa Fluor 568 secondary antibody goat anti-mouse IgG (1/500, Molecular Probes) and a 1/500 dilution of DAPI (50 μg/μL) in blocking solution were added for 2 h at room temperature. After five washings in wash buffer (1× PBS/0.1% Tween-20) coverslips were placed on the slides after addition of Vectashield drops. Slides were left at room temperature for 1 h before microscopy analysis.

sgRNAs and Cas9 mRNA generation

sgRNA sequences (listed in Supplemental Table S1) were cloned into the BsaI-digested pDR274 (Addgene, #42250) vector. The *sgRNAs* were synthesized by in vitro transcription (using the Megascript T7 transcription kit #AM1334, Ambion). After transcription, *sgRNAs* were purified using an RNAeasy Mini Kit (Qiagen). The quality of purified *sgRNAs* was checked by electrophoresis on a 2% agarose gel. As a control, we used RFP-specific *sgRNAs*, whose sequence is not present in the fish genome (Supplemental Table S1). *Cas9* mRNA was generated as described previously (Hwang et al. 2013a).

FACS

Fluorescent *Cas9*-expressing cells were isolated from wild-type cells by fluorescence-activated cell sorting. 3 dpf embryos were dissociated as previously described by Manoli and Driever (2012). Cell sorting was performed on FACS Aria (BD Biosciences), and data were analyzed using FACSDiva version 6.1.2 (BD Biosciences). The GFP fluorescence was detected in the gfpBlue-B-530/30-A channel. GFP-positive and -negative cells were sorted in lysis buffer provided in the NucleoSpin Tissue Kit (Macherey-Nagel), and genomic DNA was extracted with the same kit. PCR on target genomic loci and DNA sequencing were performed as described above.

Microscopy

Low magnification images were acquired with a Leica MZ FLIII stereomicroscope (Leica) equipped with a Leica DFC310FX digital camera (Leica). Whole-eye pictures were taken with a Leica upright wide-field epifluorescence microscope using a 20× oil immersion objective. A Zeiss LSM 780 confocal microscope (Zeiss) was used for confocal microscopy, employing a 40× water immersion or 10× objective. Z-volumes were acquired with a 1- to 2-μm

resolution, and images were processed using ImageJ, Adobe Photoshop, and Adobe Illustrator software.

Data access

The sequences of mutant *tyr* clones from this study have been submitted to the NCBI GenBank (<http://www.ncbi.nlm.nih.gov/genbank/>) under accession numbers KU751772–KU751776. The sequences and the maps relative to the plasmids pUAS:Cas9T2AGFP;U6:sgRNA1;U6:sgRNA2 and pUAS:Cas9T2ACre;U6:sgRNA1;U6:sgRNA2 are available in Addgene (<https://www.addgene.org>). Plasmid numbers are #74009 and #74010.

Acknowledgments

We thank Allison Bardin, Allison Mallory, Yohanns Bellaiche, Christoph Gebhardt, Shahad Albadri, Celine Revenu, and Valerie Bercier for critical reading of the manuscript. We also thank Herwig Baier, Estuardo Robles, Joachim Wittbrodt, Koichi Kawakami, Claire Wyart, Nadine Peyri ras, and Georges Lutfalla for sharing reagents and transgenic lines. We thank all members of the Del Bene lab for fruitful discussions. We thank the Developmental Biology Curie imaging facility (PICT-IBISA@BDD, Paris, France, UMR3215/U934) member of the France-BioImaging national research infrastructure for their help and advice with confocal microscopy and the Flow Cytometry and Cell Sorting Platform at Institute Curie for their expertise. The Del Bene laboratory “Neural Circuits Development” is part of the Laboratoire d’Excellence (LABEX) entitled DEEP (ANR -11-LABX-0044), and of the  cole des Neurosciences de Paris Ile-de-France network. V.D.D. was supported by a doctoral fellowship of the Fondation Pierre-Gilles de Gennes pour la recherche and Fondation Recherche Medicale (FRM) 4th year doctoral fellowship. F.D.S. was supported by a doctoral fellowship of the Curie International PhD program. T.O.A. was supported by a Boehringer Ingelheim Fonds PhD fellowship. H.S. was funded through FPU12/03007. This work has been supported by an ATIP/AVENIR program starting grant (F.D.B.), ERC-StG #311159-Zebractum (F.D.B.), ANR-II-INBS-0014 (J.P.C.), CNRS, INSERM, Institut Curie (F.D.B.), and Mus um National d’Histoire Naturelle (J.P.C) core funding, the Fundaci n CNIC Carlos III (N.M.), the Fundaci n ProCNIC (N.M.), the Spanish Ministry of Economy and Competitiveness (Tercel and BFU2011-25297) (N.M.), and ERC Starting grant 337703 – zebraHeart (N.M.).

Author contributions: V.D.D., F.D.S., T.O.A., J.P.C., and F.D.B. conceived and designed experiments. V.D.D., F.D.S., and N.T. performed molecular cloning experiments. V.D.D. and F.D.S. performed microinjections, immunohistochemistry, and imaging experiments. T.O.A. generated essential transgenic lines. V.D.D. and F.D.S. analyzed the data. V.D.D., F.D.S., J.P.C., and F.D.B. wrote the manuscript with inputs from all the coauthors. H.S. and N.M. provided essential unpublished reagents (*Tg[−3.5bb:loxP-lacZ-loxP-eGFP]cn2* transgenic line).

References

Ablain J, Durand EM, Yang S, Zhou Y, Zon LI. 2015. A CRISPR/Cas9 vector system for tissue-specific gene disruption in zebrafish. *Dev Cell* **32**: 756–764.

Akitake CM, Macurak M, Halpern ME, Goll MG. 2011. Transgenerational analysis of transcriptional silencing in zebrafish. *Dev Biol* **352**: 191–201.

Amsterdam A, Nissen RM, Sun Z, Swindell EC, Farrington S, Hopkins N. 2004. Identification of 315 genes essential for early zebrafish development. *Proc Natl Acad Sci* **101**: 12792–12797.

Asakawa K, Kawakami K. 2008. Targeted gene expression by the Gal4-UAS system in zebrafish. *Dev Growth Differ* **50**: 391–399.

Asakawa K, Suster ML, Mizusawa K, Nagayoshi S, Kotani T, Urasaki A, Kishimoto Y, Hibi M, Kawakami K. 2008. Genetic dissection of neural circuits by *Tol2* transposon-mediated Gal4 gene and enhancer trapping in zebrafish. *Proc Natl Acad Sci* **105**: 1255–1260.

Auer TO, Duroure K, Concordet JP, Del Bene F. 2014a. CRISPR/Cas9-mediated conversion of *eGFP*- into *Gal4*-transgenic lines in zebrafish. *Nat Protoc* **9**: 2823–2840.

Auer TO, Duroure K, De Cian A, Concordet JP, Del Bene F. 2014b. Highly efficient CRISPR/Cas9-mediated knock-in in zebrafish by homology-independent DNA repair. *Genome Res* **24**: 142–153.

Auer TO, Xiao T, Bercier V, Gebhardt C, Duroure K, Concordet JP, Wyart C, Suster M, Kawakami K, Wittbrodt J, et al. 2015. Deletion of a kinesin I motor unmasks a mechanism of homeostatic branching control by neurotrophin-3. *eLife* **4**. doi: 10.7554/eLife.05061.

Balciunas D, Wangensteen KJ, Wilber A, Bell J, Geurts A, Sivasubbu S, Wang X, Hackett PB, Largaespada DA, McIvor RS, et al. 2006. Harnessing a high cargo-capacity transposon for genetic applications in vertebrates. *PLoS Genet* **2**: e169.

Balciuniene J, Nagelberg D, Walsh KT, Camerota D, Georgette D, Biemar F, Bellipanni G, Balciunas D. 2013. Efficient disruption of Zebrafish genes using a Gal4-containing gene trap. *BMC Genomics* **14**: 619.

Branda CS, Dymecki SM. 2004. Talking about a revolution: the impact of site-specific recombinases on genetic analyses in mice. *Dev Cell* **6**: 7–28.

Camp E, Lardelli M. 2001. Tyrosinase gene expression in zebrafish embryos. *Dev Genes Evol* **211**: 150–153.

Campbell PD, Marlow FL. 2013. Temporal and tissue specific gene expression patterns of the zebrafish *kinesin-1* heavy chain family, *kif5s*, during development. *Gene Expr Patterns* **13**: 271–279.

Cho SW, Kim S, Kim JM, Kim JS. 2013. Targeted genome engineering in human cells with the Cas9 RNA-guided endonuclease. *Nat Biotechnol* **31**: 230–232.

Chuang JC, Raymond PA. 2001. Zebrafish genes *rx1* and *rx2* help define the region of forebrain that gives rise to retina. *Dev Biol* **231**: 13–30.

Cong L, Ran FA, Cox D, Lin S, Barretto R, Habib N, Hsu PD, Wu X, Jiang W, Marraffini LA, et al. 2013. Multiplex genome engineering using CRISPR/Cas systems. *Science* **339**: 819–823.

Davison JM, Akitake CM, Goll MG, Rhee JM, Gosse N, Baier H, Halpern ME, Leach SD, Parsons MJ. 2007. Transactivation from Gal4-VP16 transgenic insertions for tissue-specific cell labeling and ablation in zebrafish. *Dev Biol* **304**: 811–824.

Halbig KM, Lekven AC, Kunkel GR. 2008. Zebrafish *U6* small nuclear RNA gene promoters contain a SPH element in an unusual location. *Gene* **421**: 89–94.

Heermann S, Schutz L, Lemke S, Kriegstein K, Wittbrodt J. 2015. Eye morphogenesis driven by epithelial flow into the optic cup facilitated by modulation of bone morphogenetic protein. *eLife* **4**. doi: 10.7554/eLife.05216.

Horstick EJ, Jordan DC, Bergeron SA, Tabor KM, Serpe M, Feldman B, Burgess HA. 2015. Increased functional protein expression using nucleotide sequence features enriched in highly expressed genes in zebrafish. *Nucleic Acids Res* **43**: e48.

Hwang WY, Fu Y, Reyon D, Maeder ML, Kaini P, Sander JD, Joung JK, Peterson RT, Yeh JR. 2013a. Heritable and precise zebrafish genome editing using a CRISPR-Cas system. *PLoS One* **8**: e68708.

Hwang WY, Fu Y, Reyon D, Maeder ML, Tsai SQ, Sander JD, Peterson RT, Yeh JR, Joung JK. 2013b. Efficient genome editing in zebrafish using a CRISPR-Cas system. *Nat Biotechnol* **31**: 227–229.

Jao LE, Wente SR, Chen W. 2013. Efficient multiplex biallelic zebrafish genome editing using a CRISPR nuclease system. *Proc Natl Acad Sci* **110**: 13904–13909.

Kawakami K. 2004. Transgenesis and gene trap methods in zebrafish by using the *Tol2* transposable element. *Methods Cell Biol* **77**: 201–222.

Kawakami K, Abe G, Asada T, Asakawa K, Fukuda R, Ito A, Lal P, Mouri N, Muto A, Suster ML, et al. 2010. zTrap: zebrafish gene trap and enhancer trap database. *BMC Dev Biol* **10**: 105.

Kay JN, Finger-Baier KC, Roeser T, Staub W, Baier H. 2001. Retinal ganglion cell genesis requires *lakritz*, a zebrafish *atonal* homolog. *Neuron* **30**: 725–736.

Kim JH, Lee SR, Li LH, Park HJ, Park JH, Lee KY, Kim MK, Shin BA, Choi SY. 2011. High cleavage efficiency of a 2A peptide derived from porcine teschovirus-1 in human cell lines, zebrafish and mice. *PLoS One* **6**: e18556.

Kwan KM, Fujimoto E, Grabher C, Mangum BD, Hardy ME, Campbell DS, Parant JM, Yost HJ, Kanki JP, Chien CB. 2007. The *Tol2*kit: a multisite gateway-based construction kit for *Tol2* transposon transgenesis constructs. *Dev Dyn* **236**: 3088–3099.

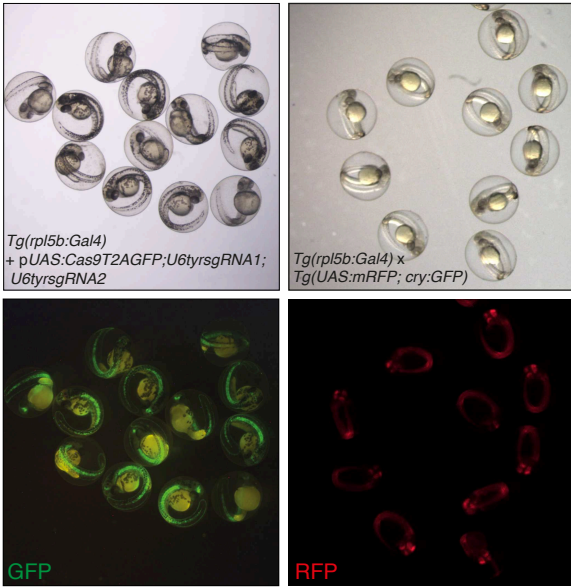
Livesey FJ, Cepko CL. 2001. Vertebrate neural cell-fate determination: lessons from the retina. *Nat Rev Neurosci* **2**: 109–118.

Livet J. 2007. [The brain in color: transgenic “Rainbow” mice for visualizing neuronal circuits]. *Med Sci (Paris)* **23**: 1173–1176.

- Love NR, Thuret R, Chen Y, Ishibashi S, Sabherwal N, Paredes R, Alves-Silva J, Dorey K, Noble AM, Guille MJ, et al. 2011. pTransgenesis: a cross-species, modular transgenesis resource. *Development* **138**: 5451–5458.
- Mali P, Yang L, Esvelt KM, Aach J, Guell M, DiCarlo JE, Norville JE, Church GM. 2013. RNA-guided human genome engineering via Cas9. *Science* **339**: 823–826.
- Manoli M, Driever W. 2012. Fluorescence-activated cell sorting (FACS) of fluorescently tagged cells from zebrafish larvae for RNA isolation. *Cold Spring Harb Protoc* **2012**. doi: 10.1101/pdb.prot069633.
- Moreno-Mateos MA, Vejnar CE, Beaudoin JD, Fernandez JP, Mis EK, Khokha MK, Giraldez AJ. 2015. CRISPRscan: designing highly efficient sgRNAs for CRISPR-Cas9 targeting *in vivo*. *Nat Methods* **12**: 982–988.
- Mosimann C, Kaufman CK, Li P, Pugach EK, Tamplin OJ, Zon LI. 2011. Ubiquitous transgene expression and Cre-based recombination driven by the *ubiquitin* promoter in zebrafish. *Development* **138**: 169–177.
- Nevin LM, Taylor MR, Baier H. 2008. Hardwiring of fine synaptic layers in the zebrafish visual pathway. *Neural Dev* **3**: 36.
- Novak A, Guo C, Yang W, Nagy A, Lobe CG. 2000. Z/EG, a double reporter mouse line that expresses enhanced green fluorescent protein upon Cre-mediated excision. *Genesis* **28**: 147–155.
- Pan X, Wan H, Chia W, Tong Y, Gong Z. 2005. Demonstration of site-directed recombination in transgenic zebrafish using the Cre/loxP system. *Transgenic Res* **14**: 217–223.
- Pan YA, Freundlich T, Weissman TA, Schoppik D, Wang XC, Zimmerman S, Ciruna B, Sanes JR, Lichtman JW, Schier AF. 2013. Zebrafish: multispectral cell labeling for cell tracing and lineage analysis in zebrafish. *Development* **140**: 2835–2846.
- Perrimon N. 1998. Creating mosaics in *Drosophila*. *Int J Dev Biol* **42**: 243–247.
- Platt RJ, Chen S, Zhou Y, Yim MJ, Swiech L, Kempton HR, Dahlman JE, Parnas O, Eisenhaure TM, Jovanovic M, et al. 2014. CRISPR-Cas9 knockin mice for genome editing and cancer modeling. *Cell* **159**: 440–455.
- Port F, Chen HM, Lee T, Bullock SL. 2014. Optimized CRISPR/Cas tools for efficient germline and somatic genome engineering in *Drosophila*. *Proc Natl Acad Sci* **111**: E2967–E2976.
- Provost E, Rhee J, Leach SD. 2007. Viral 2A peptides allow expression of multiple proteins from a single ORF in transgenic zebrafish embryos. *Genesis* **45**: 625–629.
- Robles E, Filosa A, Baier H. 2013. Precise lamination of retinal axons generates multiple parallel input pathways in the tectum. *J Neurosci* **33**: 5027–5039.
- Scott EK, Baier H. 2009. The cellular architecture of the larval zebrafish tectum, as revealed by Gal4 enhancer trap lines. *Front Neural Circuits* **3**: 13. doi: 10.3389/neuro.04.013.2009.
- Scott EK, Mason L, Arrenberg AB, Ziv L, Gosse NJ, Xiao T, Chi NC, Asakawa K, Kawakami K, Baier H. 2007. Targeting neural circuitry in zebrafish using GAL4 enhancer trapping. *Nat Methods* **4**: 323–326.
- Shen Z, Zhang X, Chai Y, Zhu Z, Yi P, Feng G, Li W, Ou G. 2014. Conditional knockouts generated by engineered CRISPR-Cas9 endonuclease reveal the roles of Coronin in *C. elegans* neural development. *Dev Cell* **30**: 625–636.
- Shi J, Wang E, Milazzo JP, Wang Z, Kinney JB, Vakoc CR. 2015. Discovery of cancer drug targets by CRISPR-Cas9 screening of protein domains. *Nat Biotechnol* **33**: 661–667.
- Sprague J, Bayraktaroglu L, Bradford Y, Conlin T, Dunn N, Fashena D, Frazer K, Haendel M, Howe DG, Knight J, et al. 2008. The Zebrafish Information Network: The zebrafish model organism database provides expanded support for genotypes and phenotypes. *Nucleic Acids Res* **36**: D768–D772.
- Suster ML, Abe G, Schouw A, Kawakami K. 2011. Transposon-mediated BAC transgenesis in zebrafish. *Nat Protoc* **6**: 1998–2021.
- Westerfield M. 2000. *The zebrafish book. A guide for the laboratory use of zebrafish (Danio rerio)*, 4th ed. University of Oregon Press, Eugene, OR.
- Wijgerde M, McMahon JA, Rule M, McMahon AP. 2002. A direct requirement for Hedgehog signaling for normal specification of all ventral progenitor domains in the presumptive mammalian spinal cord. *Genes Dev* **16**: 2849–2864.
- Yin L, Maddison LA, Li M, Kara N, LaFave MC, Varshney GK, Burgess SM, Patton JG, Chen W. 2015. Multiplex conditional mutagenesis using transgenic expression of Cas9 and sgRNAs. *Genetics* **200**: 431–441.

Received June 22, 2015; accepted in revised form February 24, 2016.

A



B

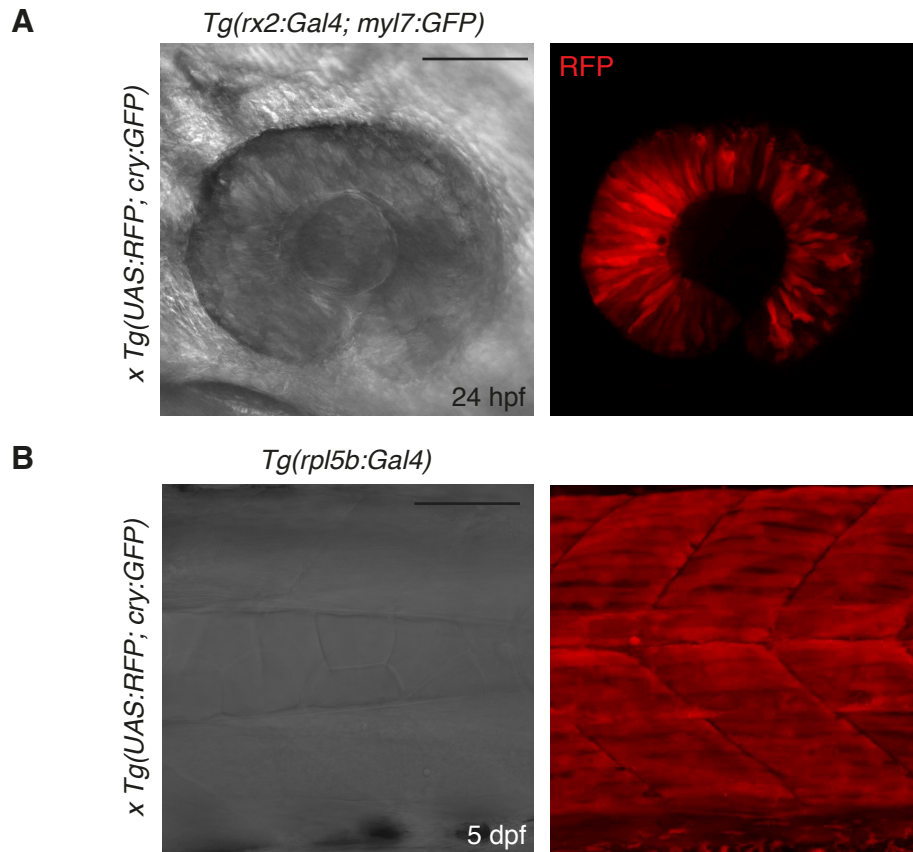
Target 1 mutations

5'-AGCGTTTGGACTGGAGGACTTCTGGGGAGGTGCAGACT-3'

5'-AGCGTTTGGACTGGAGGACTTCTG - - - - - ACT-3' Δ11 (x3)

5'-AGCGTTTGGACTGGAGGACTTCTGGGG - TGTGCAGACT-3' Δ2; +1

Supplementary Figure 1



Supplementary Figure 2

sgRNA name	Target gene	Target sequence	Mutagenesis efficiency
TyrsgRNA1	Tyrosinase	GGACTGGAGGACTTCTGGGG	90% (18/20)
TyrsgRNA2	Tyrosinase	GGCGTTTCTGCCTTGGCATC	10% (2/20)
Ath5sgRNA1	Ath5	GGCATATAAACCCAATCCAC	20% (4/20)
Ath5sgRNA2	Ath5	GGCCGAGCTGTGCAGACTCC	13% (4/32)
Kif5aasgRNA1	Kif5aa	GGAATGATGCCCATCTGCTG	22% (4/18)
Kif5aasgRNA2	Kif5aa	GGGACGACACGGTCATCATC	38% (6/16)
Pvalb6sgRNA	Pvalb6	CGCTATTGTCGGCATCCAGG	47% (9/19)
ctlsgRNA1	RFP	GGCCACGAGTTCCGAGATCGA	-
ctlsgRNA2	RFP	GGACATCACCTCCCACAACG	-

Supplementary Table 1

Transgenic or mutant zebrafish line used in this study	Gene	Description	Original Reference
<i>kif5aa</i> ^{T6Z +/-}	<i>kif5aa</i>	TALEN mediated loss-of-function allele of <i>kif5aa</i> .	(Auer et al., 2015)
<i>Tg(isl2b:Gal4)</i>		A promoter fragment of the <i>isl2b</i> gene drives expression of the Gal4 transactivator in the entire RGC population of the retina.	(Ben Fredj et al., 2010)
<i>Tg(gSA2AzGFF49A)</i>		Transgenic line generated by gene-trap approach. An optimized version of the Gal4 (GFF) is expressed in periventricular neurons (PVNs) at the level of the optic tectum (OT).	(Muto et al., 2013)
<i>Tg(rpl5b:Gal4)</i>		A promoter fragment of the <i>rpl5b</i> ribosomal gene drives quasi-ubiquitous expression of the Gal4 transactivator.	generated in this report
<i>Tg(s1020t)</i>		Transgenic line generated by an enhancer-trap screen. Gal4 is expressed in the thalamus, spinal cord and bipolar cells of the retina.	(Scott and Baier, 2009)
<i>Tg(mnx1:Gal4)</i>		A promoter containing three copies of the <i>mnx1</i> enhancer drives the expression of Gal4 in spinal cord primary motor neurons.	(Zelenchuch and Brusés, 2011)
<i>Tg(rx2:Gal4; myl7:GFP)</i>		A promoter fragment of the <i>rx2</i> gene drives expression of Gal4 in retinal progenitors. The heart-specific promoter <i>myl7</i> drives GFP (<i>myl7:GFP</i>) as transgenesis marker.	generated in this report
<i>Tg(UAS:Cas9T2AGFP; U6sgRNA1; U6sgRNA2)</i>		The simultaneous expression of the Cas9 endonuclease and the GFP reporter depends on the activation of an UAS. Two sgRNAs empty expression cassettes are present.	generated in this report
<i>Tg(UAS:Cas9T2AGFP; U6tyrsgRNA1; U6tyrsgRNA2)</i>	<i>tyr</i>	The simultaneous expression of the Cas9 endonuclease and the GFP reporter depends on the activation of an UAS. Two U6 promoter sequences drive the transcription of sgRNAs targeting the <i>tyrosinase</i> gene.	generated in this report
<i>Tg(-3.5ubb:loxP-lacZ-loxP-eGFP)cn2</i>		The ubiquitin promoter (Mosimann et al, 2011) is placed 5' of a floxed lacZ sequence followed by GFP cDNA. Expression of GFP in the lens driven by a crystalline promoter fragment (<i>cry</i>) is used as transgenesis reporter.	generated in this report
<i>Tg(UAS:Brb1.0L)^{s1997t}</i>		The expression of a Brainbow cassette (Pan et al., 2013) is dependent of the activation of an upstream activator sequence (UAS).	(Robles et al., 2013)
<i>Tg(UAS:RFP; cry:GFP)</i>		A UAS drives the Gal4-mediated transcription of the cDNA sequence of the red fluorescent protein (RFP). Expression of GFP in the lens driven by a crystalline promoter fragment (<i>cry</i>) is used as transgenesis reporter.	(Auer et al., 2014)

Supplementary Table 2

Figure S1 Mutagenesis efficiency at the *tyr* locus in the *Tg(rpl5b:Gal4)* line

(A) Left panel: whole mount image of *Tg(rpl5b:Gal4)* embryos transiently expressing the *pUAS:Cas9T2AGFP;U6:tyrsgRNA1;U6:tyrsgRNA2* used for FACS analysis. Right panel: double transgenic *Tg(rpl5b:Gal4) x Tg(UAS:RFP; cry:GFP)* larvae. RFP is used as an independent reporter of Gal4 transactivation and confirms non-ectopic expression of the *pUAS:Cas9T2AGFP;U6:tyrsgRNA1;U6:tyrsgRNA2*.

(B) Representative mutations at the *tyr* locus.

Figure S2 Gal4 expression domains in the *Tg(rx2:Gal4; myl7:GFP)* and *Tg(rpl5b:Gal4)* lines

(A) Confocal image of Gal4-induced eye-specific expression of *UAS:RFP* in a 24 hpf double transgenic *Tg(rx2:Gal4; myl7:GFP) x Tg(UAS:RFP; cry:GFP)* embryo. Scale bar: 100µm. (B) Confocal image of muscle cells expressing *UAS:RFP* in a 5 dpf double transgenic *Tg(rpl5b:Gal4) x Tg(UAS:RFP; cry:GFP)* embryo. Scale bar: 50µm.

Table S1 Sequence and efficiency of the sgRNAs used in this study.

The mutagenesis rate was assessed by injection of in vitro transcribed sgRNA with synthetic Cas9 mRNA into one-cell stage wild-type embryos. To estimate the number of mutations induced we extracted DNA from a pool of 25 injected embryos and subsequently PCR amplified the targeted locus. Single PCR amplicons were sequenced and mutant alleles were identified after alignment with the wild-type sequence.

Table S2 Transgenic lines used in the report

Chapter III: Discussion

1. A new function for an old protein

Understanding the basis of synaptic lamination is critical to gain deeper insights on how complex neural networks form. The vertebrate visual system has served as a valuable model for the investigation of the mechanisms underlying the segregation of neurons and neural processes in specific synaptic layers (Baier 2013). While an extremely complex molecular code has been shown to mediate cell-surface recognition in the IPL of the retina, the factors involved in the formation of distinct laminae in retinorecipient nuclei, such as the optic tectum (OT)/superior colliculus (SC), are largely unknown.

In our first study, we focused on identifying molecular cues that may regulate laminar organization of RGC axonal processes in the neuropil of the zebrafish developing OT. The technical advantages of the zebrafish model made it possible to investigate the *in vivo* function of the large secreted ECM protein Reelin during retinotectal system development.

Decades of studies have unraveled multiple functions of Reelin during brain development. However, the majority of these studies have focused on the functional dissection of the Reelin signaling pathway in neuronal migration for layer formation in mouse cortical structures (D'Arcangelo 2014). Up to date, only few reports provide experimental evidence for a possible involvement of Reelin in the process of axon guidance (Borrell et al 2007, Su et al 2011).

Although during the processes of neuronal lamination and axonal layering positional cues act on different cellular structures, our results, in line with findings from other groups, suggest that in some cases it is possible to draw a common mechanism of action.

1.1 Reelin acts as a long-range molecular cue in the zebrafish tectal neuropil

Previous mouse studies have shown that different *reelin*-expressing cell populations, such as Cajal-Retzius cells or granule cell precursors, are situated in superficial layers of laminated embryonic brain structures and promote neuronal migration in the adjacent tissue (Ogawa et al 1995). Similarly, in our study, the anatomical position of the SINs at the surface of the tectal neuropil and their high levels of *reelin* expression renders them ideal for exerting a neurodevelopmental role in addition to their previously characterized function in the processing of visual information (Del Bene et al

2010, Preuss et al 2014). Importantly, the analysis of the spatial distribution of Reelin in the larval zebrafish optic tectum revealed the presence of a superficial-to-deep concentration gradient. This study thus represents the first demonstration of a spatial gradient of the Reelin protein in the vertebrate central nervous system. Interestingly, in the mouse brain, immuno-labeling analyses of cortical slices with epitope-specific antibodies have revealed that the central fragment of Reelin is able to reach the deeper layers of the cortical plate (Jossin et al 2007). This observation suggests that the *in vivo* cleavage of the Reelin protein generates signaling molecules with long-range action, away from the secreting cells. Consistently, another study showed that Reelin influences the migratory behavior of neurons that are placed in deep layers of the developing cortical plate, by promoting the switch from a multipolar to a bipolar morphology (Jossin & Cooper 2011). In an analogous manner, in zebrafish, we reasoned that SINS-secreted Reelin could provide guidance to RGC axons across several laminae of the tectal neuropil. To test this hypothesis, we characterized the transcriptional dynamics of the main downstream components of the Reelin canonical pathway in the zebrafish retina with a focus on the RGC population. The results obtained by *in situ* hybridization revealed that the expression domains of these factors differ from those observed in mouse. In the mammalian retina the receptors VLDLR and LRP8 (also known as ApoER2) and the intracellular adaptor protein Dab1 are expressed in the ganglion cell layer (GCL) in a subset of RGCs (Su et al 2011). On the contrary, in the zebrafish retinal tissue, we detected a widespread expression of *vdldr* and *dab1a* (ortholog of the mammalian *dab1*) throughout the GCL. Additionally, these two factors were expressed in the amacrine cell (AC) population. In contrast, expression of *lpr8* and *dab1b* was detected in ACs and, to a lesser extent, in bipolar cells. This expression pattern of *vdldr* and *dab1a* argues for a presumable sub-functionalization, subsequent to a duplication event relating to the teleost-specific whole genome duplication event in the case of *dab1* (Herrero-Turrión et al 2010). At the same time, the fact that the entire GCL displays expression of *vdldr* and *dab1a* suggests that in zebrafish Reelin the whole RGC population and not only on a specific subpopulation is potentially responsive to Reelin signaling. These data are consistent with the hypothesis that, in the tectal neuropil, Reelin may act not only on RGC axons projecting in the most superficial tectal layers, close to the Reelin source (the SINS) but also on retinal afferents targeting deeper sublaminae.

1.2 Reelin signaling is involved in tectal synaptic lamination

Based on the observation that *vldlr* and *dab1a* are expressed in the GCL layer of the zebrafish retina at the developmental stage of 3 days post fertilization (dpf), concomitantly with RGC axons invading the tectal neuropil, we investigated Reelin contribution to the process of retinotectal laminar targeting.

The loss-of-function allele of *reelin* that we generated by TALENs-mediated gene disruption allowed for the *in vivo* analysis of Reelin function. Homozygous mutant fish did not show obvious phenotypic consequence during larval development and were fertile and viable at the adult stage, as is the *reeler* homozygous mouse (Falconer 1951). At the larval stage of 5 dpf, when the retinotectal circuit is established, our experimental set-up enabled the analysis of the effect of Reelin loss on axonal pathfinding at single cell resolution. While no defects in RGC axon navigation and retinotopic targeting could be detected in *reelin* mutant larvae, lamina-specific targeting was severely impaired.

Previous studies have unveiled a function for Reelin in class-specific targeting of axons in the mammalian visual system, namely in the retinogeniculate (Su et al 2011) and retinocollicular circuits (Baba et al 2007). In the retinocollicular system of the *reeler* mouse, the reported aberrant lamination pattern of RGC axons is a secondary effect of an abnormal architecture of the target retinorecipient superior colliculus (SC). In contrast, the defects in retinogeniculate targeting observed in the *reeler* mouse do not arise from a disrupted cellular lamination of the target LGN. In this case, the subset of *dab1*-expressing ipRGC axons, whose projection pattern is affected by the loss of Reelin, are truly mistargeted and not simply targeting correct synaptic partners that have migrated into inappropriate LGN subnuclei. Our data provide compelling evidence of a direct action of Reelin on RGC axons, through a mechanism that is analogous to the one observed in the retinogeniculate system.

However, while in the mouse visual system LGN-derived Reelin is proposed to be responsible for retinogeniculate axonal targeting, we formally demonstrate that tectum-derived Reelin is involved in retinotectal lamination by generating mutant/wild-type chimeric embryos *via* blastomere transplantations. The analysis of *reelin* mutant RGC axons growing into a wild-type optic tectum revealed a normal lamination pattern, while RGC wild-type axons innervating a *reelin* mutant neuropil displayed aberrant layering. Taken together, our results demonstrate a non-RGC-autonomous requirement of Reelin for retinotectal targeting, ruling out a contribution in the process of the Reelin protein expressed by RGCs.

Moreover, our findings indicate that Reelin exerts its function on RGC axons *via* VLDLR and Dab1a. CRISPRs/Cas9-mediated targeted mutagenesis of both *vldlr* and

dab1a resulted in the impairment of axon lamination in homozygous mutant fish, phenocopying the one observed in *reelin* mutant fish. While these results parallel those supporting a Dab1-mediated signaling in the retinogeniculate targeting in mouse (Su et al 2011), they differ from the observations made in previous studies on *vldlr* mutant mice. Importantly, the misrouting of retinal axons detected in the compound *vldlr^{-/-}/lrp8^{-/-}* fails to accurately recapitulate the axonal targeting defects detected in *reeler* or *scrambler* LGN, suggesting that these canonical Reelin receptors are not involved in Reelin-mediated retinogeniculate targeting (Su et al 2013). In contrast, our data strongly support that VLDLR is activated by the extracellular Reelin to regulate retinotectal targeting, which is consistent first with the phenotype observed in mutant larvae and secondly with the widespread expression of the receptor in the GCL. Therefore, it is possible that, while in fish Reelin mediates the laminar arrangement of the whole population of RGC axons via VLDLR, different Reelin-dependent and Reelin-independent mechanisms may have arose during evolution to achieve a tight regulation of class-specific targeting of retinal afferents.

Together, our loss-of-function approaches combined with *in vivo* labeling of retinal axons have allowed us to explore with unprecedented detail the function of Reelin canonical signaling pathway in lamina-specific retinotectal targeting.

1.3 Reelin acts as an attractive molecular cue for ingrowing RGC axons

Up to date, several contrasting models have been proposed to explain Reelin function. The ECM protein has been suggested to act as a chemo-attractant (Gilmore & Herrup 2000), repellent (Ogawa et al 1995, Schiffmann et al 1997), detachment (Dulabon et al 2000, Sanada et al 2004) or stop (Sanada et al 2004) signal for radially migrating neurons. However, other studies indicate that none of these models sufficiently explain Reelin function (Luque 2004, Magdaleno et al 2002) that might ultimately be context dependent.

In the attempt to influence the laminar choice of retinal axons, we induced over-expression of the canonical Reelin receptor VLDLR in an RGC-specific manner. This way, we were able to bias the laminar choice of RGCs projections towards superficial tectal layers such as the SFGS and SO. Based on this observation, we propose that Reelin acts as attractive molecular cue on RGC axons innervating the tectal neuropil. This finding could be further supported by additional experiments. For instance, retinal explants cultured in the presence of *reelin*-expressing cells would confirm a chemo-attractant role of the protein on the neural processes of the retinal ganglion cell population. The apparent shift of RGCs axons highly expressing VLDLR leads to the

hypothesis that a differentially expression of the endogenous VLDLR is present in a wild-type genetic background. In the future, different experimental approaches could be used to test this hypothesis. For example, CRISPR/Cas9-mediated strategies would allow the targeted integration of a transgene coding for a chosen fluorophore in the *vldlr* genomic locus in order to generate a fusion fluorescent receptor (Auer et al 2014, Hisano et al 2015, Hoshijima et al 2016, Kimura et al 2014, Li et al 2015). *In vivo* tracing of the Vldlr-XFP protein would give information on the relative expression of the receptor in RGC axons. Alternatively, a similar readout would be offered by a more classical transgenesis method based on the integration in the fish genome of a bacterial artificial chromosome (BAC) carrying the *vldlr* genomic locus and the in-frame sequence of an XFP reporter (Busmann & Schulte-Merker 2011, Suster et al 2011). According to our model, we would predict the presence of a gradient of expression of the VLDLR receptor in RGC axons in response to the superficial-to-deep Reelin concentration gradient. Therefore, RGCs highly expressing VLDLR may preferentially target superficial layers of the tectal neuropil and *vice versa*.

1.4 Reelin spatial distribution is important for its function

We propose that the relative expression of VLDLR might direct the RGC processes towards a defined layer in response to the concentration of the Reelin protein within the same layer. In line with this hypothesis, we provided evidence for direct correlation between the Reelin spatial distribution and correct sublamina arrangement by RGCs axons. Strikingly, induced expression of a GFP-tagged Reelin at the level of the periventricular zone, anatomically opposite to the tectal surface, caused a severe perturbation of retinotectal lamination. This phenotype is presumably due to an interference with the spatial distribution of the endogenous Reelin protein. An in-depth analysis of the laminar targeting of RGCs in presence of periventricular neurons and radial glia cells over-expressing Reelin would further support the above-discussed hypothesis of an attractive gradient. If this were the case, a preferential innervation of deeper laminae by retinal axons would be observed. A clear readout would need the experiment to be performed in a *reelin* mutant background where, in absence of *reelin*-expression by SINEs, an inverted gradient would be generated.

The idea that the spatial distribution of Reelin is crucial for its function is consistent with the findings from mouse studies. For instance, ectopic Reelin expression in the developing neocortex polarizes the dendrites of developing neurons towards the reelin source within the cortical plate (Kubo et al 2010). Another study has implicated Reelin signaling as a determinant of the deployment of the Golgi apparatus into the future leading process of cortical neurons (Meseke et al 2013b). Interestingly, the

aforementioned study shows that the selection of the dendrite that will later become the leading process depends on Reelin concentration. In fact, the authors observed that the translocation of the Golgi apparatus would selectively occur in the dendrite that was most proximal to the Reelin source.

In conclusion the spatial distribution of Reelin may contribute to the selection of the neuritic process that becomes the apical dendrite. In a similar manner, our data suggest that Reelin levels across several neuropil laminae are important for the selection by RGC axons of a specific target layer in the tectal neuropil.

1.5 Two gradients for laminar-specific RGC axonal targeting

It is noteworthy to say that to date, Slit1/Robo2 signaling pathway is the only one shown to provide long-range lamina-specific guidance to retinal afferents in the zebrafish tectal neuropil. As already described, Slit1 is presumably distributed in a superficial-to-deep gradient and its enrichment at the tectal surface depends on the presence of Collagen IV α 5 (Xiao et al 2011). Given its repulsive nature, the Slit1 gradient alone does not seem sufficient to convey proper positional information to ingrowing neurites. This suggests the presence of a counter-gradient to achieve a fine modulation of laminar segregation of axons and dendrites. In our work, we show that Reelin displays a spatial distribution that is analogous to Slit1 distribution but requires different factors, such as heparane sulphate proteoglycans (HSPGs) for anchoring to the ECM. These observations lead to the hypothesis that Reelin/VLDLR and Slit1/Robo2 pathways act simultaneously during retinotectal system development but need different ECM components for their gradient formation. According to this model, two extracellular gradients with similar distribution but opposite effects, repellent in the case of Slit1 and attractant in the case of Reelin, would ensure a precise and timely axonal lamination process. Along the same line, it would be fair to assume that a tight regulation of relative expression levels of the two receptors, Robo2 and VLDLR, in different subsets of RGC axons controls the targeting of specific sublaminae.

In the future, it would be interesting to analyze the retinotectal circuit development in a system unable to respond to both Slit1 and Reelin signaling pathways. This possibility could be assessed by the generation of double mutant fish (*astti272z/vldlr^{-/-}*) carrying loss-of-function mutation for both *robo2* and *vldlr*.

A recent study in zebrafish showed that the loss of the lamination cue provided by Robo2 does not prevent the formation of a functional direction-selective circuit in the tectal neuropil but delays the process to later stages of development (Nikolaou & Meyer 2015). The authors conclude from their observations that lamination guidance cues are dispensable for the correct wiring of neural networks but important to increase

the speed with which synaptic partners find each other. According to their findings, a crucial mechanism allowing functional recovery of the retinotectal system would be the structural plasticity of neuronal processes. This feature would enable the establishment of connections between synaptic partners even in conditions of altered lamination. This idea finds support in a very recent anatomical and functional analysis of the lemniscal pathway, a circuit conveying whisking and touch information to the rodent's brain, in the *reeler* mouse (Wagener et al 2016). This neural network is composed by thalamocortical axons (TCAs) projecting to target cells located in the layer IV of the primary somatosensory cortex. Interestingly, despite the severe cellular intermingling of the *reeler* cortex, TCAs still target misplaced layer IV neurons and form with these functional synaptic connections. Together, the results from these studies show that: 1. synaptic specificity mechanisms are in place that are independent of the correct placement of the target cells. 2. lamination is nevertheless facilitating a fast set-up of the proper connections by minimizing the time needed for a neuronal process (axon/dendrite) to find its synaptic partner. This last observation is important from an evolutionary point of view for timely function of neuronal circuits that are e.g. involved in visually evoked escape or hunting behaviors.

However, the above-described studies are limited to the analysis of animals carrying loss-of-function mutations for only one gene, either Reelin in mouse or Robo2 in zebrafish. For instance, Nikolau et al. performed their experiments in the *astti272z* mutant tectum, where the Reelin signaling pathway is still in place. The same analysis in double mutant fish (*astti272z/vldlr^{-/-}*) would allow gaining more insights on the functional requirement of the two pathways. We can predict three possible scenarios: 1. the same phenotype detected in the *astray* mutant would be observed 2. the development of a functional circuit would be additionally delayed 3. the RGC axonal mistargeting would be too severe and would prevent the correct contact formation between synaptic partners. Based on the results from this experiment, accurate conclusions on the function of synaptic layers in the nervous system can be drawn.

Altogether, our results suggest that, at least two extracellular factors, such as Reelin and Slit1, are responsible for establishment of stereotyped layers in the developing zebrafish tectal neuropil. Thereby the retinorecipient tissue would be pre-patterned before the innervation by RGCs axons to provide a substrate for axonal growth in a lamina-specific manner. Giving the widespread expression of these two molecules in various regions of the vertebrate nervous system, it is possible that this represents a conserved patterning mechanism in other regions of the central system that show lamination and discrete synaptic distribution.

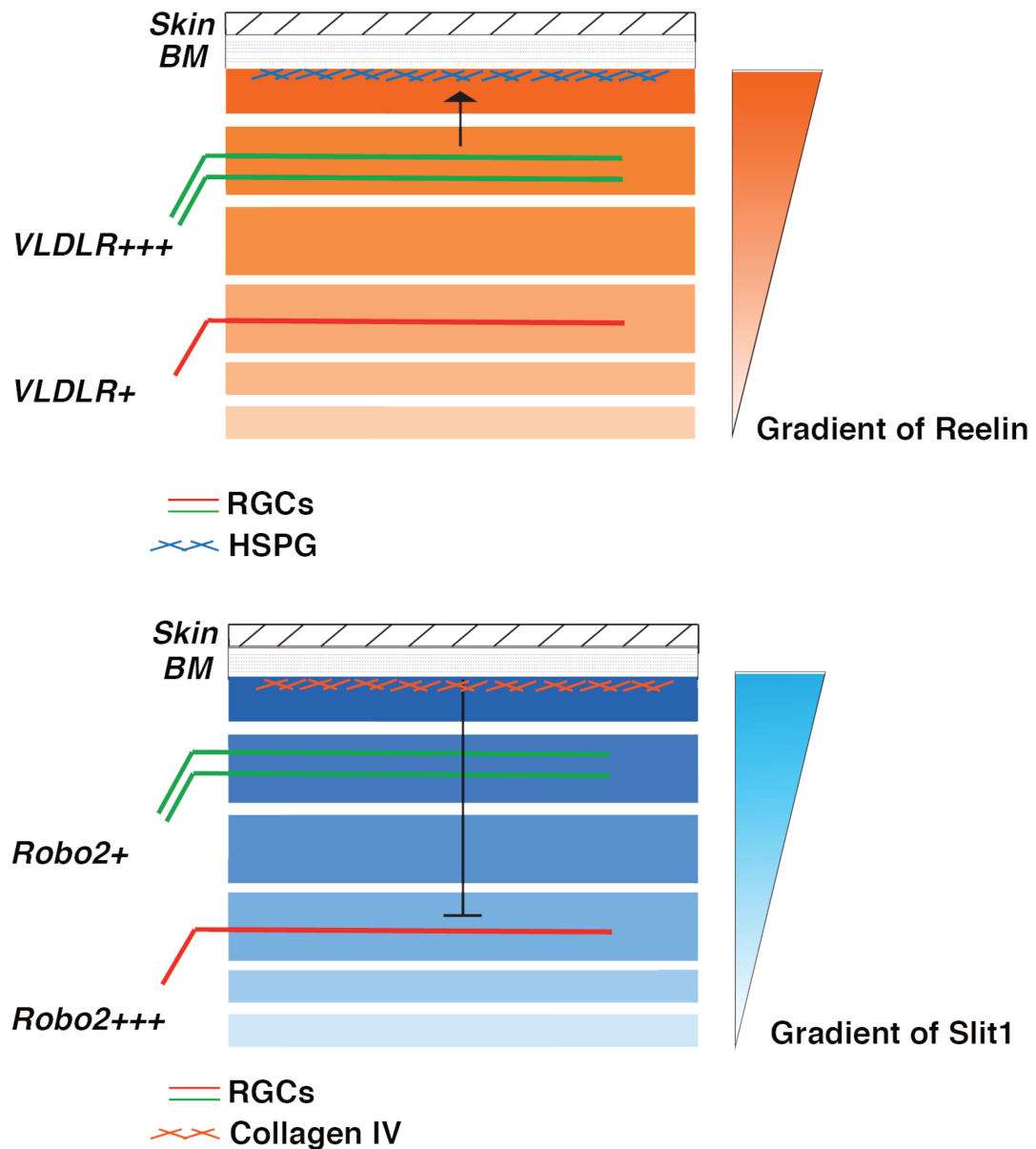


Figure 11. Model of Reelin and Slit1 mechanism of action in laminar patterning of the zebrafish tectal neuropil. Reelin is secreted by SINs from the most superficial layer of the tectal neuropil. The enrichment of Reelin protein in the basement membrane (BM), depending on HSPG, leads to the formation of a superficial-to-deep concentration gradient. The distribution in a gradient allows Reelin to act across multiple synaptic laminae as long-range attractive molecule for VLDLR-expressing RGC axons. A differential expression of VLDLR by distinct subset of RGCs may lead to precise lamina targeting (upper panel). Slit1 is secreted by tectal cells and accumulates in the BM through binding to collagen IV. Slit1 is presumably distributed in a superficial-to-deep concentration gradient in the tectal neuropil and acts as long-range repulsive molecule on Robo2-expressing RGC axons. Different expression levels of Robo2 would define lamina-specific targeting (lower panel). The two extracellular guidance system may act simultaneously to pre-pattern synaptic laminae in the zebrafish tectal neuropil during the developmental window preceding the ingrowth of RGC axons, thereby ensuring precise lamina-specific targeting *ab initio*.

2. Tissue-specific gene disruption in zebrafish

In the last few years genome-editing techniques, such as TALENs and the CRISPRs/Cas9 system, have facilitated the efficient generation of loss-of-function alleles in multiple model organisms including zebrafish. In our first study, we have ourselves employed these methods to induce targeted gene disruption of the factors involved in Reelin signaling pathway for an in-depth characterization of its function. Importantly, none of the induced loss-of-function mutations in the three alleles analyzed (*reln*, *vldlr* and *dab1a*) led to obvious phenotypical consequences. Given that the expression of Reelin is restricted to the CNS, the absence of major developmental defects could be expected. However, several studies focus on the investigation at late developmental stages or in postmitotic cells of factors also involved in crucial processes such as early embryonic development or cell-cycle progression. In these cases, a traditional loss-of-function approach would lead to early lethality limiting the analysis of specific late phenotypes. This underlies the need in the zebrafish community for an inducible system to allow targeted mutagenesis.

A previous study (Ablain et al 2015) has pioneered the use of the CRISPR/Cas9 methodology to generate conditional gene knock-out *via* tissue-specific expression of *cas9* in zebrafish. This strategy takes advantage of cell-type-specific promoters to control the spatiotemporal expression of the Cas9 enzyme. The modularity of the vector system makes it readily applicable for locus disruption of any gene of interest in the desired tissue. However, this approach requires previous knowledge on the chosen promoter sequences that will drive *cas9* expression. These genomic sequences are often unknown or not well annotated. In our work, we overcame this limitation by developing a strategy that takes advantage of the Gal4/UAS (derived from yeast) to drive expression of the Cas9 enzyme. Importantly, in zebrafish, this is one of the most common methodologies ensuring cell-specific expression of transgenes. Gene- and enhancer-trap methods have been applied to establish a significant number of Gal4 transgenic lines (Asakawa & Kawakami 2008, Balciuniene et al 2013, Davison et al 2007, Kawakami et al 2010, Scott & Baier 2009), among which several are neural-specific (Asakawa et al 2008, Scott et al 2007). Notably, in this lines the Gal4 open reading frame (ORF) is randomly integrated in the fish genome through Tol2-based transposition and the insertion site is not mapped, therefore the sequence of the promoter elements driving Gal4 expression is unknown. Thereby our strategy does not require previous knowledge on promoter sequences to induce *cas9* expression since this is provided by cell-type-specific Gal4 transcription.

In the method that we developed, the transient or stable UAS-dependent expression of Cas9, coupled with constitutive transcription of gene-specific sgRNAs, allows the inactivation of any gene of interest in any Gal4 line. Therefore, gene disruption can be achieved in multiple tissues by generating a unique transgenesis vector, containing gene-specific sgRNA, to be injected into different Gal4 driver lines.

2.1 Genetic labeling of *ca9*-expressing cells via 2C-Ca9

The visualization of cells carrying loss-of-function alleles is essential to correlate phenotype with genotype for the analysis of gene function. This represents an issue that is not addressed by previously published methods. In our approach, we marked the population of the *cas9*-expressing cells by using the viral T2A self-cleaving peptide (Provost et al 2007) ensuring the stoichiometric synthesis of the Cas9 enzyme and the fluorescent reporter GFP from the same mRNA. This enables the analysis of the phenotypes arising from Cas9-induced gene disruption. In this first approach GFP expression is strictly dependent on the temporal activity of the promoter driving Gal4 expression, thus restricting direct detection of potential mutant cells to a limited time window. This caveat reduces the possibility of analyzing loss-of-function phenotypes after Gal4 transactivation activity has terminated. To circumvent this issue we proposed to use the activity of the Cre enzyme, a topoisomerase that catalyzes the site-specific recombination of DNA between loxP sites (Branda & Dymecki 2004, Pan et al 2005), to constitutively label the population of *cas9*-expressing cells. The use of Cre allows permanent labeling and clonal analysis of potentially mutated cells even after Gal4 expression has ended. This last approach greatly expands the applicability of our system (2C-Cas9) by offering the possibility to analyze the effect of gene disruption in two main cell types: progenitor cells and differentiated cells (Figure 11). Our work provides evidence of the effectiveness of the 2C-Cas9 methodology in targeted mutagenesis in both cell types. In one case, we successfully disrupted the *atoh7* gene, involved in the specification of RGCs, in retinal stem cells of the developing zebrafish retina. We could modify cell fate determination of retinal progenitor cells and generate labeled loss-of-function clones lacking the population of retinal ganglion cells. In another set of experiments, by combining the 2C-Cas9 vector system with the Brainbow technology, we achieved differential labeling of potentially mutant and wild-type cells in the same animal. In this case, we targeted the genomic locus coding for the motor protein Kinesin family member 5A (*kif5aa*) in differentiated RGCs. Here we detected the expected cell-autonomous effect of the loss-of-function of this gene on axonal branching (Auer et al 2015). Importantly, the generation of genetic mosaics by our system allowed a direct comparison of mutant cells with reduced

axonal branching and the wild-type counterpart displaying normal branching phenotype.

Our proof-of-principle experiments open an interesting avenue for the analysis of gene function in a broad range of studies. On one hand, induced mutagenesis in progenitor cells the genetic lineage tracing of potentially mutated cells represents a powerful tool for the field of stem cell and cancer cell biology. On the other hand, cell-specific gene-knock-out in differentiated cells will be extremely useful in the field of neurobiology, being applicable for the investigation of mechanisms underlying not only neurodevelopment but also maintenance and function of neural networks.

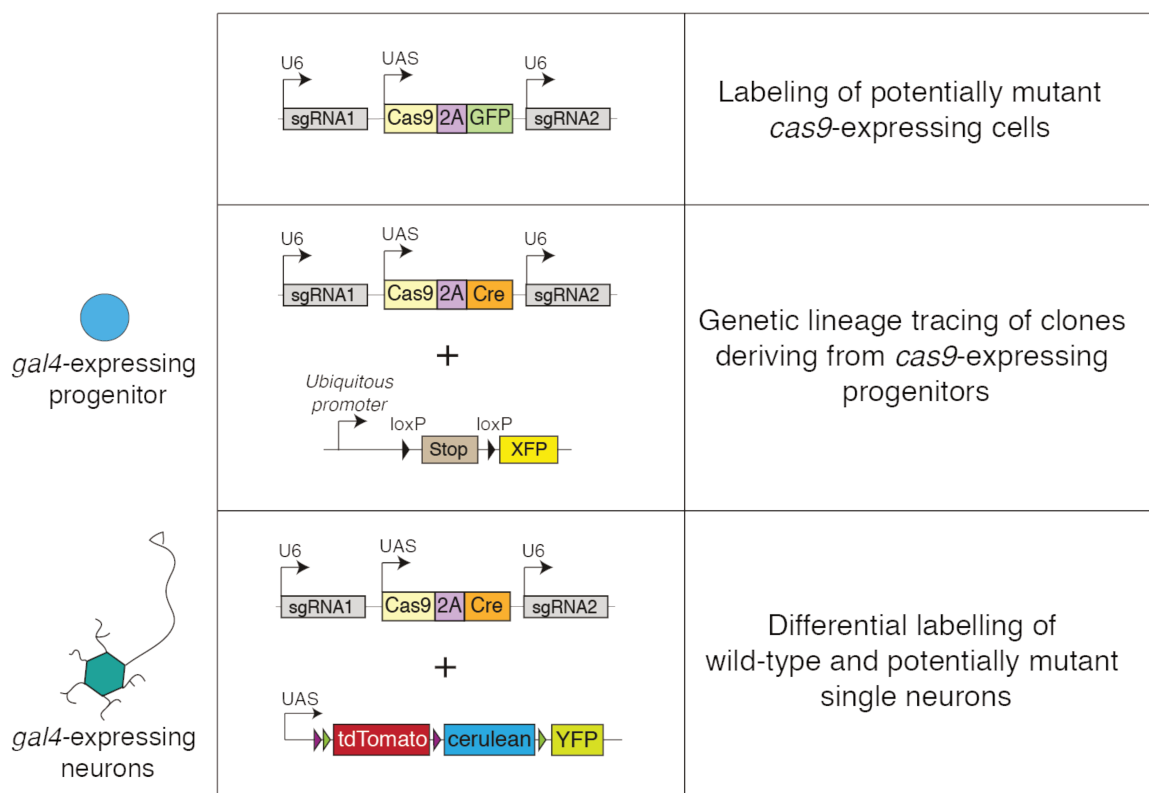


Figure 12. Schematic representation of the different methods and applications of tissue CRISPR/Cas9-mediated genome modifications. From top to bottom: i) labeling with GFP of *cas9*-expressing cells potentially mutated the in locus targeted by the *sgRNA1* and *sgRNA2* expressed with the pol III U6 promoters. ii) Genetic labeling with Cre recombinase of *cas9*-expressing progenitor cells and derived clones. Cre activity is revealed by the conditional expression of a fluorescent reporter protein (XFP) after removal of a stop cassette. iii) A similar strategy combined with a Brainbow reporter cassette allows gene disruption in differentiates neurons and the discrimination of potentially mutant cells from wild-type cells in the same animal by differential labeling.

The methods we have developed in this study offer a valuable alternative to technically challenging transplantation experiments that represent, to date, the only method to analyze cell-autonomous behavior of mutant cells in a wild-type genetic background. Furthermore, the analysis of genetic chimeras resulting from transplantations is restricted to early phenotypes and does not allow the investigation of the role of genes and pathways that are used repeatedly during development. If well established, Cre/loxP-based approaches for conditional gene inactivation in zebrafish would overcome these issues. Nevertheless they would need long generation time and are currently limited by the low efficiency of homologous recombination-based genomic manipulations.

2.2 Limitations and possible improvements of the 2C-Cas9 system

One of the main advantages of the system we have developed in this study is the genetic fluorescent labeling of *cas9*-expressing cells. Perhaps, this also represents the main drawback of the strategy. Our results suggest that a percentage of the labeled cells, varying from one experiment to the other, carries biallelic loss-of-function mutations. At the same time, a percentage of fluorescent *cas9*-expressing cells will harbor in-frame mutations. Therefore, a method to differentiate mutant and wild-type cells in the same mixed population of fluorescent cells is needed.

In our report, we propose to perform immunofluorescence experiments to obtain a clear readout of protein loss caused by targeted gene disruption. This approach allows the discrimination of immunopositive wild-type cells from immunonegative mutant cells. The aforementioned limitation of the 2C-Cas9 system could be partially overcome by optimizing the efficiency of targeted gene disruption. This would increase the proportion of truly mutant cells within the population of labeled *cas9*-expressing cells. Different possible modifications could improve the mutagenesis rate induced by our vector system. First of all, the selection of sgRNA displaying efficient mutagenesis rates is crucial to successfully induce DSBs at the target genomic locus. In addition, to achieve loss of function in the cases where indel (insertions/deletions) mutations do not disrupt the ORF of the targeted gene, designing of sgRNAs targeting essential functional domains of a protein can be advantageous. The injection of our vector system into a heterozygous mutant background, where one allele carries a null mutation, represents another way to enhance the efficiency of gene disruption. Furthermore, the use of a strong Gal4 driver line, leading to a high intracellular expression of Cas9 endonuclease levels, is recommended. In the future, additional improvements in the Cas9 expression cassette may be needed. A possibility could be the incorporation into our vector system of noncoding elements of the zebrafish

genome that have been shown to boost expression of transgenes in UAS-based plasmids (Horstick et al 2015).

Finally, despite the above-described limitations, the genetic labeling of potentially mutant cells generated by the 2C-Cas9 method provides a versatile technique to correlate phenotype and genotype, a challenge that cannot be addressed with other currently available genetic tools in zebrafish.

3. Conclusions

Conclusions 1

The predominance of synaptic laminae in the nervous system suggests that the spatial clustering of similar inputs is essential for proper function of neural networks. An in-depth knowledge of the mechanisms ruling lamina-specific targeting of neurites is needed to understand the bases of information processing in the brain. In our first work, we have shown that an endogenous concentration gradient of the ECM protein Reelin contributes to the establishment of synaptic lamination in the vertebrate visual system. Previous studies have proposed that the formation of a laminar scaffold by target-derived ECM factors would precede the targeting of neural processes. Our data provide compelling evidence that tectum-derived Reelin is distributed in a gradient in the zebrafish tectal neuropil before the arrival of RGCs projections. This finding supports a model according to which ECM molecules act as global neuropil organizers by pre-patterning the target tissue in discrete layers to provide positional information for ingrowing axons and dendrites. From an evolutionary perspective, the pre-patterning of synaptic laminae might be the result of a selective pressure because it ensures a timely circuit assembly by bringing the neurites of pre- and postsynaptic neurons in spatial proximity. An appropriate speed of synaptic contact formation is crucial to perform certain behaviours at appropriate stages of development, such as feeding or escape behaviour for the zebrafish larva. In this context, our study proposes ECM lamination cues as key factors of a strategy that the developing brain adopts to shape neuropil architecture for the timely establishment of a functional circuit. Although our results refer to the zebrafish retinotectal system, they provide a framework for the analysis of ECM contribution to neural networks assembly in other species or areas of the brain.

Conclusions 2

Since the advent of the CRISPR/Cas9 system the possibilities to perform targeted mutagenesis or more advanced genomic engineering experiments are no longer an obstacle in many organisms. A tight spatiotemporal regulation of gene disruption is a crucial step to increase the resolution at which gene function can be analyzed. Nevertheless cell-specific mutagenesis remains challenging in zebrafish. The methods pioneered in this work enables targeted mutagenesis in cell clones or single cells and allows genetic lineage tracing of mutant cells. These cells can be potentially followed until adulthood, allowing the use of our strategy in fields ranging from stem cells and regeneration to cancer biology and aging. Importantly, because none of the tools that we developed are restricted to zebrafish, similar approaches are readily applicable in virtually any organism where transgenesis and DNA injection are feasible.

References

- Ablain J, Durand EM, Yang S, Zhou Y, Zon LI. 2015. A CRISPR/Cas9 vector system for tissue-specific gene disruption in zebrafish. *Developmental cell* 32: 756-64
- Alcantara S, Ruiz M, D'Arcangelo G, Ezan F, de Lecea L, et al. 1998. Regional and cellular patterns of reelin mRNA expression in the forebrain of the developing and adult mouse. *The Journal of neuroscience : the official journal of the Society for Neuroscience* 18: 7779-99
- Androutsellis-Theotokis A, Leker RR, Soldner F, Hoepfner DJ, Ravin R, et al. 2006. Notch signalling regulates stem cell numbers in vitro and in vivo. *Nature* 442: 823-6
- Antinucci P, Nikolaou N, Meyer MP, Hindges R. 2013. Teneurin-3 specifies morphological and functional connectivity of retinal ganglion cells in the vertebrate visual system. *Cell reports* 5: 582-92
- Antinucci P, Suleyman O, Monfries C, Hindges R. 2016. Neural Mechanisms Generating Orientation Selectivity in the Retina. *Current biology : CB*
- Arber S, Barbayannis FA, Hanser H, Schneider C, Stanyon CA, et al. 1998. Regulation of actin dynamics through phosphorylation of cofilin by LIM-kinase. *Nature* 393: 805-9
- Arnaud L, Ballif BA, Forster E, Cooper JA. 2003. Fyn tyrosine kinase is a critical regulator of disabled-1 during brain development. *Current biology : CB* 13: 9-17
- Artavanis-Tsakonas S, Rand MD, Lake RJ. 1999. Notch signaling: cell fate control and signal integration in development. *Science* 284: 770-6
- Asada N, Sanada K, Fukada Y. 2007. LKB1 regulates neuronal migration and neuronal differentiation in the developing neocortex through centrosomal positioning. *The Journal of neuroscience : the official journal of the Society for Neuroscience* 27: 11769-75
- Asakawa K, Kawakami K. 2008. Targeted gene expression by the Gal4-UAS system in zebrafish. *Development, growth & differentiation* 50: 391-9
- Asakawa K, Suster ML, Mizusawa K, Nagayoshi S, Kotani T, et al. 2008. Genetic dissection of neural circuits by Tol2 transposon-mediated Gal4 gene and enhancer trapping in zebrafish. *Proceedings of the National Academy of Sciences of the United States of America* 105: 1255-60
- Assadi AH, Zhang G, Beffert U, McNeil RS, Renfro AL, et al. 2003. Interaction of reelin signaling and Lis1 in brain development. *Nature genetics* 35: 270-6
- Auer TO, Del Bene F. 2014. CRISPR/Cas9 and TALEN-mediated knock-in approaches in zebrafish. *Methods* 69: 142-50
- Auer TO, Duroure K, De Cian A, Concordet JP, Del Bene F. 2014. Highly efficient CRISPR/Cas9-mediated knock-in in zebrafish by homology-independent DNA repair. *Genome research* 24: 142-53

- Auer TO, Xiao T, Bercier V, Gebhardt C, Durore K, et al. 2015. Deletion of a kinesin I motor unmasks a mechanism of homeostatic branching control by neurotrophin-3. *eLife* 4
- Azeredo da Silveira R, Roska B. 2011. Cell types, circuits, computation. *Current opinion in neurobiology* 21: 664-71
- Baba K, Sakakibara S, Setsu T, Terashima T. 2007. The superficial layers of the superior colliculus are cytoarchitecturally and myeloarchitecturally disorganized in the reelin-deficient mouse, reeler. *Brain research* 1140: 205-15
- Baier H. 2013. Synaptic laminae in the visual system: molecular mechanisms forming layers of perception. *Annual review of cell and developmental biology* 29: 385-416
- Baier H, Klostermann S, Trowe T, Karlstrom RO, Nusslein-Volhard C, Bonhoeffer F. 1996. Genetic dissection of the retinotectal projection. *Development* 123: 415-25
- Balciuniene J, Nagelberg D, Walsh KT, Camerota D, Georlette D, et al. 2013. Efficient disruption of Zebrafish genes using a Gal4-containing gene trap. *BMC genomics* 14: 619
- Barker AJ, Baier H. 2015. Sensorimotor decision making in the zebrafish tectum. *Current biology : CB* 25: 2804-14
- Barnes AP, Lilley BN, Pan YA, Plummer LJ, Powell AW, et al. 2007. LKB1 and SAD kinases define a pathway required for the polarization of cortical neurons. *Cell* 129: 549-63
- Barrangou R, Fremaux C, Deveau H, Richards M, Boyaval P, et al. 2007. CRISPR provides acquired resistance against viruses in prokaryotes. *Science* 315: 1709-12
- Barresi MJ, Hutson LD, Chien CB, Karlstrom RO. 2005. Hedgehog regulated Slit expression determines commissure and glial cell position in the zebrafish forebrain. *Development* 132: 3643-56
- Becker CG, Schweitzer J, Feldner J, Schachner M, Becker T. 2004. Tenascin-R as a repellent guidance molecule for newly growing and regenerating optic axons in adult zebrafish. *Molecular and cellular neurosciences* 26: 376-89
- Bedell VM, Wang Y, Campbell JM, Poshusta TL, Starker CG, et al. 2012. In vivo genome editing using a high-efficiency TALEN system. *Nature* 491: 114-8
- Ben Fredj N, Hammond S, Otsuna H, Chien CB, Burrone J, Meyer MP. 2010. Synaptic activity and activity-dependent competition regulates axon arbor maturation, growth arrest, and territory in the retinotectal projection. *The Journal of neuroscience : the official journal of the Society for Neuroscience* 30: 10939-51
- Bhaya D, Davison M, Barrangou R. 2011. CRISPR-Cas systems in bacteria and archaea: versatile small RNAs for adaptive defense and regulation. *Annual review of genetics* 45: 273-97
- Borrell V, Del Rio JA, Alcantara S, Derer M, Martinez A, et al. 1999. Reelin regulates the development and synaptogenesis of the layer-specific entorhino-hippocampal connections. *The Journal of neuroscience : the official journal of the Society for Neuroscience* 19: 1345-58

- Borrell V, Pujadas L, Simo S, Dura D, Sole M, et al. 2007. Reelin and mDab1 regulate the development of hippocampal connections. *Molecular and cellular neurosciences* 36: 158-73
- Branda CS, Dymecki SM. 2004. Talking about a revolution: The impact of site-specific recombinases on genetic analyses in mice. *Developmental cell* 6: 7-28
- Brittis PA, Canning DR, Silver J. 1992. Chondroitin sulfate as a regulator of neuronal patterning in the retina. *Science* 255: 733-6
- Brittis PA, Lemmon V, Rutishauser U, Silver J. 1995. Unique changes of ganglion cell growth cone behavior following cell adhesion molecule perturbations: a time-lapse study of the living retina. *Molecular and cellular neurosciences* 6: 433-49
- Bullmore E, Sporns O. 2012. The economy of brain network organization. *Nature reviews. Neuroscience* 13: 336-49
- Burrill JD, Easter SS, Jr. 1994. Development of the retinofugal projections in the embryonic and larval zebrafish (*Brachydanio rerio*). *The Journal of comparative neurology* 346: 583-600
- Bussmann J, Schulte-Merker S. 2011. Rapid BAC selection for tol2-mediated transgenesis in zebrafish. *Development* 138: 4327-32
- Cajal SR. 1899. Textura del Sistema Nervioso del Hombre Y Vertebrados.
- Candal EM, Caruncho HJ, Sueiro C, Anadon R, Rodriguez-Moldes I. 2005. Reelin expression in the retina and optic tectum of developing common brown trout. *Brain research. Developmental brain research* 154: 187-97
- Caviness VS, Jr. 1976. Patterns of cell and fiber distribution in the neocortex of the reeler mutant mouse. *The Journal of comparative neurology* 170: 435-47
- Cayouette M, Poggi L, Harris WA. 2006. Lineage in the vertebrate retina. *Trends in neurosciences* 29: 563-70
- Chai X, Forster E, Zhao S, Bock HH, Frotscher M. 2009. Reelin stabilizes the actin cytoskeleton of neuronal processes by inducing n-cofilin phosphorylation at serine3. *The Journal of neuroscience : the official journal of the Society for Neuroscience* 29: 288-99
- Cheng TW, Liu XB, Faulkner RL, Stephan AH, Barres BA, et al. 2010. Emergence of lamina-specific retinal ganglion cell connectivity by axon arbor retraction and synapse elimination. *The Journal of neuroscience : the official journal of the Society for Neuroscience* 30: 16376-82
- Chklovskii DB. 2004. Synaptic connectivity and neuronal morphology: two sides of the same coin. *Neuron* 43: 609-17
- Cong L, Ran FA, Cox D, Lin S, Barretto R, et al. 2013. Multiplex genome engineering using CRISPR/Cas systems. *Science* 339: 819-23
- Cuntz H, Forstner F, Borst A, Hausser M. 2010. One rule to grow them all: a general theory of neuronal branching and its practical application. *PLoS computational biology* 6
- D'Arcangelo G. 2014. Reelin in the Years: Controlling Neuronal Migration and Maturation in the Mammalian Brain. *Advances in Neuroscience* 2014: 19

- D'Arcangelo G, Homayouni R, Keshvara L, Rice DS, Sheldon M, Curran T. 1999. Reelin is a ligand for lipoprotein receptors. *Neuron* 24: 471-9
- D'Arcangelo G, Miao GG, Chen SC, Soares HD, Morgan JI, Curran T. 1995. A protein related to extracellular matrix proteins deleted in the mouse mutant reeler. *Nature* 374: 719-23
- Davison JM, Akitake CM, Goll MG, Rhee JM, Gosse N, et al. 2007. Transactivation from Gal4-VP16 transgenic insertions for tissue-specific cell labeling and ablation in zebrafish. *Developmental biology* 304: 811-24
- de Wit J, Ghosh A. 2016. Specification of synaptic connectivity by cell surface interactions. *Nature reviews. Neuroscience* 17: 22-35
- Deans MR, Krol A, Abraira VE, Copley CO, Tucker AF, Goodrich LV. 2011. Control of neuronal morphology by the atypical cadherin Fat3. *Neuron* 71: 820-32
- Deiner MS, Kennedy TE, Fazeli A, Serafini T, Tessier-Lavigne M, Sretavan DW. 1997. Netrin-1 and DCC mediate axon guidance locally at the optic disc: loss of function leads to optic nerve hypoplasia. *Neuron* 19: 575-89
- Del Bene F, Wyart C, Robles E, Tran A, Looger L, et al. 2010. Filtering of visual information in the tectum by an identified neural circuit. *Science* 330: 669-73
- Del Rio JA, Heimrich B, Borrell V, Forster E, Drakew A, et al. 1997. A role for Cajal-Retzius cells and reelin in the development of hippocampal connections. *Nature* 385: 70-4
- Dell AL, Fried-Cassorla E, Xu H, Raper JA. 2013. cAMP-induced expression of neuropilin1 promotes retinal axon crossing in the zebrafish optic chiasm. *The Journal of neuroscience : the official journal of the Society for Neuroscience* 33: 11076-88
- Doudna JA, Charpentier E. 2014. Genome editing. The new frontier of genome engineering with CRISPR-Cas9. *Science* 346: 1258096
- Drenhaus U, Morino P, Veh RW. 2003. On the development of the stratification of the inner plexiform layer in the chick retina. *The Journal of comparative neurology* 460: 1-12
- Duan X, Krishnaswamy A, De la Huerta I, Sanes JR. 2014. Type II cadherins guide assembly of a direction-selective retinal circuit. *Cell* 158: 793-807
- Dulabon L, Olson EC, Taglienti MG, Eisenhuth S, McGrath B, et al. 2000. Reelin binds alpha3beta1 integrin and inhibits neuronal migration. *Neuron* 27: 33-44
- Dunn TW, Gebhardt C, Naumann EA, Riegler C, Ahrens MB, et al. 2016. Neural Circuits Underlying Visually Evoked Escapes in Larval Zebrafish. *Neuron* 89: 613-28
- Erskine L, Herrera E. 2014. Connecting the retina to the brain. *ASN neuro* 6
- Falconer DS. 1951. Two new mutants, 'trembler' and 'reeler', with neurological actions in the house mouse (*Mus musculus* L.). *J Genet* 50: 192-201
- Famiglietti EV, Jr., Kolb H. 1976. Structural basis for ON-and OFF-center responses in retinal ganglion cells. *Science* 194: 193-5

- Forster E. 2014. Reelin, neuronal polarity and process orientation of cortical neurons. *Neuroscience* 269: 102-11
- Franco SJ, Martinez-Garay I, Gil-Sanz C, Harkins-Perry SR, Muller U. 2011. Reelin regulates cadherin function via Dab1/Rap1 to control neuronal migration and lamination in the neocortex. *Neuron* 69: 482-97
- Fricke C, Lee JS, Geiger-Rudolph S, Bonhoeffer F, Chien CB. 2001. astray, a zebrafish roundabout homolog required for retinal axon guidance. *Science* 292: 507-10
- Fuerst PG, Bruce F, Tian M, Wei W, Elstrott J, et al. 2009. DSCAM and DSCAML1 function in self-avoidance in multiple cell types in the developing mouse retina. *Neuron* 64: 484-97
- Gabriel JP, Trivedi CA, Maurer CM, Ryu S, Bollmann JH. 2012. Layer-specific targeting of direction-selective neurons in the zebrafish optic tectum. *Neuron* 76: 1147-60
- Gahtan E, Tanger P, Baier H. 2005. Visual prey capture in larval zebrafish is controlled by identified reticulospinal neurons downstream of the tectum. *The Journal of neuroscience : the official journal of the Society for Neuroscience* 25: 9294-303
- Garneau JE, Dupuis ME, Villion M, Romero DA, Barrangou R, et al. 2010. The CRISPR/Cas bacterial immune system cleaves bacteriophage and plasmid DNA. *Nature* 468: 67-71
- Gebhardt C, Baier H, Del Bene F. 2013. Direction selectivity in the visual system of the zebrafish larva. *Frontiers in neural circuits* 7: 111
- Gerfen CR, Paletzki R, Heintz N. 2013. GENSAT BAC cre-recombinase driver lines to study the functional organization of cerebral cortical and basal ganglia circuits. *Neuron* 80: 1368-83
- Gilmore EC, Herrup K. 2000. Cortical development: receiving reelin. *Current biology : CB* 10: R162-6
- Godinho L, Mumm JS, Williams PR, Schroeter EH, Koerber A, et al. 2005. Targeting of amacrine cell neurites to appropriate synaptic laminae in the developing zebrafish retina. *Development* 132: 5069-79
- Goffinet AM. 1979. An early development defect in the cerebral cortex of the reeler mouse. A morphological study leading to a hypothesis concerning the action of the mutant gene. *Anat Embryol (Berl)* 157: 205-16
- Gordon L, Mansh M, Kinsman H, Morris AR. 2010. Xenopus sonic hedgehog guides retinal axons along the optic tract. *Dev Dyn* 239: 2921-32
- Hale CR, Zhao P, Olson S, Duff MO, Graveley BR, et al. 2009. RNA-guided RNA cleavage by a CRISPR RNA-Cas protein complex. *Cell* 139: 945-56
- Hashimoto-Torii K, Torii M, Sarkisian MR, Bartley CM, Shen J, et al. 2008. Interaction between Reelin and Notch signaling regulates neuronal migration in the cerebral cortex. *Neuron* 60: 273-84
- Heidenreich M, Zhang F. 2016. Applications of CRISPR-Cas systems in neuroscience. *Nature reviews. Neuroscience* 17: 36-44

- Herrero-Turrion MJ, Velasco A, Arevalo R, Aijon J, Lara JM. 2010. Characterisation and differential expression during development of a duplicate Disabled-1 (Dab1) gene from zebrafish. *Comparative biochemistry and physiology. Part B, Biochemistry & molecular biology* 155: 217-29
- Hiesberger T, Trommsdorff M, Howell BW, Goffinet A, Mumby MC, et al. 1999. Direct binding of Reelin to VLDL receptor and ApoE receptor 2 induces tyrosine phosphorylation of disabled-1 and modulates tau phosphorylation. *Neuron* 24: 481-9
- Hisano Y, Sakuma T, Nakade S, Ohga R, Ota S, et al. 2015. Precise in-frame integration of exogenous DNA mediated by CRISPR/Cas9 system in zebrafish. *Scientific reports* 5: 8841
- Hong YK, Kim IJ, Sanes JR. 2011. Stereotyped axonal arbors of retinal ganglion cell subsets in the mouse superior colliculus. *The Journal of comparative neurology* 519: 1691-711
- Hopker VH, Shewan D, Tessier-Lavigne M, Poo M, Holt C. 1999. Growth-cone attraction to netrin-1 is converted to repulsion by laminin-1. *Nature* 401: 69-73
- Horstick EJ, Jordan DC, Bergeron SA, Tabor KM, Serpe M, et al. 2015. Increased functional protein expression using nucleotide sequence features enriched in highly expressed genes in zebrafish. *Nucleic acids research* 43: e48
- Horton AC, Racz B, Monson EE, Lin AL, Weinberg RJ, Ehlers MD. 2005. Polarized secretory trafficking directs cargo for asymmetric dendrite growth and morphogenesis. *Neuron* 48: 757-71
- Hoshi H, Liu WL, Massey SC, Mills SL. 2009. ON inputs to the OFF layer: bipolar cells that break the stratification rules of the retina. *The Journal of neuroscience : the official journal of the Society for Neuroscience* 29: 8875-83
- Hoshijima K, Jurynek MJ, Grunwald DJ. 2016. Precise Editing of the Zebrafish Genome Made Simple and Efficient. *Developmental cell* 36: 654-67
- Howell BW, Gertler FB, Cooper JA. 1997. Mouse disabled (mDab1): a Src binding protein implicated in neuronal development. *The EMBO journal* 16: 121-32
- Huberman AD, Clandinin TR, Baier H. 2010. Molecular and cellular mechanisms of lamina-specific axon targeting. *Cold Spring Harbor perspectives in biology* 2: a001743
- Huberman AD, Wei W, Elstrott J, Stafford BK, Feller MB, Barres BA. 2009. Genetic identification of an On-Off direction-selective retinal ganglion cell subtype reveals a layer-specific subcortical map of posterior motion. *Neuron* 62: 327-34
- Hutson LD, Chien CB. 2002. Pathfinding and error correction by retinal axons: the role of astray/robo2. *Neuron* 33: 205-17
- Inatani M, Irie F, Plump AS, Tessier-Lavigne M, Yamaguchi Y. 2003. Mammalian brain morphogenesis and midline axon guidance require heparan sulfate. *Science* 302: 1044-6
- Jiang Y, Obama H, Kuan SL, Nakamura R, Nakamoto C, et al. 2009. In vitro guidance of retinal axons by a tectal lamina-specific glycoprotein Nel. *Molecular and cellular neurosciences* 41: 113-9

- Jinek M, Chylinski K, Fonfara I, Hauer M, Doudna JA, Charpentier E. 2012. A programmable dual-RNA-guided DNA endonuclease in adaptive bacterial immunity. *Science* 337: 816-21
- Johnson KG, Ghose A, Epstein E, Lincecum J, O'Connor MB, Van Vactor D. 2004. Axonal heparan sulfate proteoglycans regulate the distribution and efficiency of the repellent slit during midline axon guidance. *Current biology : CB* 14: 499-504
- Jossin Y, Cooper JA. 2011. Reelin, Rap1 and N-cadherin orient the migration of multipolar neurons in the developing neocortex. *Nature neuroscience* 14: 697-703
- Jossin Y, Gui L, Goffinet AM. 2007. Processing of Reelin by embryonic neurons is important for function in tissue but not in dissociated cultured neurons. *The Journal of neuroscience : the official journal of the Society for Neuroscience* 27: 4243-52
- Jossin Y, Ignatova N, Hiesberger T, Herz J, Lambert de Rouvroit C, Goffinet AM. 2004. The central fragment of Reelin, generated by proteolytic processing in vivo, is critical to its function during cortical plate development. *The Journal of neuroscience : the official journal of the Society for Neuroscience* 24: 514-21
- Joung JK, Sander JD. 2013. TALENs: a widely applicable technology for targeted genome editing. *Nature reviews. Molecular cell biology* 14: 49-55
- Kaas JH. 1997. Topographic maps are fundamental to sensory processing. *Brain research bulletin* 44: 107-12
- Karlstrom RO, Trowe T, Klostermann S, Baier H, Brand M, et al. 1996. Zebrafish mutations affecting retinotectal axon pathfinding. *Development* 123: 427-38
- Kawakami K. 2004. Transgenesis and gene trap methods in zebrafish by using the Tol2 transposable element. *Methods in cell biology* 77: 201-22
- Kawakami K, Abe G, Asada T, Asakawa K, Fukuda R, et al. 2010. zTrap: zebrafish gene trap and enhancer trap database. *BMC developmental biology* 10: 105
- Kay JN, Roeser T, Mumm JS, Godinho L, Mrejeru A, et al. 2004. Transient requirement for ganglion cells during assembly of retinal synaptic layers. *Development* 131: 1331-42
- Kennedy TE, Serafini T, de la Torre JR, Tessier-Lavigne M. 1994. Netrins are diffusible chemotropic factors for commissural axons in the embryonic spinal cord. *Cell* 78: 425-35
- Kim IJ, Zhang Y, Meister M, Sanes JR. 2010. Laminar restriction of retinal ganglion cell dendrites and axons: subtype-specific developmental patterns revealed with transgenic markers. *The Journal of neuroscience : the official journal of the Society for Neuroscience* 30: 1452-62
- Kim IJ, Zhang Y, Yamagata M, Meister M, Sanes JR. 2008. Molecular identification of a retinal cell type that responds to upward motion. *Nature* 452: 478-82
- Kimura Y, Hisano Y, Kawahara A, Higashijima S. 2014. Efficient generation of knock-in transgenic zebrafish carrying reporter/driver genes by CRISPR/Cas9-mediated genome engineering. *Scientific reports* 4: 6545

- Klar A, Baldassare M, Jessell TM. 1992. F-spondin: a gene expressed at high levels in the floor plate encodes a secreted protein that promotes neural cell adhesion and neurite extension. *Cell* 69: 95-110
- Kubo K, Honda T, Tomita K, Sekine K, Ishii K, et al. 2010. Ectopic Reelin induces neuronal aggregation with a normal birthdate-dependent "inside-out" alignment in the developing neocortex. *The Journal of neuroscience : the official journal of the Society for Neuroscience* 30: 10953-66
- Kuffler SW. 1953. Discharge patterns and functional organization of mammalian retina. *J Neurophysiol* 16: 37-68
- Kuhn R, Schwenk F, Aguet M, Rajewsky K. 1995. Inducible gene targeting in mice. *Science* 269: 1427-9
- Kuhn TB, Stoeckli ET, Condrau MA, Rathjen FG, Sonderegger P. 1991. Neurite outgrowth on immobilized axonin-1 is mediated by a heterophilic interaction with L1(G4). *The Journal of cell biology* 115: 1113-26
- Kunz S, Spirig M, Ginsburg C, Buchstaller A, Berger P, et al. 1998. Neurite fasciculation mediated by complexes of axonin-1 and Ng cell adhesion molecule. *The Journal of cell biology* 143: 1673-90
- Langley JN. 1895. Note on Regeneration of Prae-Ganglionic Fibres of the Sympathetic. *The Journal of physiology* 18: 280-4
- Lee JS, von der Hardt S, Rusch MA, Stringer SE, Stickney HL, et al. 2004. Axon sorting in the optic tract requires HSPG synthesis by ext2 (dackel) and extl3 (boxer). *Neuron* 44: 947-60
- Li J, Zhang BB, Ren YG, Gu SY, Xiang YH, Du JL. 2015. Intron targeting-mediated and endogenous gene integrity-maintaining knockin in zebrafish using the CRISPR/Cas9 system. *Cell research* 25: 634-7
- Li Q, Shirabe K, Thisse C, Thisse B, Okamoto H, et al. 2005. Chemokine signaling guides axons within the retina in zebrafish. *The Journal of neuroscience : the official journal of the Society for Neuroscience* 25: 1711-7
- Livet J, Weissman TA, Kang H, Draft RW, Lu J, et al. 2007. Transgenic strategies for combinatorial expression of fluorescent proteins in the nervous system. *Nature* 450: 56-62
- Luque JM. 2004. Integrin and the Reelin-Dab1 pathway: a sticky affair? *Brain research. Developmental brain research* 152: 269-71
- Macdonald R, Scholes J, Strahle U, Brennan C, Holder N, et al. 1997. The Pax protein Noi is required for commissural axon pathway formation in the rostral forebrain. *Development* 124: 2397-408
- Madisen L, Zwingman TA, Sunkin SM, Oh SW, Zariwala HA, et al. 2010. A robust and high-throughput Cre reporting and characterization system for the whole mouse brain. *Nature neuroscience* 13: 133-40
- Magdaleno S, Keshvara L, Curran T. 2002. Rescue of ataxia and preplate splitting by ectopic expression of Reelin in reeler mice. *Neuron* 33: 573-86

- Makarova KS, Haft DH, Barrangou R, Brouns SJ, Charpentier E, et al. 2011. Evolution and classification of the CRISPR-Cas systems. *Nature reviews. Microbiology* 9: 467-77
- Manoharan M, Muhammad SA, Sowdhamini R. 2015. Sequence Analysis and Evolutionary Studies of Reelin Proteins. *Bioinform Biol Insights* 9: 187-93
- Marc RE, Cameron D. 2001. A molecular phenotype atlas of the zebrafish retina. *J Neurocytol* 30: 593-654
- Marin-Padilla M. 1998. Cajal-Retzius cells and the development of the neocortex. *Trends in neurosciences* 21: 64-71
- Marraffini LA, Sontheimer EJ. 2008. CRISPR interference limits horizontal gene transfer in staphylococci by targeting DNA. *Science* 322: 1843-5
- Masland RH. 2001. The fundamental plan of the retina. *Nature neuroscience* 4: 877-86
- Matsuki T, Matthews RT, Cooper JA, van der Brug MP, Cookson MR, et al. 2010. Reelin and stk25 have opposing roles in neuronal polarization and dendritic Golgi deployment. *Cell* 143: 826-36
- Matsuoka RL, Chivatakarn O, Badea TC, Samuels IS, Cahill H, et al. 2011. Class 5 transmembrane semaphorins control selective Mammalian retinal lamination and function. *Neuron* 71: 460-73
- McKenney RJ, Vershinin M, Kunwar A, Vallee RB, Gross SP. 2010. LIS1 and NudE induce a persistent dynein force-producing state. *Cell* 141: 304-14
- McLaughlin T, O'Leary DD. 2005. Molecular gradients and development of retinotopic maps. *Annual review of neuroscience* 28: 327-55
- Meseke M, Cavus E, Forster E. 2013a. Reelin promotes microtubule dynamics in processes of developing neurons. *Histochem Cell Biol* 139: 283-97
- Meseke M, Rosenberger G, Forster E. 2013b. Reelin and the Cdc42/Rac1 guanine nucleotide exchange factor alphaPIX/Arhgef6 promote dendritic Golgi translocation in hippocampal neurons. *The European journal of neuroscience* 37: 1404-12
- Mikoshiba K, Nagaike K, Kohsaka S, Takamatsu K, Aoki E, Tsukada Y. 1980. Developmental studies on the cerebellum from reeler mutant mouse in vivo and in vitro. *Developmental biology* 79: 64-80
- Missaire M, Hindges R. 2015. The role of cell adhesion molecules in visual circuit formation: from neurite outgrowth to maps and synaptic specificity. *Developmental neurobiology* 75: 569-83
- Molyneaux BJ, Arlotta P, Menezes JR, Macklis JD. 2007. Neuronal subtype specification in the cerebral cortex. *Nature reviews. Neuroscience* 8: 427-37
- Morgan JL, Dhingra A, Vardi N, Wong RO. 2006. Axons and dendrites originate from neuroepithelial-like processes of retinal bipolar cells. *Nature neuroscience* 9: 85-92
- Mosimann C, Kaufman CK, Li P, Pugach EK, Tamplin OJ, Zon LI. 2011. Ubiquitous transgene expression and Cre-based recombination driven by the ubiquitin promoter in zebrafish. *Development* 138: 169-77

- Mumm JS, Williams PR, Godinho L, Koerber A, Pittman AJ, et al. 2006. In vivo imaging reveals dendritic targeting of laminated afferents by zebrafish retinal ganglion cells. *Neuron* 52: 609-21
- Nadarajah B, Brunstrom JE, Grutzendler J, Wong RO, Pearlman AL. 2001. Two modes of radial migration in early development of the cerebral cortex. *Nature neuroscience* 4: 143-50
- Nakano Y, Kohno T, Hibi T, Kohno S, Baba A, et al. 2007. The extremely conserved C-terminal region of Reelin is not necessary for secretion but is required for efficient activation of downstream signaling. *The Journal of biological chemistry* 282: 20544-52
- Nelson R, Famiglietti EV, Jr., Kolb H. 1978. Intracellular staining reveals different levels of stratification for on- and off-center ganglion cells in cat retina. *J Neurophysiol* 41: 472-83
- Nevin LM, Robles E, Baier H, Scott EK. 2010. Focusing on optic tectum circuitry through the lens of genetics. *BMC biology* 8: 126
- Nevin LM, Taylor MR, Baier H. 2008. Hardwiring of fine synaptic layers in the zebrafish visual pathway. *Neural development* 3: 36
- Nichols AJ, Olson EC. 2010. Reelin promotes neuronal orientation and dendritogenesis during preplate splitting. *Cerebral cortex* 20: 2213-23
- Nikolaou N, Lowe AS, Walker AS, Abbas F, Hunter PR, et al. 2012. Parametric functional maps of visual inputs to the tectum. *Neuron* 76: 317-24
- Nikolaou N, Meyer MP. 2015. Lamination Speeds the Functional Development of Visual Circuits. *Neuron* 88: 999-1013
- O'Dell RS, Ustine CJ, Cameron DA, Lawless SM, Williams RM, et al. 2012. Layer 6 cortical neurons require Reelin-Dab1 signaling for cellular orientation, Golgi deployment, and directed neurite growth into the marginal zone. *Neural development* 7: 25
- Odermatt B, Nikolaev A, Lagnado L. 2012. Encoding of luminance and contrast by linear and nonlinear synapses in the retina. *Neuron* 73: 758-73
- Ogawa M, Miyata T, Nakajima K, Yagyu K, Seike M, et al. 1995. The reeler gene-associated antigen on Cajal-Retzius neurons is a crucial molecule for laminar organization of cortical neurons. *Neuron* 14: 899-912
- Osterfield M, Egelund R, Young LM, Flanagan JG. 2008. Interaction of amyloid precursor protein with contactins and NgCAM in the retinotectal system. *Development* 135: 1189-99
- Ott H, Bastmeyer M, Stuermer CA. 1998. Neurolin, the goldfish homolog of DM-GRASP, is involved in retinal axon pathfinding to the optic disk. *The Journal of neuroscience : the official journal of the Society for Neuroscience* 18: 3363-72
- Pan X, Wan H, Chia W, Tong Y, Gong Z. 2005. Demonstration of site-directed recombination in transgenic zebrafish using the Cre/loxP system. *Transgenic research* 14: 217-23
- Pavlou O, Theodorakis K, Falk J, Kutsche M, Schachner M, et al. 2002. Analysis of interactions of the adhesion molecule TAG-1 and its domains with other

- immunoglobulin superfamily members. *Molecular and cellular neurosciences* 20: 367-81
- Perez RG, Halfter W. 1994. Tenascin protein and mRNA in the avian visual system: distribution and potential contribution to retinotectal development. *Perspectives on developmental neurobiology* 2: 75-87
- Pinto Lord MC, Caviness VS, Jr. 1979. Determinants of cell shape and orientation: a comparative Golgi analysis of cell-axon interrelationships in the developing neocortex of normal and reeler mice. *The Journal of comparative neurology* 187: 49-69
- Platt RJ, Chen S, Zhou Y, Yim MJ, Swiech L, et al. 2014. CRISPR-Cas9 knockin mice for genome editing and cancer modeling. *Cell* 159: 440-55
- Port F, Chen HM, Lee T, Bullock SL. 2014. Optimized CRISPR/Cas tools for efficient germline and somatic genome engineering in *Drosophila*. *Proceedings of the National Academy of Sciences of the United States of America* 111: E2967-76
- Preuss SJ, Trivedi CA, vom Berg-Maurer CM, Ryu S, Bollmann JH. 2014. Classification of object size in retinotectal microcircuits. *Current biology : CB* 24: 2376-85
- Provost E, Rhee J, Leach SD. 2007. Viral 2A peptides allow expression of multiple proteins from a single ORF in transgenic zebrafish embryos. *Genesis* 45: 625-9
- Rice DS, Curran T. 2001. Role of the reelin signaling pathway in central nervous system development. *Annual review of neuroscience* 24: 1005-39
- Rice DS, Nusinowitz S, Azimi AM, Martinez A, Soriano E, Curran T. 2001. The reelin pathway modulates the structure and function of retinal synaptic circuitry. *Neuron* 31: 929-41
- Rivera-Alba M, Peng H, de Polavieja GG, Chklovskii DB. 2014. Wiring economy can account for cell body placement across species and brain areas. *Current biology : CB* 24: R109-10
- Robles E, Baier H. 2012. Assembly of synaptic laminae by axon guidance molecules. *Current opinion in neurobiology* 22: 799-804
- Robles E, Filosa A, Baier H. 2013. Precise lamination of retinal axons generates multiple parallel input pathways in the tectum. *The Journal of neuroscience : the official journal of the Society for Neuroscience* 33: 5027-39
- Robles E, Laurell E, Baier H. 2014. The retinal projectome reveals brain-area-specific visual representations generated by ganglion cell diversity. *Current biology : CB* 24: 2085-96
- Robles E, Smith SJ, Baier H. 2011. Characterization of genetically targeted neuron types in the zebrafish optic tectum. *Frontiers in neural circuits* 5: 1
- Roska B, Werblin F. 2001. Vertical interactions across ten parallel, stacked representations in the mammalian retina. *Nature* 410: 583-7
- Ruthazer ES, Aizenman CD. 2010. Learning to see: patterned visual activity and the development of visual function. *Trends in neurosciences* 33: 183-92

- Sakai JA, Halloran MC. 2006. Semaphorin 3d guides laterality of retinal ganglion cell projections in zebrafish. *Development* 133: 1035-44
- Sakakibara S, Misaki K, Terashima T. 2003. Cytoarchitecture and fiber pattern of the superior colliculus are disrupted in the Shaking Rat Kawasaki. *Brain research. Developmental brain research* 141: 1-13
- Sanada K, Gupta A, Tsai LH. 2004. Disabled-1-regulated adhesion of migrating neurons to radial glial fiber contributes to neuronal positioning during early corticogenesis. *Neuron* 42: 197-211
- Sanchez-Camacho C, Bovolenta P. 2008. Autonomous and non-autonomous Shh signalling mediate the in vivo growth and guidance of mouse retinal ganglion cell axons. *Development* 135: 3531-41
- Sanes JR, Zipursky SL. 2010. Design principles of insect and vertebrate visual systems. *Neuron* 66: 15-36
- Sashital DG, Wiedenheft B, Doudna JA. 2012. Mechanism of foreign DNA selection in a bacterial adaptive immune system. *Molecular cell* 46: 606-15
- Sauer B, Henderson N. 1988. Site-specific DNA recombination in mammalian cells by the Cre recombinase of bacteriophage P1. *Proceedings of the National Academy of Sciences of the United States of America* 85: 5166-70
- Schiffmann SN, Bernier B, Goffinet AM. 1997. Reelin mRNA expression during mouse brain development. *The European journal of neuroscience* 9: 1055-71
- Schroeter EH, Wong RO, Gregg RG. 2006. In vivo development of retinal ON-bipolar cell axonal terminals visualized in *nyx::MYFP* transgenic zebrafish. *Visual neuroscience* 23: 833-43
- Schweisguth F. 2004. Regulation of notch signaling activity. *Current biology : CB* 14: R129-38
- Scott EK, Baier H. 2009. The cellular architecture of the larval zebrafish tectum, as revealed by *gal4* enhancer trap lines. *Frontiers in neural circuits* 3: 13
- Scott EK, Mason L, Arrenberg AB, Ziv L, Gosse NJ, et al. 2007. Targeting neural circuitry in zebrafish using GAL4 enhancer trapping. *Nature methods* 4: 323-6
- Sekine K, Honda T, Kawauchi T, Kubo K, Nakajima K. 2011. The outermost region of the developing cortical plate is crucial for both the switch of the radial migration mode and the Dab1-dependent "inside-out" lamination in the neocortex. *The Journal of neuroscience : the official journal of the Society for Neuroscience* 31: 9426-39
- Seth A, Culverwell J, Walkowicz M, Toro S, Rick JM, et al. 2006. *belladonna/(lhx2)* is required for neural patterning and midline axon guidance in the zebrafish forebrain. *Development* 133: 725-35
- Shanmugalingam S, Houart C, Picker A, Reifers F, Macdonald R, et al. 2000. *Ace/Fgf8* is required for forebrain commissure formation and patterning of the telencephalon. *Development* 127: 2549-61
- Shelly M, Cancedda L, Heilshorn S, Sumbre G, Poo MM. 2007. LKB1/STRAD promotes axon initiation during neuronal polarization. *Cell* 129: 565-77

- Shen Z, Zhang X, Chai Y, Zhu Z, Yi P, et al. 2014. Conditional knockouts generated by engineered CRISPR-Cas9 endonuclease reveal the roles of coronin in *C. elegans* neural development. *Developmental cell* 30: 625-36
- Sheppard AM, Pearlman AL. 1997. Abnormal reorganization of preplate neurons and their associated extracellular matrix: an early manifestation of altered neocortical development in the reeler mutant mouse. *The Journal of comparative neurology* 378: 173-9
- Shimoda Y, Watanabe K. 2009. Contactins: emerging key roles in the development and function of the nervous system. *Cell adhesion & migration* 3: 64-70
- Sibbe M, Forster E, Basak O, Taylor V, Frotscher M. 2009. Reelin and Notch1 cooperate in the development of the dentate gyrus. *The Journal of neuroscience : the official journal of the Society for Neuroscience* 29: 8578-85
- Siegert S, Scherf BG, Del Punta K, Didkovsky N, Heintz N, Roska B. 2009. Genetic address book for retinal cell types. *Nature neuroscience* 12: 1197-204
- Smear MC, Tao HW, Staub W, Orger MB, Gosse NJ, et al. 2007. Vesicular glutamate transport at a central synapse limits the acuity of visual perception in zebrafish. *Neuron* 53: 65-77
- Sperry RW. 1963. Chemoaffinity in the Orderly Growth of Nerve Fiber Patterns and Connections. *Proceedings of the National Academy of Sciences of the United States of America* 50: 703-10
- Stanfield BB, Cowan WM. 1979. The morphology of the hippocampus and dentate gyrus in normal and reeler mice. *The Journal of comparative neurology* 185: 393-422
- Strasser V, Fasching D, Hauser C, Mayer H, Bock HH, et al. 2004. Receptor clustering is involved in Reelin signaling. *Molecular and cellular biology* 24: 1378-86
- Su J, Haner CV, Imbery TE, Brooks JM, Morhardt DR, et al. 2011. Reelin is required for class-specific retinogeniculate targeting. *The Journal of neuroscience : the official journal of the Society for Neuroscience* 31: 575-86
- Su J, Klemm MA, Josephson AM, Fox MA. 2013. Contributions of VLDLR and LRP8 in the establishment of retinogeniculate projections. *Neural development* 8: 11
- Super H, Soriano E, Uylings HB. 1998. The functions of the preplate in development and evolution of the neocortex and hippocampus. *Brain research. Brain research reviews* 27: 40-64
- Suster ML, Abe G, Schouw A, Kawakami K. 2011. Transposon-mediated BAC transgenesis in zebrafish. *Nature protocols* 6: 1998-2021
- Suter DM, Pollerberg GE, Buchstaller A, Giger RJ, Dreyer WJ, Sonderegger P. 1995. Binding between the neural cell adhesion molecules axonin-1 and Nr-CAM/Bravo is involved in neuron-glia interaction. *The Journal of cell biology* 131: 1067-81
- Temizer I, Donovan JC, Baier H, Semmelhack JL. 2015. A Visual Pathway for Looming-Evoked Escape in Larval Zebrafish. *Current biology : CB* 25: 1823-34
- Tessier-Lavigne M, Goodman CS. 1996. The molecular biology of axon guidance. *Science* 274: 1123-33

- Theodosiou NA, Xu T. 1998. Use of FLP/FRT system to study *Drosophila* development. *Methods* 14: 355-65
- Thompson H, Andrews W, Parnavelas JG, Erskine L. 2009. Robo2 is required for Slit-mediated intraretinal axon guidance. *Developmental biology* 335: 418-26
- Thompson H, Barker D, Camand O, Erskine L. 2006a. Slits contribute to the guidance of retinal ganglion cell axons in the mammalian optic tract. *Developmental biology* 296: 476-84
- Thompson H, Camand O, Barker D, Erskine L. 2006b. Slit proteins regulate distinct aspects of retinal ganglion cell axon guidance within dorsal and ventral retina. *The Journal of neuroscience : the official journal of the Society for Neuroscience* 26: 8082-91
- Tissir F, Goffinet AM. 2003. Reelin and brain development. *Nature reviews. Neuroscience* 4: 496-505
- Triplet JW, Feldheim DA. 2012. Eph and ephrin signaling in the formation of topographic maps. *Semin Cell Dev Biol* 23: 7-15
- Trowe T, Klostermann S, Baier H, Granato M, Crawford AD, et al. 1996. Mutations disrupting the ordering and topographic mapping of axons in the retinotectal projection of the zebrafish, *Danio rerio*. *Development* 123: 439-50
- Wagener RJ, Witte M, Guy J, Mingo-Moreno N, Kugler S, Staiger JF. 2016. Thalamocortical Connections Drive Intracortical Activation of Functional Columns in the Mislaminated Reeler Somatosensory Cortex. *Cerebral cortex* 26: 820-37
- Walz A, Anderson RB, Irie A, Chien CB, Holt CE. 2002. Chondroitin sulfate disrupts axon pathfinding in the optic tract and alters growth cone dynamics. *J Neurobiol* 53: 330-42
- Wassle H. 2004. Parallel processing in the mammalian retina. *Nature reviews. Neuroscience* 5: 747-57
- Weiner JA, Koo SJ, Nicolas S, Fraboulet S, Pfaff SL, et al. 2004. Axon fasciculation defects and retinal dysplasias in mice lacking the immunoglobulin superfamily adhesion molecule BEN/ALCAM/SC1. *Molecular and cellular neurosciences* 27: 59-69
- Wiedenheft B, Sternberg SH, Doudna JA. 2012. RNA-guided genetic silencing systems in bacteria and archaea. *Nature* 482: 331-8
- Xiao T, Baier H. 2007. Lamina-specific axonal projections in the zebrafish tectum require the type IV collagen Dragnet. *Nature neuroscience* 10: 1529-37
- Xiao T, Staub W, Robles E, Gosse NJ, Cole GJ, Baier H. 2011. Assembly of lamina-specific neuronal connections by slit bound to type IV collagen. *Cell* 146: 164-76
- Yamagata M, Herman JP, Sanes JR. 1995. Lamina-specific expression of adhesion molecules in developing chick optic tectum. *The Journal of neuroscience : the official journal of the Society for Neuroscience* 15: 4556-71
- Yamagata M, Sanes JR. 2005. Versican in the developing brain: lamina-specific expression in interneuronal subsets and role in presynaptic maturation. *The*

Journal of neuroscience : the official journal of the Society for Neuroscience 25: 8457-67

- Yamagata M, Sanes JR. 2008. Dscam and Sidekick proteins direct lamina-specific synaptic connections in vertebrate retina. *Nature* 451: 465-9
- Yamagata M, Sanes JR. 2012. Expanding the Ig superfamily code for laminar specificity in retina: expression and role of contactins. *The Journal of neuroscience : the official journal of the Society for Neuroscience* 32: 14402-14
- Yamagata M, Weiner JA, Sanes JR. 2002. Sidekicks: synaptic adhesion molecules that promote lamina-specific connectivity in the retina. *Cell* 110: 649-60
- Yin L, Maddison LA, Li M, Kara N, LaFave MC, et al. 2015. Multiplex Conditional Mutagenesis Using Transgenic Expression of Cas9 and sgRNAs. *Genetics* 200: 431-41
- Zmuda JF, Rivas RJ. 1998. The Golgi apparatus and the centrosome are localized to the sites of newly emerging axons in cerebellar granule neurons in vitro. *Cell motility and the cytoskeleton* 41: 18-38
- Zuko A, Bouyain S, van der Zwaag B, Burbach JP. 2011. Contactins: structural aspects in relation to developmental functions in brain disease. *Advances in protein chemistry and structural biology* 84: 143-80

Publications

Articles

Di Donato V, Auer T, De Santis F, Duroure K, Concordet J-P, Del Bene F. *A gradient of Reelin regulates axonal lamination in the vertebrate visual system*. **Manuscript submitted**

Fontenas L, De Santis F*, **Di Donato V*** Chambraud B, Del Bene F, Tawk M. *Neuronal *ndrg4* is essential for nodes of Ranvier organization in zebrafish*. **Manuscript in revision. *equal contribution**

Di Donato V*, De Santis F*, Auer T, Testa N, Sanchez-Iranzo H, Mercader N, Concordet J-P, Del Bene F. *2C-Cas9: a versatile tool for clonal analysis of gene function*. **Genome research**. 2016 Mar 8. ***equal contribution**

Paolini A*, Duchemin AL*, Albadri S, Patzel E, Bornhorst D, González Avalos P, Lemke S, Machate A, Brand M, Sel S, **Di Donato V**, Del Bene F, Zolessi FR, Ramialison M, Poggi L. *Asymmetric inheritance of the apical domain and self-renewal of retinal ganglion cell progenitors depend on Anillin function*. **Development**. 2015 Feb 5.

Di Donato V*, Auer T*, Duroure K, Del Bene F. *Characterization of the Calcium Binding Protein Family in Zebrafish*. **PLoS One**. 2013;8(1):e53299. ***equal contribution**

Book chapters

Albadri S*, **Di Donato V***, De Santis F*, Del Bene F. *Knock-in and Knock-out approaches in zebrafish neurobiology*. Chapter for IPSEN conference **Genome editing in Neuroscience conference**, April 2016 ***equal contribution**

De Santis F*, **Di Donato V***, Del Bene F. *Clonal Analysis of Gene Loss-of-function and Tissue-specific Gene Deletion in Zebrafish via CRISPR/Cas9 Technology*. **Methods in cell biology**. June 2016. ***equal contribution**

Characterization of the Calcium Binding Protein Family in Zebrafish

Vincenzo Di Donato^{1,2,3,9}, Thomas O. Auer^{1,2,3,4,9}, Karine Duroure^{1,2,3}, Filippo Del Bene^{1,2,3*}

1 Institut Curie, Centre de Recherche, Paris, France, **2** CNRS UMR 3215, Paris, France, **3** INSERM U934, Paris, France, **4** Centre for Organismal Studies Heidelberg, Im Neuenheimer Feld 230, University of Heidelberg, Heidelberg, Germany

Abstract

Calcium Binding Proteins (CaBPs), part of the vast family of EF-Hand-domain containing proteins, modulate intracellular calcium levels. They thereby contribute to a broad spectrum of biological processes – amongst others cell migration, gene expression and neural activity. In this study we identified twelve members of this protein family in zebrafish including one gene (*cabp4b*) currently not present in the zebrafish genome assembly. To gain insight into their biological functions, we carried out a detailed analysis of the expression patterns of these genes during zebrafish late embryonic and early larval development. We detected specific transcription for most of them in different neuronal cell populations including the neuroretina, the inner ear and the notochord. Our data supports potential roles for CaBPs during neuronal development and function and provides a starting point for genetic studies to examine CaBPs' function in these tissues and organs.

Citation: Di Donato V, Auer TO, Duroure K, Del Bene F (2013) Characterization of the Calcium Binding Protein Family in Zebrafish. PLoS ONE 8(1): e53299. doi:10.1371/journal.pone.0053299

Editor: Ferenc Mueller, University of Birmingham, United Kingdom

Received: August 2, 2012; **Accepted:** November 30, 2012; **Published:** January 16, 2013

Copyright: © 2013 Di Donato et al. This is an open-access article distributed under the terms of the Creative Commons Attribution License, which permits unrestricted use, distribution, and reproduction in any medium, provided the original author and source are credited.

Funding: This work was supported by the ATIP/AVENIR program from CNRS/INSERM and an EC-IRG reintegration grant to FDB. VDD was supported by a Leonardo a scholarship of the Leonardo da Vinci project Unipharma-Graduates. TOA was supported by a Boeringer-Ingelheim Fonds Ph.D. fellowship. The funders had no role in study design, data collection and analysis, decision to publish, or preparation of the manuscript.

Competing Interests: Filippo Del Bene is currently an academic editor for PLOS ONE. This does not alter the authors' adherence to all the PLOS ONE policies on sharing data and materials.

* E-mail: Filippo.Del-Bene@curie.fr

⁹ These authors contributed equally to this work.

Introduction

Calcium signaling is a fundamental process required for communication between neurons [1]. A local and rapid increase in calcium concentration within the pre- and postsynaptic specialization is required for transmission of information throughout the nervous system. The massive influx of calcium into the postsynaptic neuron triggers the activation of specific gene expression programs leading to long-term or short-term synaptic alterations [2,3].

Since calcium-dependent gene transcription is involved in the control of crucial processes such as synapse development, maturation and refinement, it must be strictly regulated [4].

A broad spectrum of calcium sensing proteins acts as buffer for intracellular calcium, modulating and restricting the spatial and temporal impact of calcium as a second messenger. This gives these proteins a central role as regulators of the signaling pathways triggered or promoted by calcium.

Calcium binding typically elicits a conformational switch in the sensor. This switch leads to various interactions with downstream effectors and ultimately modulates neuronal activity [5]. For instance, the calcium binding protein Calmodulin (CaM) has been shown to bind the intracellular domain of the L-type voltage sensitive calcium channel and, upon calcium influx, to activate Ras/MAP Kinase signaling thus triggering gene transcription in the nucleus [6].

In mammals, the Calmodulin (CaM) superfamily, characterized by an EF-hand calcium binding motif, forms the largest class of calcium sensing proteins [7]. A related subfamily, the Calcium

Binding Proteins (CaBPs) share a very similar domain organization with CaM and have been shown to have coevolved in vertebrate animals [8]. In humans the Calcium Binding Protein family is composed of six members: CaBP1, 2, 4, 5, 7 and 8. While the *cabp6* gene has not been identified, *cabp3* is most probably a pseudogene [9]. *Cabp7* and *cabp8* were alternatively referred to as *calneuron2* and *calneuron1* respectively in earlier studies [10,11] and form a separate sub-family based on their sequence characteristics.

The expression pattern of single members of the CaBP family has been analyzed in human and mouse tissues (for a summary see Table 1.) but the localisation of the majority of them remains unknown. Furthermore, a few functional studies have been carried out, showing the involvement of CaBPs in the physiology of neural circuits. For example, *cabp4* and *5* were observed to be expressed in the retina where the respective proteins play a role in the modulation of visual stimuli, most likely by their interaction with voltage-gated Calcium channels [12] [13]. The specific expression of other Calcium binding proteins has been observed to be connected to a precise function [14] in their respective expression domains.

In the following study we describe the expression patterns of all known Calcium binding proteins during the first five days of zebrafish development. We furthermore identified a new member of this gene family, *cabp4b* that is not part of the actual Zv.9 genome assembly.

Table 1. Comparison of CaBP family member expression domains in mouse and zebrafish.

Gene in mouse	Expression domain	Reference	Gene in zebrafish	Expression domain
<i>cabp1</i>	Retina (INL* amacrine cells and subset of bipolars); Cerebellum	Haeseleer et al. (2000) [9]	<i>cabp1a</i>	Amacrine cells, heart, notochord
			<i>cabp1b</i>	Amacrine cells, otic vesicles, notochord
<i>cabp2</i>	Retina	Haeseleer et al. (2000) [9]	<i>cabp2a</i>	Retina (bipolar cells), notochord
			<i>cabp2b</i>	Inner ear; neuromasts
<i>cabp4</i>	Photoreceptors	Haeseleer et al. (2004) [12]	<i>cabp4a</i>	No specific expression
			<i>cabp4b</i>	Photoreceptors
<i>cabp5</i>	Retina (rod bipolar cells)	Haeseleer et al. (2000) [9], Rieke et al. (2008) [13]	<i>cabp5a</i>	No specific expression
			<i>cabp5b</i>	Inner ear; Retina (bipolar cells); otic vesicles
<i>cabp7</i>	CA3** region of the hippocampus; entorhinal cortex; antero-dorsal and anteroventral thalamus; inferior and superior colliculus	Mikhaylova et al.(2006) [11]	<i>cabp7a</i>	Dorsal thalamus; cerebellar plate
			<i>cabp7b</i>	Nucleus of medial longitudinal fascicle; reticular formation
<i>caln1 (cabp8)</i>	Cerebellum; Hippocampus; Cortex	Wu et al. (2001) [10]	<i>caln1</i>	Pallium; Thalamus, pronephric duct; Retina (ganglion cell layer)
			<i>caln2</i>	Pallium; Thalamus; Retina (ganglion cell layer)

*inner nuclear layer.

**curnu ammonis.

doi:10.1371/journal.pone.0053299.t001

Results

Phylogenetic analysis

To identify all Calcium binding protein family members in zebrafish we used the Ensembl orthology prediction tool. Based on their human orthologs we found two zebrafish paralogs for each gene (except *cabp4*). This is consistent with the commonly accepted theory that all teleosts underwent one additional round of whole genome duplication in evolution [15]. Surprisingly compared with the other 4 teleosts (medaka, takifugu, tetraodon, stickleback) zebrafish seemed to be the only species with just one paralog of *cabp4*. To identify a potential second zebrafish paralog for this gene we searched the NCBI expressed sequence tag collection for a suitable cDNA clone using the Tetraodon *cabp4* (2of2) cDNA sequence as bait. As the best hit, with 77% sequence identity, we identified a cDNA clone from a zebrafish retina cDNA library. This sequence was not present in the current *Zv.9* assembly. When we aligned the cDNA clone with all other zebrafish *cabps* cDNA sequences it displayed the highest degree of conservation to *cabp4a* (data not shown). Using specific primers against the identified cDNA clone (IMAGE:4145466) sequence, we were able to amplify a 530 bp fragment from wild type Tupfel long fin cDNA. The online protein domain prediction tool Prosite from ExPasy assigned two EF-Hand domains to the unknown gene (Fig. 1C). Based on these results, we decided to call this cDNA clone *cabp4b*.

We subsequently calculated a phylogenetic tree based on the protein sequences of all *H. sapiens* and *D. rerio* Calcium binding proteins (for details see Material and Methods). As previously described [10] *cabp7s* and *cabp8s* (*cabneurons*) form a separate subfamily (Fig. 1). *Cabp4* is closest related to this subtree followed by *cabp5*. Furthermore, both zebrafish *cabp5* and *cabp2* paralogs show a closer relationship to the zebrafish *cabp2* paralogs than to their human orthologs.

In situ expression analysis

In order to determine the spatial distribution of calcium binding protein mRNA, we performed whole mount *in situ* hybridisation analyses with specific antisense probes.

CaBP1s

The expression pattern at different stages of development for both *cabp1a* and *cabp1b* is consistent with the data reported in the ZFIN website [16]. At 48hpf *cabp1a* exhibits a broad expression throughout the developing brain (Fig. 2, A–D) with additional expression in the notochord and the heart. 72hpf the staining of the antisense probe is restricted to the inner half of the inner nuclear layer (INL) of the retina (Fig. 2, A'–D'). To determine the precise neuronal type showing *cabp1a* expression we employed the zebrafish transgenic line Tg(Ptf1a:GFP) [17] (pancreas transcription factor 1 a) that has been shown to label the two inhibitory neuronal types (horizontal and amacrine cells) of the retina. Thereby, we were able to indicate amacrine cells as the most likely *cabp1a*-expressing population (compare Fig. 2 F–H). This observation is consistent with previous data by Wu et al. [10] where mRNA of the mouse *cabp1* ortholog was detected in amacrine cells of the mouse retina.

When the whole mount staining pattern of *cabp1b* was investigated, we could detect at 48hpf, a strong staining in the otic vesicles and along the notochord (Fig. 3, A–D). At 5dpf the strong expression of *cabp1b* in the notochord was maintained with an additional expression domain in the amacrine cells layer of the retina (Fig. 3, A'–D'). Comparison of *cabp1b* antisense probe signal with GFP in the Tg(Ptf1a:GFP) line strongly suggests expression in this cell type (Fig. 3, E–H).

CaBP2s

Whole mount RNA expression analyses of *cabp2a* revealed no specific signal at early developmental stages. At 72hpf we could

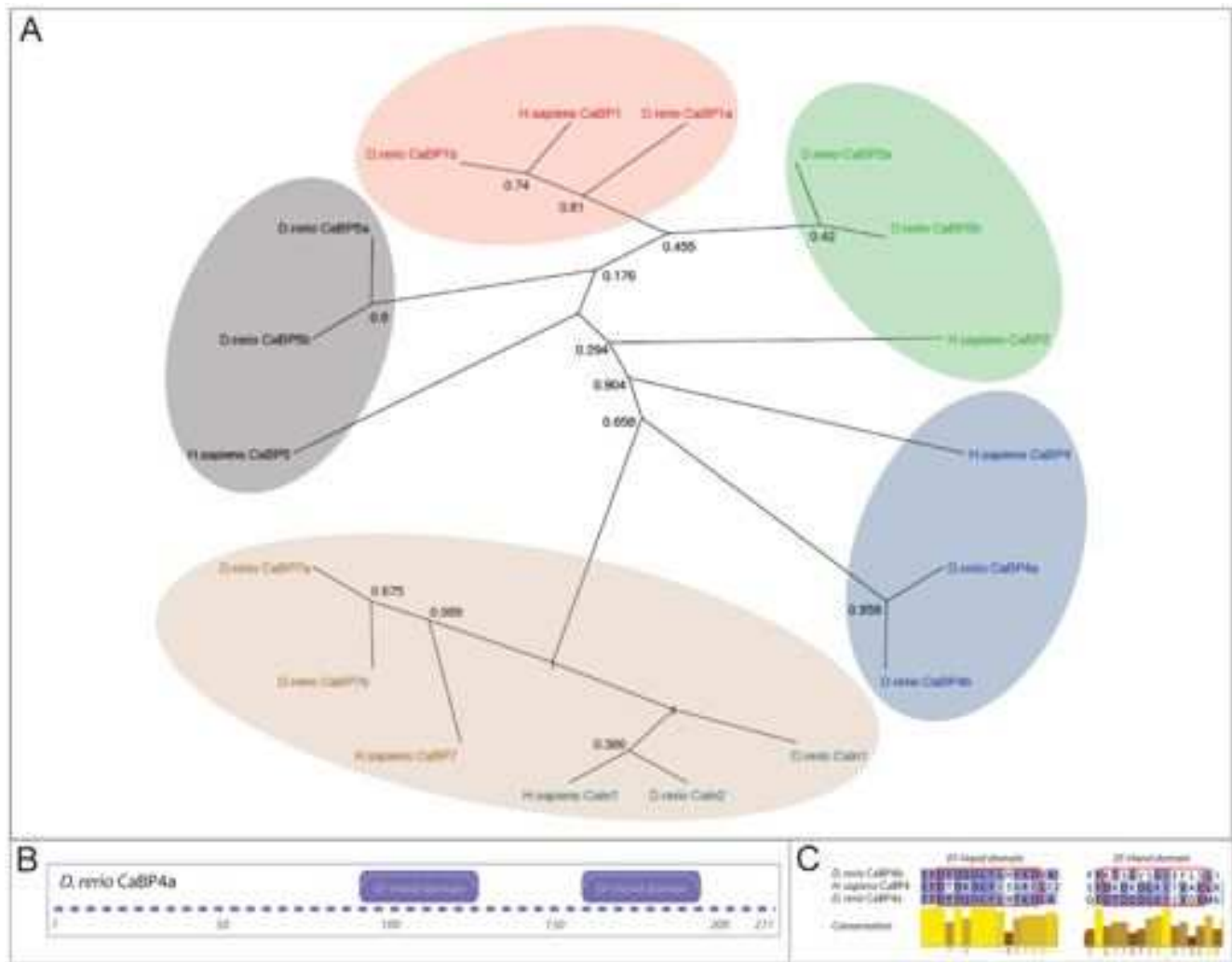


Figure 1. Phylogenetic analysis of the Calcium binding protein family in zebrafish. A) The phylogenetic tree of all human and zebrafish Calcium binding protein family members based on protein sequence. For all members there exist two paralogs in zebrafish per human paralog. *Cabp7* and *calneuron* (*cabp8*) form a separate subfamily (brown shading). B) Domain structure of CaBP4b as predicted by ExPasy (www.expasy.org). C) Protein alignment of the two EF domains of the human CaBP4 protein, the known zebrafish ortholog (*cabp4a*) and its newly discovered paralog (*cabp4b*). The blue color represents the Blossum62 score; high similarities are in dark blue while lower similarities are indicated in light blue. The first EF-Hand domain shows a higher degree of conservation than the second one.
doi:10.1371/journal.pone.0053299.g001

detect prominent expression in the retina and in the notochord (Fig. 4, A–D). To further clarify the identity of *cabp2a* expressing cells in the retinal tissue, we used the zebrafish transgenic line Tg(Vsx2:GFP) [18]. Vsx2, a homeodomain transcription factor, is initially expressed throughout the retinal epithelium, but is later enriched in a minor population of bipolar cells in the outer part of the INL. Localisation of GFP and the *in situ* signal (Fig. 4, E–H) show that *cabp2a* is expressed in the bipolar cells of the retina consistent with specific mRNA distribution of the mouse ortholog *cabp2* in the mouse retina and minor retinal component in other species [9].

For *cabp2b*, both, the inner ear and neuromasts in the lateral line exhibit strong staining from 72hpf onwards (Fig. 5). The localisation in hair cells of both sensory organs was further supported by analyzing the expression in the Tg(Brn3C:memGFP) transgenic line [19]. In this line the GFP signal can be observed in a subset of retinal ganglion cells, hair cells of the inner ear and the lateral line neuromasts.

CaBP4s

During the first five days of development no mRNA of the *cabp4a* gene could be detected. Similarly, the newly discovered *cabp4b* was not detected in any tissue within the first 72 hours post fertilization. Importantly, from day 4 onwards, a strong staining in the photoreceptor layer became visible (Fig. 6). This specific pattern of expression has also been described in mammals where *cabp4* was shown to play a crucial role in photoreceptor physiology [12]. The impairment of *cabp4* function triggers severe defects of vision like autosomal recessive night blindness [20].

CaBP5s

Endogenous *cabp5a* mRNA shows no expression in all the stages of development analyzed, while for adult eye tissue there was EST evidence reported [21]. For *cabp5b*, from 48hpf onwards, the expression pattern is consistent with the profile shown by Thisse *et al.*, 2004¹⁶: the otic vesicles display a very prominent labeling, which is maintained in later stages (Fig. 7). In addition, in 5dpf

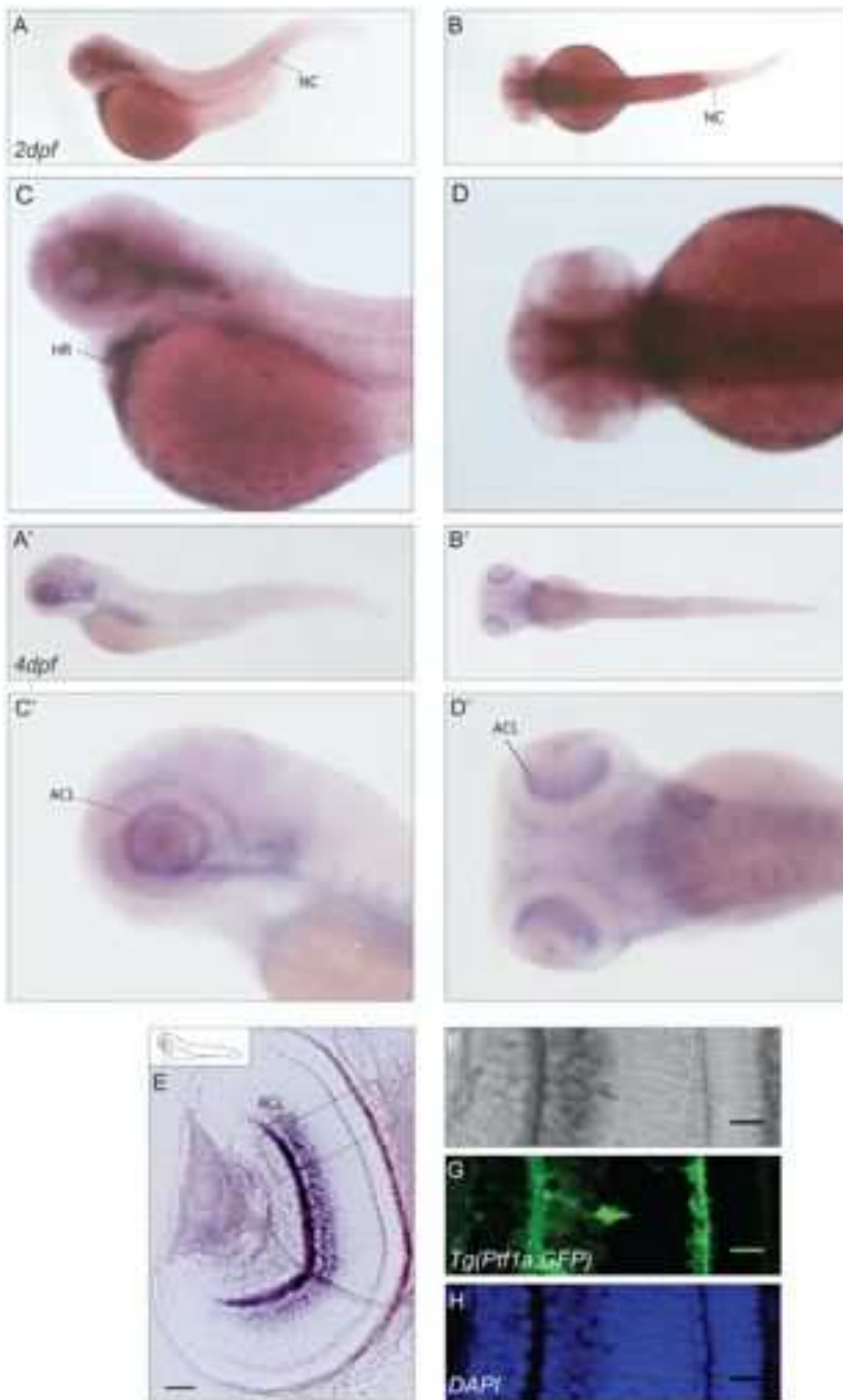


Figure 2. Expression pattern of *cabp1a*. (A–D') mRNA expression of *cabp1a* in lateral (A–A') and dorsal (B,B') views of a 2 dpf and 4 dpf zebrafish embryo with higher magnifications (C–D,C'–D'). (E–H). Cross-sections of retinae in the Tg(Ptf1a:GFP) transgenic line show staining of *cabp1a* in the amacrine cell layer. (E) Epifluorescence picture of a sectioned retina. Scale bar: 50 μm (F–H) Confocal images of the area selected in E. (F) *In situ* signal in bright field, (G) GFP signal restricted to amacrine cells, (H) DAPI nuclear stain. Scale bar: 20 μm. HR: heart, NC: notochord, ACL: amacrine cell layer. doi:10.1371/journal.pone.0053299.g002

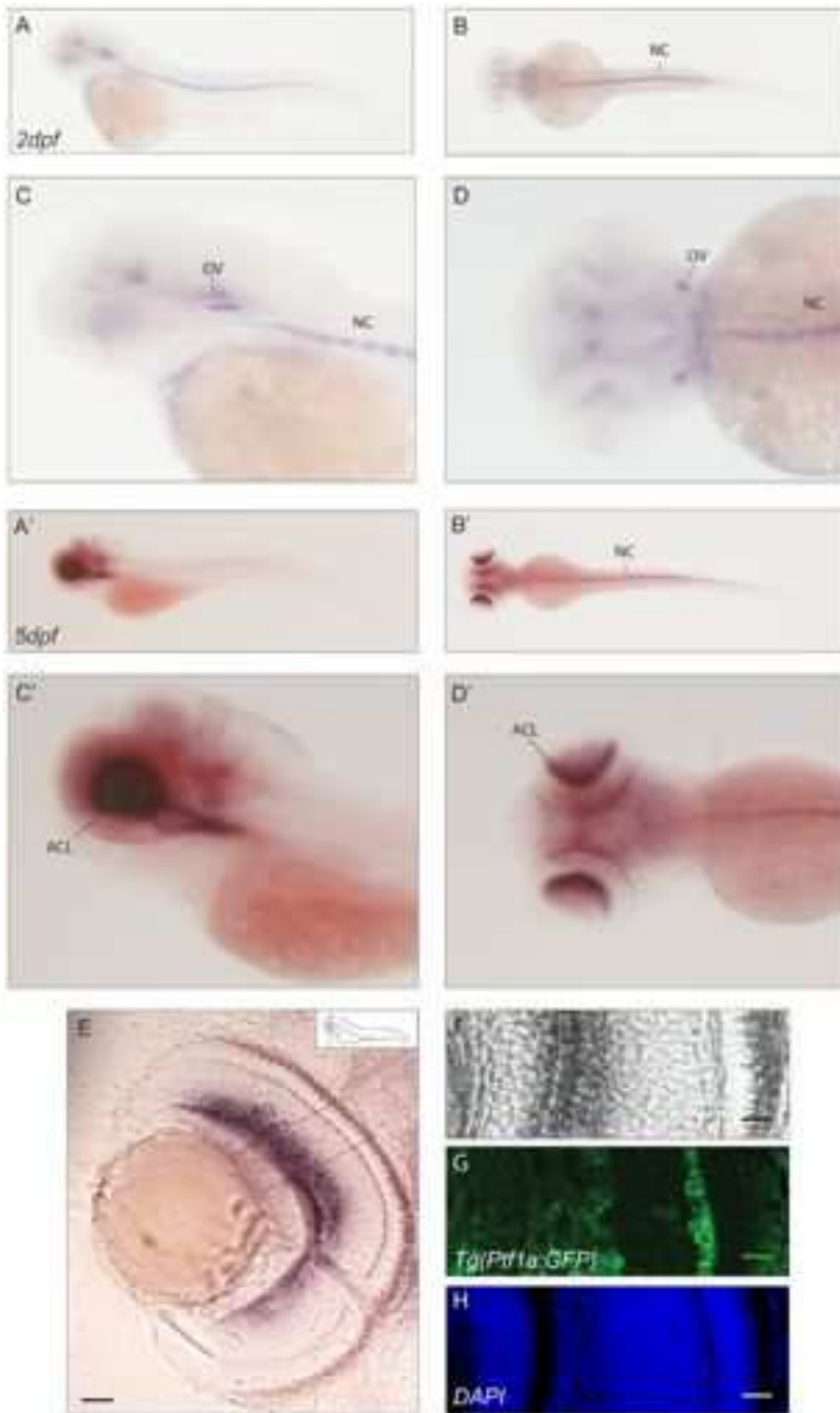


Figure 3. Expression pattern of *cabp1b*. (A–D') Expression in 2dpf (A–D) and 5dpf (A'–D') zebrafish embryos: lateral (A,C–A',C') and dorsal (B,D–B',D') views. At 2dpf a signal in the otic vesicles and the notochord can be detected. At 5dpf expression in the notochord and the amacrine cell layer of the retina is seen. (E–H). Cross-sections of retinæ in the Tg(Ptf1a:GFP) transgenic line show staining of *cabp1b* in the amacrine cell layer.(E)

Epifluorescence picture of a sectioned retina. Scale bar: 50 μm (F–H) Confocal images of the area selected in E. (F) *In situ* signal in bright field, (G) GFP signal restricted to amacrine cells, (H) DAPI nuclear stain. Scale bar: 20 μm . OV: otic vesicle, NC: notochord, ACL: amacrine cell layer.
doi:10.1371/journal.pone.0053299.g003

larvae a strong signal is detectable in the retinal inner nuclear layer and in the notochord (Fig. 7, A'–D'). To identify the *cabp5b*-expressing cells, we assayed whole-mount *in situ* hybridisation in the zebrafish transgenic lines Tg(Vsx2:GFP) and Tg(Brn3C:memGFP). In the Vsx2 transgenic line we see expression of GFP and *cabp5b* in the inner nuclear layer of the retina, in what are most probably bipolar cells. On the contrary, *brn3C* and *cabp5b* expressing cells in the ear represent distinct populations. Interestingly, for mouse *cabp5*, a role in rod to bipolar cell signaling was proposed by Rieke et al. [13]. Upon loss of *cabp5* function, the rod-mediated responses of retinal ganglion cells were reduced which might reflect a change in the presynaptic function of rod bipolar cells.

CaBP7s

Homolog to human *calcium binding protein 7* (ENSG00000100314, also known as *Calneuron2*), the two zebrafish genes *cabp7a* (annotated as *cabp7 2of2*, ENSDARG00000078272) and *cabp7b* (annotated as *cabp7b*, ENSDARG00000060846) were analyzed for their spatio-temporal expression pattern. *cabp7a* showed widespread expression throughout the brain from day 3 onwards with a prominent labeling detected in the dorsal thalamus region, as well as at the level of the cerebellar plate (Fig. 8). For *cabp7b*, the observed expression was more restricted to the midbrain and the hindbrain area anterior to the medulla oblongata (Fig. 9). Some regions, such as the migrated posterior tubercular area, the nucleus of medial longitudinal fascicle and the reticular formation, revealed a prominent staining. No expression

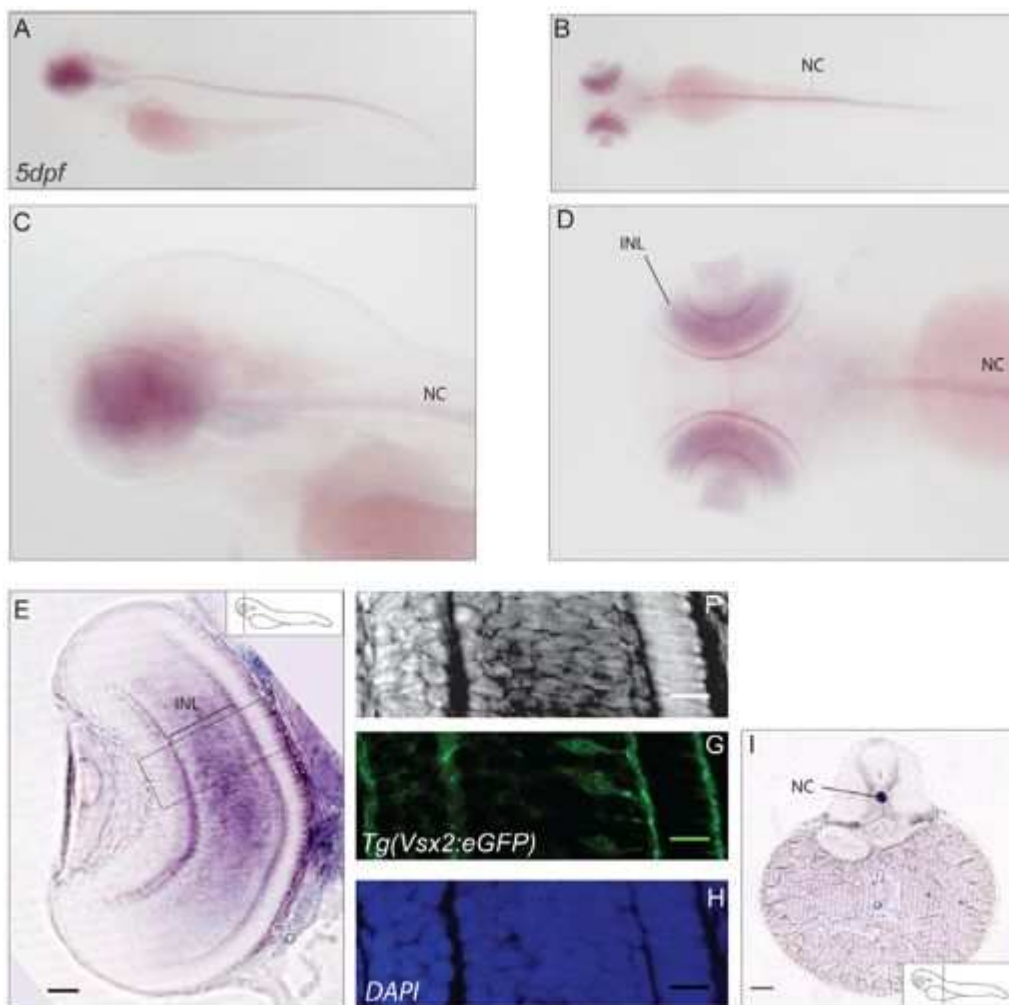


Figure 4. Expression pattern of *cabp2a*. (A–D) *In situ* hybridisation showing expression of *cabp2a* in 5dpf larvae. Lateral views (A,C), dorsal views (B, D). *Cabp2a* antisense probe exhibits diffuse retinal localisation; a strong staining is also present along the notochord. (E–H) Cross-section of a retina in the Tg(Vsx2:eGFP) transgenic line. (E) Epifluorescence image of a sectioned retina, showing prominent expression of *cabp2a* in the bipolar cell layer. Scale bar: 50 μm . (F–H) Confocal images of the area selected in E. (F) *In situ* signal in bright field, (G) GFP signal localized in bipolar cells, (H) DAPI. Scale bar: 20 μm (I) Cross-section exhibiting *in situ* staining in the notochord. Scale bar: 100 μm . INL: inner nuclear layer, NC: notochord.
doi:10.1371/journal.pone.0053299.g004

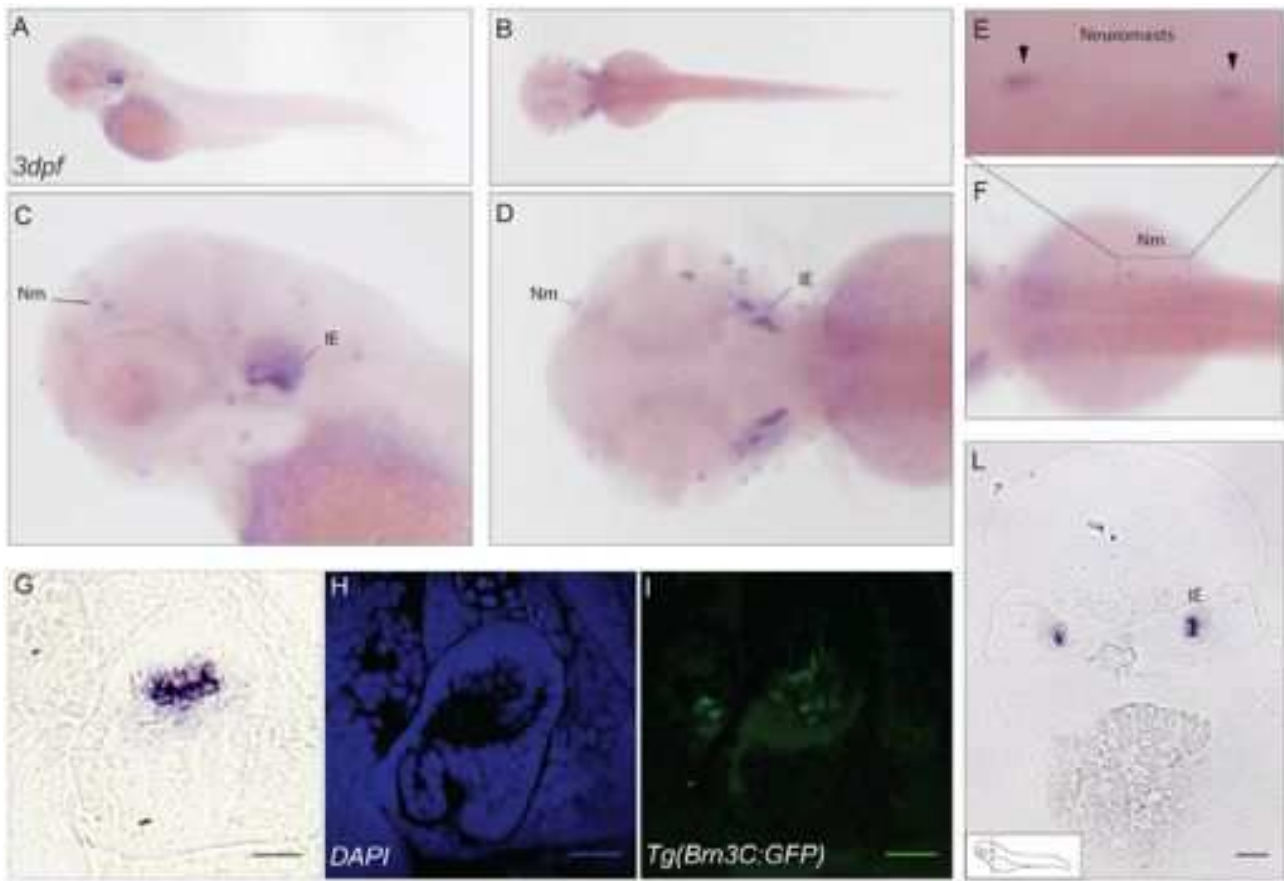


Figure 5. Expression pattern of *cabp2b*. (A–D) *In situ* hybridisation signal of *cabp2b* in 3dpf zebrafish embryos. Lateral (A) and dorsal (B) views of the embryo with higher magnification (C–D). Staining is restricted to hair cells in the inner ear and to the neuromasts. (F) View of stained neuromasts in the lateral line and (E) higher magnification of the selected area; arrowheads in E show the neuromasts. (G–L) Transverse section of the ear in the Tg(Brn3C:memGFP) transgenic line. (L) Epifluorescence image, showing strong expression of *cabp2b* in a subset of cells in the inner ear. Scale bar: 100 µm. (G) Higher magnification picture. (H–I) Confocal images. (H) DAPI signal, (I) GFP staining in the same domain as *cabp2b*. Scale bar: 20 µm. Nm: neuromast, IE: inner ear.

doi:10.1371/journal.pone.0053299.g005

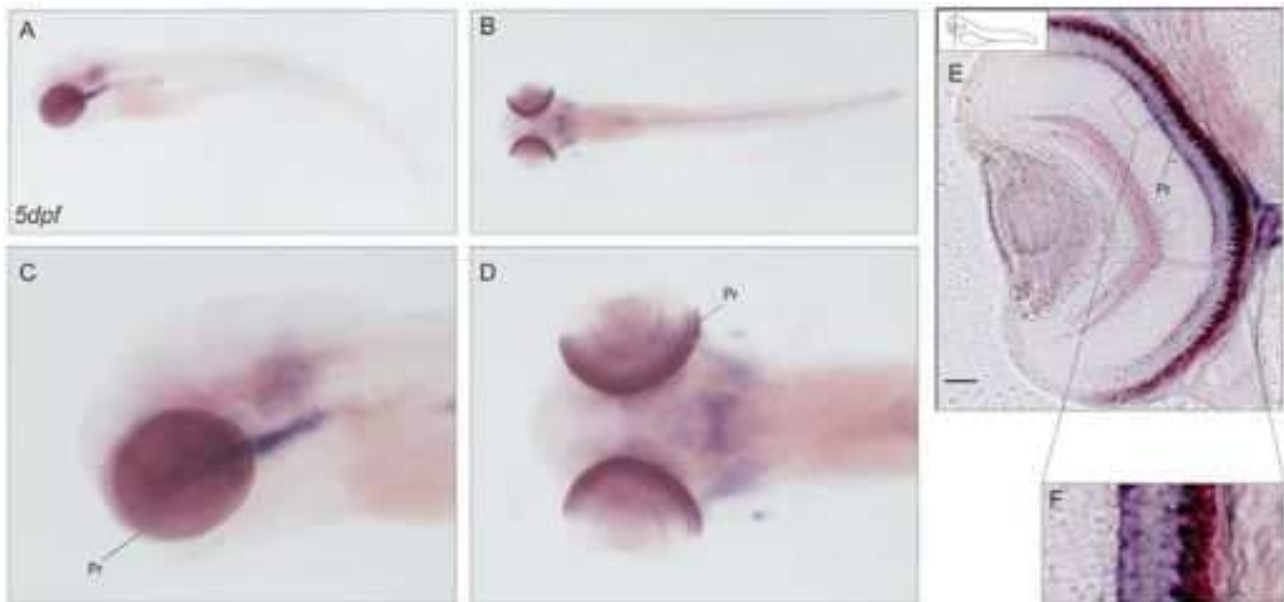


Figure 6. Expression pattern of *cabp4b*. (A–D) *In situ* localisation of *cabp4b* transcript in 5dpf larvae. Lateral (A–C) and dorsal views (B–D). A strong staining in the photoreceptor layer is detected. (E–F) Cross section of a retina (E) with zoom in to the photoreceptor layer (F). Scale bar: 20 µm. Pr: photoreceptors.

doi:10.1371/journal.pone.0053299.g006

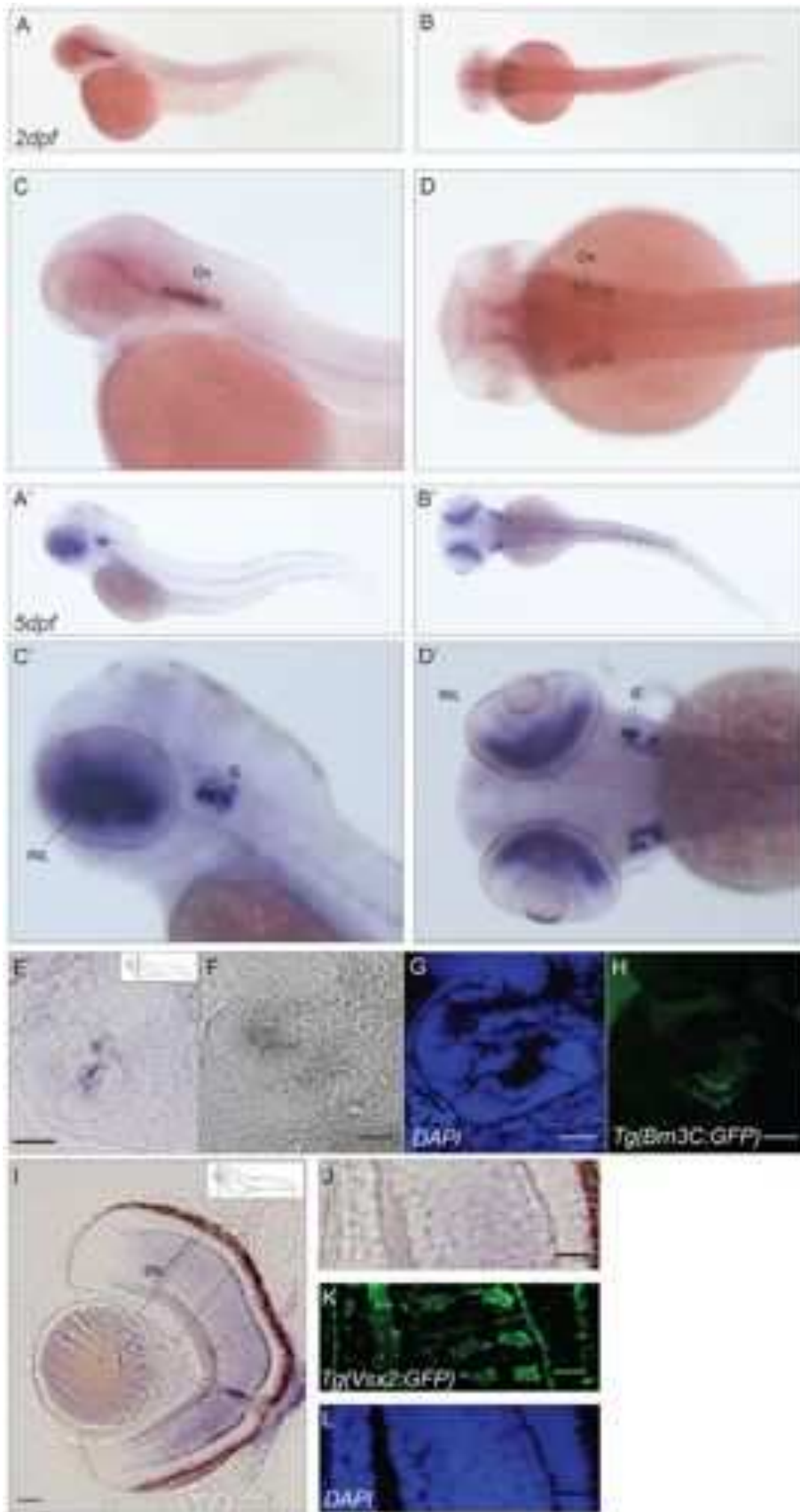


Figure 7. Expression pattern of *cabp5b*. (A–D') *Cabp5b* expression in 2dpf (A–D) and 5dpf (A'–D') zebrafish embryos: lateral (A,C–A',C') and dorsal (B,D–B',D') views. An intense staining is present in the inner ear and in the notochord at both stages of development. In 5dpf embryos, in addition, a strong signal is detectable in the retinal inner nuclear layer. (E–H) Sections of the ear in Tg(Brn3C:memGFP) transgenic line embryos.

Epifluorescence image of a sectioned ear (E) and confocal images (F–H) showing strong expression of *cabp5b* in a subset of cells in the inner ear. Picture in bright field (F), DAPI (G), GFP (H). Scale bar: 20 μm . (I–L) Cross-sections of a retina in the Tg(Vsx2:eGFP) transgenic line. Epifluorescence image of a sectioned retina (I) and magnification (J), showing *cabp5b* antisense probe signal in the bipolar cell layer. Scale bar: 50 μm . (K–L) Confocal images. GFP signal localized in bipolar cells (K), DAPI (L). Scale bar: 20 μm . Ov: otic vesicle, IE: inner ear, INL: inner nuclear layer. doi:10.1371/journal.pone.0053299.g007

in the dorsal parts of the brain such as optic tectum and cerebellum could be detected (Fig. 9, E, F).

CaBP8s

Calcium binding protein 8, also known as *calneuron1*, has the two homologs *caln1* and *caln2* in zebrafish. Both of them are characterized by an early onset (between 24hpf and 48hpf) of expression (Fig. 10, A–D, Fig. 11, A–D). In 48hpf embryos, *caln1* exhibits a specific *in situ* hybridisation pattern, restricted to a population of primary sensory neurons - most probably Rohon Beard cells (Fig. 10, A–D). Analysis at later stages, 4dpf, reveals expression of *caln1* predominantly extending from the telencephalic pallial domain to the ventral thalamus region (Fig. 10, A'–D'). In addition, *caln2* is detected in 4dpf embryos in what is most probably the head of the pronephric ducts. The expression pattern observed for *caln2* seems to overlap with that of *caln1* at later stages - a very localized staining is detectable at 48hpf in the subpallial region and in the caudal midbrain (Fig. 11, A–D). *Caln1* and 2 are also detected in a subset of retinal ganglion cells - in the case of *caln2* localized at the center of the ganglion cell layer (Fig. 11, E).

Discussion

Our work indicates that Calcium Binding Protein family members show very specific expression patterns in the course of zebrafish embryonic and larval development. Comparing our data with the published literature in mouse we observe a consistent conservation of most expression domains between the mammalian and the teleost clade (Table 1). In addition, we detected expression of *cabp2b* and *cabp5b* in hair cells of the inner ear, that has not been

previously described in mice, and the neuromasts of the lateral line.

As a consequence of the extra genome duplication in teleosts, the two zebrafish orthologs either showed distinct expression patterns (i. g. *cabp2a* and *cabp2b*) or expression could not be detected for one of the two paralogs (i. g. *cabp1a* and *cabp1b*). The separate expression domains of the two paralogs suggest a possible subfunctionalization during teleost evolution [22]. This remarkable feature of the zebrafish system and its amenability to genetic manipulation will allow a detailed dissection of CaBP function in the different neuronal subpopulations where they are expressed.

In addition, we identified a new member of the *cabp* family, *cabp4b*, that is not part of the current zebrafish genome assembly. In humans, this gene has been related to different retinal pathologies such as the congenital cone-rod synaptic disorder and autosomal recessive night blindness.

Therefore, our findings open up the possibility to further dissect the molecular mechanisms underlying the pathology in humans using zebrafish as a model organism.

Materials and Methods

Ethic statements

All fish are housed in the fish facility of our laboratory, which was built according to the local animal welfare standards. All animal procedures were performed in accordance with French and European Union animal welfare guidelines.

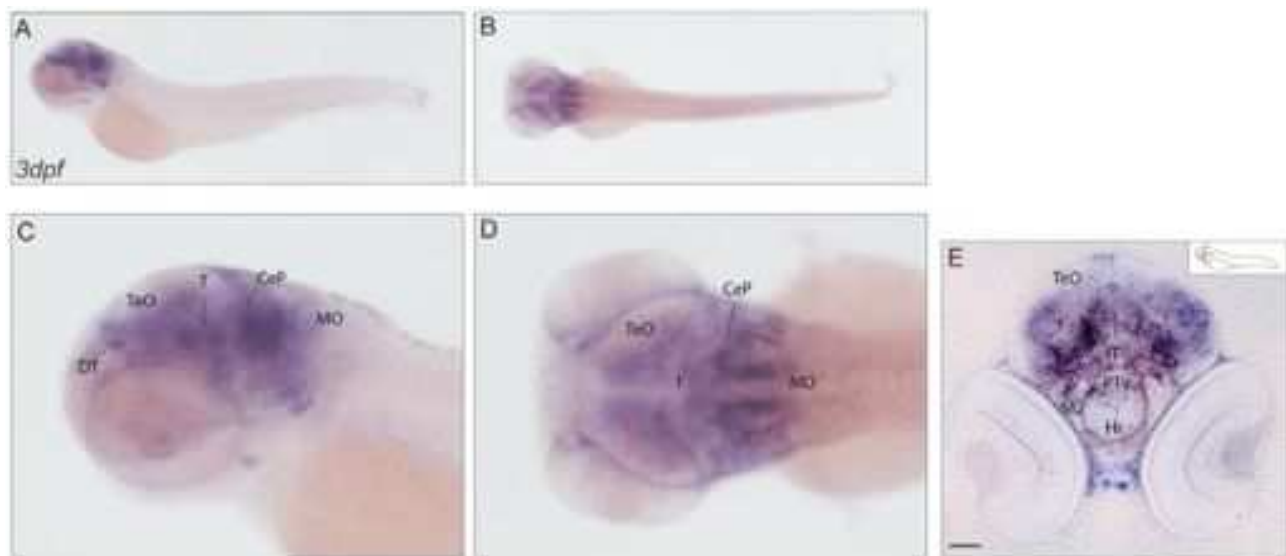


Figure 8. Expression pattern of *cabp7a*. (A–D) mRNA expression of *cabp7a* in lateral (A) and dorsal (B) views of 3dpf larvae with higher magnification (C–D). The signal of *cabp7a* antisense probe is widespread in the brain, with a stronger staining detected in the regions of the dorsal thalamus and the cerebellar plate. (E) Transverse section at the level of the eye, exhibiting diffuse expression of *cabp7a* in the developing brain. Scale bar: 100 μm . CeP: cerebellar plate; DT: dorsal thalamus; Hr: rostral hypothalamus; M2: migrated posterior tubercular area; MO: medulla oblongata; PTV: ventral part of posterior tuberculum; T: midbrain tegmentum; TeO: tectum opticum. doi:10.1371/journal.pone.0053299.g008

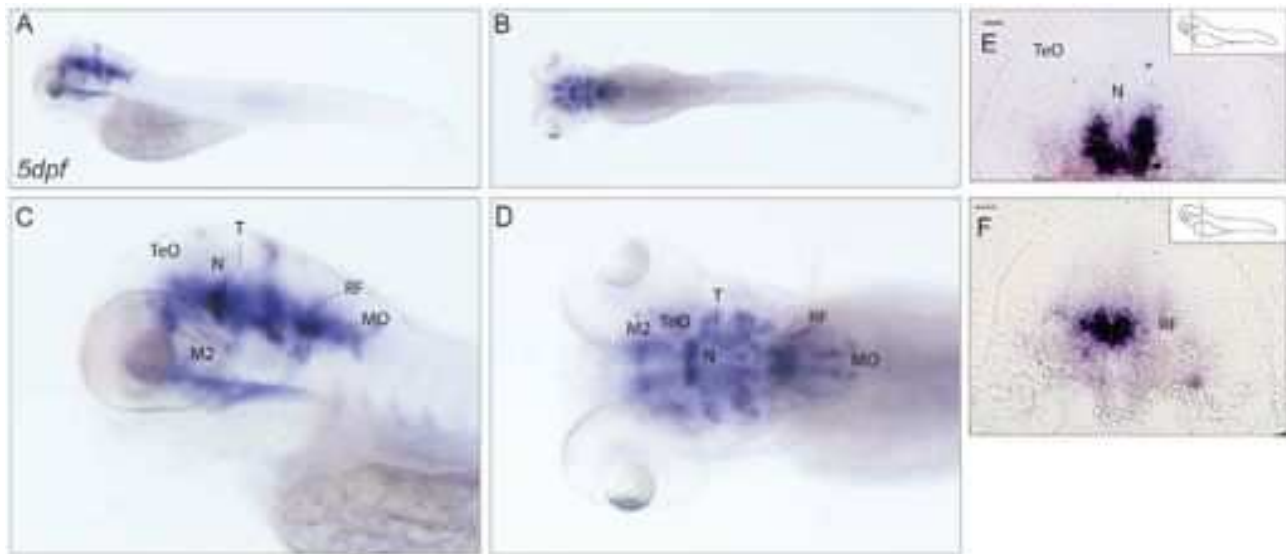


Figure 9. Expression pattern of *cabp7b*. (A–D) *In situ* localisation of *cabp7b* transcript in 5dpf larvae. Lateral (A,C) and dorsal views (B, D). A wide distribution of *cabp7b* mRNA in the brain was observed. (E,F) Transverse sections. Strongly stained cells are present in the midbrain, probably in the region of the nucleus of medial longitudinal fascicle (E) and in the hindbrain area anterior to the medulla oblongata most likely at the level of the reticular formation (F). Scale bar: 50 μ m. M2: migrated posterior tubercular area; MO: medulla oblongata; N: nucleus of medial longitudinal fascicle; RF: reticular formation; T: midbrain tegmentum; TeO: tectum opticum.
doi:10.1371/journal.pone.0053299.g009

Gene identification

Calcium binding protein members in *Danio rerio* were identified based on orthology predictions in Ensembl using the Zv9 (GCA_000002035.2) assembly. To confirm gene identities we performed multispecies alignments within the 5 teleost species *O. latipes*, *T. rubripres*, *G. aculeatus*, *T. nigroviridis* and *D. rerio* and used the following genes: *cabp1a* (ENSDARG00000033411), *cabp1b* (ENSDARG00000019990), *cabp2a* (ENSDARG00000052016), *cabp2b* (ENSDARG00000052277), *cabp4a* (ENSDARG00000008866), *cabp5a* (ENSDARG00000002576), *cabp5b* (ENSDARG00000028485), *cabp7a* (ENSDARG00000060846), *cabp7b* (ENSDARG00000078272), *cabn1 (cabp8a)* (ENSDARG00000088898), *cabn2 (cabp8b)* (ENSDARG00000069766).

In the case of *cabp4* there was just one ortholog annotated in the zebrafish Zv9 assembly. As there were two paralogs present in all other teleost fish species we used the cDNA sequence of *cabp4* (2of2) (ENSTNIG00000005250) of Tetraodon and performed a BlastN search against the EST selection of NCBI. As a result we found a cDNA clone (BG307419, fm03g10.y1, IMAGE:4145466) that showed 77% sequence similarity to the Tetraodon sequence and named it *cabp4b*.

Phylogenetic analysis

The protein sequences of *Danio rerio* and *Homo sapiens* CaBPs were obtained from Ensembl. For *cabp7b*, there was no annotated start codon and we were not able to identify a suitable translational start in the genomic upstream sequence. For *cabp4a* neither start nor stop codon were annotated. By including the flanking genomic region in the search for an ORF, both could potentially be identified upstream and downstream of the annotated gene. For the newly identified *cabp4b* the whole sequence given as BG307419 was used and translated in frame +1. Alignment of the sequences was produced using MUSCLE online at the European Bioinformatics Institute (EBI) [23]. The result of the algorithm was visualized using Jalview [24]. A phylogenetic tree was assembled using BioNJ online at phylogeny.fr performing 1000 bootstraps

and using the Jones-Taylor-Thornton matrix. This distance-based algorithm is claimed to be well suited for comparison of sequences with high substitution rates [25,26]. The tree was visualized using the open source software Dendroscope [27]. To identify the functional domains within the *cabp4b* ORF we used the ExpASy Prosite database from the Swiss Institute of Bioinformatics (SIB, www.expasy.org).

Fish husbandry and strains used

Breeding and raising of zebrafish followed standard protocols [28]. Zebrafish embryos were treated with 0.0045% 1-Phenyl-2-Thiourea (PTU) in medium after gastrulation to prevent pigment formation. For one color whole mount *in situ* hybridisation Tupfel long fin fish were used. The transgenic Tg(Vsx2:GFP) [18] and Tg(Ptf1A:GFP) [17] lines were a kind gift of Lucia Poggi and Jochen Wittbrodt; the Tg(Brn3C:memGFP) [19] line was obtained from Herwig Baier.

Molecular cloning

For generating an anti-sense probe for *cabp1a*, we ordered the clone IRBOP991H0750D from Imagenes. Subsequently, the coding fragment was cloned into the pBluescript KS vector (Invitrogen). Following linearization of the plasmid with HindIII and DNA clean-up, a Digoxigenin (DIG)-labeled antisense probe was generated using T7 RNA polymerase. Following DNaseI treatment, the synthesized probe was purified using the NucleoSpin[®] RNA II Kit (Macherey-Nagel).

The same procedure was applied for the synthesis of the anti-sense probes of *cabp2a* (IMAGp998N1115278Q(2)); into pAMP1, linearization with KpnI, transcription with SP6 polymerase; *cabp2b* (IMAGp998G1716318Q); into pBluescript Sk-, linearization with EcoRV, transcription with T7 polymerase; *cabp4a* (IMAGp998D0510667Q(4)); into pBluescript Sk-, linearization with BamHI/NotI, transcription with T7 polymerase; *cabp5a* (IRBOP991H021D); into pBluescript Sk-, linearization with NcoI, transcription with T7 polymerase; *cabp5b* (IMAG-

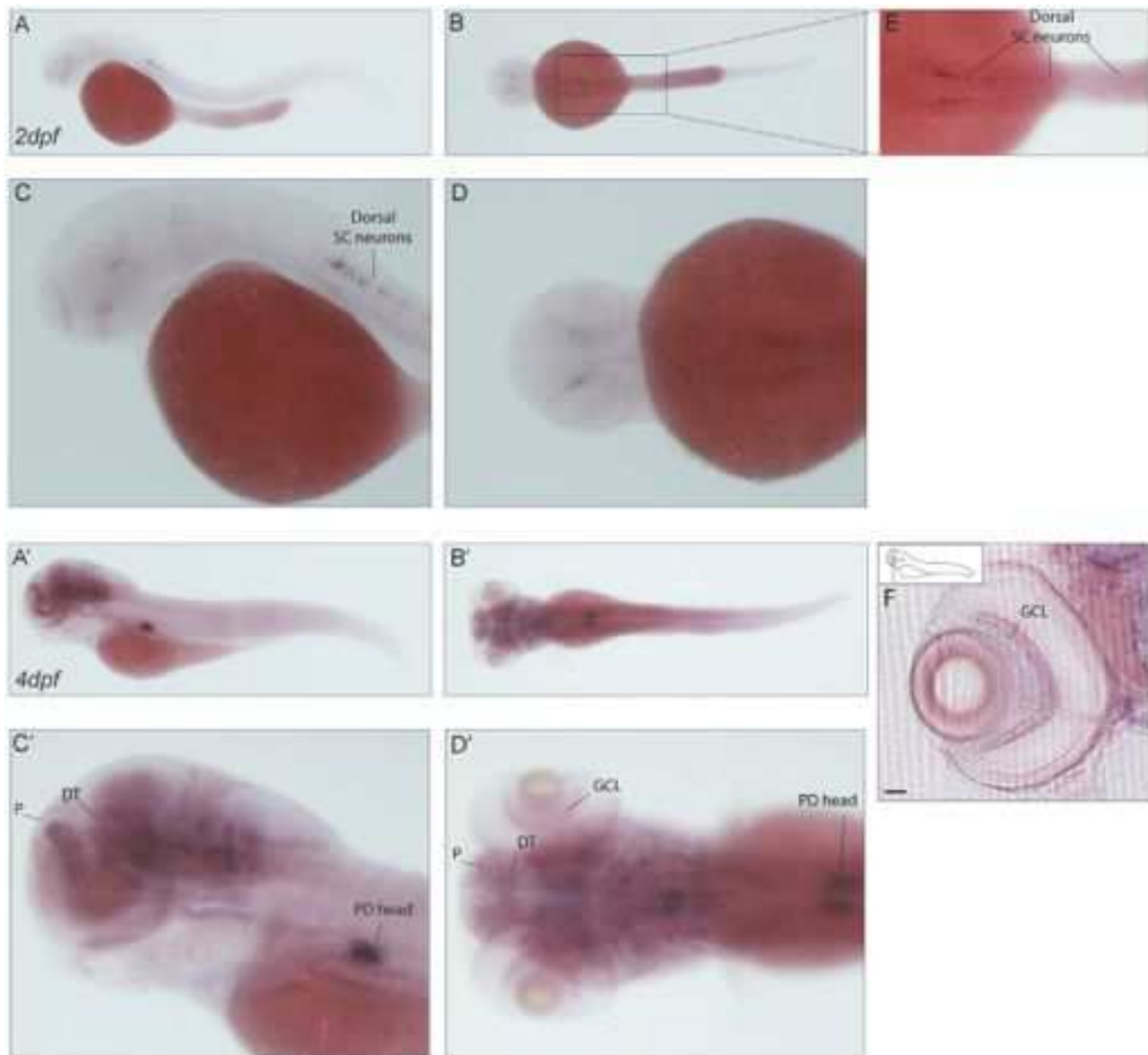


Figure 10. Expression pattern of *caln1*. (A–D') *In situ* signal of *caln1* transcript in 2dpf (A–D) and 4dpf (A'–D') larvae. Lateral (A,C–A',C') and dorsal views (B,D–B',D'). (E) Higher magnification shows specific staining in the dorsal spinal cord probably in Rohon Beard cells. (A'–D') 4dpf whole mount embryos show diffuse signal in the brain and a specific expression in what is most probably the head of the pronephric ducts. (F) A transverse section through the retina shows expression in the retinal ganglion cell layer. Scale bar: 50 μ m. SC neurons: spinal cord neurons, P: pallium; DT: dorsal thalamus; PD: pronephric duct; GCL: ganglion cell layer. doi:10.1371/journal.pone.0053299.g010

p998E2112463Q(5+3)b) into pAMP1, linearization with EcoRI, transcription with SP6 polymerase. For *cabp1b*, *cabp4b*, *cabp7a*, *cabp8a* and *cabp8b*, cDNA fragments were PCR amplified from zebrafish total cDNA using the following primers (5'prime to 3'prime): CaBP1b_fwd: CTATGGGAAACTGTGTTAAATCGCCGC; CaBP1b_rev: TTATCTCTAGCGAGACATCATTCCGAC; CaBP4b_fwd: CATCCACGATACACCATGGCAG; CaBP4b_rev: TCCACAGAGATCTTCCCATCGC; CaBP7a_fwd: AAGTGGAGGAGATCCGTGAAGC; CaBP7a_rev: ATCAAGCTCTTTCGCACACAGG; CaBP8a_fwd: AAGGAGATGAGGGCTAGGGAG; CaBP8a_rev: CACACACGTCTGACGGTCTTC; CaBP8b_fwd: GGAGCGAGCTTTCACCTGATG; CaBP8b_rev: TGGTGAGATGGTCTCTGAAGGC. PCR frag-

ments were cloned into the pCRII-TOPO vector (Invitrogen) according to manufacturers' instructions. All plasmids used were confirmed by sequencing.

In situ hybridisation

In vitro transcription of Digoxigenin-labeled probes was performed using the RNA Labeling Kit (Roche Diagnostics Corporation) according to manufacturer's instructions. Dechorionated embryos at the appropriate developmental stage(s) were fixed in 4% paraformaldehyde in 1 \times phosphate buffered saline (pH 7.4) for 2 h at room temperature and whole-mount *in situ* hybridisation was performed as previously described [29].

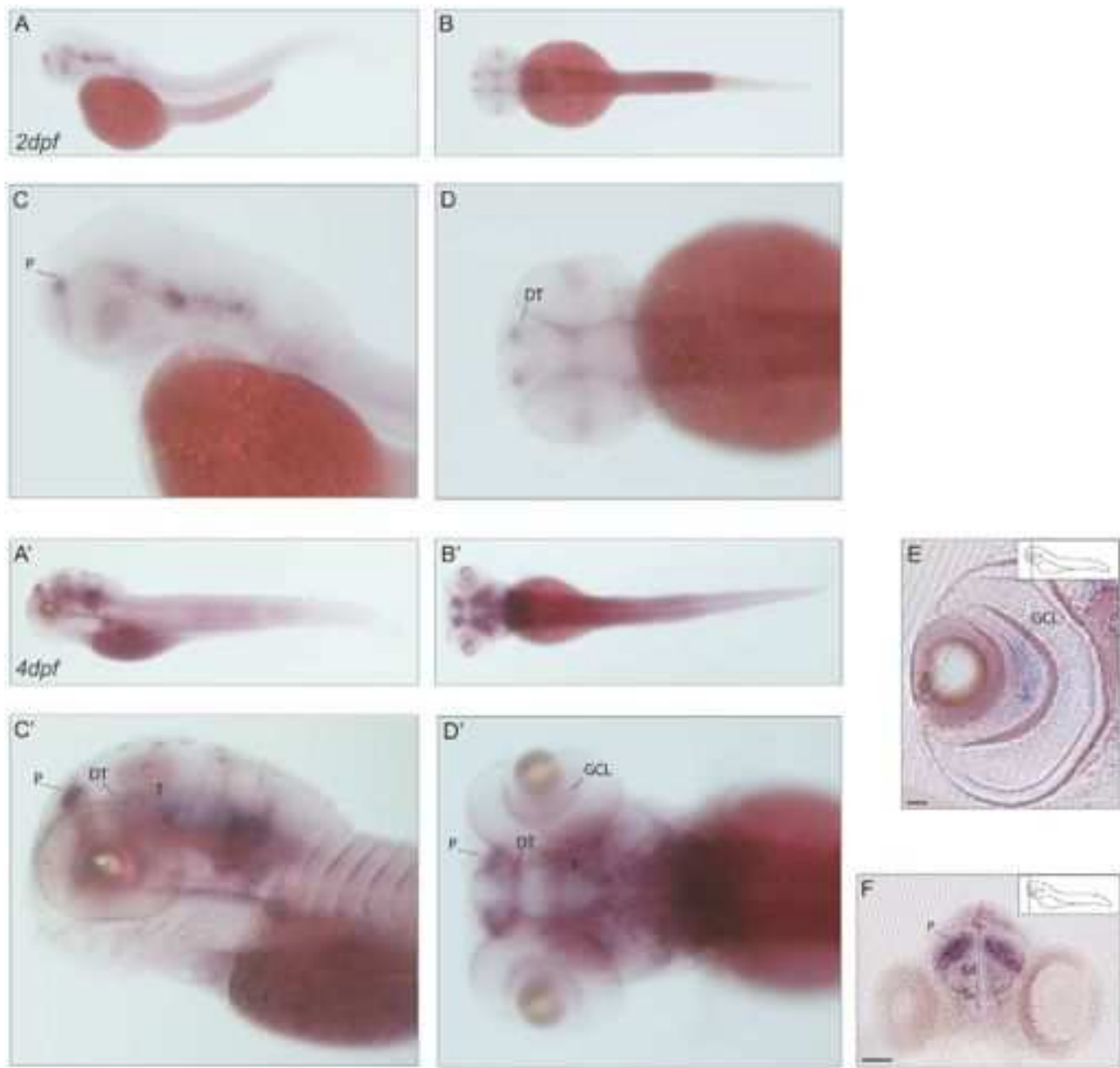


Figure 11. Expression pattern of *caln2*. (A–D') mRNA expression of *caln2* in lateral (A,C–A',C') and dorsal (B,D–B',D') views of 2dpf (A–D) and 4dpf (A'–D') larvae with zoom in (C,D–C',D'). The onset of *caln1* expression takes place within the first two days of embryonic development. (A–D) At 2dpf the *caln1* transcript localizes to the forebrain at the level of the subpallial region and in the caudal midbrain. (A'–D') The same expression profile seems to be maintained until day 4 of development. (E) Transverse section of the retina showing signal of *caln1* antisense probe in a subset of retinal ganglion cells in the central part of the ganglion cell layer. Strongly stained cells are present in the region of the telencephalic pallial domain (F). Scale bar: 50 μm. P: pallium; DT: dorsal thalamus; T: midbrain tegmentum; GCL: ganglion cell layer; Sd: dorsal division of subpallium; Sv: ventral division of subpallium.

doi:10.1371/journal.pone.0053299.g011

Antibody staining

After *in situ* hybridisation staining, whole mount zebrafish embryos from Tg(Vsx2:GFP), Tg(Brn3C:memGFP) and Tg(Ptfla:GFP) transgenic lines were washed twice in 1× PBS/0.1% Tween-20 solution. Subsequently, they were incubated 1 h at room temperature in 10% Normal Goat Serum (Invitrogen), 1% DMSO in PBS-Tw blocking solution followed by overnight incubation with 1/1000 dilution of chicken primary anti-GFP antibody (Genetex). The Alexa Fluor 488 secondary antibody goat anti-chicken IgG (1/500, Molecular probes) and a 1/500 dilution of DAPI (50 μg/μL) in blocking solution were added overnight.

After 5× washing in wash buffer (1× PBS/0.1% Tween-20) microscopy analysis was performed.

Vibratome sections and confocal microscopy

After staining, whole-mount embryos were washed twice in 0.1% Tween in PBS 1×. Afterwards, the samples were embedded in gelatin/albumin with 4% of Glutaraldehyde and sectioned (20 μm) on a VT1000 S vibrating blade microtome (Leica). The sections were analyzed on a Leica Upright Widefield epifluorescence microscope and a Zeiss LSM710 confocal microscope

(Zeiss). Images were processed using ImageJ, Adobe Photoshop and Adobe Illustrator software.

Acknowledgments

We thank E. Restrepo for sharing preliminary results and W. Norton, Ch. Gebhardt and S. Weiss for their advice and comments on the manuscript. A special thank to L.Poggi and J. Wittbrodt that kindly provided the Tg(Vsx2:GFP) [18] and Tg(Ptfla:GFP) [17] zebrafish transgenic lines and

H. Baier for the Tg(Brn3C:memGFP) line. We thank Olivier and Armelle for excellent fish husbandry.

Author Contributions

Conceived and designed the experiments: VDD TOA FDB. Performed the experiments: VDD TOA KD. Analyzed the data: VDD TOA FDB. Wrote the paper: VDD TOA FDB.

References

- Berridge MJ (1998) Neuronal calcium signaling. *Neuron* 21: 13–26.
- Catterall WA, Few AP (2008) Calcium channel regulation and presynaptic plasticity. *Neuron* 59: 882–901.
- Mochida S, Few AP, Scheuer T, Catterall WA (2008) Regulation of presynaptic Ca_v2.1 channels by Ca₂⁺ sensor proteins mediates short-term synaptic plasticity. *Neuron* 57: 210–216.
- Greer PL, Greenberg ME (2008) From synapse to nucleus: calcium-dependent gene transcription in the control of synapse development and function. *Neuron* 59: 846–860.
- McCue HV, Haynes LP, Burgoyne RD (2010) The diversity of calcium sensor proteins in the regulation of neuronal function. *Cold Spring Harb Perspect Biol* 2: a004085.
- Dolmetsch RE, Pajvani U, Fife K, Spotts JM, Greenberg ME (2001) Signaling to the nucleus by an L-type calcium channel-calmodulin complex through the MAP kinase pathway. *Science* 294: 333–339.
- Kawasaki H, Nakayama S, Kretsinger RH (1998) Classification and evolution of EF-hand proteins. *Biometals* 11: 277–295.
- McCue HV, Haynes LP, Burgoyne RD (2010) Bioinformatic analysis of CaBP/calneuron proteins reveals a family of highly conserved vertebrate Ca₂⁺-binding proteins. *BMC Res Notes* 3: 118.
- Haeseleer F, Sokal I, Verlinde CL, Erdjument-Bromage H, Tempst P, et al. (2000) Five members of a novel Ca₂⁺-binding protein (CaBP) subfamily with similarity to calmodulin. *J Biol Chem* 275: 1247–1260.
- Wu YQ, Lin X, Liu GM, Jamrich M, Shaffer LG (2001) Identification of a human brain-specific gene, calneuron 1, a new member of the calmodulin superfamily. *Mol Genet Metab* 72: 343–350.
- Mikhaylova M, Sharma Y, Reissner C, Nagel F, Aravind P, et al. (2006) Neuronal Ca₂⁺ signaling via caldendrin and calneurons. *Biochim Biophys Acta* 1763: 1229–1237.
- Haeseleer F, Imanishi Y, Maeda T, Possin DE, Maeda A, et al. (2004) Essential role of Ca₂⁺-binding protein 4, a Cav1.4 channel regulator, in photoreceptor synaptic function. *Nat Neurosci* 7: 1079–1087.
- Rieke F, Lee A, Haeseleer F (2008) Characterization of Ca₂⁺-binding protein 5 knockout mouse retina. *Invest Ophthalmol Vis Sci* 49: 5126–5135.
- Haynes LP, McCue HV, Burgoyne RD (2012) Evolution and functional diversity of the Calcium Binding Proteins (CaBPs). *Front Mol Neurosci* 5: 9.
- Wittbrodt JMA, Scharf M. (1998) More genes in fish? *BioEssays* 20: 511–515.
- Sprague J, Bayraktaroglu L, Clements D, Conlin T, Fashena D, et al. (2006) The Zebrafish Information Network: the zebrafish model organism database. *Nucleic Acids Res* 34: D581–585.
- Jusuf PR, Harris WA (2009) Ptf1a is expressed transiently in all types of amacrine cells in the embryonic zebrafish retina. *Neural Dev* 4: 34.
- Vitorino M, Jusuf PR, Maurus D, Kimura Y, Higashijima S, et al. (2009) Vsx2 in the zebrafish retina: restricted lineages through derepression. *Neural Dev* 4: 14.
- Xiao T, Roeser T, Staub W, Baier H (2005) A GFP-based genetic screen reveals mutations that disrupt the architecture of the zebrafish retinotectal projection. *Development* 132: 2955–2967.
- Zeit C, Kloeckener-Gruissem B, Forster U, Kohl S, Magyar I, et al. (2006) Mutations in CABP4, the gene encoding the Ca₂⁺-binding protein 4, cause autosomal recessive night blindness. *Am J Hum Genet* 79: 657–667.
- Vihtelic TS, Fadool JM, Gao J, Thornton KA, Hyde DR, et al. (2005) Expressed sequence tag analysis of zebrafish eye tissues for NEI Bank. *Mol Vis* 11: 1083–1100.
- Force A, Lynch M, Pickett FB, Amores A, Yan YL, et al. (1999) Preservation of duplicate genes by complementary, degenerative mutations. *Genetics* 151: 1531–1545.
- Edgar RC (2004) MUSCLE: multiple sequence alignment with high accuracy and high throughput. *Nucleic Acids Res* 32: 1792–1797.
- Waterhouse AM, Procter JB, Martin DM, Clamp M, Barton GJ (2009) Jalview Version 2—a multiple sequence alignment editor and analysis workbench. *Bioinformatics* 25: 1189–1191.
- Dereeper A, Guignon V, Blanc G, Audic S, Buffet S, et al. (2008) Phylogeny.fr: robust phylogenetic analysis for the non-specialist. *Nucleic Acids Res* 36: W465–469.
- Gascuel O (1997) BIONJ: an improved version of the NJ algorithm based on a simple model of sequence data. *Mol Biol Evol* 14: 685–695.
- Huson DH, Richter DC, Rausch C, Dezulian T, Franz M, et al. (2007) Dendroscope: An interactive viewer for large phylogenetic trees. *BMC Bioinformatics* 8: 460.
- Westerfield M The zebrafish book. A guide for the laboratory use of zebrafish (*Danio rerio*). Univ of Oregon Press, Eugene 4th ed.
- Thisse C, Thisse B (2008) High-resolution in situ hybridisation to whole-mount zebrafish embryos. *Nat Protoc* 3: 59–69.

RESEARCH REPORT

STEM CELLS AND REGENERATION

Asymmetric inheritance of the apical domain and self-renewal of retinal ganglion cell progenitors depend on Anillin function

Alessio Paolini^{1,*}, Anne-Laure Duchemin^{1,*}, Shahad Albadri¹, Eva Patzel^{1,2}, Dorothee Bornhorst¹, Paula González Avalos³, Steffen Lemke³, Anja Machate⁴, Michael Brand⁴, Saadettin Sel², Vincenzo Di Donato⁵, Filippo Del Bene⁵, Flavio R. Zolessi⁶, Mirana Ramialison⁷ and Lucia Poggi^{1,‡}

ABSTRACT

Divisions that generate one neuronal lineage-committed and one self-renewing cell maintain the balance of proliferation and differentiation for the generation of neuronal diversity. The asymmetric inheritance of apical domains and components of the cell division machinery has been implicated in this process, and might involve interactions with cell fate determinants in regulatory feedback loops of an as yet unknown nature. Here, we report the dynamics of Anillin – an essential F-actin regulator and furrow component – and its contribution to progenitor cell divisions in the developing zebrafish retina. We find that asymmetrically dividing retinal ganglion cell progenitors position the Anillin-rich midbody at the apical domain of the differentiating daughter. *anillin* hypomorphic conditions disrupt asymmetric apical domain inheritance and affect daughter cell fate. Consequently, the retinal cell type composition is profoundly affected, such that the ganglion cell layer is dramatically expanded. This study provides the first *in vivo* evidence for the requirement of Anillin during asymmetric neurogenic divisions. It also provides insights into a reciprocal regulation between Anillin and the ganglion cell fate determinant *Ath5*, suggesting a mechanism whereby the balance of proliferation and differentiation is accomplished during progenitor cell divisions *in vivo*.

KEY WORDS: Anillin, Asymmetric cell division, *Ath5* (*Atoh7*), Neurogenesis, Retina development, Apical domain inheritance

INTRODUCTION

During retinal development, asymmetric self-renewing divisions of progenitor cells prolong the temporal progression of neurogenesis (Cayouette et al., 2006; Cepko, 2014; Parameswaran et al., 2014). The asymmetric inheritance of apical components has been suggested to provide instructive information for the specification of cell fate (Clark et al., 2012; Huttner and Brand, 1997; Kechad et al., 2012). The complex cellular and molecular interactions linking this inheritance to daughter cell self-renewal and differentiation *in vivo* remain elusive. Recent studies reported

cleavage furrow components as potential signalling sources for instructing cell fate (Chen and Zhang, 2013; Dubreuil et al., 2007; Ettinger et al., 2011; Kosodo and Huttner, 2009; Pollarolo et al., 2011; Singh and Pohl, 2014). For example, newborn sensory neurons of the *Drosophila* notum inherit asymmetrically distributed cytokinesis remnants of the last mitotic cleavage (Pollarolo et al., 2011). Other studies have suggested that the extent of release of the post-mitotic midbody – a transient intercellular bridge from the cleavage furrow just before abscission – couples cell division to cell fate in neuroepithelial, stem and cancer cells (Dubreuil et al., 2007; Ettinger et al., 2011). It remains unknown whether cleavage furrow components also instruct asymmetric cell division *in vivo* in the developing vertebrate neuroepithelium.

Here, we combined *in vivo* time-lapse confocal imaging with cell biology and functional analyses to examine the role of the F-actin-binding protein Anillin – a crucial component of the cleavage furrow and midbody (Field and Alberts, 1995; Kechad et al., 2012; Rincon and Paoletti, 2012; Ronkainen et al., 2011) – in the occurrence of asymmetric divisions in the developing zebrafish retina. We report novel evidence supporting that Anillin is important not only for progenitor cell self-renewal, but also for balancing symmetric and asymmetric outcomes essential for correct retinal neurogenesis. This study further provides novel insights into the interplay between cytokinesis machinery components and the retinal ganglion cell (RGC) fate determinant *Ath5* (*Atoh7*) during asymmetric neurogenic cell divisions *in vivo*.

RESULTS AND DISCUSSION**Dynamic expression of Anillin suggests a role in asymmetric divisions generating RGCs**

To investigate the role of Anillin during retinal neurogenesis we established an *anillin:anillin-eGFP* transgenic line that recapitulates *anillin* expression *in vivo* (Fig. 1A,B). All cells in the retinal neuroepithelium are proliferative prior to 28 hours post fertilisation (hpf) (Li et al., 2000), strongly expressing *anillin* (Fig. 1B). The *ath5:gap43-RFP* transgene, in which membrane-tethered RFP (Gap43-RFP) is expressed under the control of the *ath5* promoter (Zolessi et al., 2006), highlights the cell cycle exit of RGCs – the first-born neurons in the vertebrate retina. Time-lapse imaging in double-transgenic *anillin:anillin-eGFP;ath5:gap43-RFP* embryos revealed that *anillin:anillin-eGFP* is downregulated in the differentiating Gap43-RFP-positive cells of the RGC layer, suggesting *anillin* downregulation by *Ath5* (Fig. 1C,C'). Consistently, retinæ from *lakritz* mutant (*ath5*^{-/-}) embryos, in which progenitors undergo extra rounds of proliferative divisions instead of differentiating into RGCs (Jusuf et al., 2012; Kay et al., 2001; Kelsh et al., 1996), failed to downregulate *anillin* mRNA (supplementary material Fig. S1A). The presence of a well-characterised *Ath5* consensus binding site

¹Department of Developmental Biology/Physiology, Centre for Organismal Studies (COS) Heidelberg, Im Neuenheimer Feld 230, Heidelberg 69120, Germany. ²Department of Ophthalmology, University of Heidelberg, Heidelberg 69120, Germany. ³Centre for Organismal Studies (COS) Heidelberg, Im Neuenheimer Feld 230, Heidelberg 69120, Germany. ⁴Biotechnology Center and Center for Regenerative Therapies Dresden, TU Dresden, Fetscherstrasse 105, Dresden 01307, Germany. ⁵Institut Curie - Centre de Recherche, U934/UMR3215, Paris 75248, Cedex 05, France. ⁶Sección Biología Celular, Facultad de Ciencias, Universidad de la República and Institut Pasteur de Montevideo, 11400 Montevideo, Uruguay. ⁷Australian Regenerative Medicine Institute, Monash University, Wellington Road, Clayton, Victoria 3187, Australia.

*These authors contributed equally to this work

‡Author for correspondence (lucia.poggi@cos.uni-heidelberg.de)

Received 8 October 2014; Accepted 12 January 2015

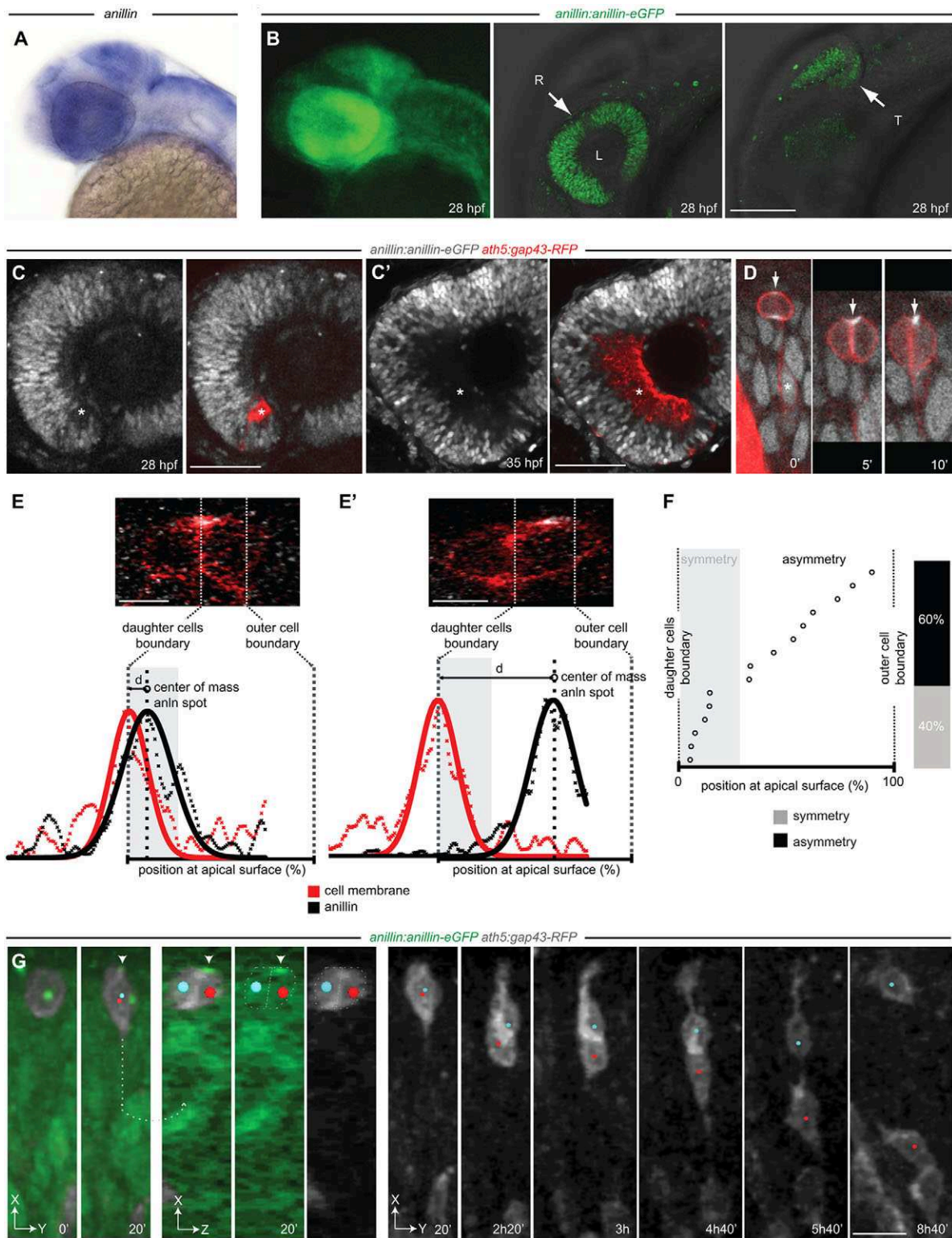


Fig. 1. Anillin expression during zebrafish retinal differentiation. (A) *anillin* mRNA (blue) at 28 hpf. (B) Expression of the *anillin-eGFP* transgene. R, retina; T, optic tectum; L, lens. Left, z-projection view; middle and right, z-plane. (C,C') *anillin:anillin-eGFP/ath5:gap43-RFP* transgenic retina. *anillin-eGFP* is downregulated in the differentiating cells of the RGC layer (asterisks). (D) Anillin-GFP localisation in the nucleus (asterisk), cleavage furrow (arrow, $t=0'$) and at the midbody (arrow, $t=5'$ and $t=10'$). Time, minutes. (E,E') Anillin-eGFP symmetric (E) and asymmetric (E') distribution and intensity profiles (data points and fitted Gaussian) used to detect the offset of the Anillin-eGFP spot from the daughter cell boundary. (F) The position of apical Anillin-eGFP ($n=15$ divisions). Distance from the cell boundary within the average radius of the Anillin spot (grey) is used to define symmetry (see supplementary material Fig. S3). (G) Frames from supplementary material Movie 1. The Anillin-eGFP spot-inheriting daughter (white arrowhead, red dot) migrates to the RGC layer. The sibling (blue dot) migrates back to the apical surface ($n=5$ out of 5 analysed divisions). At $t=20'$ a rotated frontal z-section (dotted lines, 3D slicing mode) across the centre of the dividing daughters is shown (oriented along the z-plane). The apical surface of the retinal neuroepithelium is to the top. Scale bars: 110 μm in B; 25 μm in C,C'; 6 μm in E,E'; 12 μm in G.

(CACCTG) (Del Bene et al., 2007) in an active enhancer region upstream of *anillin* [highlighted by histone H3 lysine 4 mono-methylation (H3K4me1) mark] (supplementary material Fig. S1B) further suggests that Ath5 directly regulates *anillin*.

Anillin is an established midbody component, and asymmetric inheritance of the midbody during stem cell division has been reported in multiple systems, including mouse radial glial progenitors (Dubreuil et al., 2007; Ettinger et al., 2011; Hesse et al., 2012; Kosodo et al., 2004). This led us to investigate Anillin-eGFP dynamics in dividing retinal progenitor cells. Live imaging confirmed the localisation of Anillin-eGFP in the *gap43-RFP*-expressing progenitor cell nuclei at interphase (asterisk, Fig. 1D, $t=0'$), to the contractile ring during cytokinesis (arrow, Fig. 1D, $t=0'$) and at the daughter cell apical interface consistent with the formation of a midbody at the end of cytokinesis (Fig. 1D, $t=5'$ and $t=10'$). Interestingly, 60% of analysed divisions ($n=9$ out of 15) displayed asymmetric positioning of the Anillin-eGFP spot to one daughter cell apical domain at the end of cytokinesis (Fig. 1E–F). Consistent with a correlation between Anillin-eGFP inheritance and cell fate, we observed that the daughter cell inheriting the Anillin-eGFP spot retracts its apical process and migrates basally towards the differentiating RGC layer, while the sibling cell invariably migrates back towards the apical surface ($n=5$ out of 5, Fig. 1G; supplementary material Movie 1). In addition to the observed dynamics of *anillin* expression downstream of Ath5, these data are consistent with a role for Anillin in asymmetric neurogenic cell divisions *in vivo*.

Apical domain distribution depends on Anillin

To test the role of Anillin in retinal neurogenesis we performed a loss-of-function analysis. Anillin knockdown causes cytokinesis defects that affect early vertebrate development (Gbadegesin et al., 2014; Reyes et al., 2014) (supplementary material Movie 2). We therefore generated *anillin* hypomorphic conditions (supplementary material Fig. S2A–C) and performed all analyses in mosaic zebrafish embryos as previously described (Jusuf et al., 2012). Live imaging of dividing transplanted progenitor cells labelled with H2B-RFP (nuclei, red) and LifeAct-Venus (F-actin, yellow; Riedl et al., 2008) highlighted the appearance of an F-actin-enriched spot at the basal side of the cell body before anaphase (Kosodo et al., 2008) and its basal-apical displacement during cytokinesis (supplementary material Fig. S2D,E), indicating that vertical furrowing progresses normally in the mononucleated *anillin* hypomorphic cells.

The midbody has been reported as a positional cue for apical F-actin accumulation at the daughter cell interface before the formation of new cell-cell junctions (Herszterg et al., 2013; Morais-de-Sa and Sunkel, 2013; Singh and Pohl, 2014). Expression of the *anillin-eGFP* reporter together with a red *lifeact-Ruby* construct revealed that midbody formation at the end of cytokinesis indeed coincides with the transient accumulation of F-actin around it (arrow, Fig. 2A; supplementary material Movie 3). Consistent with the apical Anillin-eGFP spot, quantification of LifeAct-Venus intensity revealed that more than half of the analysed divisions (57%, $n=8$ out of 14) distribute the apical F-actin-rich domain asymmetrically to one daughter (Fig. 2B,C; supplementary material Movie 4). This asymmetric distribution is drastically reduced in *anillin* hypomorphic conditions (15%, $n=2$ out of 13) (Fig. 2B,C; supplementary material Movie 5), indicating that Anillin is

required for proper apical domain segregation in dividing retinal progenitor cells.

The evolutionarily conserved apical polarity protein Par3 (Pard3) localises with F-actin at the level of junctional belts in neuroepithelial cells and its inheritance during cell division has been linked to neuronal fate (Alexandre et al., 2010; Bultje et al., 2009; Chen and Zhang, 2013; Dong et al., 2012; Shi et al., 2003; Takekuni, 2003; Zolessi et al., 2006). We investigated whether Par3 asymmetric inheritance depends on Anillin. Time-lapse imaging of a Par3-GFP protein revealed that, whereas in control clones most divisions distribute Par3 asymmetrically (80%, $n=12$ out of 15, Fig. 2D; supplementary material Movie 6), *anillin* hypomorphic conditions favour symmetric Par3 distribution (Fig. 2D, $n=15$ out of 15; supplementary material Movie 7). Thus, Anillin is required for the correct apical distribution of F-actin and Par3, which might be essential for asymmetric cell fate outcome.

anillin hypomorphic conditions affect retinal neurogenesis and the balance of symmetric and asymmetric RGC progenitor divisions

We next assessed whether the observed effect on Par3 and F-actin reflects changes in the mode of cell division. Hypomorphic *anillin* conditions produce an overall increase in *ath5:GFP* (Poggi et al., 2005) or *ath5:gap43-RFP* transgene expression (Fig. 3A–C; supplementary material Movies 8 and 9) and an expansion of the RGC layer (Fig. 3C), which is efficiently rescued by co-injection of *anillin-eGFP* mRNA (Fig. 3D). Although quantification of phospho-histone H3 (pH3)-positive cells at 30 hpf revealed no significant difference between the control and *anillin* hypomorphic conditions (Fig. 3E,F), the number of pH3-positive cells within the *ath5:GFP* population was significantly lower in *anillin* hypomorphic conditions (Fig. 3E,G). Thus, retinal progenitor divisions are more likely to generate *ath5*-expressing daughters, and *ath5*-expressing cells are less likely to undergo further rounds of cell division.

To assess this hypothesis we performed *in vivo* time-lapse analysis of daughter cell fate in clones transplanted from *ath5:GFP* transgenic embryos. We considered symmetric versus asymmetric divisions based on two criteria: (1) Ath5:GFP positive (A) versus Ath5:GFP negative (self-renewing progenitor, P) in sibling daughters from divisions of H2B-RFP-labelled cells; (2) neuronal fate (N) versus self-renewing progenitor (P) in sibling daughters from divisions of H2B-RFP/Ath5:GFP-positive cells (Fig. 4) (Poggi et al., 2005). We found that 56% of divisions of H2B-RFP-positive cells were asymmetric, generating one GFP-positive and one GFP-negative daughter (A/P) ($n=5$ out of 9) (Fig. 4A,D; supplementary material Movie 10). By contrast, all divisions analysed in *anillin* hypomorphic clones were symmetric, entailing GFP in both daughter cells (Fig. 4B–D; supplementary material Movie 11) ($n=10$). This is consistent with the observed increase in Ath5:GFP-positive cells. Within the Ath5:GFP-positive control clones most analysed divisions (82%, $n=9$ out of 11) were asymmetric, generating one post-mitotic daughter, which retracts the apical process and migrates to the RGC layer, and one self-renewing progenitor (N/P) (Fig. 4A,D; supplementary material Movie 12) (Jusuf et al., 2012). The concomitant appearance of an extending axon from the cell body or expression of the *cxcr4b:cxcr4b-GFP* transgene (Donà et al., 2013) further indicated differentiation into an RGC (data not shown; Fig. 4C,C') (Pujic et al., 2006). Conversely, most divisions in *anillin* hypomorphic clones were symmetric, generating two Cxcr4b-GFP-positive daughters (N/N; 70%, $n=7$ out

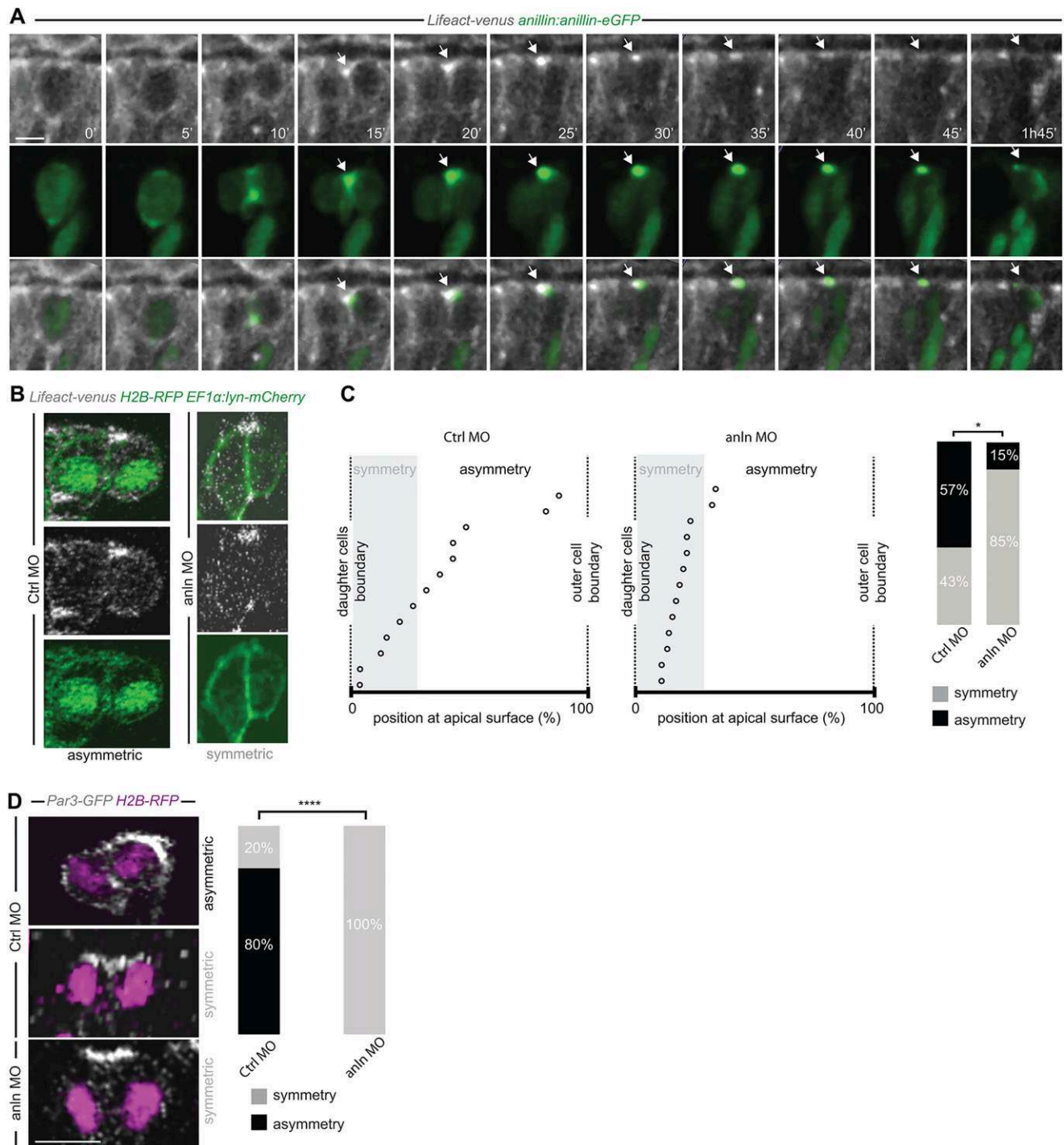


Fig. 2. Anillin is required for the apical distribution of F-actin and Par3. (A) Frames from supplementary material Movie 3. F-actin accumulates at the Anillin-eGFP-labelled midbody (arrow) at the end of cytokinesis. (B) Asymmetric (CtrlMO; frames from supplementary material Movie 4) and symmetric (anInMO; frame from supplementary material Movie 5) distribution of apical F-actin accumulation. (C) Position of the apical F-actin-rich domain (CtrlMO, $n=14$; anInMO, $n=13$) (as described in Fig. 1E–F and supplementary material Fig. S3); the frequency of asymmetry is 57% in CtrlMO and 15% in anInMO (Wilcoxon Mann–Whitney test, $*P<0.05$). (D) Symmetric versus asymmetric inheritance of Par3 in CtrlMO (frame from supplementary material Movie 6) and anInMO (frame from supplementary material Movie 7) injected embryos (two-tailed Fisher's exact test, $****P=10^{-4}$, CtrlMO, $n=15$; anInMO, $n=15$). All images represent a single z-plane of a confocal stack. The apical surface of the retinal neuroepithelium is to the top. Scale bars: 4.8 μm in A; 5 μm in D.

of 10) (Fig. 4B–D; supplementary material Movie 13). This is consistent with the decrease in pH3-positive cells among the Ath5:GFP population. Hence, when Anillin function is impaired, retinal progenitors undergo symmetric rather than asymmetric divisions, in which they are more likely to upregulate *ath5*, become post-mitotic and adopt a neuronal (RGC) fate (Fig. 4E).

Conclusions

Our study provides compelling evidence that Anillin contributes to the regulation of asymmetric neurogenic cell divisions in the retinal neuroepithelium – favouring the maintenance of proliferating progenitors while also being required for the proper distribution of F-actin and Par3 at the daughter cell

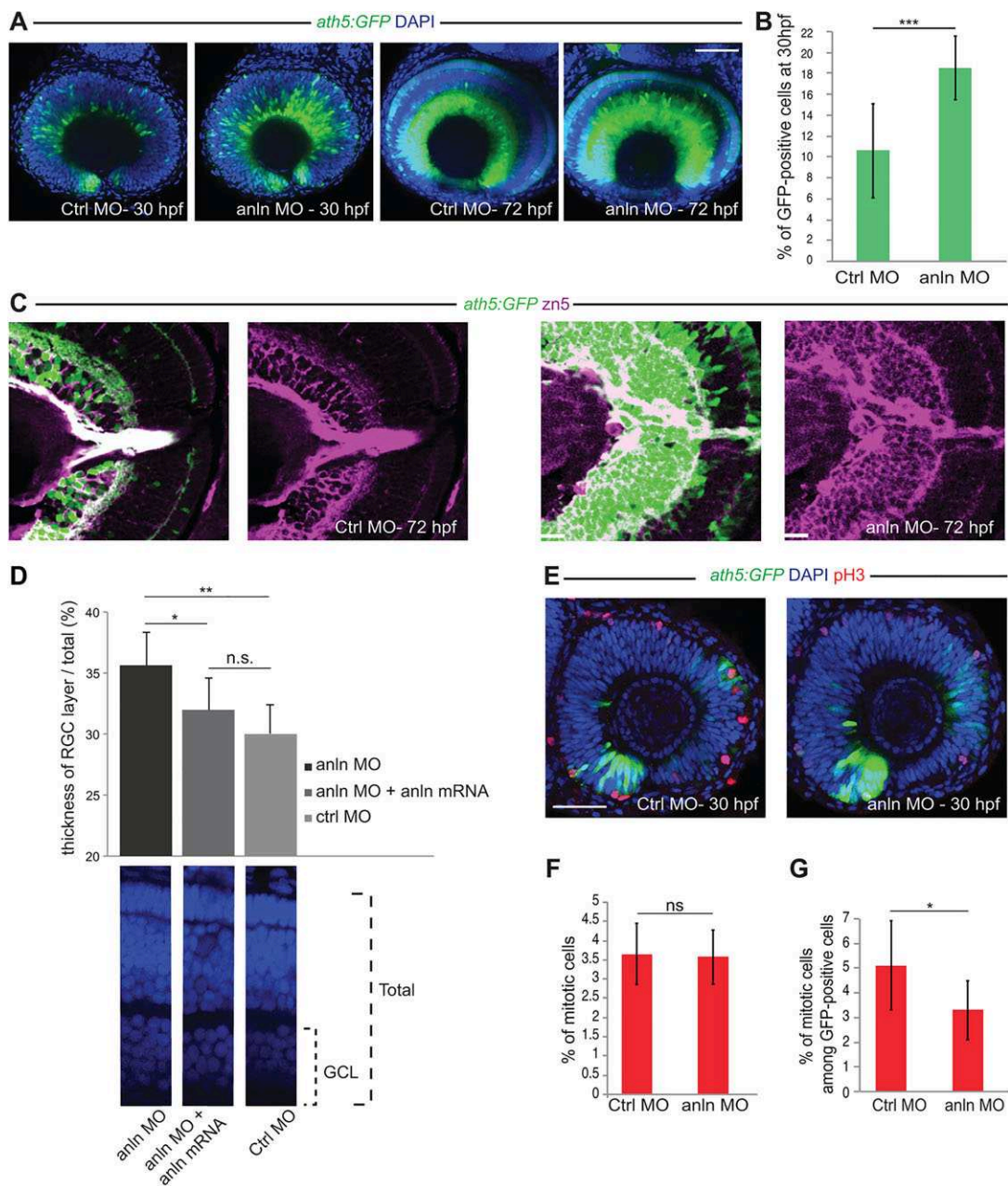


Fig. 3. *anillin* hypomorphic conditions affect RGC number. (A) *anln*MO-injected retinae (z-projections) showing increase of *Ath5:GFP* signal (CtrlMO, $n=24$; *anln*MO, $n=31$). (B) Quantification of GFP-positive among total (DAPI) cells, which increased from $10.5 \pm 1.6\%$ (s.e.m.) in CtrlMO to $18.5 \pm 1.2\%$ (s.e.m.) in *anln*MO (Student's *t*-test, $***P < 0.001$; CtrlMO, $n=8$; *anln*MO, $n=7$). (C) Retina frontal sections. Zn5 (Alcama) staining reveals expansion of the RGC layer in *anln*MO retinae. (D) Rescue of the *anln*MO phenotype. Student's *t*-test, $*P < 0.05$, $**P < 0.01$; n.s., not significant ($P=0.11$); *anln*MO and CtrlMO, $n=7$; *anln*MO+*anln*-eGFP mRNA, $n=8$. GCL, ganglion cell layer. (E) Phospho-histone H3 (pH3) labelling of mitotic cells (z-projections). (F) Ratio of pH3-positive among total DAPI-positive cells; $3.65 \pm 0.3\%$ CtrlMO, $3.57 \pm 0.3\%$ *anln*MO (Student's *t*-test, $P=0.46$; CtrlMO, $n=8$; *anln*MO, $n=7$). (G) Ratio of pH3-positive cells among GFP-positive cells is $5.1 \pm 0.6\%$ for CtrlMO versus $3.3 \pm 0.5\%$ for *anln*MO (Student's *t*-test, $*P < 0.05$; CtrlMO, $n=8$; *anln*MO, $n=7$). Scale bars: $42 \mu\text{m}$ in A,E; $23.5 \mu\text{m}$ in C.

apical domain. Our time-lapse analysis of asymmetric cell divisions of RGC progenitors suggests that the differentiating (RGC) daughter transiently inherits the Anillin-eGFP-labelled midbody. This is in agreement with the idea that instructive information accompanying this inheritance is linked to neural fate commitment (Alexandre et al., 2010; Pollarolo et al., 2011; Zolessi et al., 2006).

This study establishes a framework for future mechanistic investigations to address how apical Anillin, F-actin and associated signalling molecules contribute to long-term fate

decisions in asymmetric neurogenic cell divisions (Galvagni et al., 2012; Parameswaran et al., 2014). The nature of this information (e.g. cell cycle exit, cell polarity or neuronal fate acquisition) and the underlying signalling pathways have yet to be determined, but the evidence provided here suggests that they are likely to integrate feedback regulatory loops between *ath5* and *anillin*. Anillin expression correlates with the proliferation and metastatic potential of human tumours from many different tissue origins (Hall et al., 2005). Therefore, it is tempting to speculate that similar

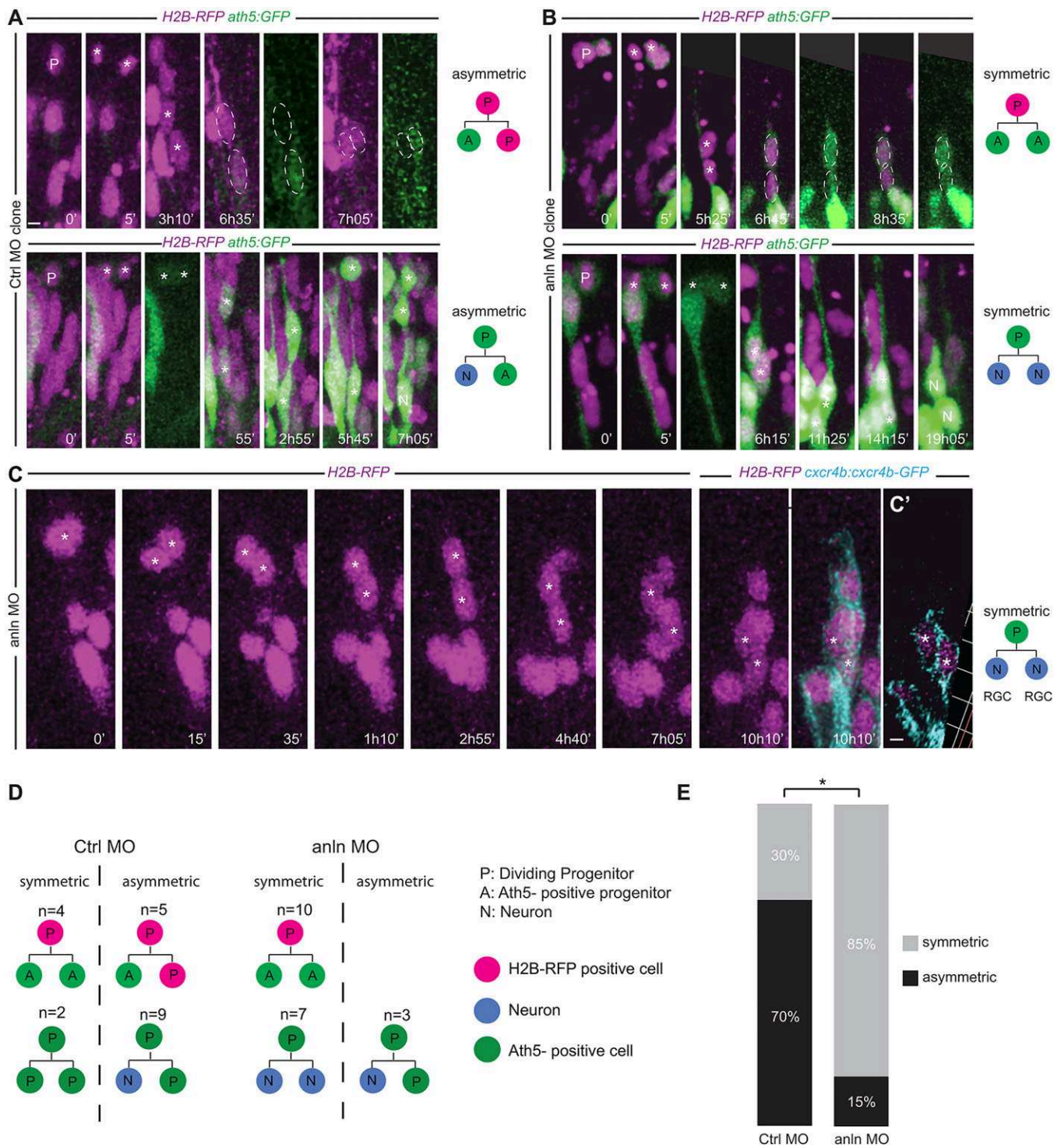


Fig. 4. *anillin* hypomorphic conditions affect the balance between symmetric and asymmetric cell division of RGC progenitors. (A,B) Frames from supplementary material Movies 10-13 showing examples of symmetric and asymmetric division outcomes in the CtrlMO (A) and anInMO (B) conditions. GFP intensity differences for A/P and A/A divisions were quantified ($P < 0.05$ for CtrlMO clones; $P = 0.92$ for anInMO clones). (C) Division (asterisk) generating two *Cxcr4b*-eGFP-positive daughters (cyan) (10 h 10'). Each time frame represents a z-projection. (C') A single z-stack. (D,E) Symmetric divisions increase from 30% in the CtrlMO to 85% in the anInMO (two-tailed Fisher's exact test, $*P = 0.011$). Apical surface of the retinal neuroepithelium is to the top. Scale bars: 5 μ m in A,B; 5.5 μ m in C,C'.

mechanisms, whereby components of the cytokinesis machinery contribute to maintaining the intrinsic asymmetry of proliferative divisions, might be common to all proliferating stem and progenitor cells.

MATERIALS AND METHODS

Animals

Zebrafish (*Danio rerio*) breeding/raising followed standard protocols (Kimmel et al., 1995). Fish care is under the supervision of animal

welfare agencies and in accordance with local (Tierschutzgesetz 111 Abs. 1 Nr. 1) and European Union animal welfare guidelines. For imaging, embryos were treated with 0.0045% 1-phenyl-2-thiourea (Sigma) to delay pigment formation. Lines used are indicated in the supplementary Materials and Methods.

Morpholinos

Morpholinos (1 ng/μl) were: CtrlMO, 5′-CCTCTTACCTCAGTTACAAT-TTATA-3′ (Gene Tools); ATGMO, 5′-GTACGCTACAAGCTGAAAAG-TAAAGT-3′; and SpMO, 5′-TTTCACAAAAGCTCTCACCTCGGT-3′. Controls and rescue experiments are described in the supplementary Materials and Methods.

pH3/Ath5:GFP analysis

The Cell Counter plugin from Fiji software was used to determine the average ratio of pH3-positive cells among total cells (DAPI staining) or among Ath5:GFP cells in every 2 μm of a 16 μm-thick z-projection.

Plasmids

Six plasmids were used: *BAC/anillin:anillin-eGFP* and *CMV:anln-eGFP_pDestTol2* (see supplementary Materials and Methods for cloning details and BAC transgenesis); *pCS2+:H2B-RFP* (Jusuf et al., 2012); *pCS2+:Lifeact-Venus* (kindly provided by R. Köster, TU Braunschweig, Germany); *pDestTol2/CMVSP6:lifeact-Ruby* vector (generated by I. Weisswange and kindly provided by J. Wittbrodt, University of Heidelberg, Germany); and *pCS2+:pard3-GFP* (kindly provided by P. Alexandre and J. Clarke, King's College London, UK).

Immunofluorescence and *in situ* hybridisation (ISH)

Immunostaining was performed as described (Jusuf et al., 2012; supplementary Materials and Methods). Primary antibodies: rabbit anti-phospho-histone H3 (Millipore, 06-570; 1:500), mouse anti-Zn5 (ZIRC Zn-5; 1:200) and chicken anti-GFP (Life Technologies, A10262; 1:200). Secondary antibodies: goat anti-rabbit IgG (H+L) conjugated to Cy5 (Invitrogen, A10523; 1:500), goat anti-mouse IgG (H+L) conjugated to Alexa fluor 546 (Invitrogen, A11003; 1:500) and donkey anti-chicken IgG (H+L) conjugated to Alexa fluor 488 (Jackson, 703-546-155; 1:250). Nuclei were counterstained with DAPI (Sigma; 1:1000).

For ISH, antisense probes for *anillin* and *ath5* were generated as previously described (Schuhmacher et al., 2011). See supplementary Materials and Methods for cloning and ISH protocol details.

Imaging

A Leica SpE confocal laser scanning microscope was used with a Leica 40×1.15 NA oil-immersion or Leica 63×1.2 NA water-immersion objective and Leica Application Suite (LAS) software (see supplementary Materials and Methods for further details of imaging). Volocity software (version 5.3, PerkinElmer) or Fiji was used for image processing and analyses. For analysis of F-actin spot displacement (supplementary material Fig. S2), coordinates (x, y, z) of the spot at the basal side of the cell body at anaphase and at the apical surface at telophase were determined. Distance covered and velocity were calculated between the two points. For lineage analysis, mosaic clones were randomly selected in the time-lapse series and daughter cells tracked manually in 4D after division. For A/P and A/A divisions (Fig. 4A,B), the ratio GFP intensity/background was assessed with Fiji. Analysis of Anillin and F-actin distributions is described in supplementary material Fig. S3 legend. Par3-GFP distribution was assessed on frontal z-sections across the centre of the dividing daughters (Alexandre et al., 2010).

Statistical analysis

Statistical tests were performed using Prism 5.0 (GraphPad), Microsoft Excel and R (Fisher's exact test, Student's *t*-test and Wilcoxon Mann–Whitney test) with *P*<0.05 considered significant. Classification of the distance between the daughter cell interface and Anillin/F-actin centre of mass was performed using R. For comparison between CtrlMO and anlnMO we used unpaired homoscedastic two-tailed Student's *t*-test

[lineage analysis (GFP-positive daughters), rescue of the RGC layer, F-actin spot displacement], Wilcoxon Mann–Whitney test (F-actin distribution in CtrlMO versus anlnMO conditions) and two-tailed Fisher's exact test (Par3 inheritance and lineage studies). All data represent three or more independent experiments.

Acknowledgements

We thank R. Köster, J. Wittbrodt, D. Gilmour, P. Alexandre and J. Clarke for constructs and transgenics; J. L. M. Cerdan for statistics; S. Bouffard for cloning; B. Wittbrodt, E. Leist, A. Saraceno, M. Majewski, B. Seiferling, T. Kellner for fish maintenance and technical assistance; M. Carl, W. A. Harris, C. Norden, N. Foulkes and D. Gilmour for constructive inputs; J. McCall for editing; J. Wittbrodt and K. Schumacher for sharing equipment and space.

Competing interests

The authors declare no competing or financial interests.

Author contributions

L.P. conceived, supervised the study and wrote manuscript. A.P. and A.-L.D. performed main experiments. S.A. and V.D.D. generated *BAC/anillin:anillin-eGFP* in the F.D.B. laboratory. A.M. generated *Tg(pToll/EF1α:lyn-mCherry)* in the M.B. laboratory. D.B. performed RT-PCR and time-lapses. E.P. and F.R.Z. performed immunoblotting and E.P. performed rescue experiments. P.G.A. and S.L. designed the quantitative method for Anillin, F-actin and Par3 analyses. S.S. provided reagents. M.R. performed bioinformatics analyses.

Funding

A.P. is supported by Landesgraduiertenförderung (LGFG; State of Baden-Württemberg) and a short-term EMBO fellowship. A.-L.D. is supported by The Hartmut Hoffmann-Berling International Graduate School of Molecular and Cellular Biology (HBIGS; Heidelberg University). M.R. is supported by a National Health and Medical Research Council/National Heart Foundation (NHMRC/NHF) Career Development Fellowship [1049980]. This work was supported by Deutsche Forschungsgemeinschaft (DFG) research grants to L.P. [PO 1440/1-1] and to S.S. [SE 1995/1-1]. We thank J. Wittbrodt for generous support.

Supplementary material

Supplementary material available online at <http://dev.biologists.org/lookup/suppl/doi:10.1242/dev.118612/-/DC1>

References

- Alexandre, P., Reugels, A. M., Barker, D., Blanc, E. and Clarke, J. D. W. (2010). Neurons derive from the more apical daughter in asymmetric divisions in the zebrafish neural tube. *Nat. Neurosci.* **13**, 673–679.
- Bultje, R. S., Castaneda-Castellanos, D. R., Jan, L. Y., Jan, Y.-N., Kriegstein, A. R. and Shi, S.-H. (2009). Mammalian Par3 regulates progenitor cell asymmetric division via notch signaling in the developing neocortex. *Neuron* **63**, 189–202.
- Cayouette, M., Poggi, L. and Harris, W. A. (2006). Lineage in the vertebrate retina. *Trends Neurosci.* **29**, 563–570.
- Cepko, C. (2014). Intrinsically different retinal progenitor cells produce specific types of progeny. *Nat. Rev. Neurosci.* **15**, 615–627.
- Chen, J. and Zhang, M. (2013). The Par3/Par6/aPKC complex and epithelial cell polarity. *Exp. Cell Res.* **319**, 1357–1364.
- Clark, B. S., Cui, S., Miesfeld, J. B., Klezovitch, O., Vasioukhin, V. and Link, B. A. (2012). Loss of Ligl1 in retinal neuroepithelia reveals links between apical domain size, Notch activity and neurogenesis. *Development* **139**, 1599–1610.
- Del Bene, F., Ettwiller, L., Skowronska-Krawczyk, D., Baier, H., Matter, J.-M., Birney, E. and Wittbrodt, J. (2007). In vivo validation of a computationally predicted conserved Ath5 target gene set. *PLoS Genet.* **3**, e159.
- Donà, E., Barry, J. D., Valentin, G., Quirin, C., Khmelinskii, A., Kunze, A., Durdu, S., Newton, L. R., Fernandez-Minan, A., Huber, W. et al. (2013). Directional tissue migration through a self-generated chemokine gradient. *Nature* **503**, 285–289.
- Dong, Z., Yang, N., Yeo, S.-Y., Chitnis, A. and Guo, S. (2012). Intralinear directional notch signaling regulates self-renewal and differentiation of asymmetrically dividing radial glia. *Neuron* **74**, 65–78.
- Dubreuil, V., Marzesco, A.-M., Corbeil, D., Huttner, W. B. and Wilsch-Bräuninger, M. (2007). Midbody and primary cilium of neural progenitors release extracellular membrane particles enriched in the stem cell marker prominin-1. *J. Cell Biol.* **176**, 483–495.
- Ettinger, A. W., Wilsch-Bräuninger, M., Marzesco, A.-M., Bickle, M., Lohmann, A., Maliga, Z., Karbanová, J., Corbeil, D., Hyman, A. A. and Huttner, W. B. (2011). Proliferating versus differentiating stem and cancer cells exhibit distinct midbody-release behaviour. *Nat. Commun.* **2**, 503.
- Field, C. M. and Alberts, B. M. (1995). Anillin, a contractile ring protein that cycles from the nucleus to the cell cortex. *J. Cell Biol.* **131**, 165–178.

- Galvagni, F., Baldari, C. T., Oliviero, S. and Orlandini, M.** (2012). An apical actin-rich domain drives the establishment of cell polarity during cell adhesion. *Histochem. Cell Biol.* **138**, 419-433.
- Gbadegesin, R. A., Hall, G., Adeyemo, A., Hanke, N., Tossidou, I., Burchette, J., Wu, G., Homstad, A., Sparks, M. A., Gomez, J. et al.** (2014). Mutations in the gene that encodes the F-actin binding protein anillin cause FSGS. *J. Am. Soc. Nephrol.* **25**, 1991-2002.
- Hall, P. A., Todd, C. B., Hyland, P. L., McDade, S. S., Grabsch, H., Dattani, M., Hillan, K. J. and Russell, S. E. H.** (2005). The septin-binding protein anillin is overexpressed in diverse human tumors. *Clin. Cancer Res.* **11**, 6780-6786.
- Herszterg, S., Leibfried, A., Bosveld, F., Martin, C. and Bellaiche, Y.** (2013). Interplay between the dividing cell and its neighbors regulates adherens junction formation during cytokinesis in epithelial tissue. *Dev. Cell* **24**, 256-270.
- Hesse, M., Raulf, A., Pilz, G.-A., Haberlandt, C., Klein, A. M., Jabs, R., Zaehres, H., Fügemann, C. J., Zimmermann, K., Trebicka, J. et al.** (2012). Direct visualization of cell division using high-resolution imaging of M-phase of the cell cycle. *Nat. Commun.* **3**, 1076.
- Huttner, W. B. and Brand, M.** (1997). Asymmetric division and polarity of neuroepithelial cells. *Curr. Opin. Neurobiol.* **7**, 29-39.
- Jusuf, P. R., Albadri, S., Paolini, A., Currie, P. D., Argenton, F., Higashijima, S.-I., Harris, W. A. and Poggi, L.** (2012). Biasing amacrine subtypes in the Atoh7 lineage through expression of Barhl2. *J. Neurosci.* **32**, 13929-13944.
- Kay, J. N., Finger-Baier, K. C., Roeser, T., Staub, W. and Baier, H.** (2001). Retinal ganglion cell genesis requires lakritz, a zebrafish atonal Homolog. *Neuron* **30**, 725-736.
- Kechad, A., Jananji, S., Ruella, Y. and Hickson, G. R. X.** (2012). Anillin acts as a bifunctional linker coordinating midbody ring biogenesis during cytokinesis. *Curr. Biol.* **22**, 197-203.
- Kelsh, R. N., Brand, M., Jiang, Y. J., Heisenberg, C. P., Lin, S., Haffter, P., Odenthal, J., Mullins, M. C., van Eeden, F. J., Furutani-Seiki, M. et al.** (1996). Zebrafish pigmentation mutations and the processes of neural crest development. *Development* **123**, 369-389.
- Kimmel, C. B., Ballard, W. W., Kimmel, S. R., Ullmann, B. and Schilling, T. F.** (1995). Stages of embryonic development of the zebrafish. *Dev. Dyn.* **203**, 253-310.
- Kosodo, Y. and Huttner, W. B.** (2009). Basal process and cell divisions of neural progenitors in the developing brain. *Dev. Growth Differ.* **51**, 251-261.
- Kosodo, Y., Röper, K., Haubensak, W., Marzesco, A.-M., Corbeil, D. and Huttner, W. B.** (2004). Asymmetric distribution of the apical plasma membrane during neurogenic divisions of mammalian neuroepithelial cells. *EMBO J.* **23**, 2314-2324.
- Kosodo, Y., Toida, K., Dubreuil, V., Alexandre, P., Schenk, J., Kiyokage, E., Attardo, A., Mora-Bermúdez, F., Arii, T., Clarke, J. D. W. et al.** (2008). Cytokinesis of neuroepithelial cells can divide their basal process before anaphase. *EMBO J.* **27**, 3151-3163.
- Li, Z., Hu, M., Ochocinska, M. J., Joseph, N. M. and Easter, S. S.** (2000). Modulation of cell proliferation in the embryonic retina of zebrafish (*Danio rerio*). *Dev. Dyn.* **219**, 391-401.
- Morais-de-Sa, E. and Sunkel, C.** (2013). Adherens junctions determine the apical position of the midbody during follicular epithelial cell division. *EMBO Rep.* **14**, 696-703.
- Parameswaran, S., Xia, X., Hegde, G. and Ahmad, I.** (2014). Hmga2 regulates self-renewal of retinal progenitors. *Development* **141**, 4087-4097.
- Poggi, L., Vitorino, M., Masai, I. and Harris, W. A.** (2005). Influences on neural lineage and mode of division in the zebrafish retina in vivo. *J. Cell Biol.* **171**, 991-999.
- Pollarolo, G., Schulz, J. G., Munck, S. and Dotti, C. G.** (2011). Cytokinesis remnants define first neuronal asymmetry in vivo. *Nat. Neurosci.* **14**, 1525-1533.
- Pujic, Z., Omori, Y., Tsujikawa, M., Thisse, B., Thisse, C. and Malicki, J.** (2006). Reverse genetic analysis of neurogenesis in the zebrafish retina. *Dev. Biol.* **293**, 330-347.
- Reyes, C. C., Jin, M., Breznau, E. B., Espino, R., Delgado-Gonzalo, R., Goryachev, A. B. and Miller, A. L.** (2014). Anillin regulates cell-cell junction integrity by organizing junctional accumulation of rho-GTP and actomyosin. *Curr. Biol.* **24**, 1263-1270.
- Riedl, J., Crevenna, A. H., Kessenbrock, K., Yu, J. H., Neukirchen, D., Bista, M., Bradke, F., Jenne, D., Holak, T. A., Werb, Z. et al.** (2008). Lifeact: a versatile marker to visualize F-actin. *Nat. Methods* **5**, 605-607.
- Rincon, S. A. and Paoletti, A.** (2012). Mid1/anillin and the spatial regulation of cytokinesis in fission yeast. *Cytoskeleton (Hoboken)* **69**, 764-777.
- Ronkainen, H., Hirvikoski, P., Kauppila, S. and Vaarala, M. H.** (2011). Anillin expression is a marker of favourable prognosis in patients with renal cell carcinoma. *Oncol. Rep.* **25**, 129-133.
- Schuhmacher, L.-N., Albadri, S., Ramialison, M. and Poggi, L.** (2011). Evolutionary relationships and diversification of barhl genes within retinal cell lineages. *BMC Evol. Biol.* **11**, 340.
- Shi, S.-H., Jan, L. Y. and Jan, Y.-N.** (2003). Hippocampal neuronal polarity specified by spatially localized mPar3/mPar6 and PI 3-kinase activity. *Cell* **112**, 63-75.
- Singh, D. and Pohl, C.** (2014). Coupling of rotational cortical flow, asymmetric midbody positioning, and spindle rotation mediates dorsoventral axis formation in *C. elegans*. *Dev. Cell* **28**, 253-267.
- Takekuni, K., Ikeda, W., Fujito, T., Morimoto, K., Takeuchi, M., Monden, M. and Takai, Y.** (2003). Direct binding of cell polarity protein PAR-3 to cell-cell adhesion molecule nectin at neuroepithelial cells of developing mouse. *J. Biol. Chem.* **278**, 5497-5500.
- Zolessi, F. R., Poggi, L., Wilkinson, C. J., Chien, C.-B. and Harris, W. A.** (2006). Polarization and orientation of retinal ganglion cells in vivo. *Neural Dev.* **1**, 2.

Clonal analysis of gene loss of function and tissue-specific gene deletion in zebrafish via CRISPR/Cas9 technology

F. De Santis^a, V. Di Donato^a, F. Del Bene¹

PSL Research University, Paris, France

¹Corresponding author: E-mail: filippo.del-bene@curie.fr

CHAPTER OUTLINE

Introduction	2
Tissue-Specific Knockout in Animal Models	2
Clonal Analysis of Gene Loss of Function	3
State of the Art in Zebrafish Tissue-Specific Gene Inactivation	4
Clonal Analysis of Gene Inactivation in Zebrafish	5
1. Methods for Tissue-Specific Gene Inactivation and Clonal Analysis of Mutant Cells	5
1.1 Rationale for the Design of a Vector System for CRISPR/Cas9-Induced Conditional Gene Disruption via Gal4/UAS	5
1.2 Experimental Workflow	6
1.2.1 Overview of the method	6
1.2.2 Technical procedure.....	6
1.3 Rationale for the Design of a Vector System for Clonal Analysis of Mutant Cells by Combining the Gal4/UAS With the Cre/loxP System	11
1.4 Experimental Workflow	12
1.5 Strategies for the Detection of Gene Loss of Function.....	12
1.5.1 Detection of protein loss in Cas9-expressing cells	12
1.5.2 Molecular assessment of the mutagenesis efficiency via fluorescence-activated cell sorting and genome locus sequencing	14
2. Discussion	15
References	16

^aThese two authors contributed equally to this work.

Abstract

In the last few years the development of CRISPR/Cas 9-mediated genome editing techniques has allowed the efficient generation of loss-of-function alleles in several model organisms including zebrafish. However, these methods are mainly devoted to target-specific genomic loci leading to the creation of constitutive knock-out models. On the contrary, the analysis of gene function via tissue- or cell-specific mutagenesis remains challenging in zebrafish. To circumvent this limitation, we present here a simple and versatile protocol to achieve tissue-specific gene disruption based on the Cas9 expression under the control of the Gal4/upstream activating sequence binary system. In our method, we couple Cas9 with green fluorescent protein or Cre reporter gene expression. This strategy allows us to induce somatic mutations in genetically labeled cell clones or single cells, and to follow them *in vivo* via reporter gene expression. Importantly, because none of the tools that we present here are restricted to zebrafish, similar approaches are readily applicable in virtually any organism where transgenesis and DNA injection are feasible.

INTRODUCTION

TISSUE-SPECIFIC KNOCKOUT IN ANIMAL MODELS

The generation of transgenic animals carrying constitutive knockout alleles represents one of the most powerful approaches to investigate gene function. However, stable gene disruption can be linked to embryonic lethality, compensation mechanisms, and pleiotropic phenotypes that might limit the analysis of mutant animals. In these cases, the possibility of inducing targeted mutagenesis in a precisely controlled spatiotemporal manner represents a great advantage in reverse genetic studies. To date, different strategies have been developed to induce tissue-specific loss of function in diverse model organisms. The golden standard techniques for conditional mutagenesis in mouse and fruit fly (*Drosophila melanogaster*) rely on the Cre/loxP and flippase (Flp)/flippase recognition target (FRT) systems (Bouabe & Okkenhaug, 2013; Theodosiou & Xu, 1998). The first approach applies homologous recombination techniques to generate animals carrying a floxed target allele, in which loxP sites are inserted at the 5' and 3' ends of the selected locus. Cre recombinase catalyzes site-specific recombination events in genomic regions containing loxP sites and can be used to excise the floxed target allele, generating gene inactivation. By crossing animals carrying a floxed sequence to driver lines in which Cre expression is controlled by a tissue-specific promoter, it is possible to induce the excision of the target locus in the desired cell population, allowing for the generation of conditional gene disruption (Kuhn, Schwenk, Aguet, & Rajewsky, 1995). A modified version of the Cre enzyme, in which the recombinase is fused to the estrogen receptor (Cre-ER), allows tamoxifen-induced temporal control of Cre activity (Feil et al., 1996). The Flp/FRT technology is an analogous strategy based on the activity of the Flp enzyme, catalyzing site-directed recombination of DNA

sequences flanked by FRT sites (Choi et al., 2009; Golic & Lindquist, 1989). Most recently, CRISPR (clustered regularly interspaced short palindromic repeats)/Cas (CRISPR-associated)—based approaches have been introduced to generate tissue-specific loss of function. The system is based on the combined activity of two components: a single guide RNA (sgRNA) containing 20 nucleotides complementary to the target genomic sequence and the Cas9 endonuclease catalyzing double-strand breaks (DSBs) at the targeted locus. In addition to the efficient generation of constitutive mutant alleles (produced by the imperfect DNA repair mechanisms occurring after Cas9-induced cleavage), the CRISPR/Cas9 technique has been used to insert loxP sites at the desired loci, thus generating floxed alleles for Cre-based conditional mutagenesis (Yang et al., 2013). In addition, it has been shown that it is possible to induce conditional knockout by coupling inducible expression of the *Cas9* enzyme with constitutive expression of sgRNAs (driven by U6 promoters recognized by type III RNA polymerase). In mouse, the generation of a floxed Cas9 allele (in which a *loxP-STOP-loxP* cassette is placed between a constitutive CAG promoter and the coding sequence (CDS) of the endonuclease) has been used to achieve Cre-dependent spatiotemporal regulation of *Cas9* expression (Platt et al., 2014). Similarly, control of Cas9 activity was obtained in *Drosophila* by using the Gal4/upstream activating sequence (UAS) binary system (Port, Chen, Lee, & Bullock, 2014). In this strategy, the use of a tissue-specific promoter to drive the transcription of the Gal4 transactivator enables conditional activation of the Cas9 enzyme, whose expression is controlled by the UAS recognized by Gal4.

CLONAL ANALYSIS OF GENE LOSS OF FUNCTION

To further improve the resolution of loss-of-function studies it is possible to manipulate gene activity in individual cells or single-cell clones and analyze the resulting phenotype within an otherwise wild-type tissue. Different strategies have been developed to generate chimeric animals in which the fate of clones derived from a mutant progenitor can be followed in a wild-type environment. In mouse, homozygous mutant embryonic stem cells, carrying the desired mutation together with an independent genetic marker, can be transplanted into host wild-type blastocysts to give rise to chimeric animals (Rossant & Spence, 1998). Similarly, transplantation strategies can be performed in *Drosophila* by introducing cells derived from a mutant donor embryo into wild-type hosts (Technau & Campos-Ortega, 1986). Nevertheless, transplantation-based approaches are often technically challenging and can only be applied to the analysis of genes acting early in development. Alternative methods are based on the Cre/loxP system and offer the possibility of inducing both targeted gene disruption and activation of a reporter for lineage tracing of mutant cells (Nakazawa, Taniguchi, Okumura, Maeda, & Matsuno, 2012; Zong, Espinosa, Su, Muzumdar, & Luo, 2005). In *Drosophila* multiple strategies have been developed over the years to generate marked clones in genetic mosaics combining

the flexibility of Gal4/UAS and Flp/FRT systems (Griffin, Binari, & Perrimon, 2014). Lately, a novel CRISPR-based strategy has been proposed in mouse. The technique takes advantage of in utero electroporation of a CRISPR-based plasmid to obtain gene inactivation together with a Piggybac transposase vector to express fluorescent reporters for lineage tracing of cells with loss-of-function mutations (Chen, Rosiene, Che, Becker, & LoTurco, 2015).

STATE OF THE ART IN ZEBRAFISH TISSUE-SPECIFIC GENE INACTIVATION

Despite the introduction in the last years of multiple approaches to induce targeted mutagenesis in the zebrafish genome, spatiotemporal control of gene inactivation remains challenging. Strategies based on the already described Cre/loxP and Flp/FRT systems have been also developed in zebrafish to achieve tissue-specific gene disruption (Ni et al., 2012). In this case, the generation of conditional alleles is induced by transgenic insertion of an inverted gene-trap cassette in an intronic region of a gene. Because the mutagenicity of the transgene is orientation dependent, Cre- and Flp-mediated recombination enables a switch from a state of conditional rescue in one orientation to a state of conditional knockout in the other. Nevertheless, the targeting of a precise locus is not possible with this method that relies on random transgene integration. More recently to circumvent this limitation, several techniques based on the TALEN or CRISPR/Cas9 systems have been established to introduce DNA fragments of variable size at predefined genomic locations (Auer & Del Bene, 2014). Among the different applications of these genome editing approaches, the efficient insertion of loxP sites in a targeted fashion has been achieved via TALEN-mediated DSB and subsequent homology-directed repair (Bedell et al., 2012). Although such a tool allows the creation of conditional alleles, the long generation time of zebrafish transgenic lines carrying stable genomic integrations of floxed alleles represents an important constraint. An alternative way to inactivate target genes in a tissue-specific manner has been developed by combining the CRISPR/Cas9 and Tol2 technologies (Ablain, Durand, Yang, Zhou, & Zon, 2015). In this report, a modular construct provides cell-type-specific expression of the Cas9 endonuclease (*Tissue-specific promoter:cas9*) and ubiquitous transcription of the sgRNA by a U6 promoter (*U6:sgRNA*). While mosaic phenotypes can be induced by transient expression of the plasmid, its inclusion into the genome by Tol2 transposition results in higher levels of tissue-restricted gene inactivation. The versatility of the vector system relies on the possibility to readily change the promoter driving *Cas9* transcription and the sgRNA to target a specific open reading frame (ORF) to obtain spatially controlled gene loss of function. A similar approach has been proposed lately to achieve also a tight temporal regulation of Cas9 expression (Yin et al., 2015). This methodology is based on the generation of two transgenic lines: one carries a transgene allowing heat-shock induction of Cas9 expression after Cre mRNA injection (*hp70:loxP-mCherry-STOP-loxP-cas9*); the

other harbors U6 cassettes for the transcription of sgRNAs (*U6:sgRNA*). Therefore, double carriers would show tissue-specific phenotypes subsequent to heat-shock and Cre activation.

CLONAL ANALYSIS OF GENE INACTIVATION IN ZEBRAFISH

CRISPRs-based methods for conditional mutagenesis represent a valid alternative to Cre- and Flp-mediated techniques. However, to date, their application has been limited to the induction and the analysis of tissue-specific gene disruption resulting in visually detectable phenotypes. In fact, genetic labeling of mutant cells, required for the examination of phenotypes that are not readily detectable, is not addressed by these systems.

In this chapter, we present two approaches that combine the Gal4/UAS (Asakawa & Kawakami, 2008) and CRISPR/Cas9 systems in order to induce simultaneously cell-type-specific locus inactivation and fluorescent marking of the targeted cells (Di Donato et al. *Genome Research Accepted*). The first strategy that we describe permits the identification of *Cas9*-expressing cells by concomitant expression of the green fluorescent protein (GFP) and Cas9, both driven by the activation of a UAS sequence (*UAS:Cas9T2AGFP*). Thus, GFP-positive cells can be detected in the spatiotemporal domain of Gal4 expression, which is defined by a chosen tissue-specific promoter. The second strategy provides a tool that enables both the permanent labeling of *Cas9*-expressing cells and the visualization of their clonal progeny, through UAS-dependent coexpression of the Cas9 endonuclease and Cre recombinase (*UAS:Cas9T2ACre*).

For both methods, the vector system used contains two U6 promoters allowing the simultaneous targeting of two sequences at any genomic locus of interest, to increase the percentage of out-of-frame mutations and large deletions.

1. METHODS FOR TISSUE-SPECIFIC GENE INACTIVATION AND CLONAL ANALYSIS OF MUTANT CELLS

1.1 RATIONALE FOR THE DESIGN OF A VECTOR SYSTEM FOR CRISPR/Cas9-Induced Conditional Gene Disruption via Gal4/UAS

CRISPR/Cas9-mediated tissue-specific gene inactivation and concomitant visualization of mutant cells requires: (1) spatiotemporal regulation of the expression of the Cas9 endonuclease; (2) expression of sgRNAs; (3) a fluorescent transgene to label cells where Cas9/sgRNA complex is present. The cell-type-specific expression of the Cas9 enzyme is achieved by using the yeast Gal4/UAS system in which the Gal4 transcriptional activator drives the expression of transgenes linked to the UAS. In our vector design, the CDS of the Cas9, flanked by two SV40 nuclear localization signals, is placed downstream of a 5xUAS cassette. To monitor *Cas9*

expression, we use a viral T2A self-cleaving peptide followed by the GFP CDS enabling the synthesis of the fluorescent reporter from the same transcript (*UAS:Cas9T2AGFP*). Two U6 promoters are subcloned in the same construct to drive ubiquitous transcription of the sgRNAs. BsmBI and BsaI restriction sites allow the cloning of the 20-bp target sequence at the transcription start site (TSS = +1) of the U6 promoters (Figs. 1A and 2). The vector contains Tol2 sites for efficient transposition of the transgenic cassette in the fish genome.

1.2 EXPERIMENTAL WORKFLOW

1.2.1 Overview of the method

The induction of conditional gene inactivation via the Gal4/UAS system consists of three steps. Step 1: design of sgRNAs targeting the genomic locus of interest and assessment of their mutagenesis efficiency. Step 2: cloning of the target sequences of the sgRNAs displaying the highest mutation rate at the TSS of the U6 promoters in the *pUAS:Cas9T2AGFP* plasmid (Fig. 1C and D). Step 3: microinjection of *pUAS:Cas9T2AGFP;U6:sgRNA1;U6:sgRNA2* plasmid for transient expression or generation of a transgenic line carrying stable genomic integration of the cassette (Fig. 1E).

1.2.2 Technical procedure

Step 1: Design of sgRNAs targeting the genomic locus of interest and assessment of their mutagenesis efficiency

sgRNA design

- Select a target site for sgRNA synthesis by using one of the available online tools (ie, <http://crispor.tefor.net/crispor.cgi>; <http://crispr.mit.edu/>; <http://zifit.partners.org/ZiFiT/>; <http://www.broadinstitute.org/rnai/public/analysis-tools/sgrna-design>; <https://chopchop.rc.fas.harvard.edu/>; <http://www.crisprscan.org/>; <http://crispr.cos.uni-heidelberg.de/help.html>).
- Filter the research for oligonucleotides suitable for cloning at the TSS of the T7 in the pDR274 vector (Addgene ref 42250).

Oligonucleotides cloning in the pDR274 vector

 - Digest 1–5 µg of the pDR274 plasmid with BsaI overnight at 37°C.
 - Run the digestion product on a 0.8% agarose gel and extract the linear plasmid with a gel and polymerase chain reaction (PCR) extraction kit.
 - Mix 3 µL of 100 µM forward and reverse oligonucleotides containing the target sequence and add 14 µL of TE buffer (10 mM Tris-Cl, pH 7.5. 1 mM EDTA).
 - Heat the mixture 10 min at 95°C and cool down for 30 min at room temperature to allow the annealing of the oligonucleotides.
 - Ligate 2 µL of annealed oligonucleotides and 100 ng of the digested pDR274 plasmid.
 - Transform the reaction in DH5α competent cells.

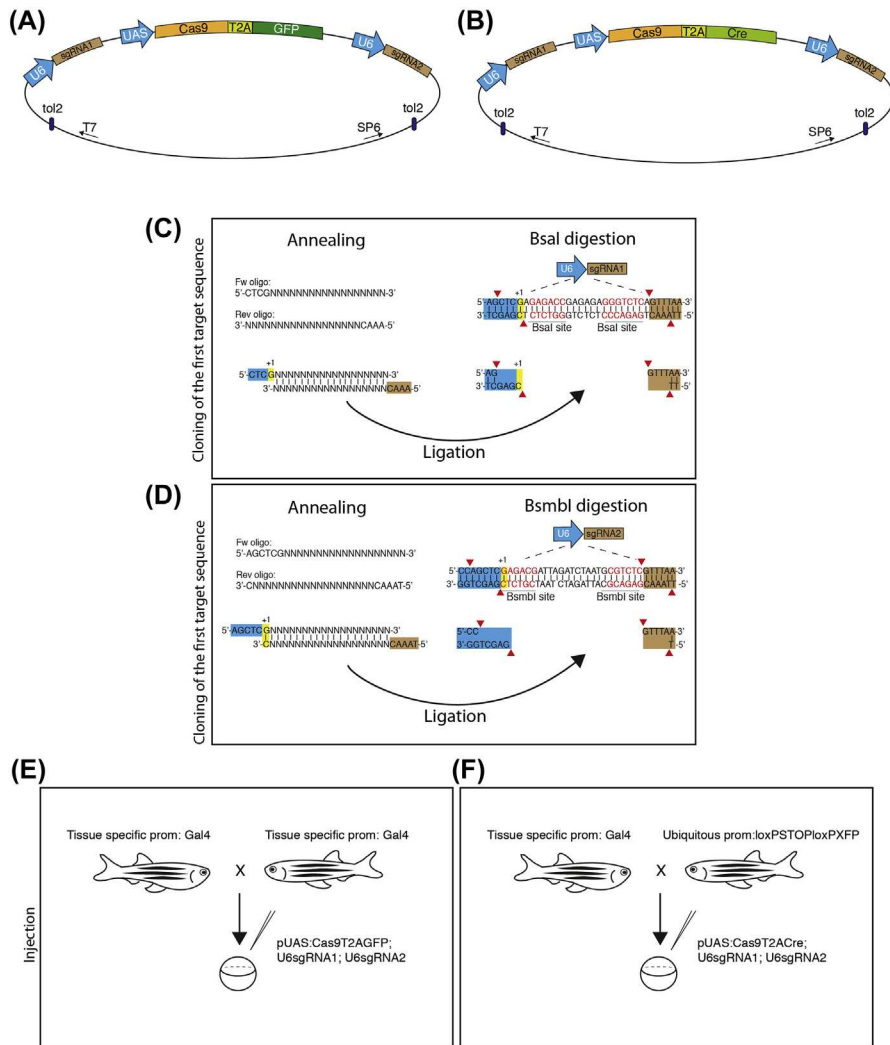
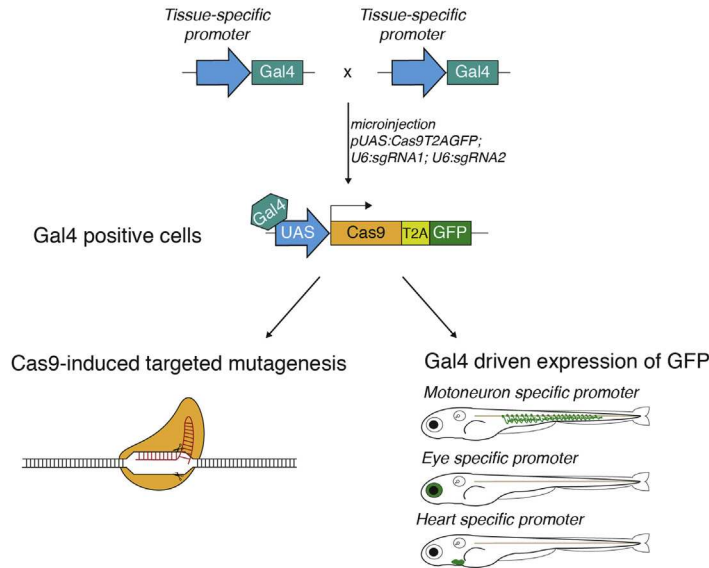


FIGURE 1

(A) Schematic of the *pUAS:Cas9T2AGFP;U6sgRNA1;U6sgRNA2* plasmid; (B) schematic of the *pUAS:Cas9T2ACre;U6sgRNA1;U6sgRNA2* plasmid; (C) insertion of the first target sequence into the transgenesis vector at the *Bsal* cloning sites; (D) insertion of the second target sequence into the transgenesis vector at the *Bsmbl* cloning sites; (E) schematic view of cross of zebrafish Gal4 transgenic driver lines and injection of the *pUAS:Cas9T2AGFP;U6sgRNA1;U6sgRNA2* plasmid; (F) schematic representation of cross of zebrafish Gal4 transgenic driver to line carrying a floxed reporter allele and injection of the *pUAS:Cas9T2ACre;U6sgRNA1;U6sgRNA2* plasmid.

**FIGURE 2**

Schematic of conditional gene inactivation and genetic labeling of *Cas9*-expressing cells after injection of the *pUAS:Cas9T2AGFP;U6sgRNA1;U6sgRNA2* plasmid in specific Gal4 driver lines.

- Plate on LB (Lysogeny broth)-kanamycin plates.
- The next day, pick two colonies from the transformation plate. Inoculate each colony into 2 mL of LB-kanamycin medium and incubate at 37°C overnight with agitation.
- Isolate DNA using a Miniprep kit.
- Sequence the plasmid with M13 forward primer to verify the presence of the target sequence.

sgRNA in vitro synthesis

- Use the pDR274 plasmid containing the target sequence as template for a PCR reaction with the primers:
 - Fw oligo: 5'-GCTCGTCCTGAATGATATGCGACC-3'
 - Rev oligo: 5'-CCAGTAGTGATCGACACTGCTCG-3'
- Set up the PCR reaction as follows:
 - pDR274 template: 10 ng
 - 5X buffer HF: 10 µL
 - dNTP (10 mM): 1 µL
 - Primers (10 µM): 2.5 µL each
 - DMSO: 1.5 µL
 - Phusion polymerase: 0.5 µL
 - H₂O up to 50 µL

Use the program:

98° 30 s

—

98° 30 s

58° 20 s } ×35

72° 20 s

—

72° 5 min

The expected size of the band is 253 bp.

The PCR product will contain a T7 promoter sequence and the sgRNA sequence.

- Gel purify the amplicon and elute in 20 µL. The PCR product will be used as template for the sgRNA synthesis.
- Proceed with sgRNA synthesis using the MegaScript T7 kit (AMBION—AM1334) assembling the reaction in a final volume of 20 µL as described below:

8 µL of PCR product

+2 µL 10X transcription buffer

+2 µL of each NTP

+2 µL of T7 RNA polymerase

- Transcribe for 4 h at 37°C.
- Add 1 µL of TurboDNase: 15 min 37°C.
- Recover RNA with RNA purification with RNeasy Mini Kit (QIAGEN—74104) according to the manufacturer's instructions and perform a double elution with 30 µL of water (Rnase/Dnase free).
- Check the quality of the sgRNA on a 2% agarose gel and with a spectrophotometer.

Microinjection of sgRNA in fish embryos

- Prepare injection solution as follows:

300 ng/µL sgRNA

25 µM Cas9 protein (NEB-M0386M or an equivalent homemade protein)

1X Cas9 10X buffer

H₂O

- Inject 1 nL of solution into one-cell—stage wild-type embryos.

Estimation of the mutagenesis rate

- Perform genomic extraction on a pool of 25 injected embryos.
- Amplify by PCR the genomic locus containing the sequence targeted by sgRNAs used.
- Clone PCR amplicons into the pCRII-TOPO (Zero Blunt TOPO PCR Cloning Kit, ThermoFisher Scientific—K2800-02) vector and sequence DNA recovered from 20 colonies.
- The frequency of insertion and deletion (indel) mutations at the targeted locus is estimated by comparison with the wild-type allele.

Step 2: Generation of pUAS:CAS9T2AGFP;U6:sgRNA1;U6:sgRNA2 construct

Design of the oligonucleotides for cloning at the TSS of U6 promoters
Two U6 promoters flank the *UAS:CAS9T2AGFP* cassette. They contain at the +1 position restriction sites for BsaI and BsmBI suitable for the cloning of desired target sequences. U6 promoters require transcription to start with a guanine nucleotide (G). Design the oligonucleotides as follows:

BsaI site (Fig. 1C):

For a target sequence starting with a G add the overhang CTC- to the 5' of the 20-nt target and the AAAC- overhang to the 5' of the reverse complement of the last 19 nt of the target (removing the final C).

Example:

Target: 5'-GCAGATACACATACAGATAC-3'

Fw oligo: 5'-CTCGCAGATACACATACAGATAC -3'

Rev oligo: 5'-AAACGTATCAGTATGTGTATCTG- 3'

For a target sequence not starting with a G substitute the first nucleotide with a G and proceed as previously described.

Example:

Target: 5'-CAGATACACATACAGATACA-3'

Fw oligo: 5'-CTCGAGATACACATACAGATACA -3'

Rev oligo: 5'-AAACTGTATCAGTATGTGTATCT- 3'

BsmBI site (Fig. 1D):

For a target sequence starting with a G add the overhang AGCTC- to the 5' of the 20-nt target and the TAAAC- overhang to the 5' of the reverse complement of the 20-nt target.

Example:

Target: 5'-GCAGATACACATACAGATAC-3'

Fw oligo: 5'-AGCTCGCAGATACACATACAGATAC -3'

Rev oligo: 5'-TAAACGTATCAGTATGTGTATCTGC- 3'

For a target sequence not starting with a G substitute the first nucleotide with a G and proceed as previously described.

Example:

Target: 5'-CAGATACACATACAGATACA-3'

Fw oligo: 5'-AGCTCGAGATACACATACAGATACA -3'

Rev oligo: 5'-TAAACTGTATCAGTATGTGTATCTC- 3'

Oligonucleotides cloning in the pUAS:CAS9T2AGFP;U6:sgRNA1;U6:sgRNA2 vector (Fig. 1C and D)

- Digest 1–2 µg of the pUAS:CAS9T2AGFP;U6:sgRNA1;U6:sgRNA2 vector with BsaI overnight at 37°C.
- Run the digestion product on a 0.8% agarose gel and extract the linear plasmid with a gel extraction kit.
- Mix 3 µL of 100 µM forward and reverse oligonucleotides containing the target sequence and overhangs for BsaI cloning and add 14 µL of TE buffer.
- Heat the mixture 10 min at 95°C and cool down for 30 min at room temperature to allow the annealing of the oligonucleotides.
- Ligate 2 µL of annealed oligonucleotides and 100 ng of the digested pUAS:CAS9T2AGFP;U6:sgRNA1;U6:sgRNA2 plasmid (Fig. 1C).

- Transform the reaction in TOP10 competent cells (ThermoFisher Scientific—K2800-02).
- Plate on LB-ampicillin plates
- The next day, pick two colonies from the transformation plate. Inoculate each colony into 2 ml of LB-ampicillin medium and incubate at 37°C overnight with agitation.
- Purify DNA using a miniprep kit
- Sequence the plasmid with T7 specific primer to verify the presence of the target sequence
- Repeat the entire process with BsmBI enzyme using oligonucleotides containing overhangs for BsmBI cloning (Fig. 1D), digesting the plasmid where the first target sequence at the BsaI site has already been inserted.
- Sequence the plasmid for correct insertion of the Sp6 specific primer.

Step 3: Establishing tissue-specific gene inactivation (Fig. 1E and 2)

Microinjection of pUAS:CAS9T2AGFP;U6:sgRNA1;U6:sgRNA2 plasmid

- Choose a specific Gal4 driver line based on the population of cells where gene function needs to be analyzed.
- Set up mating couples of the chosen Gal4 transgenic line.
- Prepare the injection mix as described:
 - 30 ng/μL of pUAS:CAS9T2AGFP;U6:sgRNA1;U6:sgRNA2 construct
 - +50 ng/μL of Tol2 mRNA
 - +RNase, DNase-free water up to 5 μL
- Inject with pUAS:CAS9T2AGFP;U6:sgRNA1;U6:sgRNA2 into one-cell–stage embryos from an incross of a *Tg(Tissue-specific:Gal4)* line.
- Screen embryos with GFP-positive cells in the expected Gal4 expression pattern.
- If a stable *UAS:CAS9T2AGFP;U6:sgRNA1;U6:sgRNA2* is needed, raise the embryos to adulthood after injection in wild-type embryos.
- Screen for F₀ adults carrying the transgene in the germline and cross them with the chosen Gal4 transgenic line.

1.3 RATIONALE FOR THE DESIGN OF A VECTOR SYSTEM FOR CLONAL ANALYSIS OF MUTANT CELLS BY COMBINING THE Gal4/UAS WITH THE CRE/LOXP SYSTEM

The use of a GFP reporter to mark *Cas9*-expressing cells allows for the phenotypic analysis of potentially mutant cells during the time span of activity of the promoter driving Gal4 transcription. Long-term tracking of these cells needs a strategy to permanently mark the cells displaying a loss-of-function phenotype. To stably label the population of *Cas9*-expressing cells, we replaced the GFP CDS in the pUAS:CAS9T2AGFP;U6:sgRNA1;U6:sgRNA2 with the ORF of the Cre recombinase (Fig. 1B). Thus, potentially mutant cells can be visualized by using fish lines carrying a transgene where a ubiquitous promoter drives the expression of a fluorescent reporter upon Cre-mediated excision of a floxed STOP sequence. The tissue-specific

promoter regulating Gal4 transcription guarantees synchronized translation of Cas9 and Cre enzymes from the same mRNA, ensuring targeted mutagenesis at the chosen genomic locus and expression of the floxed reporter within the same cell. The fluorescence of the reporter will be stable throughout the entire life of the fish and, most importantly, will be inherited in all the cells deriving from the same *Cas9*-expressing progenitor (Fig. 3). Our strategy, named 2C-Cas9 (Cre-mediated recombination for Clonal analysis of **Cas9** mutant cells) offers the possibility to induce site-specific mutagenesis in a selected cell population and, at the same time, enables genetic labeling of the clones derived from the targeted cells (Di Donato et al. *Genome Research accepted*).

1.4 EXPERIMENTAL WORKFLOW

The procedures for the cloning of the target sequences in the plasmid and for the microinjection of the resulting transgenesis vector have been previously described and are summarized in Fig. 1C,D and F. The injection of the pUAS:*CAS9T2ACre*; *U6:sgRNA1*; *U6:sgRNA2* plasmid is done in a cross between the selected Gal4 driver line and a transgenic line carrying a floxed allele. Different floxed lines can be used (Di Donato et al. *Genome Research accepted*; Bertrand et al., 2010; Hans et al., 2011; Mosimann et al., 2011).

1.5 STRATEGIES FOR THE DETECTION OF GENE LOSS OF FUNCTION

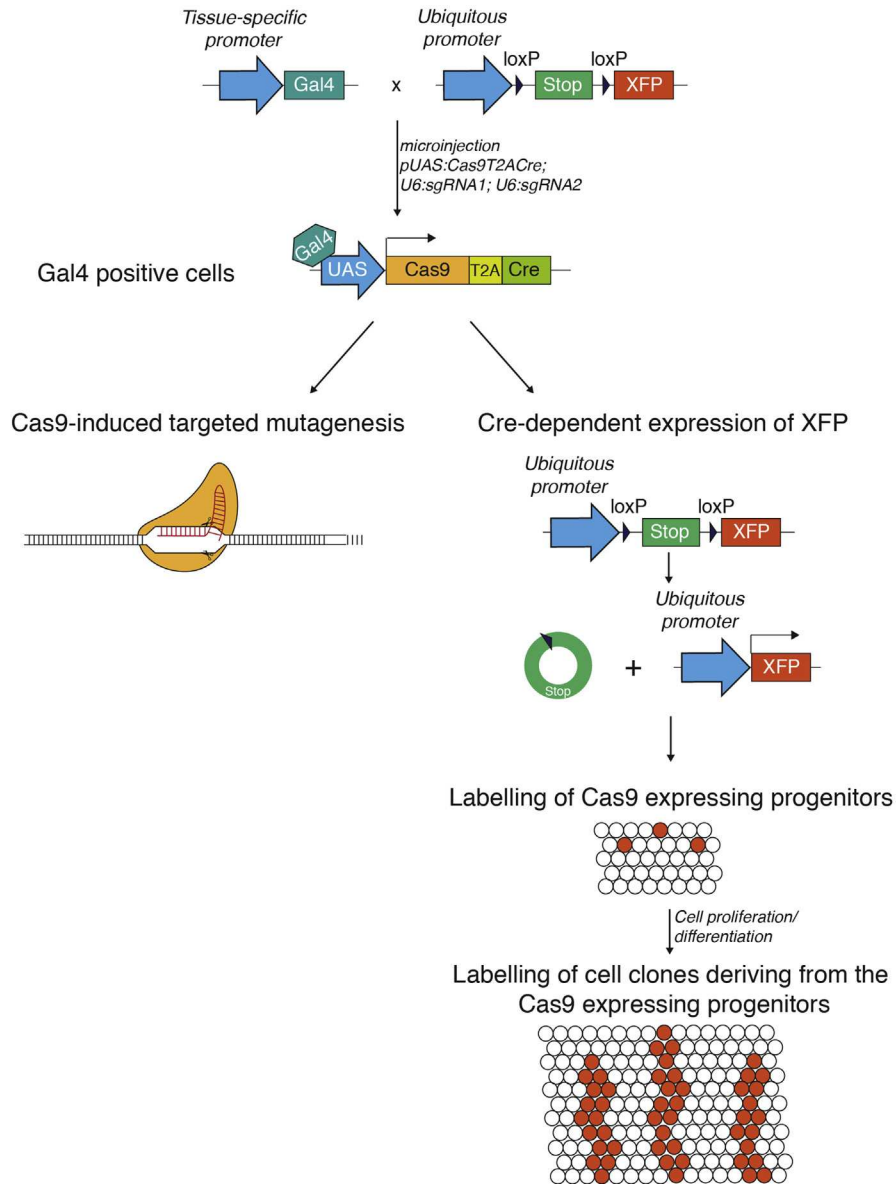
By using the 2C-Cas9 approach, all the *Cas9*-expressing cells can be identified by the expression of a fluorescent reporter. Nevertheless, the marked cells will represent a heterogeneous population in which each cell (or clone) will have independently induced mutations (some of them might not be out-of-frame mutations). To simplify the statistical analysis of the phenotypes arising from 2C-Cas9-mediated targeted gene disruption it is necessary to evaluate the proportion of mutant cells within the labeled population.

1.5.1 Detection of protein loss in *Cas9*-expressing cells

The most direct approach to identify the cells carrying *null* mutations is to perform immunohistochemistry (IHC) experiments by using an antibody recognizing the protein encoded by the targeted gene. This strategy requires a double staining to detect simultaneously the fluorescent reporter linked to *Cas9* expression and the protein coded by the targeted locus. The absence of colocalization will reveal efficient gene disruption.

1.5.1.1 Protocol for IHC on whole mount embryos

- Fix embryos in 4% paraformaldehyde in 1X PBS (pH 7.4) for 2 h at room temperature or overnight at 4°C.
- Wash three times in 1X PBS/0.1% Tween-20 (PBS-Tw), for 5 min each time.
- Incubate for 20 min in ice-cold acetone.

**FIGURE 3**

Schematic of tissue-specific gene disruption and permanent clonal labeling of *Cas9*-expressing cells after injection of the *pUAS:Cas9T2ACre; U6sgRNA1; U6sgRNA2* plasmid in a cross of a specific Gal4 driver to a floxed reporter line (2C-Cas9).

- Rehydrate in three steps (75%; 50%; 25% acetone in PBS).
- Wash twice in PBS-Tw, 5 min each.
- Incubate with 1 mg/mL collagenase diluted in PBS according to the stage (1dpf, day post fertilization: 10 min; 2 dpf: 20 min; 3 dpf: 75 min; 4 and 5 dpf: 120 min).
- Wash three times in PBS-Tw, 5 min each.
- Incubate for 1 h at room temperature in blocking solution (2% BSA; 0.5% Triton-X100 in PBS).
- Wash three times in PBS-Tw, 5 min each.
- Incubate overnight at 4°C with primary antibodies diluted in blocking solution at the appropriate concentrations.
- Wash three times in PBS-Tw, 5 min each.
- Incubate overnight at 4°C with secondary antibodies diluted in blocking solution at the appropriate concentrations.
- Wash three times in PBS-Tw, 5 min each.
- Mount for imaging in 1% low-melting agarose.

1.5.1.2 Protocol for IHC on cryosections

- Fix embryos in 4% paraformaldehyde in 1X PBS (pH 7.4) for 2 h at room temperature or overnight at 4°C.
- Incubate overnight in 30% sucrose; 0.02% sodium azide; PBS solution.
- Embed the embryos in Tissue-Tek O.C.T. compound after removal of the sucrose and place the resulting blocks on dry ice before sectioning.
- Section the blocks with a thickness of 14 µm and mount the sections on Fisherbrand Superfrost plus slides (No 12-550-15).
- Wash twice in PBS-Tw, 5 min each time.
- Incubate for 1 h at room temperature in blocking solution (10% normal goat serum in PBS-Tw).
- Incubate overnight at 4°C with primary antibodies diluted in blocking solution.
- Wash three times in PBS-Tw, 5 min each.
- Incubate for 2 h with secondary antibodies diluted in blocking solution.
- Wash five times in PBS-Tw, 5 min each.
- Add Vectashield drops on the sections and place coverslips on the slides.

1.5.2 Molecular assessment of the mutagenesis efficiency via fluorescence-activated cell sorting and genome locus sequencing

The molecular assessment of the mutagenesis efficiency of the 2C-Cas9 system in the selected Gal4 line requires the isolation of the fluorescent *Cas9*-expressing cells. Fluorescence-activated cell sorting (FACS) might be used to isolate the marked *Cas9*-expressing cells from the wild-type nonfluorescent cell population. After separation, total DNA can be extracted from the two pools of cells and the targeted locus can be analyzed to screen for the presence and the frequency of out-of-frame mutations.

1.5.2.1 Protocol for FACS

- Dissociate the embryos ($n > 200$) as previously described by [Manoli & Driever \(2012\)](#).
- Perform cell sorting and collect cells in lysis buffer (E.G. NucleoSpin Tissue kit; Macherey–Nagel—740952.10).
- Extract genomic DNA following kit instructions.
- PCR amplify the targeted genomic loci.
- Clone PCR amplicons into the pCR-bluntII-TOPO vector.
- Isolate plasmid DNA from single colonies.
- Sequence the plasmids and identify mutant alleles by comparison with the wild-type sequence.

2. DISCUSSION

In this chapter we describe a new tool allowing, with a single plasmid injection, both conditional mutagenesis and lineage tracing of potentially mutant cells. The flexibility of the approach is based on the use of the Gal4/UAS system to drive *Cas9* expression. Many Gal4 driver transgenic lines showing diverse cell-type-specific expression patterns are available to the zebrafish community. The transient or stable UAS-dependent expression of *Cas9*, coupled with constitutive transcription of gene-specific sgRNAs, allows the inactivation of any gene of interest in any Gal4 line. Therefore, gene disruption can be achieved in multiple tissues by generating a unique transgenesis vector, containing gene-specific sgRNA, to be injected into different Gal4 driver lines. Unambiguous identification of cells displaying loss-of-function phenotypes is provided by the expression of a reporter gene (GFP or Cre) together with *Cas9* endonuclease. While GFP fluorescence enables visualization of *Cas9*-expressing cells during the activity time window of the chosen Gal4 line, the use of Cre allows permanent labeling and clonal analysis of potentially mutated cells even after *Gal4* expression has terminated. Both methods represent a valuable alternative to laborious transplantation experiments that represent, to date, the only method to analyze cell-autonomous behavior of mutant cells in a wild-type genetic background. Furthermore, the analysis of genetic chimeras resulting from transplantations is restricted to early phenotypes and does not allow the investigation of the role of genes and pathways that are used repeatedly during development. If well established, Cre/loxP-based approaches for conditional gene inactivation in zebrafish would overcome these issues. Nevertheless they would need long generation time and are currently limited by the low efficiency of homologous recombination-based genomic manipulations.

Although the system described here is useful to score conditional loss-of-function phenotypes by using genetic fluorescent labeling, it does not mark exclusively populations of cells carrying *null* alleles but all *Cas9*-expressing cells. Because this is a mixed population of cells, only a percentage will harbor out-of-frame mutations.

We propose to discriminate mutant from wild-type cells by performing immunofluorescence experiments to detect loss of protein by the targeted gene at a single-cell level. Alternatively, molecular analysis of gene disruption can be performed, after DNA extraction from FACS-sorted fluorescent cells, to estimate the proportion of truly mutant cells within the labeled population.

Several parameters need to be considered to obtain highly penetrant tissue-specific phenotypes by using the 2C-Cas9 system. The selection of sgRNA displaying efficient mutagenesis rates is crucial to successfully induce DSBs at the target genomic locus. In addition, to achieve loss of function in the cases where indel mutations do not disrupt the ORF of the targeted gene, designing of sgRNAs targeting essential functional domains of a protein can be advantageous. The injection of our vector system into a heterozygous mutant background, where one allele carries a *null* mutation, represents another way to enhance the efficiency of gene disruption. Furthermore, the use of a strong Gal4 driver line, leading to a high intracellular expression of Cas9 endonuclease levels, is recommended. In the future, additional improvements in the *Cas9* expression cassette may be needed. A possibility could be the incorporation into our vector system of noncoding elements of the zebrafish genome that have been shown to boost expression of transgenes in UAS-based plasmids (Horstick et al., 2015).

The strategy presented in this chapter can be widely applied for the analysis of gene function in single cells or in clonal populations, from larval stage to adulthood. The genetic labeling of potentially mutant cells generated by the 2C-Cas9 method provides a versatile technique to correlate phenotype and genotype, a challenge that cannot be addressed with other currently available genetic tools in zebrafish.

REFERENCES

- Abblain, J., Durand, E. M., Yang, S., Zhou, Y., & Zon, L. I. (2015). A CRISPR/Cas9 vector system for tissue-specific gene disruption in zebrafish. *Developmental Cell*, 32(6), 756–764. <http://dx.doi.org/10.1016/j.devcel.2015.01.032>.
- Asakawa, K., & Kawakami, K. (2008). Targeted gene expression by the Gal4-UAS system in zebrafish. *Development, Growth & Differentiation*, 50(6), 391–399. <http://dx.doi.org/10.1111/j.1440-169X.2008.01044.x>. pii:DGD1044.
- Auer, T. O., & Del Bene, F. (2014). CRISPR/Cas9 and TALEN-mediated knock-in approaches in zebrafish. *Methods*. <http://dx.doi.org/10.1016/j.ymeth.2014.03.027>.
- Bedell, V. M., Wang, Y., Campbell, J. M., Poshusta, T. L., Starker, C. G., Krug, R. G., 2nd, ... Ekker, S. C. (2012). In vivo genome editing using a high-efficiency TALEN system. *Nature*, 491(7422), 114–118. <http://dx.doi.org/10.1038/nature11537>.
- Bertrand, J. Y., Chi, N. C., Santoso, B., Teng, S., Stainier, D. Y., & Traver, D. (2010). Haematopoietic stem cells derive directly from aortic endothelium during development. *Nature*, 464(7285), 108–111. <http://dx.doi.org/10.1038/nature08738>.
- Bouabe, H., & Okkenhaug, K. (2013). Gene targeting in mice: a review. *Methods in Molecular Biology*, 1064, 315–336. http://dx.doi.org/10.1007/978-1-62703-601-6_23.

- Chen, F., Rosiene, J., Che, A., Becker, A., & LoTurco, J. (2015). Tracking and transforming neocortical progenitors by CRISPR/Cas9 gene targeting and piggyBac transposase lineage labeling. *Development*, *142*(20), 3601–3611. <http://dx.doi.org/10.1242/dev.118836>.
- Choi, C. M., Vilain, S., Langen, M., Van Kelst, S., De Geest, N., Yan, J., ... Hassan, B. A. (2009). Conditional mutagenesis in *Drosophila*. *Science*, *324*(5923), 54. <http://dx.doi.org/10.1126/science.1168275>.
- Feil, R., Brocard, J., Mascrez, B., LeMeur, M., Metzger, D., & Chambon, P. (1996). Ligand-activated site-specific recombination in mice. *Proceedings of the National Academy of Sciences of the United States of America*, *93*(20), 10887–10890. Retrieved from <http://www.ncbi.nlm.nih.gov/pubmed/8855277>.
- Golic, K. G., & Lindquist, S. (1989). The FLP recombinase of yeast catalyzes site-specific recombination in the *Drosophila* genome. *Cell*, *59*(3), 499–509. Retrieved from <http://www.ncbi.nlm.nih.gov/pubmed/2509077>.
- Griffin, R., Binari, R., & Perrimon, N. (2014). Genetic odyssey to generate marked clones in *Drosophila* mosaics. *Proceedings of the National Academy of Sciences of the United States of America*, *111*(13), 4756–4763. <http://dx.doi.org/10.1073/pnas.1403218111>.
- Hans, S., Freudenreich, D., Geffarth, M., Kaslin, J., Machate, A., & Brand, M. (2011). Generation of a non-leaky heat shock-inducible Cre line for conditional Cre/lox strategies in zebrafish. *Developmental Dynamics*, *240*(1), 108–115. <http://dx.doi.org/10.1002/dvdy.22497>.
- Horstick, E. J., Jordan, D. C., Bergeron, S. A., Tabor, K. M., Serpe, M., Feldman, B., & Burgess, H. A. (2015). Increased functional protein expression using nucleotide sequence features enriched in highly expressed genes in zebrafish. *Nucleic Acids Research*, *43*(7), e48. <http://dx.doi.org/10.1093/nar/gkv035>.
- Kuhn, R., Schwenk, F., Aguet, M., & Rajewsky, K. (1995). Inducible gene targeting in mice. *Science*, *269*(5229), 1427–1429. Retrieved from <http://www.ncbi.nlm.nih.gov/pubmed/7660125>.
- Manoli, M., & Driever, W. (2012). Fluorescence-activated cell sorting (FACS) of fluorescently tagged cells from zebrafish larvae for RNA isolation. *Cold Spring Harbor Protocols*, *2012*(8). <http://dx.doi.org/10.1101/pdb.prot069633>.
- Mosimann, C., Kaufman, C. K., Li, P., Pugach, E. K., Tamplin, O. J., & Zon, L. I. (2011). Ubiquitous transgene expression and Cre-based recombination driven by the ubiquitin promoter in zebrafish. *Development*, *138*(1), 169–177. <http://dx.doi.org/10.1242/dev.059345>.
- Nakazawa, N., Taniguchi, K., Okumura, T., Maeda, R., & Matsuno, K. (2012). A novel Cre/loxP system for mosaic gene expression in the *Drosophila* embryo. *Developmental Dynamics*, *241*(5), 965–974. <http://dx.doi.org/10.1002/dvdy.23784>.
- Ni, T. T., Lu, J., Zhu, M., Maddison, L. A., Boyd, K. L., Huskey, L., ... Chen, W. (2012). Conditional control of gene function by an invertible gene trap in zebrafish. *Proceedings of the National Academy of Sciences of the United States of America*, *109*(38), 15389–15394. <http://dx.doi.org/10.1073/pnas.1206131109>.
- Platt, R. J., Chen, S., Zhou, Y., Yim, M. J., Swiech, L., Kempton, H. R., ... Zhang, F. (2014). CRISPR-Cas9 knockin mice for genome editing and cancer modeling. *Cell*, *159*(2), 440–455. <http://dx.doi.org/10.1016/j.cell.2014.09.014>.
- Port, F., Chen, H. M., Lee, T., & Bullock, S. L. (2014). Optimized CRISPR/Cas tools for efficient germline and somatic genome engineering in *Drosophila*. *Proceedings of the National Academy of Sciences of the United States of America*, *111*(29), E2967–E2976. <http://dx.doi.org/10.1073/pnas.1405500111>.

- Rossant, J., & Spence, A. (1998). Chimeras and mosaics in mouse mutant analysis. *Trends in Genetics*, *14*(9), 358–363. Retrieved from <http://www.ncbi.nlm.nih.gov/pubmed/9769731>.
- Technau, G., & Campos-Ortega, J. (1986). Lineage analysis of transplanted individual cells in embryos of *Drosophila melanogaster*. *Roux's Archives of Developmental Biology*, *195*(8), 489–498. <http://dx.doi.org/10.1007/BF00375889>.
- Theodosiou, N. A., & Xu, T. (1998). Use of FLP/FRT system to study *Drosophila* development. *Methods*, *14*(4), 355–365. <http://dx.doi.org/10.1006/meth.1998.0591>.
- Yang, H., Wang, H., Shivalila, C. S., Cheng, A. W., Shi, L., & Jaenisch, R. (2013). One-step generation of mice carrying reporter and conditional alleles by CRISPR/Cas-mediated genome engineering. *Cell*, *154*(6), 1370–1379. <http://dx.doi.org/10.1016/j.cell.2013.08.022>.
- Yin, L., Maddison, L. A., Li, M., Kara, N., LaFave, M. C., Varshney, G. K., ... Chen, W. (2015). Multiplex conditional mutagenesis using transgenic expression of Cas9 and sgRNAs. *Genetics*, *200*(2), 431–441. <http://dx.doi.org/10.1534/genetics.115.176917>.
- Zong, H., Espinosa, J. S., Su, H. H., Muzumdar, M. D., & Luo, L. (2005). Mosaic analysis with double markers in mice. *Cell*, *121*(3), 479–492. <http://dx.doi.org/10.1016/j.cell.2005.02.012>.